Department of Chemical and Environmental Engineering.

The Selective Heating of Pyrite in Coal Using Microwave Energy.

Peter Wardle B.Eng (Hons)

Thesis submitted to the University of Nottingham for the degree of

Doctor of Philosophy

March 2011

ABSTRACT

The objective of this research project was to investigate the effect of microwave treatment on the conversion of pyrite in coal in order to enhance its magnetic properties and to aid subsequent desulphurisation by magnetic separation. Key areas of this investigation include:- a review of the fundamental theoretical aspects of heating in an applied microwave field, a detailed literature survey of the potential applications of microwave heating to aid coal desulphurisation, a study of the transformation mechanisms of pyrite by microwave and conventional heating methods, a comprehensive review of the influence of heterogeneity on the dielectric properties of coals and the effect of high power microwave heating on the decomposition of pyrite in a high sulphur coal.

A detailed survey of the literature has shown that although a significant amount of work has been reported on the microwave heating of coal, little information is available which examines the mechanism through which different coals heat in an applied microwave field. A study is therefore presented in this thesis which quantifies, for the first time, the structural ordering of carbon in a range of coals of various ranks and the relationship with their dielectric properties. The results show a clear relationship between the structural ordering of carbon in coal and dielectric loss factor. Essentially, as the structural ordering increases, the level of free charge (per unit volume) increases together with electron mobility which results in an increase in dielectric loss factor.

The transformation of pyrite to form the more magnetic pyrrhotite and other related decomposition products by conventional radiant heating has been the focus of much research. However, little attention has been given to the effect of microwave heating on the mechanisms of pyrite transformation in inert and oxygen-containing atmospheres. The study

presented in this thesis investigates the effect of temperature, particle size and heat treatment time to establish how these affect the transformation process and the subsequent nature of the final product. This study showed that exposure of pyrite to both conventional and microwave heating methods enhanced its magnetic properties as a result phase alterations at the particle surface. Conventionally heated pyrite samples showed the highest magnetic susceptibility increases, speculated to be due difficulties surrounding the temperature control and measurement of the microwave heated samples. From a review of the literature in this field of research and by SEM observations made for each sample test in this work a general pyrite transformation model as a result of microwave exposure is proposed.

The effect of microwave radiation on the conversion of in-situ coal derived pyrite was also investigated. The study presented here extends previous work by others by assessing quantitatively the influence of higher applied microwave power levels on the conversion of pyrite in coal. Samples of run-of-mine high pyritic sulphur content (~12%wt) Kentucky coal were microwave pre-treated at varying exposure times using 8kW and 15kW of microwave power operating at a frequency of 2.45GHz. This work included initial material characterisation which consisted of TGA, optical microscopy and dielectric property measurement, followed by SEM/EDAX characterisation of both microwave treated and untreated sample specimens. This is the first time that microwave treated coal, embedded in a carnauba wax mounting medium, has been observed by this method with focus on the thermal alterations of the pyrite phase. It was demonstrated that with sufficient power and residence time, the conversion of pyrite to the more magnetic pyrrhotite is achievable using microwave irradiation. The amount of pyrrhotite formed as a result of microwave exposure varies with microwave residence time and forward power level. Comparisons of change in the iron sulphide species in the coal was made between microwave treated and untreated material. Using a multimode microwave cavity it was found that significant amounts of

pyrrhotite were formed in 20s when using 15kW of microwave power. Treatment at lower power levels in this type of cavity was found to be less effective. The overall effect of treatment on the coal proximate character was minimal.

ACKNOWLEDGEMENTS

I would to extend my thanks and gratitude to Professor Ed Lester and Professor Sam Kingman for the opportunity to undertake Ph.D research in the Department of Chemical and Environmental Engineering at The University of Nottingham. I would also like to thank them for their advice, guidance, encouragement and patience during my studies at the University.

I would also like to thank Dr Steve Plint from the Department of Chemical and Environmental Engineering for his expertise and advice in the SEM/MLA investigations described herein, the results of which have formed an important part of the thesis discussion. Further thanks go to Mr David Clift for his laboratory assistance throughout the course of this work.

I would like to thank my colleagues and friends from the University of Nottingham and Staffordshire University for their support and encouragement to complete this work.

Special thanks are also due for my parents and family for their endless support, understanding and patience throughout the course of my studies.

CONTENTS

.

LIST OF FIGURES

LIST OF TABLES

Chapter 1 - Introduction

Over the period of 1971- 2006, the World's total primary energy supply increased by 102% (OECD [Organisation of Economic Cooperation and Development], 2007). During this period, World electricity generation rose at an average rate of 3.7% per year (greater than the 2.1% growth in total primary energy supply). This energy increase was largely due to an increase in energy intensive manufacturing-led demands and the development of electrical heating in many developing countries.

Although the share of electricity production from fossil fuels has gradually fallen (displaced in particular by a rapid growth in nuclear power and to a lesser extent the development of renewable energy technologies such as wind, wave and tidal, solar and biomass systems), the share of coal usage in the fossil fuel mix remains stable.

Figure 1.1, World electricity generation by fuel (OECD Factbook, 2009).

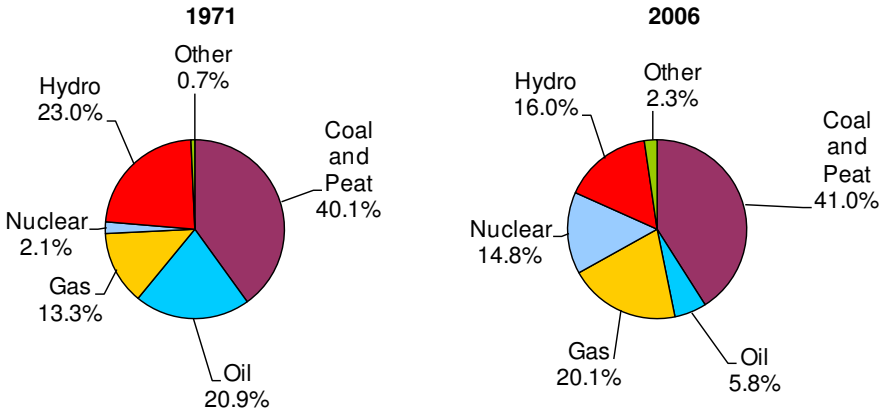

World energy production increased by 2.1% per year between 1971 and 2006, reaching 11 796 million tonnes of oil equivalent (Mtoe). The OECD, with a 33% share of the global production, was the main energy producing region in 2006. China accounted for 15% of world energy production, the United States for 14%, the Middle East region for 13% and the Russian Federation for 10%.

The share of coal in fuel – energy balances from OECD member countries is 20.3% (oil share is 40.9% and natural-gas share is 21.7%). However, the world's proven workable coal reserves at the end of 2006 was $909064x10^6$ tonnes (25,500 EJ), which is approximately 7 times more than oil reserves and approximately 9 times more than those of natural-gas (BP Global, Statistical Review of World Energy, 2007). Under the same conditions, it is estimated (accounting for current production levels) that the oil, natural-gas and coal reserves will be enough for 40, 61 and 227 years respectively. It has been predicted that this global energy mix will remain fairly stable, with fossil fuels still dominating in 2030. Due to this scenario, no fuels energy share in the mix will increase by more than a few percentage points. Fossil fuels will remain as the largest source of world energy, accounting for 80% of global demand in 2006 and approximately 82% in 2030. Although the consumption of each fossil fuel grows at different rates, their share of the total energy mix only varies slightly. In the period 2004 – 2030, oil falls from 35% to 33%, gas rises from 21% to 23% and coal rises from 25% to 26% (OECD, Energy for Sustainable Development, 2007). Global energy needs are estimated to continue to grow steadily – the underlying premise of the *World Energy Outlook's* reference scenario is that the global energy need will grow by ~50% in the period 2003 - 2030, an average annual growth rate of 1.6%. It is estimated that more than two thirds of this growth will be as a result of rapidly growing developing countries, (massive economic and population growth) and their large appetite for energy to meet these demands. In 2006, the Asia

pacific Region accounted for ~90% of global growth (4.5%) in coal consumption and 80% of the growth in production (BP Global, Statistical Review of World Energy, 2007) Any limit on the usage of coal for the global energy market will not be imposed by a limit on the availability of physical resources, but may face limits and restrictions due to its classification (rank, proximate analysis and calorific value) and its potential to produce atmospheric pollutants in the form of sulphur dioxide emissions (acid rain fall out) and the greenhouse gasses carbon dioxide (CO_2) and nitrogen oxides (NO_x). The development of clean coal technologies and carbon capture and storage is crucial in this respect. For many countries (including China) the availability of low-cost coal has been a driving factor in their large scale electrification programs. China, for example, is now 99% electrified, and 77% of this electricity is produced in coal-fired power systems (twice the average, worldwide) (Asif & Muneer, 2007).

This increase in coal usage raises serious concerns about emissions and the future global environmental impacts to follow. However, this significant increase in coal utilisation partly reflects China's resource base, having the third largest coal reserve in the world (Zhang, 1998).

One of the most serious environmental objections to the burning of coal lies in its potential to produce SO_2 emissions, which can be converted, in turn, to sulphurous and sulphuric acids. After condensation in the atmosphere, these produce acid rains, adversely affecting human health and the earth's environment. The regulation of sulphur emissions in the power industry are forcing utilities, worldwide, to seek low sulphur coals. Consequently, on the international market, price differentials have formed between coals of different sulphur contents. Thus, although the average sulphur content in coal currently

in use within the UK for example, can vary from below 0.8% to ~1.6% (by weight), there still remains some coal deposits with high sulphur contents. Moreover, some countries only have high sulphur coal stores which are not mined, despite favorable mining and geological conditions (Hayvanovych & Pysh'yev, 2003).

The SO_2 emission from coal combustion will depend generally on a number of factors including its total sulphur content (as-received), the content remaining in the ash after combustion and the combustion conditions. These will be discussed in more detail later in this work. Unabated SO_2 emissions from coal combustion are particularly high, typically around 230 (anthracite) to 390 (bituminous) and 525 (lignite) g/GJ_{NCV}. SO_2 emissions from oil (fuel & gas) are typically lower than that for coal (Graus & Worrell, 2007). The current technologies employed to control SO_2 emissions from coal fired power plants rely on gas scrubbers, sorbent injection technologies and combined NO_x and SO_2 control. These procedures allow us to reduce sulphur emissions in the stack exhaust gasses by up to 99%. Desulphurisation technologies and processes have been discussed in the literature survey carried out for this work.

Suffice to say that these desulphurisation installations are extensive and complex in design and require significant capital outlay, whether this is for retrofitting or new-build power plants. The negligible demand for the byproducts that are formed in these processes (gypsum, ammonia sulphate and dry ash etc.), mean that actually, all desulphurisation methods are unprofitable (Bazayanc, 1999). Pollution abatement technologies also affect the net efficiency of power generation. The adverse effect on the net efficiency of coal-fired power utilities is estimated to be around 2% (Graus & Worrell, 2007). Therefore, the only positive effect that these technologies will have is

environmental protection. This situation is unlikely to provide sufficient incentive for emerging economic powers to commit to such a massive investment in existing or new-build coal fired power plants and their aspiration to burn only low-sulphur coals will continue to drive up international coal prices in the short/medium term. Also, the effect of burning high-sulphur coals leads to the corrosion of the pollution control equipment and therefore the construction of desulphurisation plants is only performed in highly developed, technologically advanced countries, such as the United States and Germany. Although, even these countries make minimal efforts to use high-sulphur coals in their large combustion plants (Hayvanovych & Pysh'yev, 2003).

Naturally, this type of approach does not solve the problem of using high sulphur coals for electricity generation worldwide. The minimisation of sulphur content in coal, prior to combustion, is clearly one of immense importance if the exploitation of workable mines containing high sulphur coals is to be accomplished.

Literature data has shown that generally, sulphur is present in coal in two forms; Organic and Pyritic (iron disulphides). It is widely reported that pyrite (FeS_2) is the most commonly occurring sulphide and therefore is the major constituent of the sulphur found in coal (Stach, 1975; Male, 1984; Rowson, 1986; Hayvanovych & Pysh'yev, 2003; Uslu & Atalay, 2004; Lui, et al., 2007; Waters, et al., 2007). The main pretreatment process for removing sulphide minerals from coal is by froth flotation (Waters, et al., 2007). During this process, the pyrite (found as finely disseminated particles, framboids or clusters of individual crystals) interacts with the flotation reagents (e.g. xanthate collectors) and is floated along with the clean and valuable hydrophobic coal particles, reducing the efficiency of the flotation process (Finkelstein, 1997).

Pre-combustion magnetic separation offers considerable benefits and improvements to the sulphur – coal separation process. However, pyrite is weakly paramagnetic and so exhibits only a very small positive magnetic susceptibility (Rowson, 1986; Waters, et al., 2007). Clearly, for a successful and efficient separation process to be achieved, the magnetic properties need to be significantly improved.

This thesis investigates the use of high power microwave radiation to alter the surface chemistry of organically bound pyrite by inducing a phase alteration, resulting in a substantial increase in its magnetic susceptibility. The microwave heating of coal derived pyrite to improve its magnetic properties will allow for a fundamental investigation into the process of its conversion to a new, more magnetic phase and its effect on the physio-chemical characteristics of coal after treatment.

Chapter 2 - Theoretical Aspects of Microwave Heating

2.1 Introduction

Microwave power was first used as a means of volumetric heating up to fifty years ago and has since become readily accepted in the food industry for operations including drying, pasturisation and sterilisation and also as a means of processing both rubber and plastics (Nott and Hall, 2005; Swain et al., 2004). Industry as a whole, is continually seeking to reduce manufacturing and processing costs whilst at the same time improving the quality of the product (Menezes et al., 2007; Ostwald and Munoz, 1996). Electricity is a high grade energy source which offers a number of advantages and possibilities in this respect. There are many different ways in which electricity can be used in heating, such as resistance heating, infrared heating, ultraviolet curing, dielectric heating, induction heating, plasma and laser heating (De Alwis and Fryer, 1990; Ming-Ching, et al., 2007; Metal Finishing, 2004; Meredith and Metaxas, 1983)

Conventional radiant heating can cause problems, particularly where non-conducting or insulating materials have to be heated. This is due to the fact that heat is applied externally and allowed to ‘soak’ into the material by conduction. This can be a slow energy consuming process with materials of poor thermal conductivity. Another disadvantage of conventional heating is that overheating may occur at the surface of the heated product before the centre has reached the required temperature, particularly if attempts are made to accelerate the heating rate. Large temperature variations within a material can be overcome (or even exploited) using electromagnetic heating. Electromagnetic heating energy is delivered instantaneously throughout the mass of the

material, achieving controlled heating rates and accurate process temperatures become easier.

2.2 Plane Electromagnetic waves

Materials will differ in their ability to absorb electromagnetic energy in an applied electric field. A materials susceptibility to the heating effects in high frequency electromagnetic fields can be measured and different materials will have their own particular optimum frequency. However, microwave heating applications usually make use of the 0.915 (0.896 in the UK) and 2.45GHz frequencies in order to minimise interference with communication band microwaves. These frequencies which have been allocated to electroheat processes are designated ISM – 'industrial, scientific and medical' frequencies. Microwaves form part of a continuous electromagnetic spectrum that extends from low frequency alternating currents to cosmic rays. Figure 2.1 below illustrates the electromagnetic spectrum where microwave radiation lies between infrared and radio waves.

Figure 2.1 The electromagnetic spectrum (Serway, 1996).

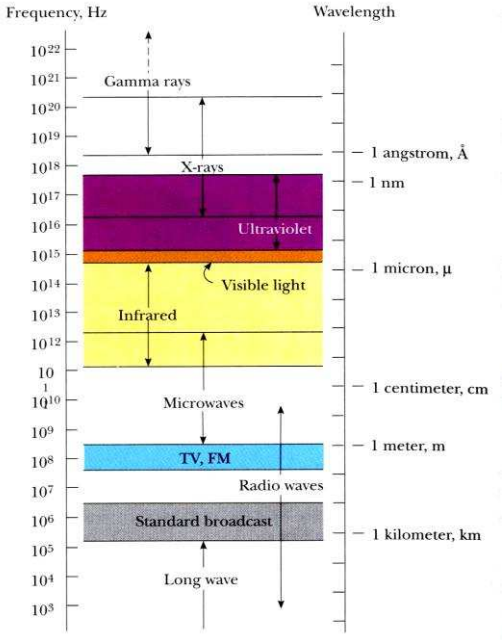

Since all electromagnetic waves travel through a vacuum with a speed c, their frequency f (Hz) and wavelength λ (m) are related by the expression

$$c = f\lambda \tag{2.1}$$

In the illustration of the electromagnetic spectrum shown in Figure 2.1 it can be seen that there is no sharp dividing point between one kind of wave and the next.

Microwaves have wavelengths ranging between approximately 1mm and 300mm and are generated by electronic devices (Serway, 1996). Because microwaves have short wavelengths they are well suited for RADAR navigation systems and for studying the atomic and molecular properties of matter.

Electromagnetic waves are produced as a consequence of two effects:

- A changing magnetic field produces an electric field:
- A changing electric field produces a magnetic field.

The electric and magnetic fields of an electromagnetic wave are perpendicular to each other and perpendicular to the direction of wave propagation. Hence, electromagnetic waves are 'transverse' plane waves which travel through a vacuum with the speed of light c, where

$$c = \frac{1}{\sqrt{\mu_0 \varepsilon_0}} = 3.00 \text{x} 10^8 \text{ m/s} \tag{2.2}$$

Where μ_0 and ε_0 are the permeability of free space (1.2566×10^{-6} H/m) and the permittivity of free space respectively (8.854×10^{-12} F/m).

Figure 2.2 below represents a sinusoidal, plane-polarised electromagnetic wave moving in the positive x direction with a speed c.

Figure 2.2 A plane-polarised electromagnetic wave. (E, electric field, B, magnetic field, c, propagation velocity) (Serway, 1996).

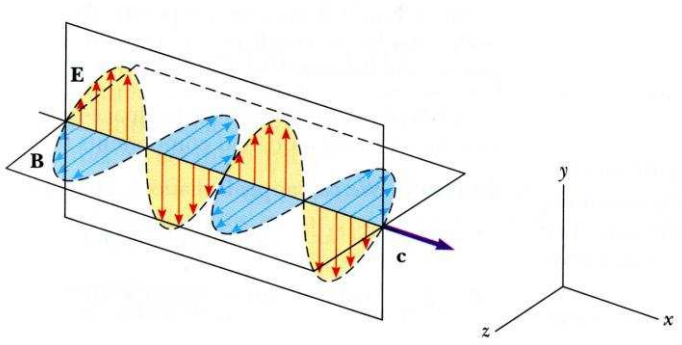

2.3 Microwave – Material Interaction Mechanisms

A dielectric material is one which is non-conducting and when inserted between the plates of a capacitor, the capacitance increases. If the dielectric completely fills the space between the charged plates, then the capacitance will increase by a dimensionless factor ε, called the dielectric constant. The relative dielectric constant ε_r of a material under given conditions is a measure to which it will concentrate electrostatic lines of flux and can be described as the ratio of the amount of stored electrical energy when a potential is applied, relative to the permittivity of a vacuum. It is commonly called the relative permittivity. Therefore, it is defined by the ratio

$$\varepsilon_r = \frac{\varepsilon}{\varepsilon_0} \tag{2.3}$$

Where ε and ε_0 represent the material static permittivity and the permittivity of free space respectively.

As shown in Figure 2.3, the electric field is oriented from the positive plate to the negative plate and its value is equal to the voltage applied to the plates divided by the distance between the plates. This is why the electric field is also called the 'voltage gradient'. Replacing the DC voltage by an alternating voltage source will make the field between the plates alternate. The frequency of its oscillations is equal to the frequency of the voltage source.

Figure 2.3 Electric Field Between a Parallel Capacitor (a) No dielectric inserted between the plates (b) Reduction in potential after dielectric insertion (Serway, 1996).

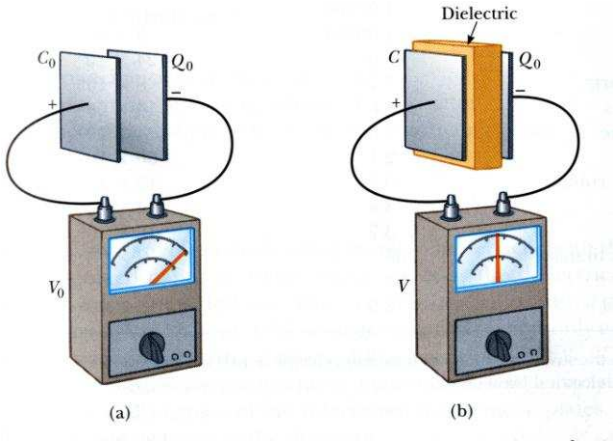

2.3.1 Polarisation

A dielectric can be heated by the application of high frequency electromagnetic energy. This occurs due to two phenomena – D.C. conductivity and polarisation (Which are both induced by the electric component of the electromagnetic field).

When an electric field is applied to a dielectric material it will align permanent dipoles present in the material (dipolar polarisation). A dipole is essentially two equal and opposite charges separated by a finite distance. An example of this is the stereochemistry of covalent bonds in a water molecule, giving the water molecule a dipole moment.

The field may also induce diploes by distorting electron orbits (electronic polarisation) or the position of atoms within their molecular framework (atomic polarisation). A third type of induced dipole is possible through the charge build up in the interfaces between components in heterogeneous systems (interfacial polarisation). These induced dipoles will become aligned with the applied electric field. The overall internal charge orientation within the material gives rise to a polarisation field vector, P .

The value of P may be given in two forms:

$$\mathrm{P} = (\varepsilon_{\mathrm{r}} - 1)\varepsilon_0 \mathrm{E} \qquad (2.4)$$

Where,

ε_{r} is the relative dielectric constant.

E is the externally applied electric field ($\mathrm{Vm^{-1}}$).

ε_0 is the permittivity of free space.

On a molecular scale,

$$\mathrm{P} = \alpha_{\mathrm{t}} \mathrm{N}' \mathrm{E}' \qquad (2.5)$$

Where,

N' represents the number of dipole moments.

E' represents the electric field experienced by the dipole ($\mathrm{Vm^{-1}}$).

With,

$$\alpha_{\mathrm{t}} = \alpha_{\mathrm{c}} + \alpha_{\mathrm{a}} + \alpha_{\mathrm{d}} + \alpha_{\mathrm{mw}}$$

Where α_{t} is the total polarisability of the medium and $\alpha_{\mathrm{c}}, \alpha_{\mathrm{a}}, \alpha_{\mathrm{d}}$ and α_{mw} are the electronic, atomic, dipolar and interfacial polarisabilities respectively.

2.3.1.1 Electronic Polarisation

Electronic polarisation may be induced to one degree or another in all atoms. This form of induced polarisation is due the distortion of the negatively charge electron cloud relative to the positively charged nucleus of the atom by the electric field. This is illustrated in Figure 2.4. Due to the low mass of the electron, the polarisation is able to follow the applied field up to optical frequencies. Consequently, at microwave frequencies it is a lossless mechanism (see 2.3.3) and contributes solely to the permittivity of a dielectric. This type of polarisation is found in all dielectric materials and only exists when an electric field is present. The temperature dependence of electronic polarisation is insignificant, with only a slight reduction in the permittivity of the material as temperature increases from the thermal expansion and subsequent reduction in density of the material (Hart, 2004)

Figure 2.4 Electronic Polarisation that results from the distortion of an atomic electron cloud by an electric field (Evans, 1995)

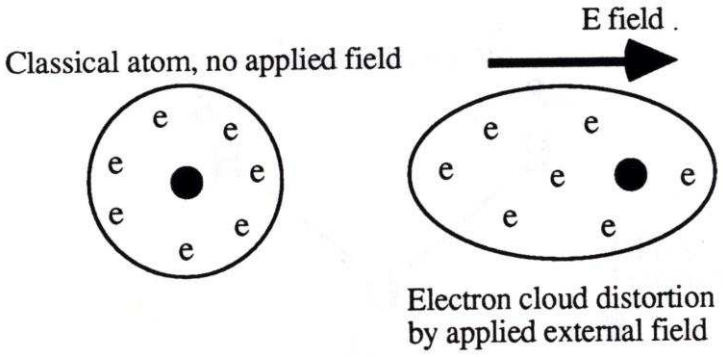

2.3.1.2 Dipole Orientation Polarisation

This type of polarisation is found in dielectrics which have permanent dipole moments. Polarisation results from a rotation of the permanent moments parallel to the direction of the applied electric field as represented in Figure 2.5. Molecules are said to be polarised when there is a separation between the 'centre of gravity' of the negative charges and that of the positive charges on the molecule. (Whittaker, 1997; Meredith and Metaxas, 1983). Water is an example of a polar liquid with molecules that are readily aligned with the applied field which can be better understood by examining the geometry of the water molecule. The molecule is arranged such that the oxygen atom is bonded to the hydrogen atoms with an angle of 105° between the two bonds. The centre of negative charge is therefore near the oxygen atom and the centre of positive charge is midway along the line joining the two hydrogen atoms (point x in Figure 2.6). Thus, the water molecule is permanently polarised (Serway, 1996). Materials that are permanently polarised in this fashion have large dielectric constants. The dielectric constant of water at 25°C is $\varepsilon_r = 80$ (Meredith, 1998).

Figure 2.5 Schematic representation of an electric dipole generated by two electric charges (of magnitude q) separated by a distance d: the associated polarisation vector P is also shown (Callister, 1999).

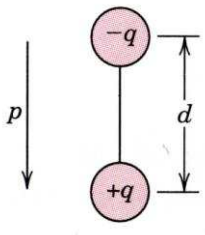

Figure 2.6 The water molecule has a permanent polarisation due to it geometry (Serway, 1996).

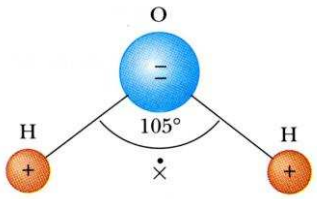

2.3.1.3 Ionic Polarisation

This type of polarisation occurs in materials with free ions. The applied field acts to displace cations in one direction and anions in the opposite direction, which gives rise to a net dipole moment. Polarisation increases with temperature due to the weakening of the elastic forces between the ions but is also reduced by thermal expansion reducing the number of ions per unit volume. In the presence of microwave radiation the induced dipoles will cause heating in the sample due to electrical resistance. If a material has a low electrical resistance, most of the microwave energy will not penetrate the surface of the material, but will be reflected from it. However, high surface voltages may still be induced and are responsible for the arcing that is observed from metals in microwave ovens (Whittaker, 1997).

Figure 2.7 shows a schematic representation of the distortion of the crystal lattice when an electric field is applied (Callister, 1999).

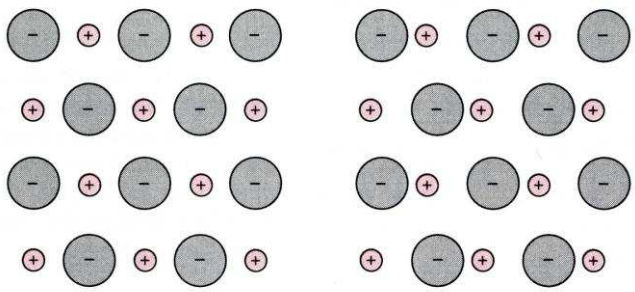

2.3.1.4 Maxwell-Wagner (Interfacial) Polarisation

In a heterogeneous dielectric material where a highly conductive phase is present and interspersed in a phase of low conductivity, charge builds up at the boundary of the two phases in line with the applied field. This mechanism is active over a broad range of the electromagnetic spectrum including the microwave region (Meredith and Metaxas, 1983). An example would be a dispersion of metallic particles in sulphur. Sulphur is microwave transparent and metals reflect microwaves. However, this combination forms a composite which is an extremely good microwave absorbing material. Interfacial polarisation is a complex effect which is difficult to treat in a simple manner and is viewed as a combination of conduction and dipolar polarisation effects (Whittaker, 1997).

2.3.2 Frequency Dependence of the Dielectric Constant.

If we consider a dielectric material that is subject to a polarisation by an a.c. electric field, with each direction reversal the dipoles will attempt to reorient with the frequency of the field. Of course this process requires some finite time and for each polarisation type there will exist a minimum reorientation time. This will depend on the ease with which the particular dipoles are capable of realignment reversals. A relaxation frequency is taken as the reciprocal of this minimum reorientation time. If the frequency of the applied electric field exceeds the relaxation frequency, the dipole will be unable to keep shifting its orientation direction, and therefore, will not make a contribution to the dielectric constant. Therefore, the value of the dielectric constant depends on the field frequency as represented in Figure 2.8.

Figure 2.8 Variation in dielectric constant with frequency of an alternating field (Callister, 1999).

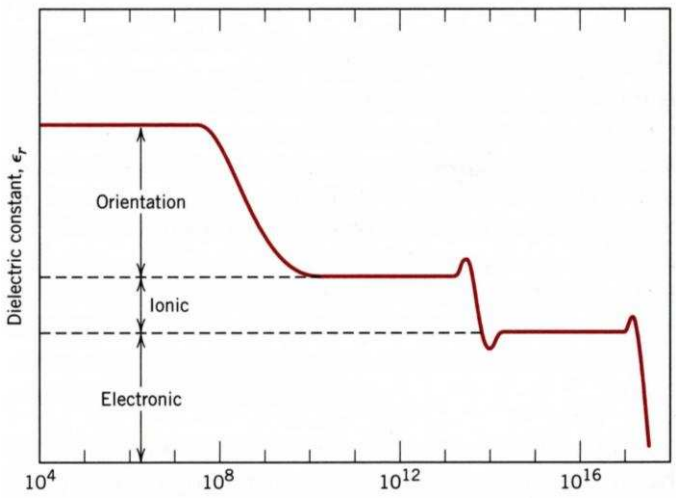

Figure 2.8 represents the dependence of ε_r on the field frequency for a dielectric medium that exhibits all three types of polarisation mechanism. Note that the frequency axis (x-axis [Hz]) is scaled logarithmically and as indicated in Figure 2.8, when a polarisation mechanism ceases to function, there is an abrupt change in the dielectric constant.

The dissipation of electrical energy by a dielectric material which is subjected to an a.c. electric field is termed dielectric loss.

Debye (1929) examined the dipolar (re-orientation) loss mechanism in dipolar electrolytes. From this work a well known relationship for the complex relative dielectric constant was deduced.

$$\varepsilon^* = \varepsilon` - \mathrm{j}\varepsilon`` = \varepsilon_0(\varepsilon_r' - \mathrm{j}\varepsilon_r'') = \varepsilon_\infty + \left[\frac{\varepsilon_s - \varepsilon_\infty}{1+\omega^2\tau^2}\right] - \left[\frac{\mathrm{j}(\varepsilon_s - \varepsilon_\infty)}{1+\omega^2\tau^2}\right] \qquad (2.6)$$

Where ε^* is the complex permittivity, ε' is the permittivity or dielectric constant, ε'' is the dielectric loss factor, ε_0 is the permittivity of free space, ε_r' is the relative dielectric

constant, $\varepsilon_r^{''}$ is the relative loss factor, ε_s is the relative dielectric constant at D.C, ε_∞ is the relative dielectric constant at high frequencies, τ is the relaxation time of the system and j is the imaginary part of the dielectric constant expressed by a complex number $\left(\sqrt{-1}\right)$.

By separating the real and imaginary parts of Equation 2.6, the parameters $\varepsilon^{'}$ and $\varepsilon^{''}$ can be obtained. Debye illustrated these parameters plotted as a function of $\omega\tau$, as shown in Figure 2.9.

Figure 2.9 Debye Relaxation Plot with $\omega\tau$ (Metaxas and Binner, 1995)

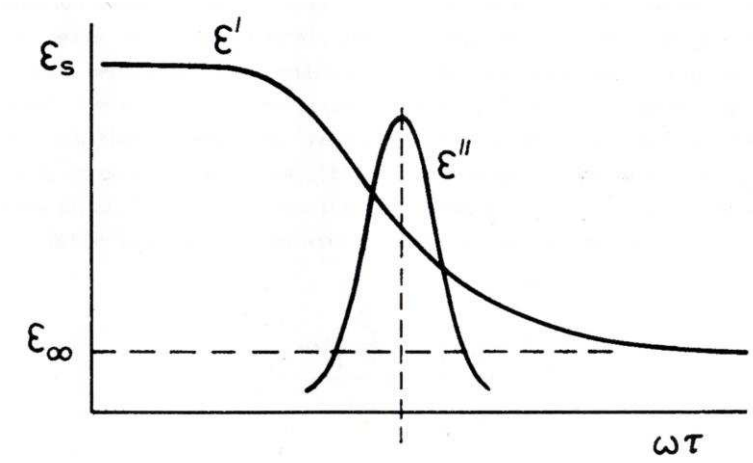

The Debye relaxation plot can be interpreted in the following way.

At very low frequencies the dipoles have ample time to follow the reversal of the electric field and thus the dielectric constant will be at its maximum. The bound charge density will attain its maximum value and the energy from the external source is stored in the material. As the frequency increases the dipoles are unable to follow the field reversals and restore their original positions. As a consequence of this, the dipolar polarisation lags behind the applied field. As the frequency increases further, the re-orientation

polarisation fails to follow the applied field and will therefore contribute less and less to the total polarisation. This fall will manifest itself as a fall in the dielectric constant ε' and a rise in the dielectric loss factor ε''. The power will now be drawn from the external source and dissipated as heat in the material. It should be noted that this interpretation does not work well for a solid dielectric since the relaxation is given in terms of dipolar rotations against frictional forces in a medium where viscosity is the dominant mechanism. Moreover, when atoms and molecules are bonded together to form a dielectric, the dipoles will be influenced by the forces of all other neighbouring particles and of course these must be taken into account (Meredith and Metaxas, 1983). The dielectric constant also defines the velocity of propagation of an electromagnetic wave through the dielectric and so can be related to its refractive index (Meredith and Metaxas, 1983, Fletcher, 1995)

2.3.3 Loss Factor and Dielectric Conductivity

The ability or receptiveness of a material to electromagnetic heating is measured by the knowledge of it dielectric loss factor. Of course not all materials will exhibit the same receptiveness to heating in applied electric fields. In general, the higher the loss factor the more receptive the material will be. However, if for example a material is highly absorptive to microwave radiation, most of the incident energy will be absorbed within the first few millimetres of its surface, leaving the internal parts unaffected. In most situations this form of non-uniform heating is undesirable. Therefore, knowledge loss factor is vitally important in electromagnetic heating applications.

Generally speaking, loss factors between the limits $10^{-2} < \varepsilon'' < 5$ provide good candidates for microwave heating applications (Meredith and Metaxas, 1983 and Bradshaw, 2002). The variation in loss factor with temperature is significant for some materials. At low temperatures some materials will respond modestly to microwave heating and so must first be heated by conventional means before treatment by electromagnetic radiation (Hamlyn, 1991). If ε_r' is a measure of a materials ability to be polarised by external electric fields, the loss factor ε_r'' quantifies the efficiency with which the electromagnetic energy is converted to heat. This can be represented in visual form by considering the total current as the vector sum of the charging current and the loss current. The angle δ is the phase lag between the electric field and the resultant orientation polarisation of the material. Water has a very high loss factor and so is particularly receptive to dielectric heating. This is of importance when considering drying applications with microwave heating.

Figure 2.10 Vector diagram of the charging current and loss current.

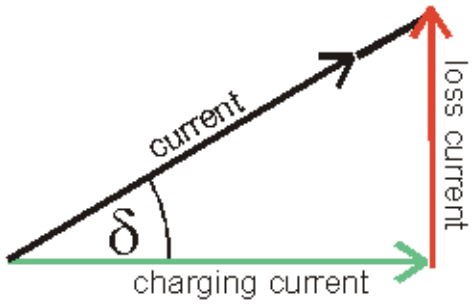

2.3.4 Dielectric Constant and Loss Angle

The relationship between the real and imaginary parts of the complex permittivity is expressed as a loss tangent.

$$\varepsilon'' = \varepsilon' \tan \delta \qquad (1.7)$$

This is given as a phase angle which is defined by the angular difference (lag) in phase between the sinusoidal alternating potential and the resultant polarisation of the dipoles within the dielectric where δ is measured in radians.

Figure 2.11 Resultant dipole polarisation lag behind applied electric field (Chaplin, 2007).

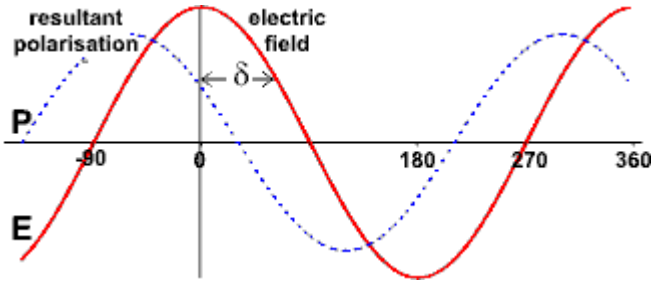

2.3.5 Power absorption and Penetration Depth

One can define the depth to which the power penetrates into the dielectric which is of great importance for the application of industrial microwave processes. The so-called penetration depth is defined as the distance from the surface of the material at which the incident power reduces to the number e^{-1} (0.368) from its value at the surface. The amplitude of the incident wave will diminish as it propagates through the material due to power absorption. Thus, the field intensity and power flux density will fall exponentially with distance from the surface since the electric field strength in attenuated by the dielectric.

The relationship between the penetration depth D_P and the wavelength of the incident radiation λ_0 is given by the expression (Metaxas and Meredith, 1983)

$$D_P = \frac{\lambda_0}{2\pi\sqrt{2\varepsilon'}} \frac{1}{\sqrt{\left[\left\{1+\left(\frac{\varepsilon''}{\varepsilon'}\right)^2\right\}^{0.5}-1\right]}} \tag{2.8}$$

The incident power interacts with the dielectric as illustrated in Figure 2.2. At the frequencies allocated for industrial use in the microwave regime, the penetration depth of some materials may be very small and the size of the treated load could be many times greater than the penetration depth. This will result in temperature non-uniformities and thus the allowable size of the component to be treated depends critically on the knowledge of the dielectric properties, emphasising the need to establish the later before microwave cavity equipment can be designed and built. The penetration depth may alter significantly due to temperature variations within the material which manifests itself in changes of the loss tangent $(\tan\delta)$ with temperature.

Figure 2.12 Power absorption profile in a dielectric medium (Metaxas and Binner, 1995).

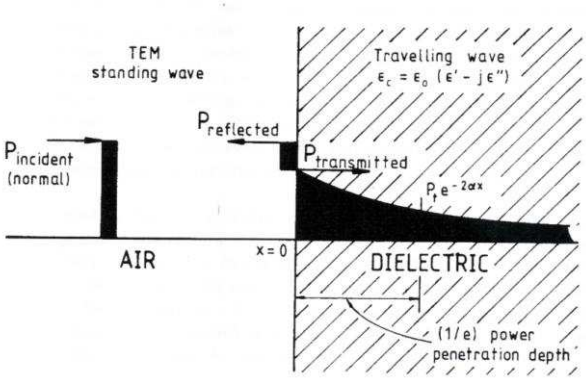

The rate at which heat is absorbed in the dielectric material can be expressed as a power density. The relationship between power density (W/m^3), RMS electric field strength (V/m) and loss factor is given by the following expression (Meredith, 1998).

$$P = 2\pi f . E^2 \varepsilon_0 \varepsilon'' \qquad (2.9)$$

Where f is the field frequency (Hz).

Assuming a uniform electric field and neglecting losses, the change in temperature will be given by

$$\frac{dT}{dt} = \frac{P}{\rho C_P} = \frac{\omega E^2 \varepsilon_0 \varepsilon''}{\rho C_P} \qquad (2.10)$$

Where ρ and C_P are the material density (kg/m^3) and specific heat capacity (J/g K) respectively (Stuchley, 1983).

It is important to note that power absorbed, or heat generation, is proportional to the square of the field strength within the material. If the change in temperature is proportional to the loss factor ε'' of the dielectric and the loss factor increases exponentially with temperature then a cumulative effect will ensue resulting in a state of thermal runaway, where the rate at which the sample is heated exceeds the rate at which heat can dissipate to other parts of the sample, which in some cases can be destructive and undesirable (sintering of ceramic materials). Thermal runaway may be controlled by reducing the power density if the dielectric is a poor thermal conductor, allowing thermal conduction to equalise the temperature gradient within the material. However, low power levels may reduce the benefits of dielectric heating. One can see from Equation 1.9 that the energy absorption increases with frequency for a constant voltage gradient and loss factor.

Thus, for materials which have very high loss factors, the attenuation of the applied energy near to the surface of the material becomes significant at high frequencies. To avoid this effect and the resulting differential heating which may occur, lower frequency applications may provide a more uniform heating regime.

2.4 Microwave Generating Devices

There are various types of electronic components able to supply microwave power (magnetrons, klystrons and solid state power sources etc.). However, the magnetron tube remains the most popular compromise in modern industrial microwave applications. The choice of technology available for such devices depends upon the output power level required, its frequency stability, efficiency and cost. Currently, solid state power sources do not provide the required power-output requirements and are comparatively more expensive than the magnetron or klystron technologies (Meredith, 1998). As such, solid state devices and klystron amplifiers will not be discussed here since they are rarely used for industrial applications.

2.4.1 The Magnetron Tube

The magnetron was developed as a source of high power microwaves during the Second World War and was crucial to the success of precision RADAR detection systems. Since then, the magnetron tube has continued to be developed to cover a large frequency range (0.5-100GHz) providing a wide range of power output for both RADAR and domestic and industrial microwave heating. The domestic microwave appliance has seen huge quantities by mass production which has meant that they are now readily available at very low cost.

The principle of operation of the magnetron vacuum tube requires a hollow copper anode in the form of a number of evacuated radial resonant cavities, tuned to the desired operating frequency at the centre of which is an electron omitting cathode. The anode vanes project radially inwards and forms slots between them which are approximately $\lambda/4$ deep and therefore resonate at the operating microwave frequency. A high-strength magnetic field is aligned axially to the anode/cathode assembly which can be provided by a permanent magnet, or an electromagnet depending on the power output of the magnetron. The theory of its operation is based around the interaction and motion of electrons under the influence of both the electric and magneric fields. The trajectory of the electron flow from the cathode to the anode is governed by the force exerted by the electric field on the electron (which is proportional to the electric field strength) and the force exerted by the magnetic field on the electron, which acts in a direction perpendicular to the electron path. Thus, the electron path to the anode is quasi-circular rather than direct. An antenna or probe is connected to the anode, which extends into one of the tuned radial cavities to extract energy. This is then coupled to a low loss waveguide, a hollow metallic enclosure which transmits the energy to the product. Heat is dissipated to the anode, as the kinetic energy of electrons reaching it is converted into heat. This heat loss is the principal energy loss in the operation of the magnetron. A cross section schematic of a typical tube magnetron is shown in Figure 2.3. The magnetron tube is considered to be the most efficient of the microwave tubes with efficiencies up to 90%. The robust construction of modern magnetron tubes provide easy rebuilding after end-of-life failure or damage (Meredith, 1998).

Figure 2.13 Schematic Diagram of a Typical Tube Magnetron.

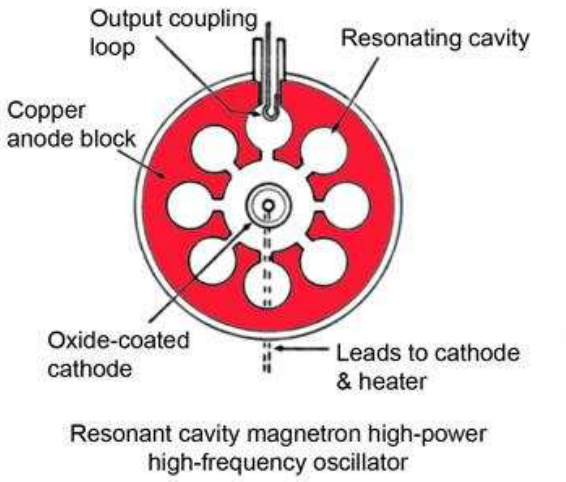

2.5 Microwave Energy – Transmission to the Product

Once the power has been produced by the magnetron in the form of an electromagnetic wave of the desired frequency, it has to be directed to the product to be processed or towards an applicator in which heating will take place. This needs to be done as efficiently as possible (minimal losses due to attenuation) using a carefully designed waveguide.

2.5.1 Waveguide Design

At microwave frequencies used for industrial processes, the energy transfer from the magnetron is transmitted toward to the product via specially designed channels called waveguides, the dimensions of which depend of the operating frequency of the system. The waveguide is simply a rectangular metal duct along which energy can travel with little loss. The construction material and dimensions of the waveguide are special in this respect. It can be shown that the shortest free-space wave that can be transmitted has a wavelength of twice that width of the waveguide.

The wavelength in the waveguide differs from that in free space as given by the expression:

$$1/\lambda_g^2 = 1/\lambda_0^2 - 1/\lambda_c^2 \quad (2.11)$$

Where,

λ_g is the wavelength in the guide.

λ_0 is the wavelength in free space.

λ_c is the critical wavelength.

The critical wavelength is given by

$$\lambda_c = 2b \quad (2.12)$$

Where,

b is the waveguide width.

With the critical dimensions of the waveguide in place which allow microwaves to be transmitted to the product, a suitable construction material will need to be selected which allows for efficient energy transfer and so one which gives minimal attenuation is necessary. The magnetic field portion of the wave will induce currents in the walls of the waveguide, and so in order to reduce the losses, a material of low resistivity, such as aluminium must be used (Hamlyn, 1991). The waveguide may be designed with bends and joints which should be constructed carefully to allow energy to flow freely past them. Waveguides are either classed TE (transverse electric, or H) mode or TM (transverse magnetic or E) mode. In transverse electric TE mode the electric field vector is perpendicular to the direction of wave propagation. Conversely, when in TM mode,

the magnetic field vector is perpendicular to the direction of wave propagation (Meredith, 1998).

Once efficient energy transmission is achieved, it must then be conveyed to an applicator where heating of the product is to take place.

2.5.2 Applicator Technology

The applicator forms part of the microwave system where electromagnetic energy is transferred to the product and where heating takes place. The overall design of the applicator will depend on the nature of the product to be processed in terms of size, shape and the volume throughput required. The applicator can be designed for batch or continuous processing which may incorporate a hybrid design where conventional radiant heating and microwave heating can take place (Hamlyn, 1991, Hart, 2004).

There are two basic designs for microwave applicators. These are the resonant waveguide or monomode applicator and the multimode or cavity applicator. In general, a mode is refers to a specific way in which the electromagnetic field establishes itself within the applicator or waveguide. To ensure that radiation leakage does not occur, most applicators take the form of a simple metallic box which is designed to reflect the electromagnetic energy within the applicator. For continuous process applications where the target load is resident in the waveguide for some finite period of time, then leakage is prevented by employing a choke device which may be manufactured from a material which will absorb ‘mop-up’ any residual power.

2.5.3 Waveguide Applicators

A typical progressive waveguide applicator is shown in Figure 2.14. The product is passed through the broad face of a folded rectangular duct. In this situation there will be a progressive attenuation caused by losses to the product with the remaining residual power dissipated to a water load at the end of the waveguide. The reflected power dissipated in the water load can be calculated using calorimetry. It is possible, with knowledge of the geometry of the waveguide to solve the Maxwell equations analytically or numerically utilising appropriate boundary conditions. Thus, the design of a cavity to support one resonant mode is based on the solution of these equations. Therefore, in general, monomode cavities have a well defined electromagnetic field in space where the position of maximum electric field strength can exploited with the target load positioned accordingly. As such, these cavities are capable of extremely high heating rates in excess of 100°C/s (Jones, 2007). They are also favoured for applications where the target load exhibits very low dielectric loss. Synchronising the coincidence of the position of maximum field strength and target load can be problematic, since the dielectric properties of the target material may change as its temperature rises resulting in a drift of the resonant frequency within the cavity, making steady matching difficult. To overcome these difficulties, most applicators are designed such that the incident and reflected waves can be automatically tuned to achieve superposition and as such the power density can be maximised. Knowledge of the forward and reflected power is important when impedance matching. (Metaxas and Meredith, 1983). Changing conditions inside the cavity due to spatial, temperature, chemical or phase changes of the product will alter the impedance.

To facilitate impedance matching of the generator and applicator, a magic-T junction, which consists of adjustable short-circuit pistons can be used to maximise the forward power into the cavity (Hart, 2004).

Figure 2.14 An example of a progressive waveguide applicator (U.I.E 1998).

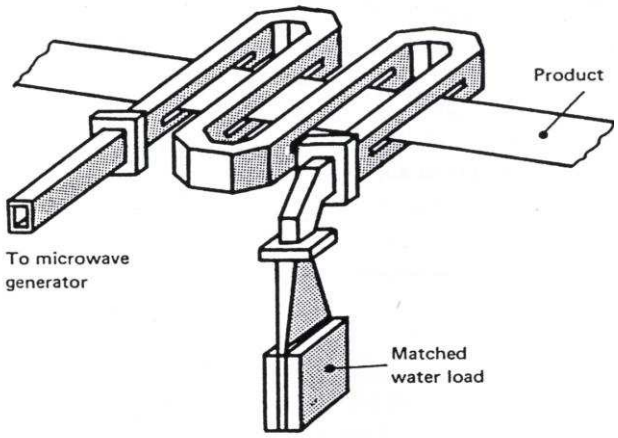

The waveguide applicator is also used with cylindrical, instead of rectangular, waveguides, which are more desirable for heating cylindrical shaped products. In this configuration the waveguide is perturbed along its longitudinal axis into a region of high electric field to achieve maximum power density.

An example of such a monomode cavity is illustrated in Figure 2.15.

Figure 2.15 An example of a cylindrical monomode cavity applicator (U.I.E 1998).

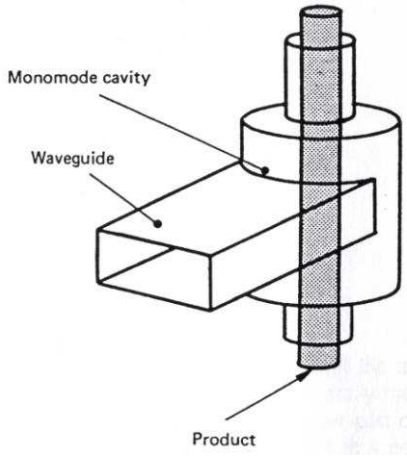

The monomode waveguide applicators share the following characteristics:

- They allow for a homogeneous electric field distribution in the product and are able to be tuned to give very high electric field values. They are useful for difficult applications, particularly when the target load is a very low loss dielectric.
- The cross sectional dimensions of the waveguide are of the same order of magnitude as the microwave wavelength being used. As such, their use is rather restricted to small/thin products which fill only part of the waveguide.

2.5.4 Multimode Cavity Applicators

The domestic microwave oven is a small multimode cavity applicator which consists of a closed metal box, with some means of coupling to a power generator, such as a magnetron. The dimensions of the cavity should be at least a couple of wavelengths long in two dimensions to maximise the number of resonant modes. A carefully designed cavity will support a number of resonant modes at a given frequency and the cavity should be designed to have as many resonant modes as possible at or near the operating frequency of the microwave generator (Hamlyn, 1991). This reduces the incidence of standing waves within the cavity that could lead to non-uniform heating. The production of a number of mode reflections within the cavity will randomise the field patterns and ensure that the electric field strength does not vary significantly throughout the cavity (Hart, 2004). The load may also be moved around, via a turntable, or the field pattern randomised using a mode stirrer, which continually perturbs the electric field by its

rotation, to ensure that the heating process is as uniform as possible, which is of vital importance in many industrial applications (Metaxas and Binner, 1995; Plaza-Gonzalez, et al., 2005). Multimode heating is sometimes not suitable for some applications where high temperatures and heating rates are required, since the energy will be dissipated over a large volume in contrast to monomode heating where the energy can be rather more targeted (Metaxas and Meredith, 1983). They have a particular disadvantage when trying to heat very low loss materials. Most industrial multimode microwave cavities are generally larger than those in domestic ovens. Their internal volume may be a few cubic metres with the product being carried through the cavity on a conveyor with multiple microwave generators and cavities along its length. A simple schematic of such a cavity is shown in Figure 2.6. The openings of the microwave cavity will be of specific design to ensure that energy leakage is minimised. These may include metal contact seals or chokes.

Figure 2.16 A multimode cavity for continuous processing (U.I.E 1998).

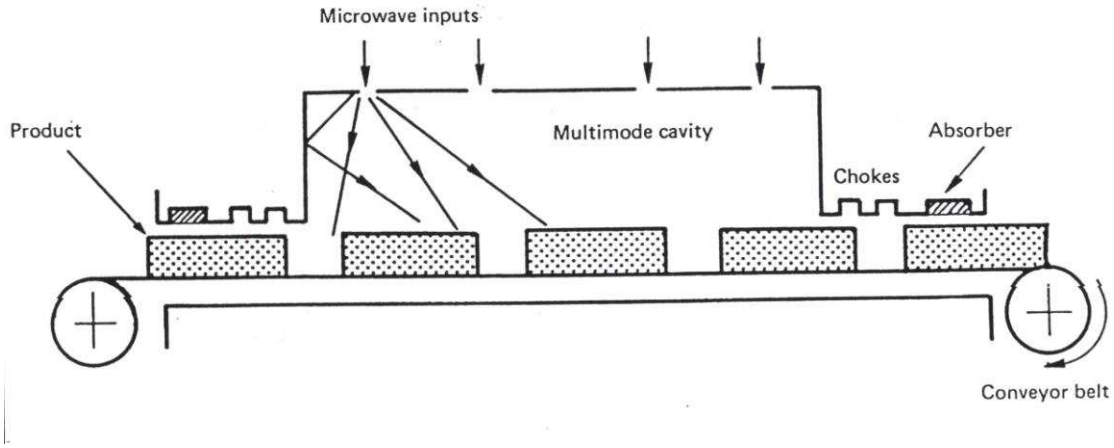

2.6 Dielectric Property Measurement

Dielectric property measurement is required to facilitate the control of a heating process and to increase the knowledge of any potential processing problem such as thermal runaway. By evaluating the dielectric properties of a material over a range of processing temperatures and at the desired heating frequency, one can evaluate its behaviour in the presence of a microwave field. This information may also be used to inform the selection of the construction materials of a microwave heating system (Hart, 2004). ASTM D 2520-81 gives an account of the different American Standard Test Methods available for complex permittivity (dielectric constant) measurement of solid insulating materials at microwave frequencies over a range of temperatures up to 1650°C. The different methods are subdivided into categories where the advantages and disadvantages are outlined, depending on the conditions with which the measurement is to take place (Guillon, 1994). A brief overview of the various technologies available for measuring dielectric properties is presented here. The various parameters measured will depend on the technique employed but ultimately they will all lead to the calculation of the crucial material property of complex permittivity or related parameters. However, not all techniques are suitable for measurement at temperatures other than ambient.

2.6.1 Shorted transmission line method (Roberts – von Hippel method)

This technique was first developed by Roberts and von Hippel (1946). The principle of this method adopts a closed end waveguide, whereby the standing waves produced are analysed with the cavity empty and then with the cavity perturbed with a precisely

machined dielectric specimen positioned at the end of the transmission line. A probe is inserted into a slot in the waveguide to measure the standing wave patterns. When a dielectric object is inserted into the cavity, the resonant frequency will shift towards lower frequencies. (Kraszewski and Nelson, 1995). By this method, values of dielectric permittivity ε' and loss factor ε'' are calculated from measurements of the length of the dielectric, the ratio of the electric field strength in the node and antinode, the distance between the surface of the dielectric and the position of the first node and the characteristic wavelength of the waveguide. There are however, some disadvantages with this technique. Firstly, more than one measurement needs to be taken with dielectric specimens of different lengths and secondly, errors may be introduced by an imperfect machined specimen causing a short circuit and line losses and imperfections in the dielectric specimen. Also, if the test is made over a range of temperatures, the shrinking or expansion of the dielectric sample will cause errors. This method has the advantage of being able to measure dielectric properties over a wide range of frequencies and a wide range of permittivities and loss factors. This technique is well suited for measurements at ambient temperatures on solid samples, however, other techniques have been developed for the measurement of the complex dielectric constant in lossy liquids (Metaxas and Meredith, 1983). This technique has been used by many researchers for both ambient and higher temperature measurements (Nelson, 1983 and 1988, Church et al., 1988, Salsman, 1991, Horderfield et al., 1992, Arai et al., 1992 and Fletcher, 1995).

2.6.2 Resonant Cavity Techniques

This method used for dielectric measurement is based upon standard theoretical dielectric principles and measurements of the change in quality factor, the so-called Q- factor and resonant frequency when the sample is inserted. The measurement of the specific resonant frequencies can be detected using a vector network analyser, in which measurements of the frequencies and their corresponding bandwidths are recorded. The frequencies at which measurements are taken are restricted to the descrete resonant modes of the cavity. Calculation of the dielectric properties of materials relies on the fact that the Q factor of the cavity will vary, as will its resonant frequency, depending on whether it is unfilled or filled with the dielectric sample. This type of cavity perurbation technique will measure the ε' and $\tan\delta$ for the sample material. The two usual definition of the Q factor are:

$$Q = 2\pi \frac{\text{stored\_energy\_in\_cavity}}{\text{energy\_loss\_per\_cycle}} \tag{2.13}$$

and,

$$Q = \omega_r \frac{\text{stored\_energy\_in\_cavity}}{\text{average\_power\_loss}} \tag{2.14}$$

Where ω_r is the resonant frequency of the cavity.

The stored energy in the cavity is equal to the sum of the instantaneous electric and magnetic stored energies. During resonance, energy is dissipated in the walls of the cavity. This loss gives rise to the Q factor of the cavity.

Using this method, the sample volume has to be small with respect to the volume of the resonant cavity and the dielectric properties of the sample are low enough so as not to disturb the internal field significantly. This means that the electromagnetic fields in the cavity with and without the sample inserted should be approximately equal (Klein et al., 1993).

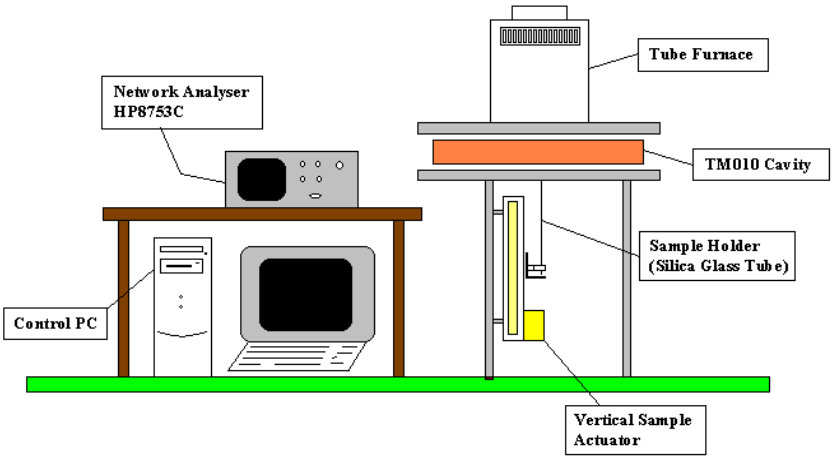

Figure 2.17 Schematic Layout of Cavity dielectric measuring Equipment

This type of cavity perturbation technique is suitable for measuring the complex permittivity at frequencies between 50 MHz and 3GHz (depending on cavity dimensions), and up to temperatures of 1400°C. The system can measure the dielectric constant of materials during conventional heating, curing or sintering. The hot sample and its holder are rapidly removed from a conventional tube furnace and inserted into the high electric field region of a conducting thick-walled cylindrical cavity. The resonant frequency and loaded Q factor of the cavity are recorded by a Hewlett-Packard 8753 vector network analyser and stored for off-line analysis.

The test sample and holder are either left in the cavity for further measurements at lower temperatures as the sample cools, or are quickly returned to the furnace for further processing. A schematic layout of the cavity and tube furnace is shown in figure 2.8 below.

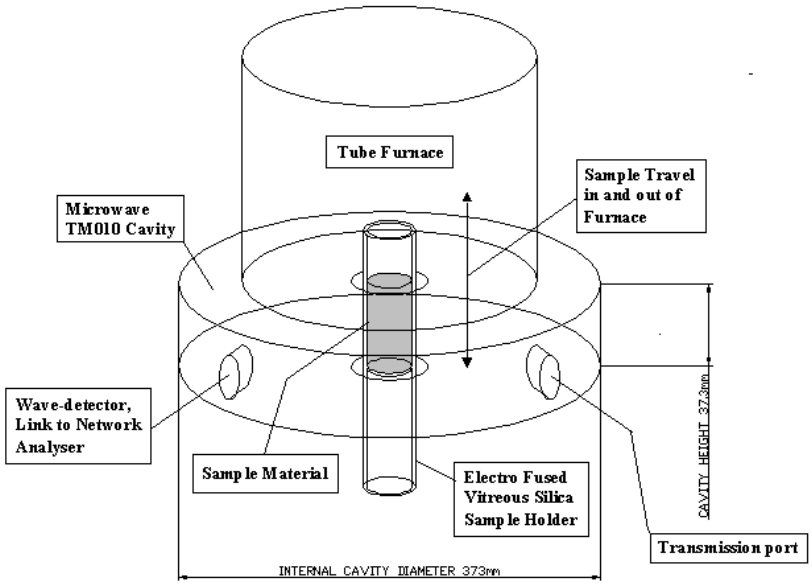

Figure 2.18 Resonant cylindrical cavity schematic.

The small cylindrical sample is inserted into the longitudinal axis of the TM_{0n0} cavity into a position of uniform electric field. In cavities of this type the electric field is parallel to the longitudinal axis of the perturbed sample and will diminish in the radial direction. (Metaxas and Meredith, 1983 and Klein et al., 1993). As a result of the electromagnetic field orientation in the cavity, the magnetic field in a TM_{0n0} is zero along its longitudinal axis and so the mode distribution in the vicinity of the sample is purely electric.

The characterisation of the electromagnetic field inside the cylindrical cavity can be obtained from the solution of Maxwell's equations. Mathematical expressions relating to its resonant wavelength and cavity dimensions can be found elsewhere (Metaxas and Meredith, 1983).

The dielectric property of a perturbed sample can be calculated from the measured frequency shift and change in the cavity Q factor before and after insertion using the following relationships developed from perturbation theory.

For the real Permittivity or dielectric constant:

$$\varepsilon' = 1 + 2J_1^2(X_{l.m})\frac{V_C}{V_S}\frac{f_0 - f_s}{f_0} \tag{2.15}$$

and for the imaginary permittivity or loss factor:

$$\varepsilon'' = J_1^2(X_{l.m})\frac{V_C}{V_S}\left(\frac{1}{Q_S} - \frac{1}{Q_0}\right) \tag{2.16}$$

Where,

V_C is the volume of the cylindrical cavity (m^3).

V_S is the volume of the perturbed sample (m^3).

f_s is the resonant frequency of the cavity and sample (Hz).

f_0 is the resonant frequency of the unperturbed cavity (Hz).

Q_S is the quality factor of the cavity and sample.

Q_0 is the quality factor of the unperturbed cavity.

J_1 is the first order Bessel function.

$X_{l.m}$ is the m^{th} root of J_o.

The relationship between sample density and dielectric properties can be used to estimate the dielectric properties of a solid medium from measurements on pulverised powdered samples, particularly when solid samples cannot be obtained or when measurements on solid materials is not convenient. This is sometimes the case when using the cavity perturbation technique, since the samples are small and can be pulverent. The density of powdered samples must be considered and accounted for when analysing the dielectric properties of particulate materials since it is intuitively obvious that the less material there is present, the nearer the sample becomes to free space (Nelson and Beck-Montgomery, 1981; Nelson, 1983). The best compaction process can only yield samples that are about 55% dense and so it s common to use regressing models to predict dielectric properties from a number of standard tests (Evans, 1995). The analysis of the mathematical relationships required for particulate mixtures and the development of a suitable experimental technique will be discussed and presented in detail later in this work.

2.6.3 Coaxial probe

The high temperature coaxial probe is a variation on the principle described on the shorted transmission line. In this case, an open ended coaxial probe is terminated with a sample of dielectric material. The reflection coefficient of the probe terminated with the dielectric sample is measured. This can be related to the complex permittivity of the sample by using an algorithm associated with the probe. Measurement using this method may be made at elevated temperature by heating the sample via a ceramic work tube (Arai et al., 1996). This is a broadband technique with the advantage that sample

preparation time is short, although the sample must have a smooth flat surface in contact with the probe.

2.7 Conclusion

The fundamental theoretical aspects of microwave heating and the associated material interactions in an electromagnetic field have been discussed, along with a range of suitable methods for measuring the crucial dielectric properties of the material to be heated. The technology available to generate and transmit microwaves to the product has also been outlined. It can be seen, therefore, that by using relatively simple techniques, one can efficiently deliver high power microwave energy to a range of products for both "one off" batch heating or continuous progressive heating. These facts facilitate the current laboratory research into the controlled microwave pre-treatment of coal to aid desulphurisation.

Chapter 3 - Literature Review

3.1 The Origin of Coal

Coal is a physically heterogeneous solid which is chemically complex and organoclastic in nature. It consists of organic material containing carbon, hydrogen, nitrogen, sulphur and other primary and secondary mineral inclusions. The composition and character of each coal will be defined firstly by the makeup of the original organic and inorganic accumulation, and secondly by the degree of diagenesis it has undergone. The natural agencies which cause the changes in the chemical and physical properties of coals include the action of bacteria and fungi (oxidation, reduction, hydrolysis and condensation; the effects of heat and pressure in the presence of water).

Sedimentary sequences containing coal and peat are found world wide and range in age from Upper Palaeozoic to Recent. The accumulation of the plant debris is effected by syn-sedimentary and post-sedimentary influences which produce coals of various ranks and structural complexity (which are closely interlinked). There are remarkable similarities which exist in coal-bearing sequences due to particular sedimentary associations which are required to generate and preserve coals. Even sequences from areas geographically separate and of different ages exhibit a similar lithological framework and will be similar structurally (van-Krevelin, 1993).

There is no model that can act as a panacea for all coal deposits but there are a number of coal deposits that have been identified with particular depositional regimes. Coal can be divided into humic (low hydrogen content) and sapropelic (high hydrogen content) types.

Sapropelic coals are laid down as sub-aquatic mud under more or less anaerobic conditions. They are composed of fine detritus water plants, plankton and spores washed and blown into ponds. They may also be composed of some shore plants and reworked peat. Sapropelic coals are therefore typically fine-grained and homogeneous and include coal types known as Cannel and Boghead coals. Cannel coals are composed mainly of miospores and organic mud debris laid down under water, whereas boghead coals originate from algal material. Intermediate forms are also recognised such as boghead-cannel or cannel-boghead transitions (Thomas, 1992).

Humic coals are composed of a diverse mixture of macroscopic plant debris and typically have a banded appearance. Humic coals are predominantly deposited as peats, although occasionally as humic muds under partially aerobic conditions.

Coal goes through several stages during its formation. With increased pressure and time caused by overlying sediments, tectonic movements and the forces of erosion, impurities and moisture are removed and peat begins to transform into low-grade coal (lignite or brown coal). Continued pressure from the accumulation of overlying sediments and increases in temperature, further metamorphose the lignite into bituminous coal and then further into a hard, high lustre coal known as anthracite (Van-Krevelin, 1993; Thomas, 1992; Stach et al., 1982)

3.2 Coal Classification

The composition and character of each coal may vary depending on the diversity of its origin. Depending on the properties and thus its potential application, several systems

have been developed to classify coals into different groups. From the different classification systems available, the ASTM (American Society for the Testing of Materials) is most commonly used. Table 3.1 shows this classification system (ASTM D338, 1991).

The degree of transformation or coalification of peat through lignite, sub-bituminous, bituminous to anthracite, is termed the coal rank. The identification of the rank of a coal deposit can be used to determine its future potential and so is of great importance to a coal geologist. The coalification process is essentially an initial biochemical transformation followed by a geochemical or metamorphic phase. Typically, the older the coal, the higher the rank and so anthracite and lignite may be termed high and low rank respectively. Another useful property of the coal which can be used to define rank is considered to be: Carbon content, volatile matter content, moisture capacity and calorific value. The knowledge of these properties is known as proximate analysis. The proximate analysis is the most fundamental of all coal analyses and is of great importance in understanding the practical use of a coal.

During the geochemical or metamorphic stage, the progressive changes that occur within coals are an increase in the carbon content and a decrease in the hydrogen and oxygen contents resulting in a decrease in the volatile content of the coal. Determination of the chemical properties of the coal, known as ultimate analysis is also important and so the calculation of the amounts of these elements may have a direct bearing on the usability of the coal.

Table 3.1 the ASTM coal classification system.

Class/Group	Fixed Carbon Limits (% dmmf[a])	Volatile Matter Limits (% dmmf)	Gross Calorific Value[b] (BTU/Lb)	Agglomerating Character
Anthracite				
1. Meta-Anthracite	>98	<2	…	Non-
2. Anthracite	92-98	2-8	…	agglomerating
3. Semianthracite	86-92	8-14	…	
Bituminous				
1. Low Volatile	78-80	14-22	…	Commonly
2. Medium Volatile	69-78	22-32	>14000	agglomerating
3. High Volatile A	<69	<31	1300-14000	
4. High Volatile B	…		11500-15000	
5. High Volatile C	…		10500-11500	agglomerating
Sub-bituminous				
1. Sub-bituminous A	…	…	10500-11500	Non-
2. Sub-bituminous B	…	…	9500-10500	agglomerating
3. Sub-bituminous C	…	…	8300-9500	
Lignite				
1. Lignite A	…	…	6300-8300	Non-
2. Lignite B	…	…	<6300	agglomerating

[a]dmmf = Dry, Mineral Matter Free Basis, [b]Moist, Mineral Matter Free Basis.
'Moist' Refers to coal containing it natural moisture but not being visible water on the surface.
***The agglomerating property of coal can be evaluated using Caking Tests and is useful for evaluating the potential of coals for coking and combustion.**

Figure 3.1 the dependency of coal property on rank.

	Low Rank →			High Rank
Rank	Lignite →	Sub-bituminous →	Bituminous →	Anthracite
Age	→	Increases	→	
Carbon Content %	→	Increases	→	
Volatile Matter %	→	Decreases	→	
Moisture Content %	Decreases →		→	Increases
Calorific Value	→	Increases	→	

Figure 3.1 above, shows the four main coal groups and the changes in the proximate analysis of the coal with increasing rank.

Figure 3.2 Seyler`s coal chart (Thomas, 1992)

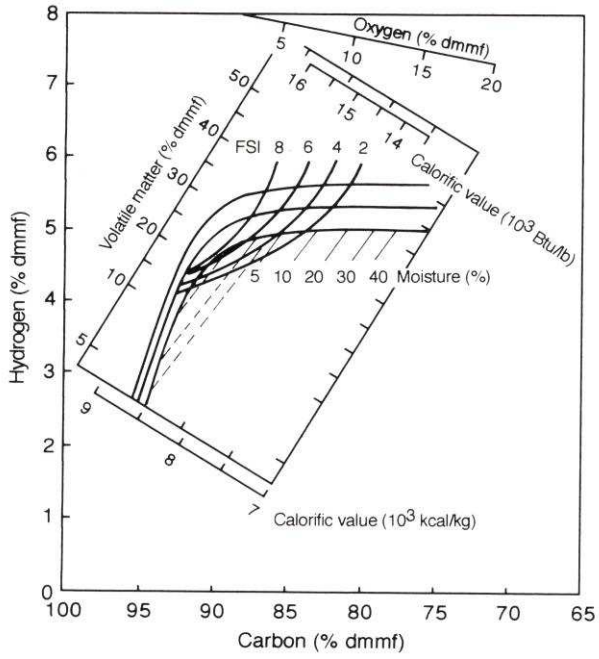

The Seyler`s coal chart shown above in Figure 3.3 shows the relationship between elemental composition, volatile matter contents and moisture contents. This chart is useful for the classification of coals which use carbon/oxygen or carbon/hydrogen

correlations. It should be noted, however, that Seyler`s classification chart is only applicable to British Carboniferous coals and takes little account of lower rank coals. There are two kinds of coal classification systems for either `scientific` or `commercial` applications. These are used to serve different kinds of utilisation purposes. Scientific systems will generally concentrate on coal origin, constitution and other fundamental properties discussed previously (proximate and ultimate analyses etc.). On the other hand commercial systems deal with aspects of coal, such as market value, utilisation, technological properties and its suitability for a particular use (Thomas, 1992; Liu, 1986, British Geological Survey - Mineral Profile - Coal, 2007). The technological properties of coal such as the ash fusibility, free swelling index and plasticity, among others, have also been introduced as second classification parameters to characterise coals in different fields of utilisation.

3.3 Coal Petrography

Coal is composed of a number of organic and inorganic entities which may not be visible to the naked eye. While the heterogeneous structure of a coal may be obvious to the naked eye, it is only on a microscopic level that one can see in detail the constitution of coal. In the same way that inorganic rocks are composed of minerals, coals are mainly composed of macerals and mineral matter interspersed throughout the structure. Therefore, the petrographic description of coal is based on a geological approach to identify organic rocks. Using standard petrographic techniques, a coal can be defined in terms of lithotype and maceral composition. Whereas a mineral is characterised by a

fairly well-defined chemical composition due to its uniformity and the fact that most minerals are crystalline, a coal maceral may vary widely in its chemical composition and physical properties and is not crystalline. The uses of petrographic studies on coal in assessing its geochemical parameters and combustion characteristics have been studied at length. Coals which differ in petrographic composition show quite different combustion and electrical/dielectric characteristics, even for coals of the same rank .

3.3.1 Coal Macerals

The organic units or macerals that make up a coal mass can be identified across the entire rank range under a microscope. The term maceral is used to describe both the shape and nature of the microscopically recognisable constituents of a coal (Stach et al., 1982) and was first used in this context by Stopes (1935). The word maceral originates from the latin verb `macerare` and means to soften or weaken, with or without heat, or to wear away. In order to distinguish between macerals, it is necessary to choose a set of parameters which can be determined while under microscopic examination (Stach et al., 1982). These are defined as reflectance and fluorescence, colour, morphology and polishing hardness (relief). However, as metamorphosis advances and rank increases these apparent differences can become less evident as the reflectance values of all macerals virtually coincide (Van-Krevelen, 1993). In an attempt to eliminate any ambiguity that may arise in the definitions of different macerals, an established set of rules have been developed for petrographic microscopy, which provide a description that macerals will correspond to their appearance under reflected light using oil immersion objectives. (AS 2856.2-1998). All macerals have the suffix `inite`, and are classified into

three groups; Vitrinite, Liptinite and Inertinite. The three maceral groups are to a certain degree characterised by their chemical composition. Upon the comparison of isometamorphic maceral groups, the vitrinite maceral contains relatively more oxygen, the liptinite contains relatively more hydrogen and inertinite more carbon. The volatile matter yield is also highest in the liptinite maceral. The Stopes-Heerlen classification of maceral groups is shown in Table 3.2 (Thomas, 1992). The correlation between microscopically observed shapes and structures of macerals and certain plant organisms and tissues is well established. Macerals from the same group differ from one another in terms of morphology and structure rather than in reflectance. This is to say that the difference in elemental composition amongst macerals of the same group is slight.

Table 3.2 Stopes-Heerlen classification of maceral groups, macerals and submacerals of hard coals (Thomas, 1992)

Maceral Group	Maceral	Submaceral
Vitrinite	Vitrodetrinite	Telocollinite
	Telinite	Gelocollinite
	Collinite	Desmocollinite
		Corpocollinite
Liptinite	Sporinite	…
	Cutinite	…
	Suberinite	…
	Resinite	…
	Alginite	…
	Liptodetrinite	…
	Fluorinite	…
	Exudatinite	…
	Bituminite	..
Inertinite	Fusinite	
	Semifusinite	
	Macrinite	…
	Micrinite	…
	Sclerotinite	…
	Inertodetrinite	…

3.3.1.1 Vitrinite

Vitrinite macerals are derived from cell wall material (woody tissue) of plants, which are chemically composed of polymers, cellulose and lignin. It mainly originated from trunks, branches, stems, leaves and roots. Vitrinite is the most frequent and probably the most important maceral occurring in bituminious coals. The vitrinite maceral typically makes up 50% - 90% of most North American coals. However, the Gondwanaland coals of the southern hemisphere are vitrinite poor and the inertinite macerals tend to dominate in these coals. There are three different macerals that can be distinguished in vitrinite, namely telinite, collinite and vitrodetrinite. These can be seen in Table 2.3 with their corresponding submacerals. In low rank coals, i.e lignite and sub-bituminous coals, the vitrinite maceral group is sometimes referred to as huminite and is regarded as a precursor of the vitrinite macerals found in higher rank coals. In reflected light, the reflectance of the vitrinite maceral, which is intermediate in comparison with the other two maceral groups, increases with increasing rank and therefore the optical properties of vitrinite have enabled it to be used as a rank indicator. In transmitted light, organic materials become opaque and the plant structure becomes difficult to recognise (Stach et al., 1975).

Cellular structures derived from vegetable material are sometimes visible under the microscope. This is particularly evident in low rank coals, where these cell walls are called telinite. (from ‘tela’ → tissue). The cell cavities may be filled with other macerals or indeed minerals or clays, and so pure telinite is rare (Stach et al., 1975). The term collinite is derived from the greek word `kolla` which means glue and is a structureless constituent of vitrinite. Collinite was formed when the cell walls were thickened with

gelatinous humus and hence it is responsible for the colloidal medium which dominates in all bright coals. If broken gelified grains are mixed together from the vitrinite maceral group then the maceral is termed vitrodetrinite. In reflected light under oil immersion, vitrodetrinite particles may only be identified when they are surrounded by a material of different reflectance. As a concequence, vitrodetrinite may be difficult to recognise. Since the identification of individual vitrinite macerals can be difficult, the undifferentiated vitrinite content of coal will normally suffice.

3.3.1.2 Liptinite

The liptinite group comprises the macerals sporinite, cutinite, suberinite, resinite, alginite and liptodetrinite. These macerals consist of sporine, cutine, suberine, resins, waxes, fats and oils of vegetable origin which are resistant to weathering and digenesis (Stach et al., 1975). This maceral group is usually minor in coal and was formally termed exinite which was used to describe the exines in spores in coal. In low rank coals they can be distinguished from vitrinite by a higher hydrogen content and contain more aliphatic groups when compared to vitrinite (Barranco, 2001). The liptinite maceral is also the most volatile. Table 3.3 gives a survey of the macerals in the liptinite group. They generally make up about 5% - 10% of North American coals, and are usually more abundant in the Appalachian coals than any other U.S. coals except for boghead and cannel coals where they dominate (sporinite in boghead and alginate in cannel). One of the petrographic features of the liptinite macerals is that they have a reflectance lower than the vitrinite macerals in the same coal and tend to retain their original plant form, which is the basis on which they are classified. Further to this, when the coal sample is

viewed under blue light, three further macerals may be identified namely fluorinite, bituminite, and exsudatinite.

3.3.1.3 Inertinite

The inertinite macerals are derived from plant material, similar to those of vitrinite, which has been strongly altered in the early stages of coal formation in the presence of oxygen. The inertinite macerals have the highest reflectance of all the macerals and are distinguished by their relative reflectance and structures. Table 3.3 gives a survey of the macerals in the inertinite group. The most common macerals in the inertinite group are fusinite and semifusinite. Fusinite can be identified in most coals and has a char-coal like structure. Fusinite is the highest reflecting maceral in the inertinite group and depending on the extent of oxidation, a well preserved cell-like texture can be observed under the microscope. Fusinite has the highest carbon and oxygen content of all the coal macerals and is the least volatile with the lowest H/C ratio, however, the physical and chemical properties of fusinite in general show only small changes with increasing rank (Stach et al., 1975).

Fusinite occurs in varying quantities in peat, brown coal and bituminous coal, and in general its proportion does not exceed a few percent.

The intermediate stage between vitrinite and fusinite is termed semifusinite. Semifusinite always shows a lower reflectance than fusinite and the cell-like texture evident in fusinite, is mostly not as well preserved. The semifusinite maceral has the highest reflectance range of all coal macerals which ranges from the upper end of the vitrinite range to fusinite. As such, the physical and chemical properties vary widely, ranging

from those of vitrinite on the one hand to fusinite on the other, depending on the degree of coalification. Semifusinite is normally the most abundant of the inertinite macerals and are richer in carbon and poorer in hydrogen than vitrinites, but poorer in carbon and richer in hydrogen than fusinites (Stach et al., 1975).

3.3.2 Coal Lithotypes

The distinction between humic and sapropelic coals in terms of their chemical and petrographic properties depends upon the genesis and the degree of maturation. The macroscopic description of coal requires a distinctive system to describe its physical character. The term lithotype designates the different macroscopically recognisable bands of a coal seam (Stach et al 1975). Seams of humic coal usually consist of bright bands, semi-bright bands and rather dull bands. Thus, Stopes (1919), proposed the following lithological types (lithotypes), for describing humic coal.

(i). **Vitrain:** black, brittle, glassy, vitreous material, occurring as thin bands.

(ii). **Clarain:** semi-bright, black with a silk lustre, very finely stratified.

(iii). **Durain:** grey to black bands with a dull lustre, rough surface fractures.

(iv). **Fusain:** black, soft, friable, easily disintegrates into a black fibrous powder.

The four lithotypes usually occur as thin layers or lenses, often only millimetres in thickness and the alternation of the different layers of lithotypes in a seam produces so-called “banded coal”.

3.3.3 Coal Microlithotypes

The combination of the three main maceral groups, when identified petrographically, are known as microlithotypes, which can give an indication of the texture of a coal.

Microlithotypes can be divided in to three groups, monomaceral, bimaceral and trimaceral. The classifications and associations of the three microlithotype groups can be seen in Table 3.3. If two coals have equal overall contents of vitrinite and one has a higher vitrite content than the other, this may be due to different thicknesses in the bands of vitrinite, which, in turn may influence the preparation of coal. The size distribution of the masses of inertinite may be important when considering the coking behavior of a coal (Thomas, 1992).

Table 3.3 Composition and maceral associations of microlithotypes. (Stach et al., 1975).

Group	Name	Composition (Vol%)
Monomaceral	Vitrite	Vitrinite (V) >95
	Liptite	Liptinite (L) >95
	Inertite	Inertinite (I) >95
Bimaceral	Clarite	V + L >95 (each>5)
	Vitrinertinite	V + I >95 (each>5)
	Durite	I + L >95 (each>5)
Trimaceral	Duroclarite	V>I, L (each>5)
	Trimacerite Vitrinertoliptite	L>I, V (each>5)
	Clarodurite	I>V, L (each>5)

3.3.4 Mineral matter in coal

The mineral content of coal is the non-combustible inorganic fraction which is made up of minerals which are either detrital or authigenic in origin. Detrital minerals are those which have been transported into the bog or swamp by means of water or air bourn particles. Authigenic minerals are those that are introduced to the peat during or after deposition, or into coal during coalification. Precipitated minerals may be disseminated through the peat as aggregates, or mineral rich solutions may precipitate minerals on joints, cracks and fissures etc. These are introduced into the coal during the first and second stage of coalification respectively. These inorganic components are classified into three groups according to their origin.

(i). The inorganic matter from the original plant debris.

(ii). Inorganic – organic complexes which were introduced by means of water or wind during the first stage of coalification. This is sometimes called synergetic mineral matter (Suelves et al., 2000).

(iii). Minerals deposited after the consolidation of the coal, which were introduced by ascending or descending solutions into cavities, fissures and cracks (Stach et al., 1982). This is sometimes called epigenic mineral matter.

Some of the most abundant minerals in coal are the clay minerals. These minerals can occur in coal in two ways. Either as tonsteins, or as dispersed inclusions in maceral lithotypes. Tonsteins are associated with volcanic activity and been formed by either detrital or authigenic processes.

It may be possible to differentiate between synergetic and epigenic minerals, from the mode of occurrence in the seam. Synergetic mineral matter is usually intimately associated with the coal substance, whereas epigenic inorganic minerals are rather more spasmodic in occurrence and are usually clearly differentiated from the coal substance (Francis, 1961). Clay minerals can contaminate all microlithotypes. Coals with <20% (by volume) clay minerals are described as being `contaminated by clay`. Coals with clay contents of >20%<60% (by volume) are described as `carbargillite` coals. If there are higher proportions of clay minerals present, then the lithology is no longer a coal, but is argillaceous shale. Suffice to say that the mineral matter in coal can vary quite considerably, even from coal from the same mine (Cerny et al., 1997). Table 3.4 shows a survey of the known mineral groups in coal. Vassilev and Vassileva (1996) classified the inorganic constituents in coal as solid crystalline mineral matter, solid non-crystalline (amorphous) mineral matter and fluid matter. The mineral matter of coal consists of various mineral species (mostly crystalline) that belong to sulphides-sulphosalts, oxides-hydroxides, silicates, sulphates, carbonates, phosphates, chlorides, native elements, vanadates, tungstates and some other mineral classes that have been strictly divided and characterised in the mineralogical sense. It is a well known fact that the nature and distribution of mineral matter in coal plays an important role it its behaviour during handling, storage and use (Hower, 1998; Vuthaluru, 1999; Gupta et al., 1999; Huggins, 2002; Ward, 2002; Mardon and Hower, 2004; Wells et al., 2004, 2005). A number of well proven methods exist for the identification and quantification of mineral matter in

coal. These include X-ray diffraction (XRD), thermal analysis techniques, electron microprobe analysis and Scanning Electron Microscopy (SEM).

Table 3.4 Minerals in coal. (Stach et al., 1975).

Mineral group	First stage of coalification: syngenetic formation, synsedimentary, early diagenetic (intimately intergrown)		Second stage of coalification: epigenetic formation	
	Transported by water or wind	Newly formed	Deposited in fissures, cleats and cavities (coarsely) intergrown)	Transformation of syngenetic minerals (intimately) intergrown)
Clay minerals	Kaolinite, illite, sericite, clay minerals with mixed-layer structure; montmorillonite, tonstein (smectite)			Illite, chlorite
Carbonates	—	Siderite–ankerite concretions; dolomite, calcite, ankerite, siderite, calcite	Ankerite, calcite, dolomite; ankerite in fusite	—
Sulphides	—	Pyrite concretions, melnikovite–pyrite, coarse pyrite, (marcasite), concretions of FeS_2–$CuFeS_2$–ZnS; pyrite in fusite	Pyrite, marcasite, zinc sulphide (sphalerite), lead sulphide (galena), copper sulphide (chalcopyrite); pyrite in fusite	Pyrite, from transformation of syngenetic concretions of $FeCO_3$
Oxides	—	Haematite	Goethite, lepidocrocite ('needle iron ore')	Goethite, lepidocrocite ('needle iron ore')
Quartz	Quartz grains	Chalcedony and quartz from the weathering of felspars and mica	Quartz	—
Phosphates	Apatite	Phosphorite, apatite	—	—
Heavy minerals	Zircon, rutile, tourmaline, orthoclase, biotite	—	Chlorides, sulphates, nitrates	Chlorides, sulphates, nitrates

3.3.4.1 The Origin of Sulphide minerals

Sulphur in coal is found in both inorganic and organic forms. The inorganic sulphur is mostly pyrite (FeS_2). Besides pyrite there may be marcasite and sulphates. In addition to these, some coal seams may contain small quantities of sphalerite, galena, and chalcopyrite, in particular if hydrothermal veins are close to the coal seam. Sulphur bacteria have a vital role to play in peats and organic muds by reducing sulphates to sulphur, making possible the formation of pyrite and marcasite. It has been shown that FeS_2 can only be formed in peats from bacterial activity since from basic reaction kinetics, it has been shown that there is insufficient energy available for a purely chemical reduction of sulphates to disulphides, providing, of course that there is a sufficient supply of sulphur and iron (Stach, et al., 1975)

The sulphur will have originated from plants and animal protein, largely from bacterial protein, or it may have been introduced from outside areas where silicate minerals weather or perhaps where ground water carries Fe-ions. Information about the abundance, distribution and origin of sulphur in coal is important in coal combustion due to the adverse effect of sulphur oxide emissions on human health and the environment. The variation in sulphur content in coals depends largely on geological conditions, with the sulphur available during plant growth the principal source of sulphur in low-sulphur coals (<1%) (Dai et al., 2002). In contrast, in medium (1%-3% total sulphur) and high sulphur (>3% total sulphur) coal overlain by a marine environment, most of the sulphur is derived from seawater sulphate (Chou, 1990). The bacterial reduction of sulphate (from coastal swamp seawater) produces H_2S, which reacts with organic matter during early digenesis to produce sulphides and organosulphide compounds (Dai et al., 2002).

3.4 Coal Characterisation

The precise characterisation of coal is vitally important when considering its use as feedstock for the energy or chemical industry. Efforts to reduce the cost of coal mining and utilisation are achieved by increasing efficiency and reducing pollution. Thus, a clear understanding of the characteristics of coal and the products of coal combustion are required (Whateley, 2001). However, the characterisation of coal requires a detailed knowledge of its petrology and rank since its chemical and physical properties can vary enormously with age and origin. As such, a great deal of work has been carried out by researchers on coal properties and characterisation (Remeysen and Swennen, 2005; Lester and Kingman, 2004; O`Brien et al., 2003; Barranco et al., 2003; Wells et al., 2003; Cloke et al,. 2001; Sengupta, 2001; Bjorkman, 2001; Harmer et al., 2001; Haas et al., 2000; Van Geet et al., 2000; Thomasson et al., 2000; IFRF, 2002). Modern coal characterisation techniques allow for rapid identification and quantification of maceral and mineral compositions, rank analysis, proximate analysis, ultimate analysis, thermogravimetric analysis, particle size distribution, fouling index. grindability index and heavy metals analysis, using only relatively small sample sizes. Coal petrography is a standard method for characterising a coal in terms of its organic (maceral) and inorganic (mineral) constituents. Generally, two types of data can be determined from this method. The coal rank may be defined (in terms of its vitrinite reflectance) and composition (maceral proportions). This type of information can be used to understand coal deposition, coking potential, and quality of the mined product (O`Brien et al., 2003). These techniques can also provide a useful tool for monitoring coal blending. The success

of new technologies, such as specialist fluidised bed combustion and combined cycle regeneration is based upon characterisation data (Whateley, 2001).

3.4.1 Petrographic Analysis

3.4.1.1 Maceral Analysis

Maceral distributions in coal have a significant effect on utilisation processes and can influence the overall combustion performance. The physical properties of the major maceral groups as described by Stach (1975) in terms of their resistance to grinding (liptinites), brittleness (vitrinite), high density (inertinite) and mineral associations will need to be considered when assessing their limitations and suitability for a given use. Since macerals are non-cystalline organic compounds and are difficult to separate from coal, little is known about their properties. However, petrographic analysis methods have been a most successful characterisation tool, in which the separation of individual macerals from coal is not necessary. The method is recognised internationally and is important in the context of continuity. In addition to the macerals, it is also possible to identify mineral proportions in the coal sample which may be considered as a total, separately or ignored. The principle of manual maceral analysis requires a representative sample to be prepared to a particular size and then mounted on a cylindrical particulate resin block. Several grinding and polishing stages are then necessary using suitable polishing media and polisher. The sample is then analysed under a microscope using reflected light and an oil immersion objective. A mechanical semi-automatic stage should be employed which is capable of advancing the coal specimen laterally by equal steps (1/3mm) of such length as to ensure that only a small number of particles receive more

than one count. In addition to this, the stage should be equipped with a counter, capable of registering counts for each maceral category (Lester, 1994). Each time the eyepiece crossline falls on a maceral, it must be identified as belonging to a certain group and counted as such. A total of at least 500 points are counted and the results are presented as a volume percentage of each maceral group in the coal sample (BS 6127-3, 1995). Should the eyepiece crossline fall on the mounting resin, this point in question should not be counted. In most cases an analysis by maceral groups – vitrinite, liptinite and inertinite is sufficient, although for the purposes of this work, differentiation between semi-fusinite and fusinite macerals have been quantified in the inertinite maceral group.

Manual maceral analysis techniques can be time consuming and unavoidably subjective. As a consequence of these disadvantages, many efforts have been made to perform maceral analysis automatically by using software to perform an analysis on a coal image or series of images. This is of course not without its potential difficulties, since distinguishing the various maceral groups from each other and liptinite from the background resin can be difficult. Despite these difficulties, many researchers have been successful in obtaining acceptable results using an automated approach when compared to data collected manually (Lester et al., 1993; Lester et al., 1994; Cloke et al., 1995; Gilfillan et al., 1999). A novel approach to automated image analysis has successfully overcome these difficulties by introducing two images of different exposure settings under a microscope to enable the software to separate liptinite from the background mounting resin (Lester et al., 2002). At normal exposure, liptinite has a grey-scale similar to that of the surrounding resin. However, by using a longer exposure time, the resin

remains black while the grey-scale of the liptinite increases such that it can be distinguished from the resin, which is related to the differences in absorbtivity of the resin and maceral phases. A grey-scale profile of the macerals present in the sample is developed and displayed as a reflectogram (frequency histogram), which illustrates the reflectance distribution of the coal without any contribution from the background resin. From this data, maceral proportions can be calculated (Lester et al, 2002). Figure 3.3 shows a reflectance histogram for a typical UK coal sample.

Figure 3.3 Reflectance Histogram for Asfordby Coal (background resin removed).

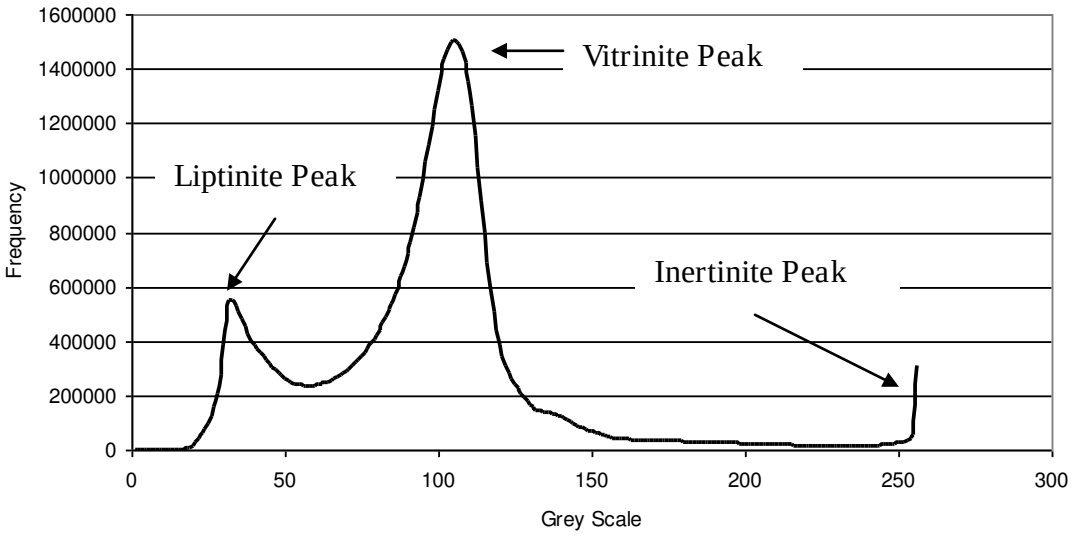

Based on this automated image analysis technique, a Reactivity Assessment Program (RAP) was developed at the University of Nottingham (Lester et al., 1994; Cloke et al., 1995). The aim of this program was to determine the "% Unreactives" in a coal sample to predict its combustion potential. The cumulative percentage of material higher than a

specific grey-scale threshold was measured and the technique was validated on a suite of coals from around the world. (Lester et al., 1995; Gilfillan et al., 1999).

3.4.1.2 Rank Analysis (vitrinite reflectance)

The rank of coal is a characteristic of the stage it has reached during coalification or maturation from decaying vegetable debris to the final stage which is represented by graphite (Stach et al., 1975). The changes in the physical and chemical properties of a coal as coalification advances are in reality, changes to inherent coal constituents. It is important to note that during the geochemical or metamorphic stage, the progressive changes in pressure and temperature, cause reactions that change much more quickly in the organic constituents than in the mineral phases. Thus, coals can therefore indicate a degree of metamorphism in sequences which show none or little mineralogical change. Also, as metamorphosis advances, progressive changes in the coal occur, such as an increase in carbon content and a decrease in the hydrogen and oxygen content resulting in a loss of volatiles. During these chemical and physical changes the three maceral groups become enriched with oxygen. As such, each maceral group will follow a distinct coalification path. The petrographic properties of the vitrinite maceral change uniformly with increasing rank and in reflected light, the reflectance of vitrinite increases progressively. These unique optical properties displayed by vitrinite, have enabled it to be used as a reliable rank indicator, provided that care is take over the selection of the component to be measured.

The preparation of a coal sample for rank analysis, follows the same procedure as the as that described for maceral analysis. The principle of operation requires that a beam of

monochromatic light, at a wavelength of 546nm, is reflected at near normal incidence from a specific area of well polished vitrinite and measured under oil immersion. This is then compared with light reflected under identical conditions from standards of known reflectance.

The reflectance, R_{vi}, is calculated as the percentage of normal incident light that is reflected from a polished vitrinite surface. Details of the full procedure and equipment set up can be found from British Standard (BS 6127, 1995).

3.4.2 The Physical Properties of Coal

The evaluation of a coal for commercial use requires the knowledge and determination of several physical properties such as density, hardness, grindability, abrasiveness and size distribution.

3.4.2.1 Coal Density

The density of a coal will depend largely on its rank and the mineral matter content. As a general rule, the density of coal will increase with increasing rank or carbon content. The density of coal can be reported in many ways based on specific features such as, apparent density, true density, bulk density, specific or relative densities (with reference to water at 4°C) etc. The density of coal is commonly measured by the gas displacement pycnometer (using helium as the probe gas) or standard density bottle methods. Of course porosity and its dependency on rank will affect the specific gravity, surface area and its ability to absorb or defuse gases into or away from the material. The density variation of coal macerals has also been reported and although the variations are not great, the general

ordering of density of macerals with approximately the same carbon content is; Liptinite<Vitrinite<Inertinite (Speight, 1983).

3.4.2.2 Coal Hardness and Grindability

There is much information available on the properties of coal which relate to it hardness, such as friability and grindability, although little is known about hardness of coal as an intrinsic property. One of the methods used to evaluate the hardness of coal employs a "scratch hardness technique". The scratch hardness of a coal can be determined by measuring the load on a pyramidal steel point required to make a scratch 100μm in width on the polished surface of a specimen. The scratch hardness of anthracite is 6 times that of soft coal, whereas pyrite is almost 20 times as hard as soft coal (Speight, 1983). The resistance of coals to abrasion is commercially significant since the abrasive action of coal on grinding elements results in major maintenance charges. As a consequence, the evaluation of the abrasiveness of coal must be considered when coals are selected for pulverised fuel systems.

The grindability of coal is a composite physical property which relates to other specific properties such as hardness, strength, tenacity and fracture. In modern commercial operations, coals are required to be crushed to a fine powder (-75μm) before being fed into a boiler. The ease with which the coal can be pulverised is measured by the Hardgrove Grindability Index (HGI) (ASTM D409). This is an index where the ease with which a coal can be pulverised is measured against coals chosen as standards. Coal with relatively high HGI values are soft and relatively easy to grind, whereas coals with a low HGI are hard and troublesome to grind. A general relationship exists between grindability

and rank, insofar as “easy-to-grind” coals are in the medium and low volatile groups, although reproducibility in this range is poor, perhaps hampered by the high moisture content of some coals in this rank range. As such, the trend is only approximate and cannot be used with confidence to estimate grindability from coal analysis. Figure 2.4 shows a generalised plot of HGI with rank.

Figure 3.4 Hardgrove Grindability Index with coal (Thomas, 1992)

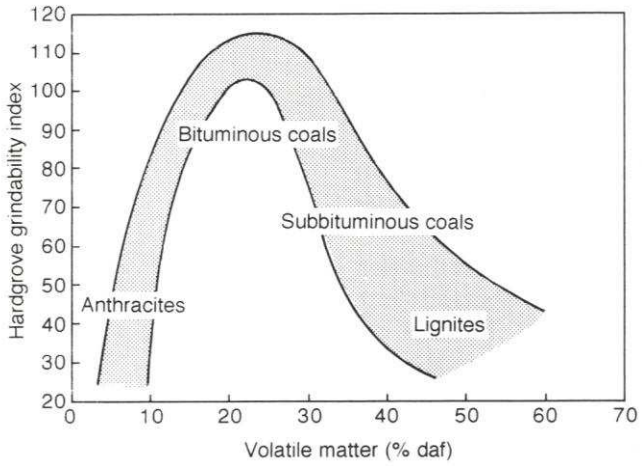

3.4.3 The Chemical Properties of Coal

Coal analyses are often reported as proximate and ultimate analysis. Proximate analysis is a very broad analysis which determines the amount of moisture, volatile matter, fixed carbon and ash. The ultimate analysis is the determination of the principal chemical elements in coal i.e. carbon, hydrogen, nitrogen and oxygen. In addition these, further analysis may be necessary to investigate the amount of other elements present which may have a direct bearing on the usability of the coal. These include, sulphur, chlorine, phosphorous, an elemental analysis of the ash residue and selected trace elements.

However, before one can proceed with the analysis of coal, it is vitally important to understand the basis with which the analytical data is presented. For example, it is necessary to understand how moisture, ash, volatile matter and fixed carbon relate to one another.

Coal analysis my be reported in the following ways;

(i). *"As received"* basis or *"as sampled"* (a.r.). The data analysis here is expressed as percentages of the coal which include the total moisture content (the moisture condition when the sample arrived in the laboratory).

(ii). *"Air dried"* basis (a.d.b.). A frequent practice is to air-dry the coal sample to bring it into approximate equilibrium with the laboratory atmosphere, in order to minimise gain or loss during sampling operations.

(iii). *"Dry basis"* (dry). The data presented is expressed as percentages of the coal after all the moisture has been removed from the sample.

(iv). *"Dry ash free basis"* (d.a.f.). The coal is considered to consist of fixed carbon and volatile matter on the basis that moisture and ash have been removed from recalculation. However, this basis does not allow for the volatile matter found in the mineral matter present in the air dried coal.

(v). *"Dry, mineral matter free"* basis (d.m.m.f.). The total amount of mineral matter is calculated rather than ash, so that the volatile matter in the mineral matter is taken into account.

3.4.3.1 Proximate Analysis

The proximate analysis of coal is a means with which to determine the composition of a coal in terms of its moisture, volatile matter, fixed carbon and ash.

There is no exact method for determining moisture content in coal. Even so, the coal industry has developed a set of empirically determined definitions which are summarised as follows:

(i). The surface or adventitious moisture that does not naturally occur in the coal and can be removed upon air drying at about 40ºC. The moisture remaining after this step is known as air-dried moisture

(ii). The moisture content of the coal when it is delivered to the laboratory is known as the as-received moisture. It is normally the procedure to air-dry the sample to obtain the "loss on air drying" and then employ a more aggressive step to determine the air-dried moisture. These results can then be added together to give the total moisture.

(iii). The total moisture is that which can be removed by aggressive drying (about 105ºC in a vacuum or nitrogen atmosphere).

High moisture content in coal is undesirable since it is chemically inert and absorbs heat during combustion. It can also create difficulties in handling, transport and storage. High moisture contents can lower the calorific value in steam coals and lower the amount of carbon available in coking coals (Thomas, 1992).

The volatile matter in coal represents that component, except for moisture, that is liberated at high temperature (900ºC) in the absence of air. Normally at this temperature

the weight loss in a sample becomes stationary. The volatile matter material is derived principally from the organic fraction of the coal. However, minor amounts may be due to the mineral matter present. The differentiation between volatile matter from the organic and inorganic matter is not usually necessary in commercial practice.

The ash remaining after coal has been incinerated in air is derived from the inorganic complexes which are present in the mineral matter of the original coal. The principal of operation to determine ash normally requires a test sample to be heated in air to a temperature of 815ºC ± 10ºC. This temperature is maintained until the sample becomes constant in mass. The ash of the sample analysed is expressed in terms of a percentage of the test sample before incineration.

The carbon found in the residue remaining after the volatile matter has been liberated is known as the fixed carbon content of coal. Fixed carbon is not normally determined directly but is the difference, in an air-dried coal, between the total percentages of the other components i.e. moisture, ash, volatile matter and 100%. Details of the methods for analysis of proximate analysis of coal can be found in British Standard (BS 1016-104, 1998).

3.4.3.2 Ultimate Analysis

The ultimate analysis of a coal is the determination of carbon and hydrogen as gaseous products of its combustion, the determination of sulphur and nitrogen in the material as a whole and the estimation of oxygen by difference. The carbon and hydrogen are liberated as CO_2 and H_2O when the coal (which has been air-dried) is incinerated and collected in an oxygen stream. Nitrogen is measured using the macro-Kjeldahl method. This method

converts nitrogen to ammonium sulphate and sulphuric acid and then uses titration to determine the amount of ammonium sulphate. Sulphur can be present in coal in three forms: Organic sulphur - present in the organic fraction of the coal: Pyritic sulphur – present in sulphide minerals (principally iron pyrites): Sulphate minerals – usually produced by oxidation of the sulphate fraction of the coal. In the ultimate analysis of a coal, the total sulphur content is determined. If an analysis requires the relative amounts of each form of sulphur, a separate analysis is required. Total sulphur is determined by the Bomb Washing Method in which sulphur is precipitated as barium sulphate from the residue of an oxygen bomb calorimeter washing. The precipitate is filtered, ignited and weighed. Oxygen estimations are usually calculated from the difference from the other elements from 100%. Details of the methods of analysis for the ultimate analysis of coal can be found in British Standard (BS 1016-106.1.1, 1996; BS 1016-106.2, 1997; BS 1016-106.4.1, 1993).

3.4.3.3 Thermal and Combustion Properties

The effects of combustion on a coal will influence its selection for particular industrial uses. A series of test can be carried out to investigate the performance of a coal inside a furnace. The tests can evaluate a coals calorific value, its ash fusion temperature and where required, the caking and coking properties if it is intended for use in metallurgical processes.

The calorific value (CV), sometimes referred to as the enthalpy of combustion or specific energy (SE), is a measure the amount of heat produced per unit mass of material when combusted. This property is associated with the bond energies between atoms and may be

calculated with fair accuracy from the determination of the elementary composition alone (Van Krevlin, 1993). The CV of a coal can be expressed in two ways. The Gross calorific value is the amount of heat liberated from the coal when it is combusted under standardised conditions, at constant volume, so that the water in the sample remains in liquid form. The gross calorific value of a coal can be determined using a standard adiabatic bomb calorimeter (BS 1016-105, 1992). The gross calorific value is determined from knowledge of the relationship between the temperature rise and the mean effective heat capacity of the system immediately before and after combustion. The gross calorific value is never achieved during combustion in furnaces since some products, such as water, are lost with their associated latent heat of vaporisation. The maximum achievable calorific value under these conditions is expressed as the net calorific value. The calorific value can be calculated and is usually expressed in terms of absolute joules per kilogram (J/kg) or British Thermal Units (BTU) (Thomas, 1992). A schematic representation of the variation of the calorific value of coal with coal rank is shown in Figure 3.5.

Figure 3.5 Variation of calorific value with coal rank.

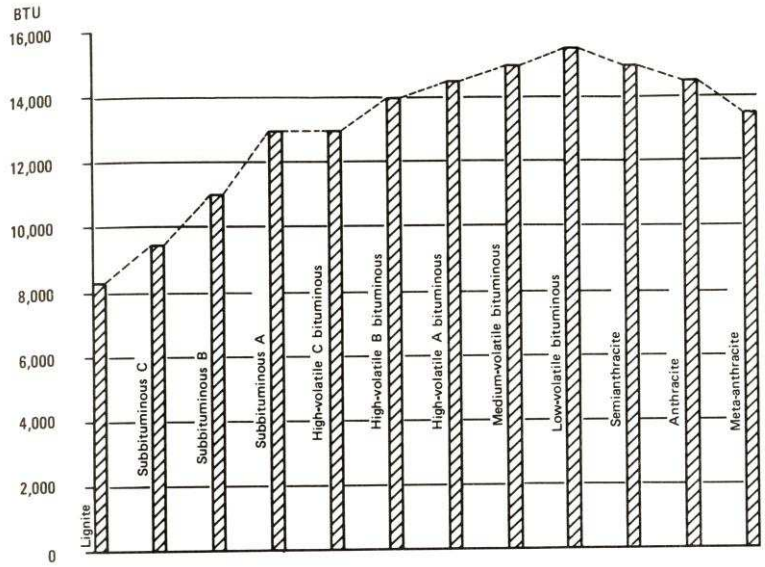

All coals will undergo some chemical changes when heated and certain types of coal will undergo physical changes when subject to the influence of heat. Such coal are known as caking coals and will pass through a series of physical changes when they soften, melt, fuse, swell and solidify within a specific temperature range. These physical changes are often referred to as the "plastic properties" of coal. The caking tendency of a coal increases with increasing volatile matter and reaches a maximum in the range 25-35% volatile matter content but then tends to decrease. The caking tendency is also high in the 81-92% carbon coals and also has a tendency to increase with hydrogen content but decrease with oxygen and mineral matter content. When noncaking coal are heated their residue tends to be pulverent and noncoherent.

The Free Swelling Index (FSI) is a standard test to measure the increase in te volume of a coal when heated, without the restriction of the exclusion of air. This test is used to evaluate the suitability of coals for coking and combustion. During this test the coal is heated for a specific time, and when all the volatiles have been liberated, a small coke "button" remains. The cross section of the button is then compared to the cross section of a series of standard profiles. Coals which exhibit a low swelling index (0-2) are deemed unsuitable for coke manufacture. Conversely, coals with a high swelling index (+8) cannot, by themselves, be used to produce coke as the resultant coke is weak and will not support loads imposed upon it in a blast furnace environment. However, such coals can often be blended to produce strong coke.

The details of the analysis method for testing the plasticity and coking potential of coals, can be found in British Standard (BS 1016-107-3, 1990).

3.5 Pulverised fuel power generation

Pulverised coal combustion in the Rankine steam cycle has been the main mode of coal utilisation in the power industry. The average efficiency of a standard coal fired power utility is η~32%. However, new technologies such as combined cycle and integrated coal gasification plants are now providing overall efficiencies of η~45% (Beer, 2006). It is generally accepted that efficiency improvements that are consistent with low cost electricity are economically beneficial, but the effect this has on the plant emissions, without additional installation of environmental protection equipment is less appreciated. It is widely accepted that efficiency is the only practical tool, in the short term, for the control of CO_2 emissions from fossil fuel plants. As such energy efficiency has become the key concept for the choice of technology for new plant design and upgrade of existing plant. Figure 3.6 show diagram of a modern advanced coal fired power plant.

Figure 3.6 Advanced pulverised fuel power plant (Beer, 2006)

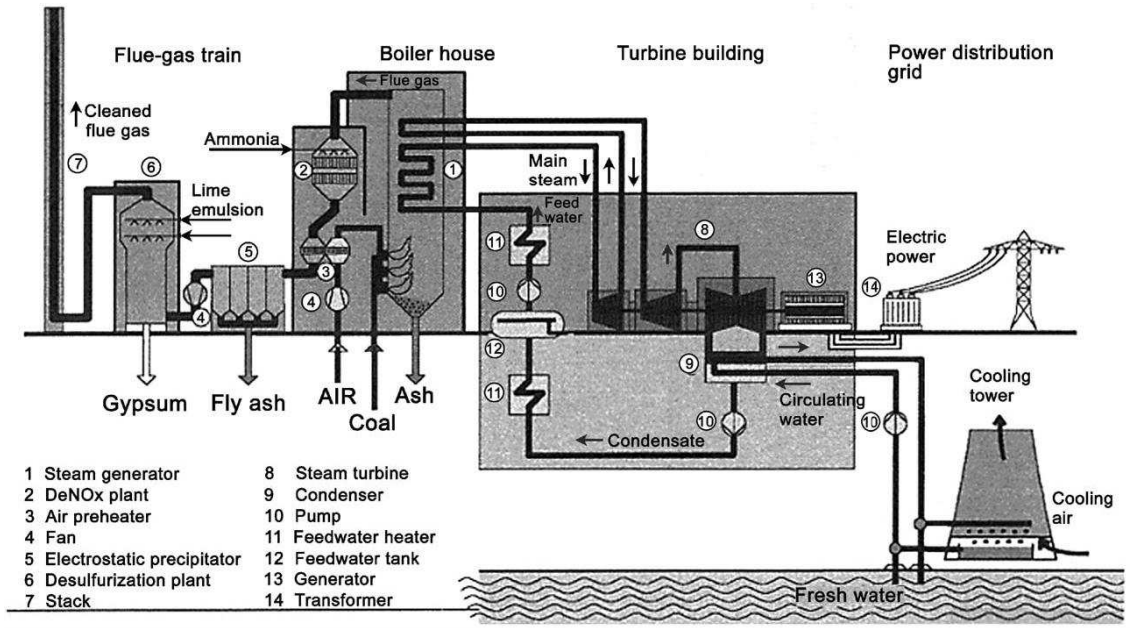

Supercritical steam plants have been used since the 1930s in Europe. Significant improvements in materials and the drive for high efficiency plants are making this system the favorite choice for new coal-fired utilities worldwide. The schematic diagram in Figure 2.6 shows an advanced power plant with forced circulation boiler equipment, flue gas desulphurization scrubbers (FGD), Electrostatic precipitators (ESP) and selective catalytic reactor (SCR) for NO_x reduction. These technologies are reviewed in brief in section 2.7. The principals of power generation will vary from plant to plant depending on its steam and gas cycles and the combustion conditions. In a typical coal combustion plant, coal will be milled to 60-75% below 75μm size. The coal it then injected into the furnace after milling with part of its air supply. The particles are almost instantly entrained in a high turbulence gas stream while resident in the furnace. Substantial burnout of carbon is completed within a couple of seconds with flame temperatures in the region of 1300°C to 1700°C (depending on the rank of coal and design of burner used). After this, the hot gasses are past to post-combustion control stages after the removal of the bulk of the fly ash. These post combustion technologies are primarily for sulphur dioxide removal and NO_x reduction.

3.6 Pulverised fuel power generation emissions

The combustion of coal for the generation of electrical power and process heating necessitates the need for strict control of emissions and pollutants which are potentially harmful to human beings and their environment. The control of emissions from power station utilities has received a great deal of attention due to ever demanding regulations. Regulations in various countries cover many aspects of coal use, with some covering the

planning of new plant, while others relate to operating conditions. All power plants have to meet regulations and targets governing the emissions of particulates, CO_2, SO_2 and NO_x in the exhaust gases and the current UK SO_2 and NO_x emission estimates and targets for these pollutants is presented here.

3.6.1 Sulphur dioxide emissions and targets

The total sulphur dioxide emissions in the UK fell by 77% between 1990 and 2004 to 833 thousand tonnes. The targets for 2010 as set by the UNECE (United Nations Economic Commission for Europe) Gothenburg Protocol and the EU national Emissions Ceiling Directive were 625 thousand tonnes and 585 thousand tonnes respectively. Total UK emissions fell by 84% between 1980 and 2004. The targets for 2010 as set by the UNECE Second sulphur Protocol were reductions of 50% by the year 2000, 70% reductions by 2005 and 80% by 2010. Emission from large combustion plants (LCP) fell by 83% between 1980 and 2003. This compares with EC LCP directive targets which were set at a 40% reduction by the year 1998 (based on 1980 levels), 60% reduction by 2003. Power stations still account for 60% of emissions, with 19% coming from the fuel use in the manufacturing industries and construction. Figure 3.7 shows the sulphur dioxide emissions and targets for 1970 – 2010.

Figure 3.7 UK Sulphur dioxide emission targets (DEFRA, 2006).

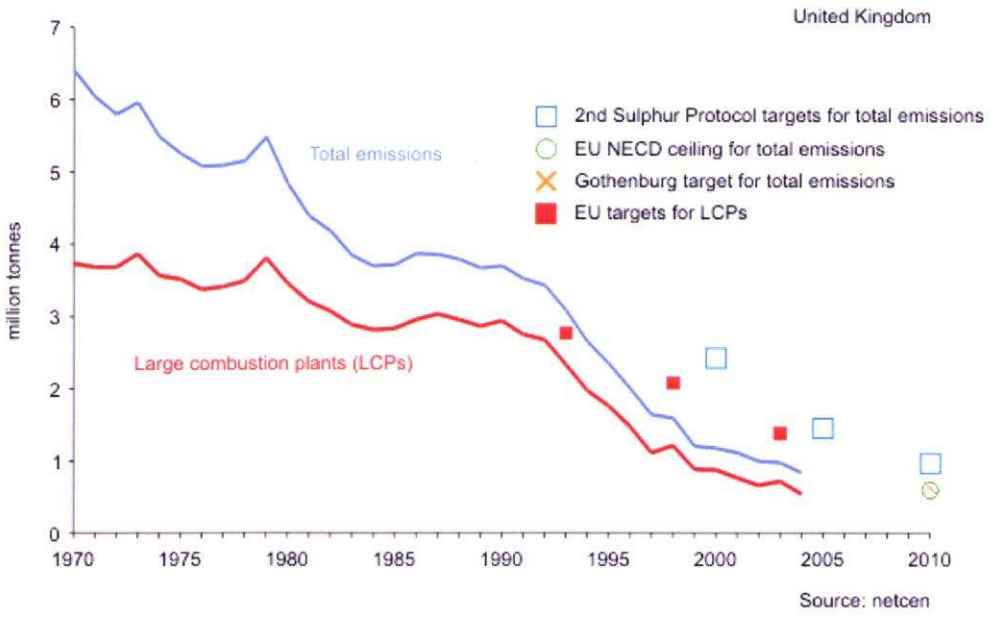

3.6.2 Nitrogen oxides emissions and targets.

Total Nitrogen oxides emissions fell by 45% between 1990 and 2004 to 1.621 million tonnes. This compares with targets set by UNECE Gothenburg Protocol of 1.81 million tonnes by 2010 and 1.167 million tonnes by 2010 under the EU National Emissions Ceiling Directive. The EC LCP Directive required the UK to reduce NO_X emissions by 30% by 1998 (1980 baseline). In 1998, large UK combustion plant emissions of NO_X were 61% below the 1980 baseline. Figure 2.8 shows the nitrogen oxides emissions and targets for 1970 – 2010.

Figure 3.7 UK Nitrogen oxides emission targets (DEFRA, 2006)

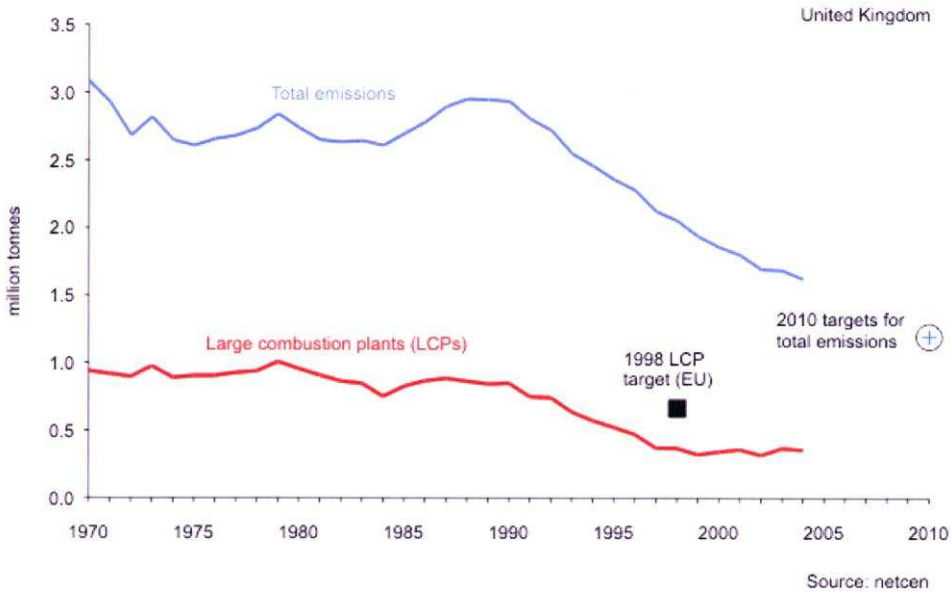

3.7 Clean Coal Technology – A Review

In recent years, a great deal of attention has been given to the pre-combustion and post-combustion cleanup of coal, as a means to reduce SO_2, NOx, particulates and CO_2 emissions from power generation utilities. Most of the current processes available for controlling sulphur emissions have involved either pre-treatment by chemical methods and/or post-treatment of the flue gases by stack scrubbing (Flue Gas Desulphurisation) along with the use of Electrostatic Precipitators (ESP) to remove particulate pollutants. The pre-combustion cleanup of coal by removing ash and inorganic sulphur (mainly pyrite) has been investigated extensively as a means to improve boiler performance and of course controlling objectionable pollutants. The production of coals which comply with the new strict environmental legislations for SO_2, NOx, and CO_2 emissions when burned in large power utility boilers remains the driving force and incentive for new

cleaning process developments. Currently and potentially available methods for controlling SOx, NOx and particulate emissions from coal fired combustion fall into the following categories.

- The use of low sulphur coal (ultra clean coal - <1% total sulphur) either naturally occurring or physically cleaned.
- The removal of sulphur oxides from the combustion flue gases using stack scrubbing technology (Flue Gas Desulphurisation).
- The chemical treatment to separate sulphur from coal.
- The conversion of coal to a clean fuel by such processes as gasification cycles and fluidised bed combustion.
- Flue gas particulate emission control with Electrostatic Precipitators (ESP) and gas conditioning.
- The use of low NOx burners to reduce NOx emissions.

A review of these existing methods and current industrial practices are discussed briefly here.

3.7.1 Flue Gas Desulphurisation

The use of flue gas desulphurisation (FGD) technologies to reduce sulphur dioxide (SO_2) and sulphur trioxide (SO_3) emissions from power station flue gasses, are widely used. There are a wide variety of FGD processes available, but most use an alkali sorbent to recover the acidic sulphur compounds from the flue gas. The main differences in the available technologies are the types of sorbent used in the process, the by-products produced, the removal efficiency, the capital cost of installation and the operating costs.

The most common FGD process in operation is the limestone gypsum wet scrubbing process. During this process the flue gasses are treated with limestone slurry, in order to remove the SO_2 and to neutralise it. As in most processes the limestone has been milled to increase the surface area available for absorption. The final product is calcium sulphate dihydrate (Gypsum). It is common practice to locate the FGD facility down stream of electrostatic precipitator (ESP or bag filter) so that most of the fly ash from combustion is removed before it reaches the FGD plant. Flue gases from the ESP are mixed with process liquor after reheating and then the gas is scrubbed with recirculating limestone slurry to remove the required amount of SO_2. Limestone/gypsum slurry is pumped from a sump, to spray headers at the top of the scrubber. As the slurry comes into contact with the flue gases, the SO_2 is dissolved in the water and thus removed from the flue gas. The calcium carbonate from the limestone reacts with the SO_2 and O_2 from the air, ultimately to produce gypsum, which precipitates from the solution in the sump. HCl is removed from the flue gas in the scrubber to produce calcium chloride solution along with trace quantities of fly ash not captured by the ESP plant treatment. It is generally claimed by FGD plant manufacturers that >95% of SO_2 can be removed from flue gases with the absorber. Some recent plants have been designed for up to 98% removal (DTI/Pub URN 00/652). The process also removes 100% of hydrogen chloride (HCl) in the flue gas. At the end of the process the scrubbed gas is passed through a de-mister to remove suspended water droplets and then the gas is reheated, to raise its temperature (80°C in the UK) to improve dispersion and reduce the frequency of a visible plume before being exhausted to the stack.

3.7.2 Particulate Control – Electrostatic Precipitators (ESP)

Electrostatic Precipitators are the particulate emissions control technology which is most widely used on coal-fired power generating facilities. Conventional electrostatic precipitators have been modernised over the past decades and new methods of construction have been proposed with increased cleaning efficiency, particularly for particles in the submicrometer range. The driving force for this new technology lies in the fact that rigorous new regulations have been imposed on power plant dust emissions which now require maximum particle emissions on the level of 10-50 mg/Nm^3, and restrictions on the emission of particles smaller than 2.5μm (Jaworek et al., 2006). To meet these new requirements, new methods to clean flue gas with collection efficiencies greater than 99% have been developed and tested. The components of the fly ash emitted by coal fired power plants consist of Al_2O_3, SiO_2 and Fe_2O_3, along with other non-volatile trace element and toxic metals (Hower et al., 2004).

The ESP is a device which uses electrostatic force to remove particles from an exhaust gas. Electrical energy is required for gas ionisation, particle charging, particle coagulation or agglomeration, or vapour condensation. The ESP contains a set of discharge electrodes placed between two parallel collection plates. Electrical discharge from the electrodes, usually maintained at a high negative potential, produces gaseous ions by attachment of free electrons to gas molecules. The two mechanisms for charging particle by ionic current consist of Field Charging and Diffusion charging (White, 1963). For particles larger than 1μm, field charging is the dominant mechanism. For particles smaller than 1μm, the charging is principally due to ion diffusion. The collection electrodes are

mechanically rapped periodically to dislodge the collected dust which falls into a hopper beneath, for collection and disposal. The two common types of ESP, namely the parallel plate, and the tubular model are show in Figure 3.6.

Figure 3.6 the parallel plate (a) and tubular (b) ESP (Jaworek et al., 2006)

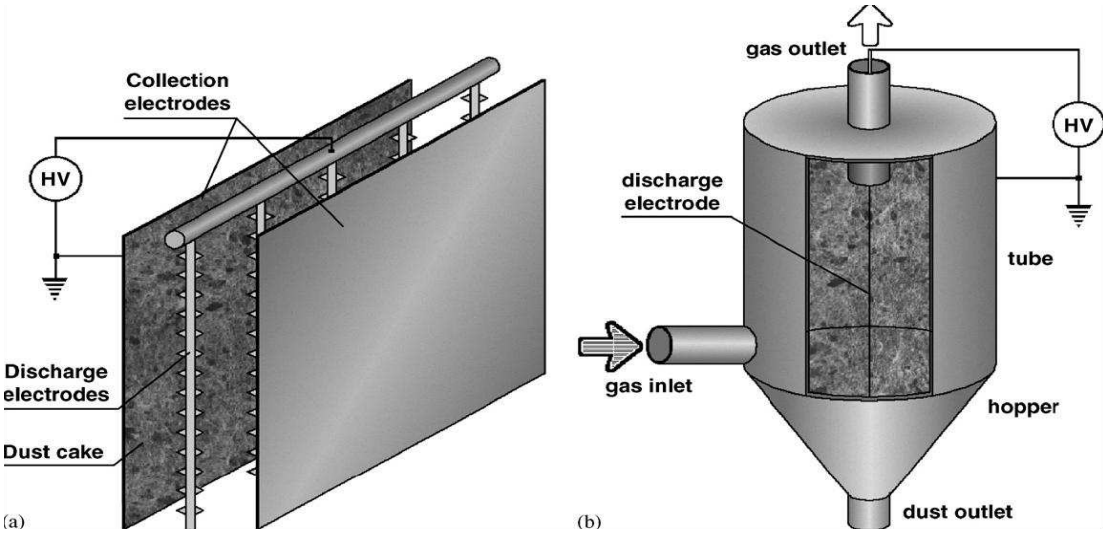

For low sulphur coals containing less than 1.5% sulphur, when the gas humidity is lower than 15%, gas conditioning is required. Gas agents such as water, steam, ammonia (NH_3), sulphur trioxide (SO_3), sulphuric acid (H_2SO_4), amongst others, are used to cause adsorption of moisture on the particle surface, thus increasing its conductivity. The effect of the gas conditioning on the dust particle depends on its composition, but NH_3 and SO_3 are the most popular agents used. The disadvantage with certain flue gas conditioning agents is that they can decrease the breakdown potential and increase adhesion and cohesion forces making rapping more difficult and less effective. It is also important to note that if sorbents are injected (as in FGD process), the resistivity of the particles in the

flue gas will change. This would almost certainly require change in operating conditions for the ESP.

Other common ESP models include the electrically energised cyclone (electrocyclone) and electrically energised fibrous filters (Jaworek et al., 2006)

3.7.3 Coal Preparation Techniques

In order to add value to run-of mine (ROM) material, coal preparation technology has been applied to meet the market requirements for quality cleaner coal. The pre-treatment of raw coal, includes crushing, sizing, cleaning and beneficiation. It has been recognised that coal pre-treatment can also bring considerable environmental benefits including the reduction of sulphur dioxide (SO_2), carbon dioxide (CO_2) and particulate emissions. It also provides a low ash product that is quality consistent to downstream power plant utilities (DTI/pub URN 01/605, 2001).

For courser coal grain sizes, density medium separation (DM) and jig washing are the preferred pre-treatment processes. These are based on two main separating principles: Separation is based upon difference in the relative density (RD) between organic coal and associated inorganic matter (mineral matter) and on differences in the surface properties between organic coal and associated inorganic matter. Coal is hydrophobic, whilst mineral matter is generally hydrophilic (Liu, 1982).

The density separation technique simulates the effect of using a heavy liquid media at a calculated density to effect a float/sink separation of coal from mineral matter. In commercial practice this can be achieved using finely ground magnetite (RD of 5.2), in water. Jig washing, on the other hand, is a water based process which relies on the

pulsation of water through a particle bed to stratify particles of different density (the higher RD particles formed in the in the lower layers, are separated using a discharge system). The jig system is a relatively low cost, simple system which is efficient only when coals are considered to be easy to clean (IEACR/44, 1991).

For fine coal cleaning (<3mm), density separation techniques, such as spiral concentrators and teeter-bed separators have been widely used (DTI/pub URN 01/605, 2001). However, for coal <0.6mm, froth flotation is still the most widely used process, particularly for ultra-fine coal, where column flotation technology is used. This technology uses froth flotation alongside impellers which are employed to disperse air bubbles within the fine coal slurry. Air-avid or water repellent (hydrophobic) particles are floated to the surface by the finely dispersed air bubbles and are collected as a froth concentrate. The mineral impurities which are readily wetted by water (hydrophilic), do not adhere to the air bubbles and thus remain submerged in the pulp. These systems are used in all coal producing countries and are efficient in terms of recovery. Flotation cells are usually combined to form a flotation bank, with volumetric capacities of up to ~120m^3 (Liu, 1982). Froth flotation in its normal mode is effective in reducing high-ash materials from coal, however, it does little in its operation to remove sulphur (pyrite). New processes have been development for the removal of pyrite using a froth flotation system. This involves a two stage process by floating pyrite form coal with xanthate. This process is called coal-pyrite floatation (Liu, 1982).

3.7.4 Low NO_x Burners

All combustion processes in air produce oxides of nitrogen. Nitrous oxides (NO_x) produced from coal combustion are considered to be responsible for 20% of the total UK annual NO_x emissions (DEFRA, Air quality strategy for England, Scotland, Wales and Northern Ireland, 2000). It has been identified as one of the greenhouse gasses present in the atmosphere that is increasing at a rate of 0.2-0.3% per year (Ogawa et al., 2005). During fossil fuel combustion, four strategies are currently used to control NO_x emissions. They are; 1) the use of low-NO_x burners, 2) staged combustion in air, 3) the use of secondary fuels "reburning" and 4) selective non-catalytic conduction.
Burner optimisation for low NO_x emissions is achieved by modifying the boiler operating conditions, excess air control and balance the air fuel ratio to various burners in order to obtain minimal NO_x formation at the burner. It has been reported that buy reducing the excess air to the burners along with fine tuning the boiler one can achieve as much as 39% reduction in NO_x emissions (Levy et al., 1993). Two-stage combustion or overfire air (OFA) is one of the features of low NO_x burners. This technique requires the combustion air to be separated into primary and secondary flow sections, to encourage complete burnout and promote the production of N_2 instead of NO_x. The primary air, oxygen deficient and at a low temperature, is mixed with fuel (fuel rich) and therefore moderate amounts of NO_x are produced. The secondary air is injected above the combustion zone through nozzles mounted above the burner. Therefore, a large flame volume is achieved at a low temperature which limits the production of NO_x. The improved flame structure also promotes a reduction in oxygen available to the hottest part

of the flame, thus improving burner efficiency. Another NO_x reducing technique is to use a staged firing or staged combustion approach. This technique produces fuel lean and fuel rich zone to promote complete combustion by starving some burners of fuel in controlled positions. Using this technology, NO_x emissions may be reduced by 30%. Flue gas recirculation can also be used to control NO_x emissions. In this case between 20 30% of the flue gas (at 350-400°C) is recirculated and mixed with the combustion air. This dilution results in a decrease in the temperature and oxygen availability reducing thermal NO_x formation at the burner (Smart & Morgan, 1994).

3.7.5 Fluidised Bed Combustion (FBC)

In fluidised combustion, coal is combusted in a hot bed of sorbent particles that are suspended (fluidised) by combustion air that is introduced from below through a series of nozzles. The so called 'circulating fluidised bed combustion' (CFBC) is the most common design in use today. By entraining a large portion of the particles, which are then separated from the flue gas and recirculated to the lower portion of the furnace, good carbon burnout is achieved. Typically a cyclone is positioned at the furnace exit to act as a separation device. Since the combustion process required relatively low temperatures NO_x production is relatively low when compared to traditional coal fired boilers (Beer, 2006). This technology has received much attention in view of its potential as an economic and environmentally acceptable method for burning low grade coal and biomass (McIlveen-Wright et al., 2006; Gayan et al., 2004; Campbell et al., 2000; Liu & Gibbs, 1998). For SO_2 capture, limestone is fed into the fluidised bed in addition to the pulverised fuel. A portion of the limestone reacts with the SO_2 to form calcium sulphate.

Due to the fact that the particles within the FBC plant have long residence times and are well mixed, efficient combustion can be maintained in temperatures as low as 843 - 899°C. This combustion is the optimum temperature range for the in-situ capture of SO_2 by free lime (Beer, 2006). The use of non-catalytic reduction technology for flue gas treatment has also been associated with advances in CFB technology to reduce NO_x emissions. Selective non-catalytic reduction (SNCR) is attractive due to its simplicity and inexpensive operating costs and is also considered simple to install and operate. The SNCR method removes NO_x from the flue gas by the thermal conversion of nitrogen oxides to N_2 and water vapour. Amine-based compounds such as ammonia and urea are used as the NO_x reductant (Zandaryaa et al., 2001; Radojevic, 1998).

3.8 Chemical and Physical Coal Desulphurisation by Microwave Energy

Coal is a complex fuel with a variety of impurities These impurities include organic and inorganic sulphur, clay minerals and a variety of elemental impurities, all of which have a negative impact on the coal-to-electricity chain. Several factors have combined to necessitate an examination of traditional practice in terms of where to remove the impurities. These include:

- Tightening of emission limits for particulates, sulphur dioxide (SO_2) and nitrogen oxides (NOx).
- Concerns over carbon dioxide (CO_2) emissions.
- The environmental effects of residues disposal.
- The requirement for high energy efficiencies in power plants.
- The competitive pressure to reduce power station operating costs.

- Research into technical developments which investigate new solutions which are economically viable.

Such impurities present in coal can increase the cost of transportation, can cause operating problems in the plant and harm the environment if released in an uncontrolled way.

The main elemental impurities in coal are:

- Sulphur, present mainly as pyrite (FeS_2), as sulphates or organically bound
- Silicon, present as SiO_2 (quartz) and in clays
- Aluminium
- Iron
- The alkali metals and alkaline earths, Ca, Mg, K, Na
- Halogens, particularly F and Cl
- Nitrogen
- Phosphorous

The concentrations of the remaining elements are less than 0.1% (1000ppm). By far the most abundant and therefore the most important group of minerals in most coals are the clay minerals. They commonly account for some 60% - 80% of mineral matter associated with coal. The clays include illite, montmorillonite, kaolinite and sericite (mica). Other common minerals include quartz, calcite, siderite, ankerite and pyrite. The major elements present in the mineral matter are commonly Si, Ti, Al, Fe, Mn, Mg, Ca, Na, K, and P. Within the coal to electricity chain, the impurities are of great concern due to environmental, plant performance, and legislation issues. The principle adverse effects

of impurities on the environment are associated with emissions of SO_2 and NOx, particulate emissions and solid residues

Iron sulphide or pyrite (FeS_2), is the primary inorganic from of sulphur found in coal. Pyrite can occur in two crystalline forms: pyrite (cubic) and marcasite (orthorhombic). Pyrite is generally more common and so collectively they are simply known as pyrite.

Pyrite occurs in coal as:

1. Narrow seams or veins up to 150mm thick and up to several hundred millimetres long.
2. Nodules, which consist of framboids, which range from a few microns to several hundred microns on diameter.
3. Discrete crystals of pyrite dispersed throughout the coal and occur in the size range of about 1 to 40μm in diameter with a large majority of the crystals being 1 to 2μm in diameter. This form of pyrite is not removed easily from coal by physical means and it is uneconomical to grind coal to this order of size (IEA Coal research – Chemical Desulphurisation of Coal, ICTIS/TR15 1981)

Reserves of coal which contain sufficiently low concentrations of sulphur to enable current sulphur dioxide emissions to be met when they combusted are limited and restricted to specific geographical areas (Stach, 1982). The cost of current technologies, such as FGD plants, represents significant proportions of the equipment cost of a modern coal fired power plant. The remaining options for controlling sulphur emissions is that of

pre-treatment to remove sulphur prior to combustion. The physical cleaning of coal prior to combustion, using washing and gravity separation techniques is already widely practiced in the coal industry. However, these are predominantly employed to remove mineral matter. Some sulphur may be rejected with the higher density material but that which is intimately associated with the organic portion will not be removed. Therefore, in order to decrease the sulphur contents of these coals to acceptable levels it is necessary to use more advanced chemical and physical techniques to remove both the organic and inorganic sulphur. High levels of pyrite (and quartz) in coal has been associated with mill wear. Their presence above specified quantities would possibly result in restricted mill throughput and higher energy consumption as they tend to be recycled within the mill and classifier system. These impurities are hard to grind and denser than organic coal (Scott et al., 1994). A review of the developments of the physical and chemical cleaning of coal with microwave energy is discussed here.

3.8.1 Desulphurisation by Microwave Energy

The separation of fine pyrite particle from coal in an attempt the reduce its sulphur emission upon combustion is difficult by conventional coal cleaning method simply because of the small sizes of the particle and that they, more often than not, will be trapped within the carbonaceous coal matrix after comminution. To overcome these problems, separator magnets have been used alongside efforts to enhance pyrite magnetisation.

The oxidation of sulphides has been investigated extensively (Belzile e tal., 2004; Dunn and Chemberlain, 1997; Huang and Rowson, 2002; Jagadeesh and Seehra, 1980; Mikhlin

et al., 2006; Peters and Thompson, 1998; Raichur et al., 2000; Rosso et al., 1990; Vaughan et al., 1997; Wang et al., 1996).There have been many studies that suggest that the magnetic susceptibility of pyrite in coal can be significantly improved by heating to sufficient temperature as to shift its stoichiometery toward magnetic phases. This can be achieved by conventional heating techniques, but heating consequently causes the pyrolysis of the coal matrix. Moreover, the oxidation of sulphides without creating adverse by-products such as SO_2, which would incur a further processing stage, remains a key objective. In order to fully understand the magnetic enhancement of pyrite to pyrrhotite, one needs to consider the fact that pyrrhotite has two distinct chemical phases, one of which magnetically very anisotropic (stoichiometric/monoclinic). For previous research by others, the nature of the chemical phase developed by a heating process is controlled by temperature, atmospheric conditions (inert or oxidising), gas pressure and flow rate and particle size (Hu et al., 2006). By using microwave technology one can potentially avoid the problem of pyrolysis of the coal matrix by using sufficiently high energy densities so as to heat quickly for minimal heat loss to the coal, with the pyritic phase absorbing more electromagnetic energy than the rest of the coal matrix. This is due to the differences in the dielectric properties of coal and pyrite which is supported in the literature (Shuey, 1976; Marland et al., 2001. The magnetic susceptibility of pyrite improves on heating due to the conversion of FeS_2 to FeS, a strongly magnetic material (Maxwell et al., 1982). By changing all or even a small part of the pyrite (FeS_2) particle to a more magnetic mineral, (e.g. pyrrhotite, FeS) the economic and technical feasibility

of magnetic separation of pyrite from coal would be greatly improved. In previous studies, researchers have assessed the mechanisms and kinetics of pyrite transformation both in inert and oxygen-containing atmospheres at elevated temperatures. These studies have shown that depending on the atmospheric conditions, the transformation process will follow a multi-step process which can be described in the following way. In inert atmospheres, pyrite will proceed through a multi-step process in the sequence of pyrite $\rightarrow$ pyrrhotite $\rightarrow$ troilite $\rightarrow$ iron. The process is determined by temperature and the total sulphur gas pressure in the system (Hu et al., 2005). A proposed model for the transition of pyrite through to iron is discussed in detail in Chapter 4.

Experiments have shown that up to 80% of the pyritic sulphur can be removed using high gradient semi-conductor magnetic separator (15 Tesla) (Maxwell et al., 1982). It is well known that pyrite will couple with and heat rapidly in microwave field. It has also been reported that pyrite behaves like a semiconductor whose conductivity is around 1000 S/m (Shuey, 1976). Since pyrite has such a high conductivity it would suggest that pyrite will heat in a microwave field by conduction or surface heating (Al-Harasheh et al 2005). (The degree of selective dielectric heating obtained will be a function of the power absorbed by the pyrite and conduction of the heat away to the surrounding coal matrix). Weng, (1993) has shown that by exposing coal to microwave irradiation, localised heating occurs and pyrite will decompose according to the following reaction; $FeS_2 \rightarrow Fe_{1-x}S \rightarrow FeS$ or $FeSO_4$ ($0<x<0.125$). Much work has been carried out on the effect of microwaves on the magnetic properties of minerals. Work assessed by Birmingham

University has revealed that some minerals show dramatic change in magnetic susceptibility after microwave irradiation. They concluded that these changes may facilitate the possibility of magnetic recovery of some of these mineral phases from complex ores previously not considered suitable for magnetic processing.

Through dielectric measurements on coal and a selection of associated minerals, the principal heating sources can be identified.

Marland et al., (2001) demonstrated that the dielectric properties (dielectric constant and loss factor) depend largely on coal rank. However it was also suggested that the dielectric properties of coal were also affected by temperature and microwave frequency. It was found that a change in applied frequency exhibited no specific trends in the dielectric properties and that the change was so small, it was neglected in the conclusions.

Typically, dielectric measurements on UK coals have shown that the electric permittivity decreases with coal rank on a dry, mineral free basis. However the moisture and mineral matter content may increase the bulk permittivity. The effects of increasing aromaticity with increasing rank and thus changes in dielectric conductivity were not discussed. It was shown, however that most coal associated minerals such as quartz and mica were relatively transparent to microwave radiation and thus showed low dielectric properties. Pyrite showed higher dielectric properties than any other coal associated mineral tested. Thus, these properties gave an indication of the heating characteristics of the selected minerals and it was therefore expected that pyrite should heat readily in a microwave environment, with most other low loss materials exhibiting a lower heating rate. It was concluded that the principal heating sources within the coal were water (moisture) and

pyrite and that a substantial reduction in dielectric properties occurred between 80ºC and 180ºC due to moisture removal (Marland et al., 2001).

New Methods were described of sulphur removal from a Silverdale coal using microwave energy and exploiting the increased magnetic susceptibility of pyrite (FeS_2) for magnetic separation (Butcher et al., 1994). It was suggested that the magnetic susceptibility of pyrite improves on heating to temperatures in the region of 300ºC, due to the conversion of FeS_2 to FeS (pyrrhotite), a strongly magnetic material. Due to the significant differences in the dielectric properties of bulk coal and pyrite, one can selectively heat the pyrite phase, resulting in increased magnetic susceptibility without adversely affecting the physical properties of the fuel. The investigations were carried out at 2.45GHz in a 650W microwave heater. Initially the screened samples were subjected to microwave radiation for 30, 60, 90 and 120 seconds before magnetic separation. Magnetic separations on non-pretreated samples were also conducted to compare the effectiveness of microwave enhanced desulphurisation. For the tests carried out on non-pretreated samples, ash reduction was achieved, but little reduction was observed in total sulphur content. It was found that in the majority of cases the sulphur was concentrated in the 'cleans' (non-magnetic fraction). It was therefore assumed that the pyrite remained unaffected by the magnetic field through which it passes. Thus, since only ash is removed the percentage of total sulphur content in the clean product effectively rises. During this investigation no effort was made to either predict or measure the temperature of the pyretic phase during the heating process. Alterations in the overall magnetic

susceptibility of the coal were not measured and the chemical phases (hexagonal or monoclinic) of pyrrhotite were not identified.

The same results were also true where the samples were pre-treated by microwave energy at 2.45GHz and 650W prior the magnetic separation. Again the majority of the total sulphur remained in the product. Minimal sulphur reduction was reported in the majority of cases. It was assumed that the microwave pre-treatment did not facilitate the rise in temperature required for the $FeS_2 \rightarrow FeS$ oxidation reduction to occur. For experiments without pre-treatment, ash reductions of up to 33.5%, for -1000 + 500μm size fraction were achieved from a feed ash content of 33.57% to a non-magnetic fraction of ash content 22.32%, with a loss in calorific value of 15.68%. The majority of sulphur remained in the product fraction. It should be noted that laboratory bench-top scale experiments such as these, offer little insight into the practical and economic implications of an industrial scale process where a significant throughput is required.

An investigation into the amenability of Askale coal desulphurisation by magnetic separation following microwave exposure was carried out by Usla & Atalay, (2003). The investigation employed a 2.45GHz, 850W microwave unit. Again, it was found that direct magnetic separation with no pre-treatment did not reduce the pyritic sulphur content of the samples significantly. This trend was also evident in the microwave treated samples where it was assumed that insufficient enhancement of the pyrite to a high magnetic pyrrohtite caused minimum sulphur reduction by magnetic separation. Evidence of the transformation of pyrite to a magnetically enhanced form of pyrrhotite was not

investigated here. For non-treated samples, ash and pyritic removals were 15.79% and 22.29% respectively for -1500 micron particle size. After microwave treatment, pyritic sulphur removals were over 37% for -1500 micron fractions. To attempt to significantly increase the bulk temperature of the coal sample, magnetite was added, which is an excellent absorber of microwave energy and hence heats readily and rapidly by microwave radiation. This was hoped to increase the heating capacity of the pyrite in the coal and thus enable the conversion of FeS_2 to FeS. With the addition of only 5% magnetite, pyritic sulphur contents were reduced by as much as 55.11% by magnetic separation at 2 Tesla. A 21.54% decrease in ash content was observed along with 20.39% increase in calorific value. It was found that the amount of ash and sulphur removal, increased with decreasing particle size. An increase in calorific value can be explained by the decreasing ash content. Alterations of the magnetic susceptibility of the sample and the quantification of any pyrite to pyrrhotite phase change were not investigated. The problem associated with the use of low power microwaves is that it will inevitably necessitate high residence times to achieve sufficient temperatures for pyritic phase change to occur. The possibility of treating materials with microwaves for several minutes in a commercial process is unlikely, particularly if high volume throughput is required. It is also unlikely that doping the target load with a good microwave absorber such as magnetite will improve the efficiency of sulphur removal after treatment. Although the effects of doping may serve to increase the bulk temperature of the coal, it is unlikely this will be sufficient to achieve temperatures which allow pyrite transformation to take place. A significant increase in the bulk temperature of the coal is

undesirable and may adversely effect the physical properties of the coal after treatment. Fanslow et al., (1980) studied the dielectric properties of coal and pyrite which he used to predict heating rates. He suggested that the solution to successful magnetic separation was due to the fact that the dielectric properties of coal and pyrite were sufficiently different so that the pyrite will absorb more electromagnetic energy that and thus heat faster than the coal. Thus, a study was conducted to measure the dielectric properties of coal and pyrite and using this data, predict the degree of selective dielectric heating of pyrite in coal. Then the predicted results for heating rate can be compared with actual dielectric heating of mixtures containing coal and pyrite. Run-of-mine coal was separated by gravitational techniques into know fractions of 1.30 float (cleans) and 2.00 Sink (Pyrite and ash). The predicted values for heating rates suggested that pyrite and ash would heat 1.3 to 3.3 times faster than clean coal. The experimental results suggested that the pyrite and ash fraction was heated from 1.6 to 2.6 times faster than clean coal.

Huang et al., (2001) investigated the dielectric heating characteristics of pyrite and marcasite. It was found that microwave power level, crystal structure and particle size had an effect on the dielectric heating rates of the material. Marcasite exhibited a higher heating rate than pyrite, and the study found that marcasite was more readily decomposed than pyrite. Microscopic examinations and x-ray diffraction analysis showed that both materials were decomposed into pyrrhotite and elemental sulphur. The investigations concluded that microwave heating rate increased with increasing particle size and power level, and it was evident that marcasite had a higher heating rate than pyrite although the precise reasons for this remain unresolved.

Kingman et al., (2000) presented a review of the microwave treatment of minerals which considered many applications including fundamental heating rate studies, microwave assisted grinding, possible exploitation in the area of extractive metallurgy and also microwave treatment of coal.

Microwave assisted grinding results were good, with further work involving higher power levels and shorter exposure times required. The use of microwave energy in the desulphurisation of coal displayed potential which could soon become a commercial reality, allowing for the use of high sulphur coals on an environmentally and economically sound way. Researchers also considered the effect microwave radiation would have on the magnetic properties of minerals. Firstly, in a study of mineral heating rates, a clear link between heating rate and microwave power level was established. In general the heating rate increased with increasing power level. The heating rates for groups of minerals were classified into: group 1: minerals which exhibit a large change in temperature when subjected to microwave radiation of 2.45GHz; group 2: minerals which show a slight change in temperature when subjected to microwave radiation of 2.45GHz; group 3: minerals which show little change in temperature when subjected to microwave radiation at 2.45GHz. A correlation was also evident when looking at the optical properties of the test materials. It was stated that; group 3: poor absorber of microwave radiation and poor absorber of light refracted. Group 2: Medium to poor absorber of microwave radiation and can absorb much light but refract much back. Group 1: Excellent absorber of microwave radiation and an excellent absorber of light.

It was also shown that large changes in magnetic susceptibility are apparent after microwave treatment. The large changes in magnetism are consistent with chemical alteration due to microwave heating. Chalcopyrite, Ilmenite, Hematite and Wolframite, all exhibiting significant increases in magnetic susceptibility. However Bornite, Pyrrhotite and Magnetite all exhibited decreases in magnetic susceptibility. It was concluded that such changes in magnetic properties may facilitate the possibility of magnetic recovery of some of theses mineral phases from complex ores previously not considered suitable for magnetic processing.

3.8.2 Desulphurisation by Magnetic Separation

There are many forms of electrostatic separation techniques available to remove sulphur, in the form of pyrite from coal. It was reported that electrostatic separation has several advantages in coal cleaning. These were the ability to process fine particles (-45 μm), high separation efficiency, environmentally friendly and is a dry process.

Butcher et al., (1995) reviewed the electrostatic separation of pyrite from coal using a roll separator which uses the corona charging technique. The tests on Moira Pottery coal at various size fractions were carried out at ambient atmospheric conditions, with no feed heating, feed heating at 60ºC and feed heating at 100ºC. Other operating variables such as roll speed, feed rate, electrostatic potential and splitter plate positions all remained constant so that a direct comparison could be made. A potential of 20kV was adhered to where possible. The separation under ambient conditions gave ash reductions between 16% and 23.1%, and sulphur reductions between 10.6% and 15.4% over the size ranges tested. The treatment of coal under different atmospheres of CO_2, N_2 and compressed air

showed that ash reductions were quite improved at low relative humidity (30%) produced when treated in a compressed gas environment. Ash reductions of up to 50.64% was achieved in a compressed air atmosphere using -500+300 micron size range, compared to a reduction of 19.07% under ambient conditions on a similar size range.

Rowson et al., (1989) investigated the desulphurisation of coal by magnetic separation and highlighted that the magnetic susceptibility of pyrite increases on heating due to the physical alteration of pyrite (FeS_2) to pyrrohotite (FeS) which is a highly paramagnetic material. Pyrite and mineral matter in coal are very weakly paramagnetic and thus have a very small positive magnetic susceptibility. The organic part of the coal structure is diamagnetic and posses a negative magnetic susceptibility and is repelled from converging lines of flux in a magnetic field. It is possible theoretically to magnetically separate these materials although in order to capture a pyritic sulphur particle it is necessary to produce a strong field or high field gradient. It was reported that the reaction to alter pyrite to pyrrohtite occurs between 300ºC and 400ºC for mineralogical pyrite. However, previous research suggests that this reaction occurs at temperatures around 250ºC for coal derived pyrite (Bluhm et al).

Under conventional heating techniques, the temperatures needed for the phase change to occur would result in the combustion of the coal. However, by using the novel approach of microwave heating, only the pyritic phase will be heated as the organic coal; matrix is relatively transparent to microwave irradiation. The result is that the majority of the microwave energy is channelled into the pyrite producing high heating rates without overheating the bulk coal and affecting its calorific value. In experiments using

potassium and sodium hydroxide leaching slurries and subjecting that coal to microwave radiation for short period resulted in up to 60%-70% of sulphur removal, while the calorific value was found to drop between 4%-5% (Rowson & Rice, 1990).

Saeid et al., (1993) presented data demonstrating the effect of high gradient/high strength magnetic fields on UK coals. The experiments were carried out using high-intensity (HIW) magnetic separator and a permanent magnetic roll separator capable of producing exceptionally high magnetic field gradients. Total sulphur and ash removal was analysed after magnetic treatment plus X-ray diffraction and magnetic profile analysis provided identification of the mineral constitution of the ash fraction of the coal. The HIW trial presented gave successful results at reducing the ash content of the coal by max 25% after only one pass through the separator. This gave the concentrated magnetic fraction of 45%-50% ash. Sulphur removal was not observed during these trials. The dry magnetic separation trials removed both ash and sulphur from coal by 40% and 10% respectively. It was concluded that only ash was removed in the wet magnetic separation trials because any liberated pyrite itself does not have a large enough magnetic susceptibility to be removed.

Data regarding the performance of high gradient magnetic separation (HGMS) in removing mineral pyrite from coal was presented by Kelland et al., (1988). Separations were made on conventional 2-Tesla iron magnet separators. The work concluded that the physical enhancement of coal pyrite by selective heating by microwave radiation improves physical coal desulphurisation by HGMS technology and that microwave

radiation for short times at sufficient power facilitates the conversion of pyrite to magnetically enhanced monoclinic pyrrhotite.

3.8.3 Chemical Desulphurisation with Microwave Heating

Chemical coal cleaning separates impurities (sulphur bearing minerals) from coal by treatment of a variety of chemical products and processes. Ash removal from coal can be theoretically reduced by physical means such a magnetic separation or float-sink means.

Since 1979, there has been substantial investigations into the role of caustic alkali solutions (NaOH and KOH) in the microwave assisted desulphurisation of coals. Zavitanos, (1979) recognised that alkali caustic were very good microwave absorbers and referred to the removal pyritic and organic sulphur from coals in this context. Due to the heating of the caustic solution in sulphur rich areas, sulphur bearing compounds will readily decompose into water soluble sulphates and acids that can be washed out.

Andres et al., (1996) discovered that hydroiodic acid allowed sulphur to be removed from coal when used in a sealed reactor with a reducing atmosphere. Using concentrated hydroiodic acid as a desulphurising agent and microwaves as an energy source, sulphate and pyritic sulphur were completely removed in 10 minutes. In studies with low-rank coals, variable amounts of organic sulphur, up to 70% in 20 minutes were removed, with total sulphur elimination greater than 80%. It was discovered that the residence time and temperature were the deciding factors affecting the process. Experiments with other acid types of different concentrations showed poor sulphur removal yields. The concentration of the hydroiodic solution was the driving force behind the reaction. Variation of microwave power did not alter the effect of microwave irradiation on sulphur removal.

The dielectric properties of coal and aqueous NaOH solution were investigated by Yang et al., (1987) to determine a study of thermo-chemical desulphurisation by microwave energy. In this study, sodium hydroxide slurry was used as a media for irradiation. The coal samples were treated in a rectangular cavity with 2.45GHz microwave frequency. The results showed 70%-80% desulphurisation efficiency. The dielectric property tests on various coal leachant mixtures indicate that the dielectric loss of sodium hydroxide was very high compared to that of coal which was low. Thus the resulting conclusion was by adding a high loss solution such as sodium hydroxide one can enhance the ability of the coal to absorb microwave energy and heat rapidly. 70%-80% of total sulphur which contains >90% inorganic and 30%-70% organic sulphur can be removed with sodium hydroxide solution as a leachant, and irradiated by microwave energy at a frequency of 2.45GHz for 60 seconds.

It is known that weakly paramagnetic pyrite particles are difficult to remove from coal by using standard magnetic separation techniques. However, when coal is treated to caustic microwave leach pre-treatment, before dry magnetic separation, a significant increase in the removal of total sulphur is observed.

Butcher et al., (1995) carried out tests on non-treated samples and leached samples for sulphur removal comparison. The test carried out on non-treated samples achieved ash reduction but very little sulphur reduction when magnetic separation techniques were applied. In most cases the sulphur was still contained in the product (clean fraction). Similar results were obtained when treating the coal samples with microwaves alone. Again some ash reduction was achieved but little or no sulphur was removed by magnetic

separation. However, the tests conducted using a NaOH leach slurry in a microwave a considerable amount of success was achieved. Reductions of total sulphur were between 26.7% and 48.7% with losses in calorific value between 22.25% and 68.42%. Reduction in ash was as low as 14% in most cases. These results were fairly typical over all size fractions. Thus, it was concluded that the pre treatment of feed coal by microwave radiation using a sodium hydroxide media was successful in enhancing the magnetic susceptibility of pyrite and as such large amounts of sulphur removal was achieved by magnetic separation. This is due the NaOH ability to leach out some sulphur and the production of a magnetic pyrite product. It was noted however, that sulphur reduction in the samples were not altered by increasing the pre-treatment time. Only differences in calorific value losses and sulphur emission values were observed.

Rowson et al., (1990) investigated coal desulphurisation using low power microwave energy. The application of 500 watt 2.45GHz for the preferential heating of pyritic sulphur in high sulphur coals was investigated. The sole purpose of such experimentation was to facilitate a more magnetic pyritic phase to allow for low-gradient magnetic separation. It was found that although the pyrite in the coal was heated at a higher rate than the organic coal matrix itself the heating rates were not high enough the reach temperature necessary for the conversion of pyrite to pyrrhotite. This was mainly due to the low power microwave applicator employed in this investigation. However, when the coal was mixed with a strong caustic (KOH or HaOH) solution of concentration 300g/l at 20% solids, which are excellent microwave absorbers, a degree of heating was sufficient to enable desulphurisation to take place. Coal samples were screened to -212μm after

exposure to microwaves for 60 seconds, which were not significantly altered in character and varied with the degree of exposure and the concentration of the alkali. Once again the described mechanisms for sulphur removal by magnetic separation were the increased magnetic susceptibility of the pyritic phase within the coal matrix and the dissolution of both pyrite and organic sulphur which was washed out in the leach liqueur after treatment. Using this method of wet caustic microwave leaching gave total suphur reductions of up to 70% in some cases.

Chemical desulphurisation research using high sulphur coals which were treated by different heating and contacting procedures including an investigation into molten alkali hydroxides were discussed by Kusakabe et al., (1988). It was found that microwave irradiation was effective in the enhancement of the reaction of sulphur and ash with alkali hydroxides. The temperature of the molten caustic immediately after microwave exposure was 563K in the experiment. A critical amount of caustic had to be used in order to prevent spark discharge in the sample. The amount needed was 4-5 times larger than the amount needed for a reaction to take place. The lowest value for the caustic-coal ratio required was 0.3-0.4 for Illinois coal. The sulphur content of the coal was not significantly reduced for residence times greater than 60 seconds. The report also concluded that caustic-coal ratios should be kept minimal to reduce loss of coal in the wash stages.

Rhee et al., (1987) conducted bench scale trials to evaluate a continuous process for removing sulphur and ash from caustic treated coals using microwave energy. The majority of the work entailed the design and installation of a reactor system and then a

series of trial studies. Ninety five tests were conducted during the mid 1980s and the results indicated that the primary mechanism for coupling microwave energy with the coal slurry were by ionic conduction with the caustic and by absorption by the dipolar water molecules, not by the coal. The primary operating parameter in the studies for the reaction rate was the absorbed microwave power density. Some energy was lost in the system by conduction from the coal and the caustic material to the transport belt (in this case Nickel). Additional absorbed microwave energy was required to compensate for this loss. In addition, double pass runs were conducted and 30%-40% of sulphur was removed and 60%-86% of ash was also removed.

In a report produced by Rowson et al., (1990) outlining the reasons for the magnetic desulphurisation of coal after microwave irradiation in caustic slurry, X-ray diffraction, EDAX, ESCA and magnetic susceptibility studies were carried out on mineral pyrite and the magnetic concentrate from coal after leaching in NaOH. The report discovered that the magnetic desulphurisation of the pyrite content in coal after NaOH 300g/l leaching in the presence of microwave radiation was due to the formation of small amounts of a strongly magnetic phase, most probably pyrrhotite or magnetite and the loss of sulphur dissolved in the leach liquor of washing (sulphide and sulphate). Using x-ray diffraction, an attempt was made to identify any new phases present in the coal structure in the magnetic fractions after treatment. It was discovered that only a loss of crystallinity in the pyrite fraction was detected by extensive examination. However, when EDAX (energy dispersive X-ray Analysis), small sulphur deficient areas were discovered on the surface of the pyrite particles. These areas were discovered to have a 1:1 FeS atomic ratio rather

than 1:2 ratio associated with pyrite. ESCA (Electron Spectroscopy Chemistry Analysis also confirmed the presence of iron rich, sulphur deficient areas on pyrite particles).

Hayashi et al., (1990) demonstrated that the rate of desulphurisation in coal was promoted by exposure to microwave radiation with molten caustic slurry of NaOH and KOH. The role of the microwave process in this respect was investigated by the rate of penetration of the caustics into a porous body. This was measured by a graphite tip which was inert to the molten caustics. When the graphite tip was impregnated with surfactants by immersing in an aqueous alkaline solution, the penetration rate increased without microwave radiation. The desulphurisation rate of coal samples pre-treated by this procedure also increased without the use of microwaves. Such finding suggest that microwave irradiation facilitates the contact between coal and molten caustics, and that the rate determining step is not chemical reaction but mass transfer of the molten caustics into the matrix.

Ferrando (1995) treated coal in a sealed reactor with HI in H_2 with microwave heating for 10 minutes. 99% removal of pyritic sulphur was removed along with 70% removal of organic sulphur which was removed as H_2S and S. Extraction was then required to remove the free sulphur from the coal. Elsamak et al., (2003) confirmed that the microwave desulphurisation of coal was much faster than thermal treatment when leaching coal with concentrated HI, which is probably due to localised superheating effects (Al-Harahsheh and Kingman, (2007).

3.9 Conclusion

The potential application of microwaves to coal desulphurisation is suggested by many authors and scope for further research in this area is vast. A comprehensive literature review of the current "state of the art" in the area of microwave coal desulphurisation has been presented. It is clear that there are many methods employed for use in microwave desulphurisation (both physical and chemical reactions) with varying degrees of success. Some of the work has demonstrated that coal desulphurisation by magnetic separation through the magnetic enhancement of pyrite has potential, although the fundamental process of conversion of pyrite within the complex coal structure by a microwave field is still open for debate. Moreover, the effects of a particular microwave desulphurisation heating regime on the end product quality of material, in terms of its effect on the physio-chemical characteristics of coal have not been fully addressed. The majority of research conducted in the field of coal desulphurisation using microwave energy has been developed using small, low power units charged with small samples. The problem associated with the use of low power microwaves is that it will inevitably necessitate high residence times to achieve sufficient temperatures for pyritic phase change to occur. Therefore the possibility of treating materials with microwaves for several minutes for a commercial process is unlikely, particularly if high volume throughput is required. There is much scope for the use of high energy density microwave treatment at a high throughput to achieve a more favourable energy balance along with novel coal characterisation techniques to monitor the condition and coal quality after treatment and to quantify the effects of microwave interaction with the pyritic phases.

Chapter 4 - Decomposition & Oxidative Desulphurisation of Pyrite by Conventional and Microwave Heating.

4.1 Introduction

Pyrite (FeS_2) is an iron disulphide and is the most abundant of all metal sulphide minerals. Pyrite is ubiquitous in the earth`s crust and is present in significant quantities in some coals and many other minerals (Hu et al., 2006; Yan et al., 2008). The wide occurrence of pyrite in coal makes it the one of the main sources of SO_2 emissions from coal fired power plants and other industrial processes. SO_2 is formed when pyrite is oxidised in industrial processes (Hu et al., 2006). Previous research investigations have reported that pyrite (FeS_2) exhibits weak paramagnetic tendencies, with a very small, positive magnetic susceptibility. However, ferromagnetic tendencies have also been reported (Waters et al., 2007; Schneider et al., 2004; Male, 1980, 1984). It has been shown that upon thermal treatment, pyrite will undergo an oxidation process that will produce new phases which exhibit increased magnetic properties. The transformation of pyrite is complex and may proceed by different mechanisms under different experimental conditions. Previous research suggests that the whole process, in the sequence **pyrite → pyrrhotite → troilite → iron**, is determined by the surrounding atmospheric conditions at elevated temperatures and the total sulphur gas pressure in the system (Hu, et al., 2006). Consequently, a controlled thermal treatment process may increase the recovery of such minerals by magnetic separation (Water et al., 2007; Wills, 1985). The mineralogical alterations of pyrite upon thermal treatment and the subsequent increase in magnetic susceptibility will have obvious benefits when considering the removal of

sulphur from coal by magnetic separation. It has been shown by others that it is possible to oxidise sulphide minerals using microwave heating (Walkiewicz et al., 1988; Chen et al., 1984; Haque et al., 1999; Groves, 2007; Rowson and Rice, 1989; Waters, et al., 2008). The decomposition and oxidation of pyrite by microwave heating is one of interest when considering the benefits of desulphurisation in coal by magnetic separation, since conventional heating is likely to adversely affect the physio-chemical characteristics of coal, particularly at elevated temperatures.

Current understanding of pyrite oxidative decomposition is superficial and general. In this chapter the thermal behavior of pure pyrite will be investigated using both conventional roasting and microwave heating methods with a view to enhancing its magnetic susceptibility. The monitoring of any changes in the magnetic properties of the sample will be related to the potential removal from coal by magnetic separation.

4.2 Decomposition and Oxidation of Pyrite – A review

4.2.1 Pyrite and Pyrrhotite

Pyrite (FeS_2) is the most abundant sulphide found in coal. As such, its influence on the operational, economic and environmental performance of coal is significant. In most natural specimens of pyrite, the molar proportions of Fe and S are close to the ideal of 1 and 2 respectively. Since significant deviations from the 1:2 Fe to S ratio have not been reported, it would appear that natural pyrite is essentially stoichiometric. Marcasite, an iron sulphide polymorph, has the same chemistry as pyrite and identical features of local coordination but exhibits a different crystal structure (orthorhombic structure – see Figure 4.1).

Pyrite typically contains a host of minor trace elements which include Ag, As, Au, Bi, Cd, Co, Cu, Hg, Mo, Ni, Pb, Pd, Ru, Sb, Se, Sn, Te, Tl and Zn. (Abraitis, et al., 2004). Variation has been reported in the semi conducting properties of natural pyrite, which are either n-type or p-type, with conductivities varying by four orders of magnitude (0.02 – 562 $(\Omega\ cm)^{-1}$. The conductivity of p-type pyrites is in general much lower than that of n-type samples. However, pyrite commonly shows p-type and n-type properties or so called p-n-type behaviour (Abraitis, et al., 2004). Pyrite originating from high temperature veins has predominantly n-type conductivity whereas pyrite formed in sedimentary and lower temperature hydrothermal deposits has predominantly p-type conductivity. P-types are also known to have a positive thermal coefficient, making the form less resistant with higher temperatures (Abraitis et al., 2004, Rimstidt and Vaughan, 2003, Shuey, 1975). Since pyrite is a well known cubic disulphide mineral, the iron atoms are arranged in a

FCC (face centered cubic) array. Its arrangement is analogous to the NaCl structure, with the iron atoms occupying the sodium positions and the disulphide group occupying the chloride positions.

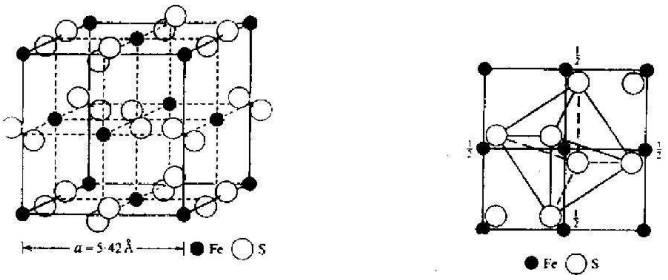

Figure 4.1 Simple cubic pyrite structure (Szargan, et al., 2001).

The transformation of pyrite to form pyrrhotite ($Fe_{1-x}S$) and other related decomposition products has been the focus of much research. The reported methods used for the oxidation of sulphides include, conventional roasting, smelting, bio-oxidation and electromagnetic heating (Hu, et al., 2006; Uhlig, et al., 2001, Belzile, et al., 2004, Rimstidt, et al., 2003; Dabrowski, et al., 2006, Chen, et al., 1986; Uslu and Atalay, 2004; Olubambi, et al., 2007; Nanthakumar, et al., 2007; Rowson and Rice, 1990; Yan, et al., 2008; Pysh'yev, et al., 2004, Boon and Heijnen, 1998, Dunn and Chamberlain, 1997). After pyrite, pyrrhotite is the most common sulphide found on earth. It is commonly found in hydrothermal deposits and volcanic rocks and deposits associated with pyrite (FeS_2), sphalerite ((Zn, Fe)S), galena (PbS) and chalcopyrite. ($CuFeS_2$) (Belzile, et al., 2004). Pyrrhotite can show a non-stoichiometric composition $Fe_{1-x}S$ with x varying from 0 to 0.125 or FeS to Fe_7S_8 respectively. It is an important sulphide waste mineral in many mining environments and is often found as a gangue

mineral in Cu – Ni deposits, associated with valuable minerals. Fe-deficient forms of pyrrhotite have monoclinic symmetry whereas the least Fe-deficient forms show hexagonal and orthorhombic structures. Monoclinic pyrrhotite is ferromagnetic at room temperature and can hold a strong remanent magnetism (Becker, et al., 1997).

4.2.2 Current state of the art.

4.2.2.1 Decomposition and Oxidation by Conventional Heating

An assessment of the mechanisms and kinetics of pyrite transformation in inert and oxygen-containing atmospheres at elevated temperatures has been extensively investigated by Hu et al., 2006. This body of work investigated parameters such as temperature, particle size, flow conditions and properties of the surrounding atmosphere to see how they affect the transformation process and the subsequent nature of the transformed product. The transformation of pyrite in an inert atmosphere follows a multi-step sequential process **(pyrite → pyrrhotite → troilite → iron)** depending on the total sulphur gas pressure in the system and temperature. The thermodynamic properties of this process have been investigated by a number of researchers (Hong, et al., 1998; Barker and Parks, 1986; Toulmin and Barton, 1964). According to Toulmin et al, under equilibrium conditions, the composition of pyrrhotite from pyrite decomposition will be determined by temperature in an inert atmosphere. The research concluded that at elevated temperatures, pyrite will decompose to form pyrrhotite and sulphur gas when the sulphur gas pressure is lowered to the corresponding equilibrium pressure of the system. Under equilibrium conditions, the sulphur content in the formed pyrrhotite (x) will be

determined by the temperature. The process was described by the following overall reaction;

$FeS_2 \rightarrow FeS_x\,(s) + (1\text{-}0.5_x)S_2\,(g)$

The dependence of 'x' moles of S per mole of Fe in FeS_x on the decomposition temperature of pyrite shown in Figure 4.2 was created by using an empirical polynomial equation developed by Hu et al., 2006).

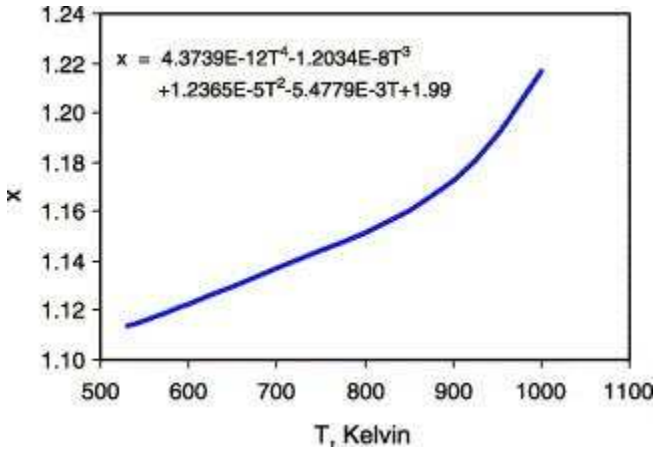

Figure 4.2 Correlation between x moles of S per mole Fe in pyrrhotite on the decomposition temperature of pyrite.

According Lambert et al., 1998, if the total sulphur gas pressure in the system is lowered from the equilibrium state, then the pyrrhotite formed from the decomposition of pyrite will continue to release sulphur gas and will result in pyrrhotite of lower sulphur content. However, practically, there will be a gradient of the partial pressure of sulphur gas across the formed pyrrhotite layer due to the diffusion of the formed sulphur gas. Thus, as a consequence of this gradient, the partial pressure of sulphur gas in the pyrrhotite layer will not be at equilibrium and will cause further decomposition of the pyrrhotite layer before the pyrite is completely decomposed. Research by Fegley and Lodders, 1995 and

Lambert et al., 1998 has identified two phases of pyrrhotite in partially decomposed pyrite particles. The deviation of the partial pressure of sulphur gas from the equilibrium pressure is a reasonable explanation for their observations. A continuation of this process will form FeS and if the sulphur gas pressure is lowered further, FeS will decompose to form elemental iron. Pyrite has an incongruent melting point of around 1016K under normal conditions which is also the maximum decomposition temperature of pyrite (since pyrite cannot exist at a temperature that is higher than its incongruent melting point). In an inert atmosphere and at its incongruent melting point, pyrite will decompose to form pyrrhotite and a sulphur-rich liquid (Hu, et al., 2006).

The kinetics of pyrite decomposition have been studied by a number of authors (Hong and Fegley, 1998; Fegley and Lodders, 1995) who observed that the decomposition of pyrite progressed with a boundary between the pyrite and the forming layer of pyrrhotite. This so called '*unreacted core'* model demonstrated that the decomposition reaction of pyrite → pyrrhotite takes place at the interface of the unreacted solid core. This 'reaction front' can be observed using the SEM picture shown in Figure 4.3 below.

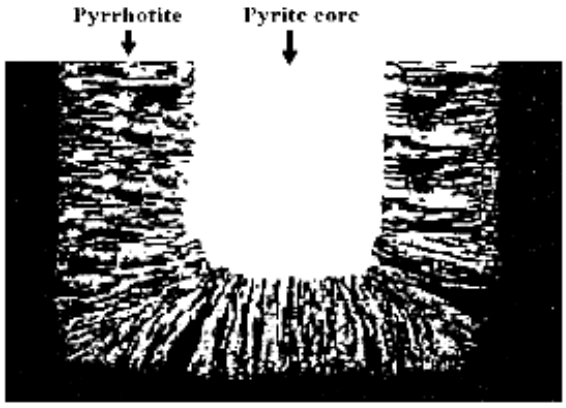

Figure 4.3 Partially decomposed pyrite particle showing the porous pyrrhotite layer surrounding a solid pyrite core (Hu, et al., 2006).

It was observed that with time, the 'reaction front' moves inwards towards the centre of the solid pyrite core with the whole reaction process being controlled by gas film/product layer diffusion. However, the influence of the heat transport resistance to the 'reaction front' through the gas film/product layer was deemed to be a significant influence on the reaction. For example, when considering large particle sizes, the particle temperature may be significantly lower than the temperature of the main gas phase due to heat transport resistance (under certain heating conditions). Hu, et al., (2006) suggested that the pyrite core temperature will not increase proportionally with the increase in the gas phase temperature since the heat transport to the core increases linearly with the temperature differential, whereas the reaction rate increase exponentially with increasing temperature. This will result in a lower reaction rate than would be expected under equilibrium conditions and could lead to an under estimation of the activation energy if this difference was neglected (Hu, et al., 2006). The temperature gradient between the particle temperature and the gas phase explained the existence of a solid pyrite core at temperatures higher than its melting point. Fegley and Lodders (1995) reported that pyrite from different geological locations and settings (e.g. hydrothermal and magmatic deposits) showed no difference in decomposition rates between samples and no effect from their minor impurities. Boyabat, et al., (2003) studied the thermal decomposition of pyrite in a horizontal tube furnace in the temperature interval 673K to 1073K in a nitrogen atmosphere using particle samples ranging between 0.5 to 1.3mm. This work concluded that the conversion rate was significantly influenced by the gas flow rate,

temperature and particle size. Essentially, the process was influenced initially through the heat transport through the gas film layer.

The transformation process of pyrite in oxygen-containing atmosphere is somewhat more complex and has been studied by a number of authors (Dunn, et al, 1989, Fegley & Lodders, 1998, Waters, et al., 2008, Hu, et al., 2006). It has been reported that under oxygen-containing atmospheres, pyrite will decompose to form a number of final products. These include Fe_2O_3 (hematite), Fe_3O_4 (magnetite), $Fe_2(SO_4)_3$, $FeSO_4$ (iron sulphate) and SO_2 (Sulphur dioxide). In the case of direct oxidation, the overall reaction sequence (according to Hu et al., 2006) will be:

$$2FeS_2(s) + 5.5O_2(g) \rightarrow Fe_2O_3(s) + 4SO_2(g)$$

It was observed that the decomposition of pyrite an oxygen-containing atmosphere is influenced by reaction conditions, such as temperature, oxygen concentration, particle size and the gas flow conditions with the overall transformation taking place in two ways. This is consistent with the observations made by Jorgensen and Moyle, (1982) who performed pyrite oxidation in air using simultaneous DTA (differential thermal analysis) and TGA (thermogavimetric analysis) with a 10K/min heating rate on particles 0.053-0.074mm in diameter. Observations made using SEM (scanning electron microscope) and XRD (X-ray diffraction) show that the pyrite was directly oxidised to form hematite at a temperature <803K. At higher temperatures however, pyrrhotite was formed as an intermediate, which then successively oxidised to form hematite (as in an inert atmosphere). This process is shown in the SEM picture in Figure 4.4.

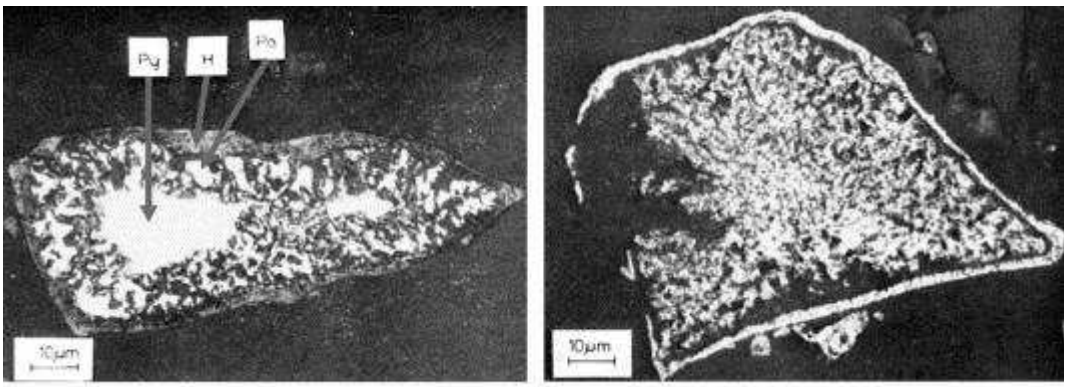

Figure 4.4 SEM pictures illustrating the oxidation of pyrite particle (53-74μm) in an oxygen-containing atmosphere (Hu, et al., 2006). (Adapted from Jorgensen and Moyle, 1982)

Figure 4.4(a) A partially reacted pyrite particle with an unreacted core (PY). A porous pyrrhotite (PO) layer can be seen with a rim of hematite (H) surrounding the particle.

Figure 4.4(b) A completely oxidised pyrite particle with two parts of different texture, showing a rim due to the direct oxidation of the pyrite particle at the earlier heating stage and the inner part from the oxidation of the pyrrhotite (note that the inner part of this particle has maintained the texture of the pyrrhotite that was formed from the thermal decomposition of the pyrite).

In the study performed by Jorgensen and Moyle (1982), the phases were preserved by quenching the sample in liquid nitrogen at different stages of the reaction. Results from DTA and TG traces were used to identify 'positions' of significance (heat effects and mass loss) so that quenched specimens could be produced for characterisation. The initial predictions made by Jorgensen and Moyle were as follows; (a) hematite would be formed directly on the pyrite surface below temperatures of 677K, whereas at higher temperature magnetite would intervene; (b) pyrrhotite would be stable above 825K; (c) ferrous and

ferric sulphates would be formed in the outer layers at temperature below 856K and 917K respectively. They noted however, that there was much controversy about the nature of the phases formed during oxidation since agreement as to the intermediate phases was far from unanimous. Using sensitive thermal analysis techniques to provide information on weight changes and heat effects accompanying oxidation, and developing a suitable quenching technique to preserve the phases, pyrrhotite was positively identified above 803K and at higher temperatures a narrow rim of sulphate was detected towards the outer edge of the ferric oxide layer (using microprobe analysis). Also, they reported that pyrrhotite was an intermediate oxidation product above 803 – 823K with oxides formed via pyrrhotite having a porous structure giving oxygen freer access to the unreacted sulphide allowing a more intense reaction to occur.

The literature associated with the thermal behaviour of a number of mineral sulphides was appraised by Dunn, et al., (1997) where particular attention was paid to the importance of experimental variables on the thermal analysis results together with the importance of correctly characterising the material before treatment (as well as any intermediate products which are formed during the process). The decomposition of pyrite was studied at different oxygen concentrations and by using DTA and TGA analysis techniques. XRD analysis was then used to identify the reaction products. The experiments were performed on two particle sizes (<0.045mm and 0.09 – 0.12mm) Observations made with the smaller (<0.045mm) particle size shows that at a heating rate of 2.5 K/min in air, pyrite was directly oxidised to hematite. This oxidation was

completed at around 773K (shown as an exothermic peak on the DTA trace). Upon SEM examination of the samples, the results indicated that the oxidation reaction process occurred according to shrinking core model whereby the overall rate of reaction is controlled by oxygen diffusion through product coatings. It was shown by Dunn, et al., that if the heating rate is sufficiently slow (that is sufficient time is allowed), then the pyrite particle will be completely oxidised by this mechanism.

With the larger pyrite particle size (0.09 -0.12mm) and a heating rate of 2.5 K/min in air, they observed that the sample directly oxidised to form hematite at a temperature lower that 783 K. This was evident upon SEM examination of the sample, where a well-defined rim of oxide was formed around a core of unreacted pyrite. Above 783 K the appearance and character of the particles changed such that the inner core now had a porous structure, indicative of gas evolution. This phenomenon was also evident in the small particles (<0.045mm) when subjected to higher heating rates (40 K/min). Dunn, et al., (1997) concluded that for the larger particles at the higher heating rate, the reaction sequence proceeds by two different mechanisms. Firstly, up to 773 K the reaction mechanism is controlled by oxygen diffusion through the surface product layer. This was evident in an exothermic peak on the DTA trace due to the direct oxidation of pyrite to hematite (Fe_2O_3). After the initial oxide rim has been formed the oxygen diffusion is retarded and slows rapidly. Combining this with the high heating rate and large particle size ensures that the reaction is nowhere near completion even at temperatures as high as 783 K. Beyond this temperature pyrrhotite is formed as an intermediate due to the decomposition of pyrite from sulphur diffusion outwards as opposed to oxygen diffusion

inwards. During the direct oxidation of the pyrite, sulphates were observed at the product layer making this layer less porous due to the large molar volume of the sulphates. Dunn, et al., (1997) reported that no further oxidation is evident until all the sulphur has been evolved. The sulphur burns at the surface of the particle and the resulting pyrrhotite becomes porous. This then allows oxygen diffusion into the particle and the pyrrhotite is rapidly oxidised further through to hematite.

Hansen, (2003) studied the transformation of pyrite in an entrained flow reactor in an atmosphere containing 5% oxygen and at a temperature of 520°C. The particle size used in the experiment was 0.032 – 0.064mm and the residence times for the particle in a reactor was 3sec. Subsequent SEM analysis on the particles showed that the particle had partially reacted showing a porous pyrrhotite layer with an unreacted pyrite core. Further EDAX (Energy dispersive X-ray microanalysis) also showed a rim of Fe_2O_3 at the surface of the particle. These observations pointed to evidence that it was thermal decomposition rather than direct oxidation of the pyrite. Henson (2003), suggested however, that the hematite rim may have been formed at the initial stage of heating by direct oxidation of pyrite or may have formed during the later stages of the process due to the simultaneous oxidation of the pyrrhotite. An SEM picture of a partially reacted pyrite particle is show here in Figure 4.5.

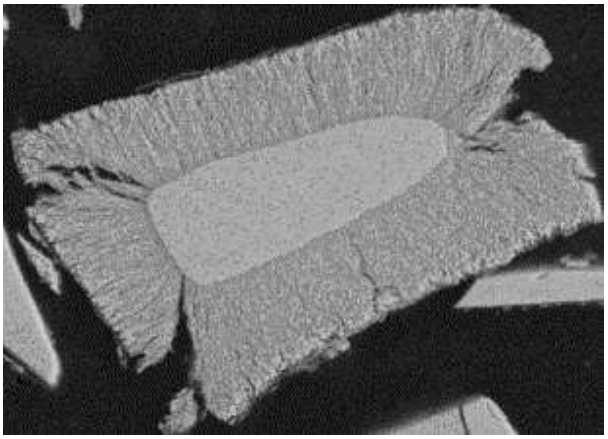

Figure 4.5 Partially reacted pyrite particle (0.06mm particle size)(Henson, 2003).

The transformation of pyrite powder by roasting on a porcelain crucible in air was investigated by Prasad, et al., (1985). At a temperature of 610°C it was noted that pyrite initially decomposed to pyrrhotite. The formed pyrrhotite was then oxidised to form other oxides. The existence of pyrite, pyrrhotite and hematite/magnetite was evident in the later stages of the process, an indication that simultaneous thermal decomposition of the pyrite followed by the oxidation of the formed pyrrhotite had taken place. It was observed that hematite was the final oxidation product with a small amount of magnetite present before the completion of the oxidation reaction.

The identification of magnetite in the oxidation products has been reported by a number of authors (Brink, et al., 1996; Hubbard, et al., 1984) with others (Prasad, et al., 1985; Srinivasachar, et al., 1990; McLennan, et al., 2000). In some cases magnetite has been found to be the dominant oxide in conditions where hematite should be the stable oxide. Brink, et al., studied the mechanisms of slag formation by minerals from coals rich in pyrite. Under the oxidising conditions in the superheater and at a temperature of about 1473K the presence of both hematite and magnetite were identified.

Groves, et al., (1987), Huffman, et al., (1989), and McLennan, et al., (2000) studied the oxidation of pyrite in a drop tube furnace. In an atmosphere containing 5% oxygen and at temperatures of 1311 – 1727K Huffman, et al., observed that magnetite was dominant across the whole temperature interval. However, it was found that with increased residence time in the furnace the fraction of hematite increased. This was most significant at the lowest furnace temperature (1311K). Groves, et al., found that in an atmosphere containing 2% oxygen and at temperatures lower than 1073K, hematite was the dominant oxide. They found that magnetite began to form at temperature higher than 1073K and 1223K in an air atmosphere.

In an experiment performed by McLennon, et al., in a drop-tube furnace at temperatures of 1573 – 1873K it was observed that magnetite/hematite and pyrrhotite were present in the oxidation products and in the case of reducing atmospheres, only wustite and magnetite were identified in the oxidation product.

Hu, et al., concluded, based on a comprehensive literature review, that oxygen deficiency at the reaction front favours the formation of magnetite/wustite, which may be caused, in practice, by relatively fast reaction rates (e.g. oxidation pyrite/pyrrhotite) and/or slow oxygen diffusion rate at the reaction front under specific conditions. An increase in hematite formation with increased oxygen concentration observed by others supports this theory with experimental parameters such as temperature, particle size, residence time and gas flow conditions also affecting the formation and nature of the oxides. This theory is also shared by Schwab and Philinis, (1947) who performed pyrite oxidation by the thermogravimetric method in air at 673 – 773K. Again it was concluded that the

oxidation process was controlled by oxygen diffusion through the product layer. However, they observed that the formation of ferric sulphate towards the outer surface of the particle had a pore blocking effect that would retard oxygen diffusion through the gas layer and eventually cause a complete cessation of the oxidation process. The resulting formation of sulphates (mainly ferrous sulphate – ($FeSO_4$) and ferric sulphate $Fe_2(SO_4)_3$)) will result in mass gain and volume increase since the molar weights and molar volumes of both ferrous and ferric sulphates are higher than those of pyrite and iron oxides. The formation of ferrous and ferric sulphate upon the oxidation of pyrite has also been observed by others (Enroth, et al., 2003; Jorgensen and Moyle, 1982; Allen, et al., 1995; Cole, et al., 1987).

From such observations as discussed above, Hu, et al., (2006), proposed a general model to illustrate pyrite transformation in an oxygen containing atmosphere. The proposed model can be seen in Figure 4.6.

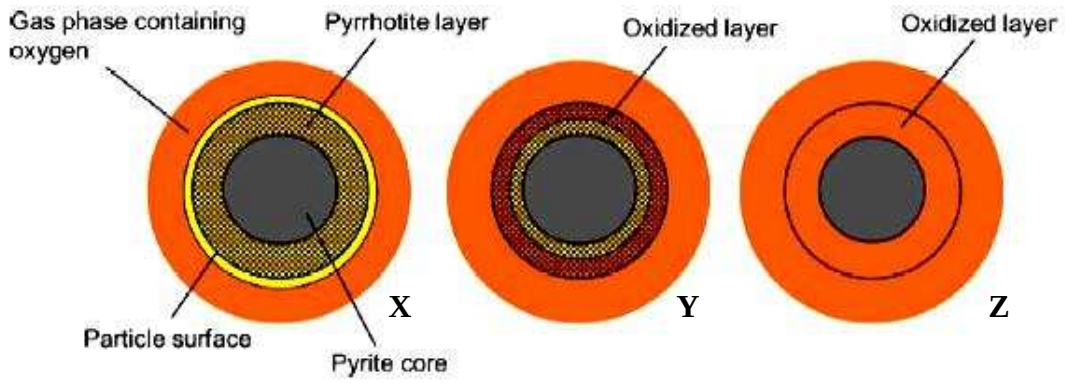

Figure 4.6 Pyrite transformation in an oxidising atmosphere (Hu, et al., 2006)

The model proposed by Hu, et al., can be interpreted in the following way;

Model X :- Pyrite does not come into contact with oxygen and undergoes thermal decomposition, as in an inert atmosphere consistent with observation made by Hong and Fegley (1997). In this case, the diffusion of sulphur gas from the reaction front will consume all oxygen (as in high temperature low oxygen concentration). The pyrrhotite formed will not oxidise further until the pyrite has fully decomposed allowing oxygen to penetrate through the reaction front.

Model Y :- In this case, oxygen has contact with the surface of the particle. However, in the situation where the reaction temperature is not very high and the oxygen concentration relatively high, the pyrrhotite formed will be directly oxidised alongside the gas phase oxidation of S to SO_2.

Model Z :- In this case, oxygen is in direct contact with the core of the particle allowing the pyrite to be oxidised directly. For this to occur, the oxygen concentration must be high and the temperature must be low. Evidence of a hematite layer surrounding a solid pyrite core observed by Jorgensen and Moyle (1982) and Dunn, et al., (1989) could be due to this process (Hu, et al., 2006). This direct oxidation could, to a certain degree, occur in the case of model **X** & **Y** during the first stage of the heating process. However, in practice, the direct oxidation of the core may be retarded if the oxygen transportation is restricted inwards by a denser iron sulphate product formed by the outward diffusion and oxidation of sulphur gas. Therefore, the mechanism for direct oxidation is limited where high heating rates are present (assuming the oxidation of sulphur gas is infinitely fast) (Hu, et al., (2006).

According to the model presented by Hu, et al., the key controlling factors that will influence the sequence of the overall transformation process are as follows;

(a) Thermal decomposition of the pyrite will only take place if the oxygen transport through the gas film is retarded either by the formation of pore blocking iron sulphates-or-Oxygen transport to the reaction front through the gas film is slower than that needed for the oxidation of sulphur gas generated by the decomposition of the pyrite (i.e. oxygen is consumed before it reaches the reaction front).

(b) Direct oxidation will take place if the oxygen transport through the gas film/product layer is faster than that needed for the oxidation of the sulphur gas released. This will then allow oxygen to penetrate through the gas/product layer to the unreacted pyrite core.

(c) Oxidation of the formed pyrrhotite phase can be vigorous (in the case of X & Y) at high temperatures and O_2 concentrations (Dunn, et al., 1991,1992,1993).

(d) The pyrite particle will remain in a solid state until it has been fully decomposed in a combustion environment. Even at temperature of up to 1427°C, the high thermal decomposition rate of the pyrite will cause a large temperature gradient between the pyrite particle and the main gas phase. The large endothermic enthalpy change as a result of this process will mean that the pyrite particle will not reach its incongruent melting point of 743°C (Jorgensen and Moyle, 1982; Dunn, et al., 1989).

There are clear experimental variables, such as heating rate, partial pressure of oxygen, particle size, sample pan geometry and composition, all of which may have

an impact on the overall oxidation reaction and therefore such procedural differences must be reported in any experimental investigation. Changes in the thermal mass and conductivity of the sample will alter the temperature of key thermal events and so any results reported must be analysed extremely carefully if one is to draw a credible hypothesis.

Dunn, et al.(1997) reported that changes in experimental variables can result in a complete change in the reaction mechanism and produced TG-DTA traces which were totally different to one another to prove this point. They reported that when using sample pans to heat the pyrite with geometry to give good gas exchange between the sample and the atmosphere (i.e. wide and shallow) then the phases present will tend to be the higher oxidation states of iron, namely Fe_2O_3 and $Fe_2(SO_4)_3$. If the crucible is shaped such to inhibit gas exchange between the particle and the atmosphere (i.e. tall and narrow causing oxygen deficiency) then the phases present will tend to be the lower oxidation states of iron, namely Fe_3O_4 and $FeSO_4$. Jorgensen and Moyle (1982), demonstrated that the rate of oxidation of pyrite decreases by about half as the wall height for the crucible increases from 2 to 4mm. The experiment used silica crucibles with large open cross sectional areas.

Having recognised the significance of alterations in the combinations of these variables, Dunn, et al., (1997), discussed the use of predominance diagrams for predicting the phases likely to be found during an oxidation process. Moreover, identification of certain phases may be used to make some assumption about the composition of the gas phases above the sample. The predominance diagram for the iron sulphur system is shown in Figure 4.7. The diagram is a log-log plot of the

sulphur partial pressure along the x-axis and the oxygen partial pressure along the y-axis. The bottom left-hand corner of the diagram is an area of low partial pressure of sulphur and oxygen (an area where the metal is thermodynamically stable). The sulphides are stable in high sulphur concentrations and the sulphates are stable in high concentrations of sulphur and oxygen. The dashed lines on the diagram indicate the partial pressure of sulphur dioxide and the effect that changes in this value has on the phases produced. Reports that identify Fe_3O_4 as a product is most probably an indication of oxygen deficiency to the reaction front (Jorgensen and Moyle, 1982).

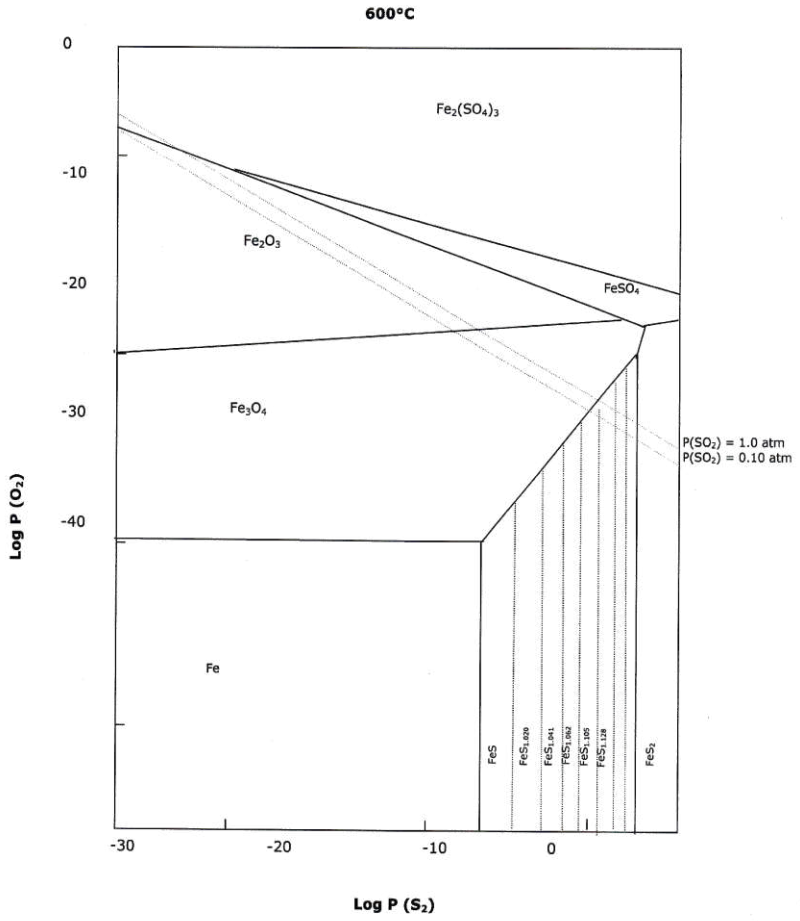

Figure 4.7 The Iron-Sulphur predominance diagram at 600°C

+

The temperature at which oxidation of pyrite commences can vary considerably, as indicated by Table 4.1 (taken from Dunn, et al., 1997).

Formula	Mineral	Reaction temperature (°C)	Reported product	Reference
FeS_2	Pyrite	380	FeS, SO_2	Jorgensen and Moyle, (1984)
		400	FeS, S	Schorr and Everhart, (1969)
		445	Fe_{1-x}, SO_2	Paulik,*et al., (1982)*
		500	$FeSO_4$, SO_2	Banerjee, (1976)
		420	Fe_2O_3, SO_2	Jorgensen and Moyle, (1982)

Table 4.1 Reported onset oxidation temperatures of pyrite (Dunn, et al., 1997).

Waters, et al., (2008), investigated the effect of thermal treatment on the magnetic properties of Peruvian pyrite by heating 50g of <125μm size particles in air using a small Carbolite muffle furnace for 1hr. Over the temperature range 373K to 1273K, the samples were analysed using XRD and SEM/EDS (Energy Dispersive Spectrum) instruments to detect phase changes induced by oxidation. The mass of each sample was recorded before and after treatment and calculated theoretical mass changes as a result of phase alterations compared well with experimental observations. A summary of the phases detected by XRD analysis in presented in table 4.2.

Formula	Mineral	Reaction temperature (°C)	Reported product
FeS_2	Pyrite	100	FeS_2
		200	FeS_2
		300	FeS_2
		400	FeS_2, $Fe_{1-x}S$
		500	FeS_2, $Fe_{1-x}S$
		600	FeS_2, $Fe_{1-x}S$
		700	FeS_2, $Fe_{1-x}S$, Fe_3O_4
		800	α-Fe_2O_3
		900	γ-Fe_2O_3
		1000	γ-Fe_2O_3

Table 4.2 Mineral phases detected by XRD analysis after thermal treatment. (Adapted from Waters, et al., 2008).

4.2.2.2 Decomposition and Oxidation by Microwave Heating

The investigations discussed so far have been concerned with the thermal decomposition and oxidation of pyrite (and associated minerals) using a conventional means of heating only. However, much research has been published on the use of novel microwave heating in attempt to decompose sulphide minerals efficiently and selectively.

The dielectric properties and heating characteristics of sulphide minerals have been investigated previously (Huang and Rowson, 2000; Rowson and Rice, 1990, Harrison, 1997; Chen, et al., 1984; Husk and Seehra, 1978). The work has shown that in general, sulphide minerals readily couple with microwaves and can be heated to high temperatures very quickly. It has also been reported that pyrite behaves like a semiconductor whose conductivity is around 1000 S/m (Shuey, 1975). Since pyrite has such a high conductivity it would suggest that pyrite with heat in microwave field by conduction or surface heating (Al-Harasheh et al 2005). Furthermore, studies have also shown that some minerals intrinsically associated with sulphide minerals are relatively transparent to microwave radiation. Preferential microwave heating has shown to be advantageous in attempting to liberate and recover (thermally induced fracturing or magnetic property enhancement) valuable minerals in an energy efficient manner (Jones, et al., 2005 & 2007; Whittles, et al., 2003; Salsman, et al., 1995; Uslu and Atalay, 2003; Kingman, et al., 2004; Al-Harahsheh, et al., 2005; Marland, et al., 1998; Haque, 1998; Vorster, et al., 2000).

Huang and Rowson, (2001) investigated the heating characteristics and decomposition of pyrite and its polymorph (marcasite) using novel microwave heating techniques.

A 1.5kW mono-mode microwave device was used to heat 5g pyrite samples with a particle size of 125 - 250μm in an atmosphere of nitrogen. Microscopic examination of the heated product showed that the pyrite and marcasite decomposition developed according to the unreacted core model and XRD analysis confirmed that both pyrite and marcasite had been converted into porous pyrrhotite. The decomposition fraction increased with prolonged microwave exposure time. However, the results showed that marcasite was more readily decomposed than pyrite when subjected to microwave radiation, which is likely to be as a result of differences in crystal structure, suggesting pyrite is more stable. This may also explain why, like other authors, marcasite showed a higher heating rate when compared to pyrite due to its thermal instability. The experimental results also showed that the heating rate for both pyrite and marcasite increased with increasing particle size. The effect of temperature on the dielectric loss factor was also attributed to the higher heating rate of the course samples, however, this was not quantified.

The use of microwave energy to facilitate the comminution of ores has been investigated by a number of authors (Walkiewicz, et al., 1991; Sahyoun, et al., 2004; Jones, et al., 2007, 2005; Salsman, et al., 1995; Kingman, et al., 2004; Whittles, et al., 2003). Ores of interest will contain minerals which will absorb microwave energy contained in a low absorbing gangue matrix. Conventional comminution processes (crushing and grinding) are very energy-intensive where bulk thermal pre-heating is required. Microwave heating offers advantages in this respect, not least because the heating will only take place in absorbing phases within the bulk material and heating rates can be much higher than

conventional heating with relatively small energy input. This kind of differential heating occurs within a material because each phase will have different absorbing properties or different dielectric properties (permittivity and loss factor).

A feasibility study using short-pulsed microwave energy as a pretreatment step in comminution was carried out by Salsman, (1995). A theoretical and experimental thermomechanical analysis was carried out on the effects of microwave power density and particle size of a single pyrite particle in a calcite host matrix. To enable a better understanding the microwave absorption characteristics of fine particles, high absorbing materials were mixed in varying proportions to non-absorbing minerals to simulate selected ores. Each 100g mixture was exposed to microwave radiation for 120s using a 1kW multi-mode cavity. The effects of sample composition and absorbing mineral particle size on microwave absorption and heating rate were noted. It was demonstrated that the mass of the sulphide mineral present in the mixtures was directly proportional to the heating rate of the bulk sample. Furthermore, the heating rate was influenced by the absorbing mineral particle size. This behavior is rationalised from volume/surface area properties and thus the heat transfer effects. The laboratory tests also verified rapid, selective heating of the pyrite particle within the calcite matrix. The simulations developed also predicted that intense bursts of short-pulsed microwave energy will heat the trapped pyrite particle but not the surrounding gangue. Simulations made here, also predicted that, with large microwave power densities, large thermal gradients will develop at grain boundaries, resulting in large thermal stresses. Thus, it was calculated that the high tensile stresses induced from the thermal gradient at the grain boundaries

would far exceed the tensile strength of common rock materials. However, the temperature gradient (and tensile stress) between the absorbing mineral and host rock were reduced as the absorbing mineral particle size reduced. It was noted, however, that for a low microwave energy density (10^{10} W/m^3) the heating rate in the absorbing particle was relatively slow. This permitted the thermal diffusion of heat to the surrounding calcite host material. Therefore, a steady state scenario developed where the pyrite particle did not reach the required temperature for breakage or phase alteration to occur as heat is given up to the surrounding calcite. Salsman, (1995) found that by increasing the energy density by two orders of magnitude (10^{12} W/m^3), the timescale over which significant temperature in the absorbing material occurred shortened substantially. In this case a temperature differential of 300K was observed between the pyrite particle and the calcite matrix in just 40ms. A further increase in energy density by two orders of magnitude, (10^{14} W/m^3) resulted in a timescale in the microsecond to reach significant temperature gradients. One can conclude that with very large energy densities, the calcite will remain close to its initial temperature and is influenced very little by the high temperature of the pyrite particle over short time intervals.

Groves, (2007) investigated the opportunities to use microwave energy to aid the magnetic separation of iron sulphide impurities from talc ore. Details of the magnetic properties of iron sulphide minerals will be discussed in detail later in this chapter. The rapid, selective heating of pyrite occurred due to the differences in the dielectric properties between the absorbing pyrite and the relatively transparent talc ore host material.

Initially, a set of test experiments were designed to asses a suitable heating regime (power level and exposure time). The tests involved artificially mixing museum grade pyrite with high grade talc. The tests were designed such that 25g of varying grain sized pyrite (±600μm to +38μm) was mixed with 1kg of high grade talc. Then the artificial samples were treated in a cylindrical, fluidised microwave cavity. The cavity was fluidised with 40%O_2 and 60% N_2 gas preheated to 100°C. After 30sec of exposure at 3kW the evidence taken from SEM analysis showed that the microwave energy had indeed coupled with the pyrite and limited oxidation had taken place. In some cases the particle had been affected only on one side of the grain. An example of this is shown in Figure 4.8.

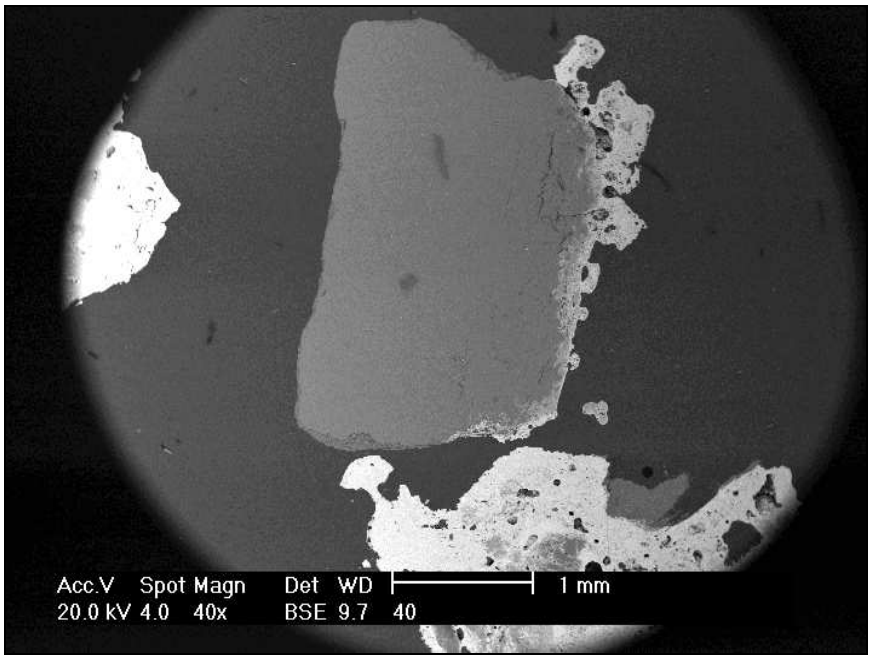

Figure 4.8 Showing a pyrite particle subjected to 3kW microwave power for 30s. (Groves, 2007).

SEM analysis of the pyrite grain, shown in Figure 4.8 reveals that the pyrite had only been affected on the left hand side (shown as a lighter shade) and has been oxidised directly to hematite. In contrast, however, analysis on other grains showed rather more uniform heating had taken place with both pyrrhotite and hematite being formed around the edges of the particle leaving a solid pyrite core only. An example of this can be seen in Figure 4.9.

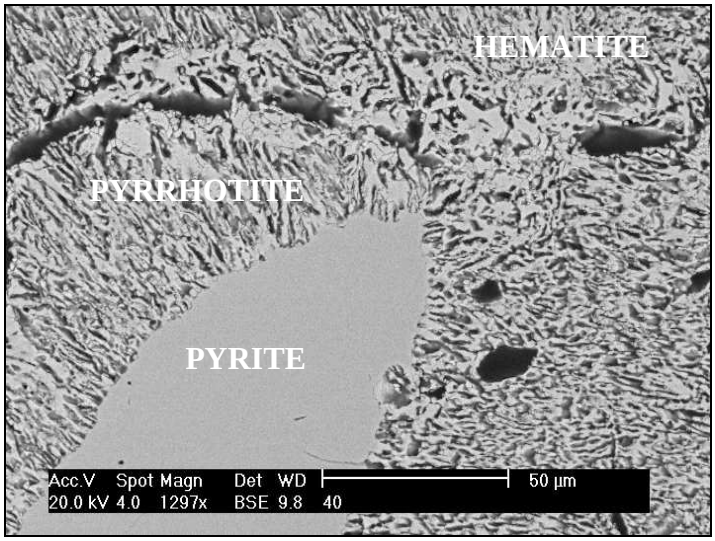

Figure 4.9 Showing a pyrite particle with porous pyrrhotite and hematite surrounding an unreacted core treated at 3kW microwave power for 30s. (Adapted from Groves, 2007).

Other particles also showed complete circumferential oxidation to pyrrhotite after treatment. The overall results demonstrated that pyrite in talc could be treated successfully with microwave energy and that partial oxidation is likely to occur under these experimental parameters. However, due to the fact that the samples were artificially manufactured by doping talc with pyrite and also the oxygen atmosphere

was likely to be in direct contact with the particle (due to fluidization), it is not possible to conclude that this experiment would have the same impact on 'as-received' talc ores, where the iron sulphide particles are likely to be locked within the host matrix. No assessment was made as to the effect of particle size on the degree of oxidation. The fact that not all particles were affect in the same way may have been due to electric field patterns within the cavity or insufficient gas distribution through the bed.

In a study to enhance the magnetic susceptibility of pyrite in coal using microwave heating, Uslu and Atalay, (2003) used a domestic variable power multi-mode microwave cavity to treat 12.5g of sample at varying size fractions in air. The initial experiments involving post-treatment magnetic separation were deemed unsuccessful and so the coal sample was doped with magnetite (a good microwave absorber) in an attempt to increase the bulk temperature of the sample and so facilitate the correct conditions for pyrite to oxidise to form pyrrhotite. Also, with magnetite addition the magnetic separation of iron sulphide from coal increased, however, no comment was made as to the transformation of pyrite to other iron sulphide species. However, in a later experiment by the same authors, using similar microwave equipment, XRD patterns and chemical analysis were used to identify the products formed after treatment. The predominant species identified were pyrite, pyrrhotite, α-hematite and γ-hematite. The microwave experiment was conducted again with sample treated in nitrogen. However, the XRD product analysis post-treatment revealed that no hematite was present in any sample. It was noted, in both experiments, that the heating rate and the maximum attained bulk

temperatures were achieved with increasing microwave power and decreasing particle size. The maximum bulk temperature attained was 850°C. It is unclear as to what form of pyrrhotite was formed in these tests (monoclinic or hexagonal). The use of small scale low power domestic microwave appliances is a disadvantage in these tests since it is unlikely that the pyrite particle will reach the desired temperature to facilitate a phase alteration. Moreover, the increased residence time required to reach suitable temperatures makes the process extremely inefficient. The lack of magnetite detected in the air treated products by XRD analysis is consistent with the fact that magnetite is reported to be formed at a higher temperature and less available oxygen compared to hematite (Hu, et al., 2007; Rimstidt and Vaughan, 2003; Scott, 1974).

The use of microwave energy to pre-treat double refractory gold ore was investigated by Nanthakumar, (2007). Double refractory gold ore contains carbonaceous matter and pyrite and the former results in the loss of gold from solution during cyanide leaching. One remedy is to conventionally roast the ore and thus oxidise the pyrite and remove the organic carbon. Nanthankumar investigated the use of microwave heating as an alternative to conventional roasting and compared the results for each heating method. The samples were treated in a variable power (max 700W) multi-mode microwave device at 2.45GHz. Samples weighing 50-100g were placed in a quartz crucible supported by an alumina platform located in the centre of the cavity. The samples were microwaved for 5min and then removed to allow for slow cooling in air. This procedure was repeated 15 times under the same conditions (75min total exposure for each sample). The samples were treated at power settings of 30%, 50%, 70% and 100%. The experimental conditions

for the conventional treatment consisted of roasting a 75g ore sample placed in a fireclay crucible and held at a temperature of 580°C for processing times of 1.15, 3, 6, 9, 12, 18 and 26hrs. The as-received ore sample was characterised using SEM and XRD analysis and showed the major components to be quartz, dolomite, pyrite and muscovite. TGA(DTGA) analysis in air showed that roasting temperatures of 650°C were required to convert the pyrite to hematite and to eliminate the organic carbon. Nanthakumar, et al., 2007 noted that using direct microwave heating the minimum roasting temperature of 650°C could not be achieved to oxidize the pyrite and to eliminate the carbon. This was partly due to the fact that the sample sizes were too small (heat loss decreasing as sample size increases). The maximum temperature achieved in the microwave test was 630°C and thus total carbon and sulphur contents were little affected. However, with conventional roasting, the heating was for more uniform than microwave heating and the samples were able to reach the critical recovery temperature eliminating carbon and converting pyrite to hematite. Even though the products were characterised before and after treatment using SEM and XRD techniques, it is unclear as to whether the pyrite was completely oxidized to hematite or whether any intermediate products were found (e.g pyrrhotite).

4.2.2.3 Magnetic Properties of Iron Sulphides.

Iron sulphides are present in magmatic, metamorphic and sedimentary rocks. Greigite (Fe_3S_4) and monoclinic pyrrhotite (Fe_7S_8) are ferrimagnetic and so are able to carry permanent magnetisation. On the other hand, pyrite (FeS_2) and hexagonal pyrrhotite

(Fe_9S_{10}) are paramagnetic at ambient temperature and so will exhibit magnetisation only when in the presence of an external field. Paramagnetic materials are those having permanent atomic dipoles, which are acted on individually, and are temporarily aligned in the direction of the externally applied magnetic field. Since the magnetisation is very small, paramagnetic materials are considered to be non-magnetic. However, their alterations during heating imply the appearance of magnetic materials. As such it is important to recognise these magnetic changes and phase transformations in order to better identify suitable conditions where magnetic enhancement is required. It is well understood that pyrite, after differential thermal analysis, changes during heating in air into iron oxides. The nature of these iron oxides will of course depend on temperature and environmental conditions (gas pressure and oxygen concentration) as discussed in detail earlier. The exothermal transformation of pyrite to hematite in air can be observed with a high resolution DTA trace and will occur in several steps starting at about 440°C and finishes at about 540°C (Bollin, 1970). However, as discussed earlier, if conditions are such that oxygen exchange is impeded then other intermediate product can occur (e.g. pyrrhotite). Magnetic susceptibility is a common parameter used to measure how easily a material can be magnetised. It is defined as the ratio of the induced magnetisation to the applied magnetic field and is thus dimensionless. It has been reported that the magnetic susceptibility of pyrite improves upon heating due to its conversion to its neighbouring sulphide pyrrhotite ($Fe_{1-x}S$ $0<x<0.125$)(Rowson, 1986). Table 4.3 shows the apparent magnetic susceptibilities of pyrite when 1% of it is converted into the compounds of iron indicated.

Compound Present	Apparent Suceptibility (x 10^6 cgs emu per gram)
Iron, Fe	159
Cementite, Fe_3C	103
Magnetite, Fe_3O_4	101
Gamma-Hematite, γ-Fe_2O_3	104
Monoclinic Pyrrhotite, Fe_7S_8	22
Melanterite, $FeSO_4 \cdot 7H_2O$	1.2
Alpha-Hematite, α-Fe_2O_3	0.4
Pyrite, FeS_2	0.3

Table 4.3 The apparent magnetic susceptibilities of a composite pyrite particle (Adapted from Uslu and Atalay, 2003).

Tudryn and Tucholka, (2004) monitored the magnetic responses of natural pyrite during thermal treatment. After identification by XRD analysis, the samples were submitted to Curie balance experiments. Three pyrite samples were heated to 700°C for 25min, 1hr and 2 hrs. The thermomagnetic behaviour of the samples was determined on a horizontal force translation balance (Curie balance) in atmosphere, in a magnetic field of 0.375 Tesla. The experiment was designed such that the sample temperature increased linearly from ambient with immediate linear cool back. The thermomagnetic behaviour of pyrite at ambient before heating showed a typical paramagnetic response and hence presented a very low magnetization. However, upon heating to 440°C the magnetization of the sample increased up to 540°C. After 540°C the magnitisation fell sharply to almost 0 at 580°C. After this critical point on the heating cycle the magnetisation does not increase further up to 700°C. Upon cooling (for samples heated quickly) the magnetization of the sample increases significantly. Once again this increase in magnetization starts at about 580°C on the cool back cycle. It was noted by Tudryn and Tucholka, (2004), that for samples heated slowly (2hrs) the magnetisation during cooling was much lower than

those heated relatively quickly (25min, 1hr). The experiments show that pyrite altered to magnetite during heating. This happened between 400°C and 540°C. The degree of alteration depended largely on the experimental conditions, particularly the residence time of the sample in the furnace. Moreover, given the fact that the degree of alteration is largely based the time of the heating process, then the oxidation would continue towards a more oxidized form of iron oxide (maghematite and then hematite). The thermomagnetic traces from pyrite heated in air for 25min, 1hr and 2hrs is presented in Figure 4.10 (a), (b) and (c) respectively.

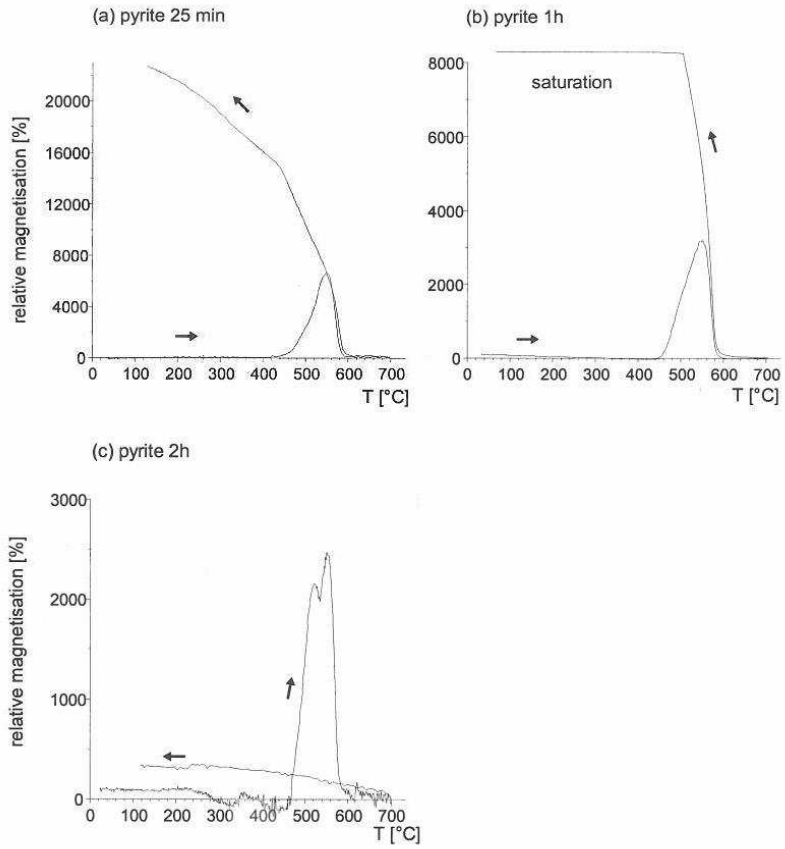

Figure 4.10 Thermomagnetic heating and cooling curves for pure pyrite. (Adapted from Tudryn and Tucholka, 2004).

It is unclear as the whether pyrrhotite or other intermediate products were detected in these experiments during the heating cycle. The fact the pyrite oxidised to magnetite before subsequent oxidation to hematite is indicative of an oxygen deficiency that would, under normal circumstance, have lead to the direct oxidation to hematite. Gas exchange to the sample may have been limited/impaired due to the sample holder geometry, however, these important details were not discussed in the published work.

Waters, et al., (2008) studied the effect of thermal treatment on the magnetic properties of pyrite. Milled and screened pyrite (<125μm) was representatively sampled in 50g batches and then heated in a conventional muffle furnace for 2hrs at set temperatures, ranging from 100 to 1100°C. Characterisation of the samples was conducted at each temperature increment using XRD and SEM/EDS analysis. Theoretical mass changes due to pyrite oxidation were calculated and corresponded well with changes in the mass observed using DTGA. For example $FeS_2 \rightarrow FeS$ would result in an overall mass decrease of 27%. Similarly, $FeS \rightarrow Fe_3O_4$ would result in an overall mass decrease of 35.7%. Characterisation of the untreated pyrite using EDS techniques showed that the ratio of sulphur to iron was 2:1, with no impurities detected which was consistent with the phases detected by XRD. The characterisation of the sample heated to 800°C using EDS and XRD analysis showed the presence of hematite. A saturation magnetisation of 900 A m^{-1} was recorded for untreated pyrite, using a vibrating sample magnetometer. It was noted that this value indicates a degree of ferromagnetism. It was suggested by the authors that this is perhaps due to small amounts of impurities in the sample, although no

such impurities were detected by EDS/XRD investigations, which is probably because the volume fraction of any impurities is likely to be outside the detection capabilities of XRD. However, evidence of such ferromagnetic behaviour was reported by Male, (1980, 1984) who speculated that a small amount of surface oxidation impurity (magnetite or low-temperature monoclinic pyrrhotite) could be responsible for the ferromagnetic anomaly observed. The magnetic properties of the new phases formed upon heating were displayed using magnetisation hysteresis curves for each sample. Waters, et al., (2008), reported that the magnitude of the magnetisation only started to increase (from less than 1kA m^{-1}) with samples treated to temperatures above 400°C. At this point both pyrite and pyrrhotite phases were detected by XRD analysis. Maximum magnetisation in the samples occurred at 700°C (~60kA m^{-1}) where pyrite, pyrrhotite and magneitite were detected by X-ray diffraction. It was reported that the magnetisation of samples treated to temperatures >700°C, <800°C decreased dramatically. This was due to the formation of antiferrimagnetc hematite (α-Fe_2O_3). Hematite is much less magnetic than pyrrhotite, magnetite and maghematite (Martinez, et al., 1999). Once the temperature increased above 800°C, the magnetisation of the sample increased due to formation of ferromagnetic maghematite (γ-Fe_3O_4). The formation of maghematite at this temperature is in agreement with other work (Sahyoun, et al., 2003), however, in order for new phases to be detected using XRD analysis the new phase needs to be greater than 5% of the bulk volume of the sample. It is possible therefore that the onset of each new phase in the transition of pyrite through to hematite may have started to occur at a lower temperature

than those reported here. Figure 4.11 shows the mineral phases detected by XRD analysis after the thermal treatment if pyrite taken from Waters, et al., (2008).

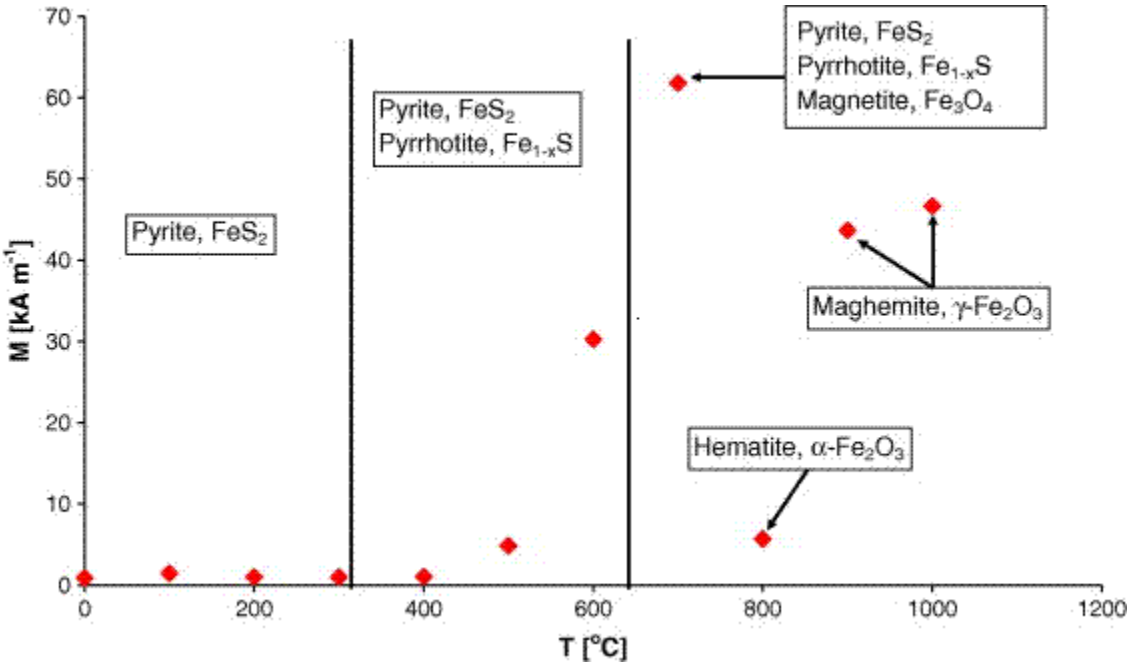

Figure 4.11 XRD detected phases and corresponding magnetisations in the transformation of pyrite upon thermal treatment in air. (Waters, et al., 2008).

After treatment at 600°C, the magnetic recovery increased from 23% (untreated) to 94% after treatment using a high intensity wet magnetic separator set at 0.7T.

In an experiment using microwave heating to alter the magnetic properties of pyrite, Waters, et al., 2008, used a multimodal 1900W and 2.45GHz microwave unit to heat 50g samples, split into two size fractions. XRD analysis was performed on untreated pyrite which shows no other discernable phases present. After 150s microwave exposure the XRD trace showed slight alterations, however, no new phase was obviously detected using this method. This was attributed to the fact that any possible new phases formed by

microwave heating may have been so small as to be below the threshold for the XRD equipment sensitivity. Problems associated with determining phase change alterations by XRD after microwave treatment was also reported by Sahyoun, et al., 2003. Other techniques have been employed to measure the oxidation of pyrite, such as SEM analysis (Groves, 2007) and X-ray photoelectron spectroscopy (Mattila, et al., 2004). Nonetheless, magnetic recovery of pyrite was improved by its exposure to microwave radiation. Even though identification of any phase alteration by XRD analysis was inconclusive, the magnetic recover rate increased with increasing microwave exposure time, from 25% untreated to a maximum of 88%. The increased magnetic recovery corresponded well with alterations in the magnetisation of pyrite detected using a vibrating sample magnetometer (VSM) device. Magnetic saturation occurred at 0.4T for untreated pyrite compared to 0.5T for the treated samples.

Groves, (2007), investigated the opportunities for the magnetic separation of iron sulphide from talc using microwave heating to enhance its magnetic susceptibility. The talc samples were treated in a fluidised bed microwave cavity with a maximum power output of 3-15kW at 2.45GHz. The samples, which were riffle split into four size classes (<5.6mm, <2.0mm, <1.0mm, <0.6mm), were treated in the fluidised cavity for 120secs at an operating power of 3kW. After treatment the samples were screened into individual size classes using a standard $\sqrt{2}$ sieve nest. The samples were then tested for total sulphur content, wet and dry magnetic separation, SEM analysis and heavy liquid density separation. The sulphur content in the treated and untreated samples showed a great deal of inconsistency with negligible differences in the finer size fractions. Groves, (2007)

suggested that this was due to the fact that the pyrite particle were intrinsically locked within the talc matrix preventing oxidation. This theory was supported by SEM data which showed fine grained pyrite (>2μm) hosted in the talc matrix. There was little evidence that oxidation had taken place as a result of microwave heating on the smallest pyrite grains. Magnetic analysis of the untreated 'feed' samples showed a large magnetic component. Groves, (2007) summarised that pyrrhotite must have existed in the sample before microwave treatment and could be removed with the application of a modest magnetic field. However, no significant increase in the magnetic susceptibility was recorded in the treated sample, possibly as a result of pyrite entrapment within the talc host. Another possibility discussed was that if oxidation had taken place (preferentially in the courser pyrite fractions) the conversion may have been to paramagnetic pyrrhotite (hexagonal crystal structure). The enhancement of magnetic properties versus particle size did not factor in the separation of magnetic and non-magnetic fractions.

The potential application of microwave energy for hydrometallurgical technologies has been studied by a number of researchers (Huang and Rowson, 2002; Rowson and Rice, 1989; Al-Harahsheh et al., 2005 & 2006, Xia and pickles, 1999; Olubambi et al., 2007; Al-Harahsheh and Kingman 2004; Zavitsanos, 1978 and 1979). For example, high pressure oxidation is the commonly applied hydrometallurgical technology in the pre-treatment of refractory gold ores. Other areas of particular interest are the extraction of copper from chalcopyrite (Al-Harahsheh, et al., 2005 & 2006) and the hydrometallurgical decomposition of pyrite and marcasite (Huang and Rowson, 2002). A review of several

authors work in this area have concluded that the application of microwaves can in fact reduce energy costs and enhance mineral surface chemistry to improve recovery yields.

4.3 Experimental Investigation.

4.3.1 Analysis Techniques

A defined experimental program is described here which investigates the conditions required to magnetically enhance pyrite upon heating using both conventional (furnace) and microwave energy heating techniques. In order to establish and measure accurately the outcome of this investigation program a number of standard analysis techniques have been used to characterise each sample before and after the heat treatment regime. This includes XRD analysis, thermogravimetric analysis (TGA), differential scanning calorimetry (DSC), vibrating sample magnetometry (VSM), scanning electron microscopy (SEM), mineral liberation analysis (MLA). A brief description of the analytical equipment used is given here.

4.3.1.1 X-Ray Diffraction

Historically X-ray diffraction (XRD) has been used for investigations to identify atomic and molecular arrangements in solids and plays an important role in the quest to develop new materials. Other uses for x-rays include qualitative and quantitative chemical identifications, residual stress determination, crystal size and crystallographic orientations. XRD analysis is a fast and reliable technique which has been used for routines mineral identification. X-rays are a form of electromagnetic radiation that have high energies and short wavelengths (wavelengths in the order of atomic spacing for

solids). A beam of X-ray directed on a crystalline material may experience diffraction (as a result of its interaction with atomic planes). A portion of the incident beam will be scattered in all directions by the electrons associated with each atom or ion than lies within its path. Using simple mathematical expressions which relate the x-ray wavelength (λ) and interatomic spacing (d) to the angle of the refracted beam (θ) → λ=dsinθ [Bragg`s Law], diffraction patterns can be developed. These patterns can be used to determine crystal structure, where the unit cell size and geometry may be resolved from the angular positions of the diffraction peaks. The arrangement of atoms within the unit cell is associated with the relative intensities of the peaks. A typical diffraction pattern for polycrystalline α-iron is shown in Figure 4.12 below.

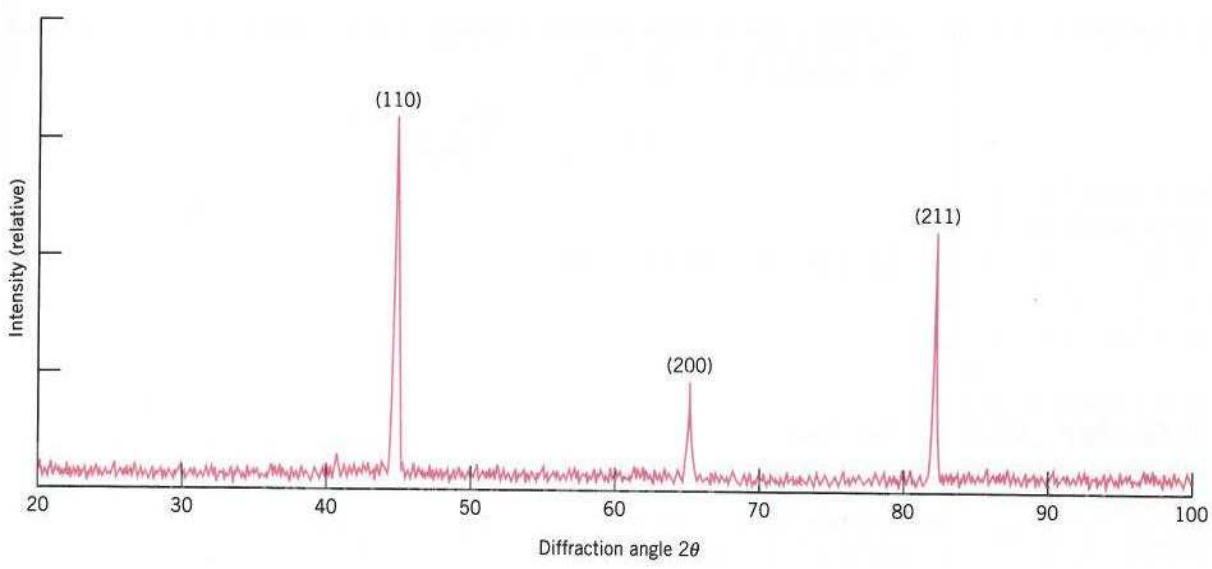

Figure 4.12 XRD pattern for polycrystalline α-iron with (h,k,l) atomic plane indices.

The results presented in this report were produced on Hiltonbrookes 3kW generator operating at 40kV and 20mA. The results were processed using “Traces V3” software.

Representative samples were finely ground to a uniform particle size to ensure that all possible crystallite orientations are present in the sample and then are mounted on flat-plate aluminium samples holders. The deffractometer control and data acquisition is handled through a dedicated PC.

4.3.1.2 Thermogravimetric Analysis.

Thermogravimetric analysis (TGA) is a technique principally used to determine weight loss with temperature. The analyser usually consists of a high-precision balance loaded with the sample which sits in a small sample pan (ceramic or platinum). The sample is placed within a small electrically heated tube furnace perturbed with a thermocouple to measure temperature during operation. The atmosphere within the furnace may be purged to prevent undesired reactions at normal or reduced pressures. Static or dynamic atmospheres of inert or reactive gasses (with gas switching facility) may be injected into the furnace when required via a software controlled gas station. Temperature heating and cooling rates (along with scanning rate) may also be controlled.

The equipment used for this work is a Pyris 1 Perkin Elmer TG analyser with auto-ampler carousel and simultaneous gas analysis detection equipment. The operating temperature of the equipment is -20°C to 1000°C with scanning rates of 0.1°C/min to 50°C/min. Small samples (<5g) were riffle split into representative batches after sieving and roll crushing. Sub-samples of this (split using a Quantachrome micro-riffler to <0.2g) were then loaded into ceramic sample pans and mounted in the automatic carousel. Heating and cooling rates, along with gas injection were controlled via a standalone PC and Pyrite Player Control software.

4.3.1.3 Differential Scanning Calorimetry

Differential Scanning Calorimetry (DSC) is a thermoanalytical technique used to measure the energy necessary to establish a near zero temperature difference between a material and a reference substance, both of which subjected to identical temperature regimes and environmental conditions where both heating and cooling rates are precisely controlled. There are two types of technique used for such systems are;

(1) Power Compensation DSC and (2) Heat Flux DSC.

The equipment used for this work is a TA-DSC TA-SDT Q600 simultaneous DSC TGA instrument. The main application of DSC is in the study of phase transitions (melting, glass transitions etc.) or exothermic decompositions. The operating temperature of the equipment is ambient to 1500°C. Small samples (<5g) were riffle split into representative batches after sieving and roll crushing. Sub-samples of this (split using a Quantachrome micro-riffler to <0.2g) were then loaded into ceramic sample pans and mounted on the horizontal balance. Heating and cooling were performed in static air during all experiments. Heating and cooling rates were controlled via a PC and TA Player Control software.

4.3.1.4 Scanning Electron Microscopy / Mineral Liberation Analysis

Microscopic examination of a material specimen is a tool of fundamental importance in this study. Scanning Electron Microscopy (SEM) is the examination of the surface of a material which is scanned with an electron beam and the reflected (back-scattered) beam of electrons is collected. This is then displayed (at the same scanning rate) on a CRT. Essentially, the image represents the surface features of the specimen. The surface of the specimen may or may not be polished, however if the specimen is electrically

nonconductive, metallic surface coating must applied. SEM instruments (along with other accessory equipment) permits qualitative and quantitative analysis of the elemental composition of assemblages, material textures and particle size and geometry.

The development of sophisticated SEM-based image analysis methods have advanced rapidly over the last 10 years. Measurement times have been greatly reduced and texture resolutions can now be submicron. Using advanced image analysis techniques, particles can be identified, separated and the mineral grains within can be delineated for discreet X-ray analysis in order to determine mineralogy. Routine analysis and automated elemental quantification are assisted by automated standards collection (standards library) which enables the target mineral to be identified. Analysis of a sufficient number of particles to obtain a statistically valid set of data is of primary concern, which in turn motivated the new generation of automated SEM technology.

The Mineral Liberation Analyser (MLA) is an SEM-based mineral measurement tool which combines BSE (Back Scattered Electron) image analysis and X-ray mineral identification instruments.

High resolution images are essential for valid mineral identification. This then allows the MLA to accurately discriminate between mineral phases within a particle. The MLA will use two types of image analysis functions for phase identification/discrimination. These functions are (1) Phase Segmentation and (2) Particle De-agglomeration.

In the first instance samples will be prepared before presentation to the SEM. This will usually involved mounting representative (of the bulk) particulate or powdered samples onto a wax or epoxy resin hardened block (~30mm dia). The particles may be defined to

a narrow size fraction beforehand. The block is then carefully ground and subsequently polished and lapped to a fine finish exposing a representative cross-section of particles. . In order to avoid the build-up of electric charge in the sample (electrons accelerated at the insulating sample do not conduct away from where they are absorbed) it must be coated with a small amount of conductive material e.g. Carbon, Gold and Platinum. The most common methods employed to produce a thin conductive layer is sputter or Evaporation coating. In this scheme of work evaporation coating is used by heating the conductive material (carbon rods) in a vacuum chamber until it evaporates and settles on the sample. It is inevitable, particularly with fine powder (<10μm) samples, that particles will touch each other when mounted on a sample block. This agglomeration of particles will, if not addressed, result in biased liberation results. The MLA system used here has a de-agglomeration function that will detect agglomerates and separate them either by (1) Shadow identification, (2) linear feature recognition or (3) a dilation procedure. These functions and their weighting can be controlled by the operator who should asses the correct or most appropriate procedure for the sample under examination.

The MLA system will identify all distinct mineral phases present in the sample once individual particles have been recognised. The process will define phase boundaries accurately and is performed on all particles. The system will also identify areas and regions of homogeneous grey level within the BSE image and assign a grey level value to it. Each grey level will correspond to a mineral of unique average atomic number (AAN). The number of back-scattered electrons omitted is directly proportional to its grey level

registered in the BSE image. Shading, cracks and voids will not be represented as an independent phase if the correct method phase segmentation is used.

Once each phase has been segmented (using the grey-scale histogram), it is assigned a unique colour. An example of a tessellated BSE image, an unclassified false colour and classified false colour image is shown in Figures 4.13, 4.14 and 4.15 respectively.

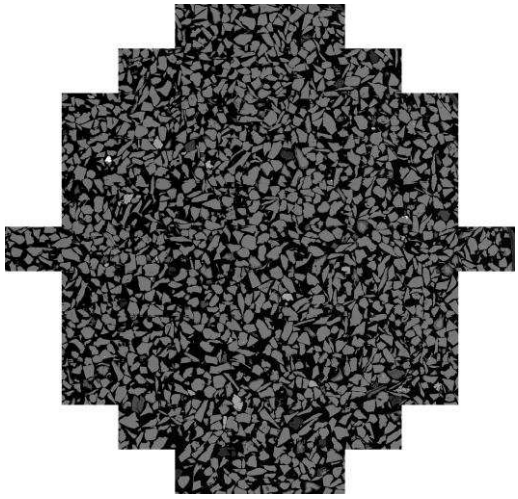

Figure 4.13 An example of a tessellated BSE image of +425μm treated pyrite (x86mag).

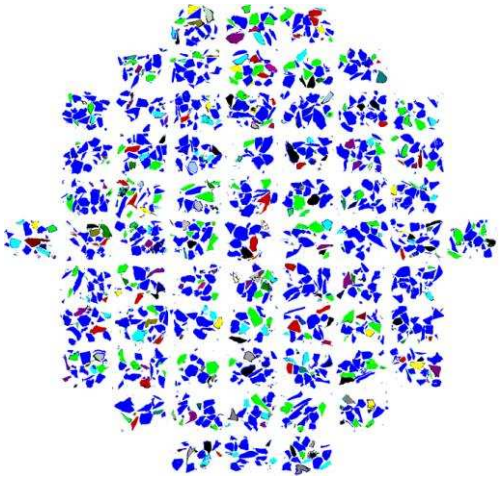

Figure 4.14 An example of a tessellated unclassified false colour image of +425μm treated pyrite (x86mag).

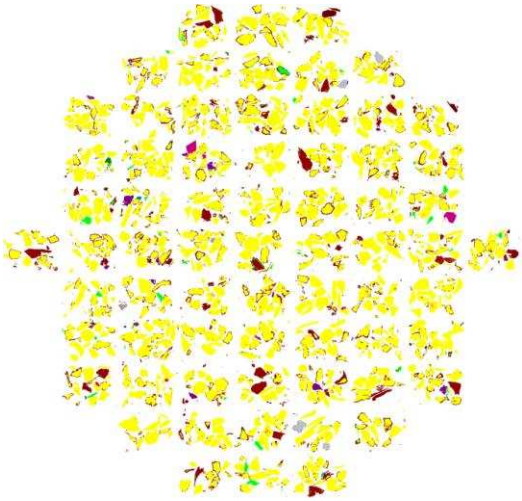

Figure 4.15 An example of a tessellated classified false colour image of +425µm treated pyrite (x86mag).

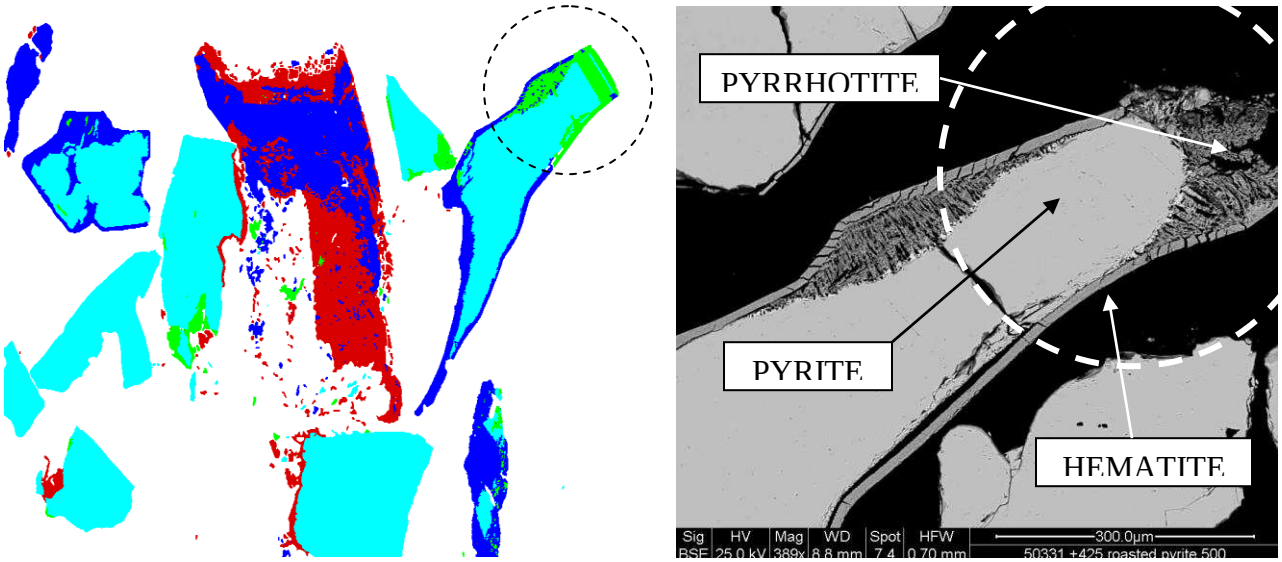

(a) **(b)**

Figure 4.16 (a) Classified image frame of +425µm treated pyrite showing some sulphide conversion. (b) BSE image treated pyrite showing some sulphide conversion and textural changes.

The classified image and BSE image shown in Figure 4.16 indicates where conversion has taken place. The identification is made from X-ray mapping across the whole particle resulting in a colour classified image.

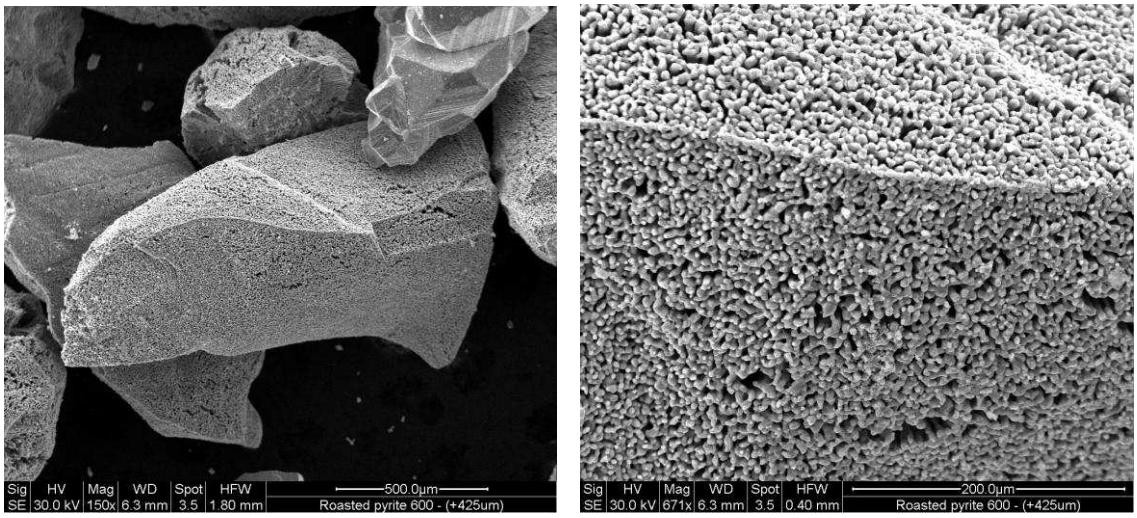

(a) **(b)**

Figure 4.17 Secondary Electron (SE) images of roasted pyrite particles +425µm (a) topography of treated pyrite particles at x150 magnification. (b) topography of treated pyrite particles showing extensive porous texture.

4.3.1.5 X-ray Analysis and Mineral Identification Procedure

For each grey-level region within the sample the MLA will perform X-ray analysis, collecting spectra from the central region of each phase (to ensure that the "cleanest" areas are measured). Spectra from the X-ray image developed will be compared to standard mineral spectra (where one exists) and a classified image is constructed. Data contained within the classified image and the pixel data contained within, will form the basis for further quantitative analysis. This data (including particle location) is stored on the MLA software for further analysis and presentation.

The X-ray beam collects the required spectra by rastering over the area/particle/phase to be analysed. This technique is known as are X-ray area analysis. This is known as XBSE (Extended BSE liberation analysis). The edge near the boundary of the phase being X-rayed is not measured to avoid possible contamination of results and so avoiding invalid identification. This technique is suitable to identify and resolve mineral phase boundaries that were not identified by BSE grey-level contrast (i.e. minerals having the same AAN).

Another technique used for mineral identification is X-ray mapping. X-ray mapping superimposes a grid over the entire image/grain and an X-ray measurement is taken at each grid point. The size of the grid may be altered, however generally speaking, X-ray mapping is a time consuming process although a comprehensive X-ray map will be formed by this technique. Grain-based X-ray mapping (GXMAP) mode may also be used by the operator can select specific grains for mapping using a BSE trigger or specific X-ray trigger. This method ensures that only grains of interest are mapped which can cut measurement and processing time significantly.

A library of mineral standards may be collected from the sample to ensure correct identification of minerals is achieved and better reflects the sample chemistry and measurement conditions such as beam energy (i.e. keV).

4.3.1.6 Post-processing of Results and Presentation

The pixel data, elemental composition and densities of the phases identified in the sample can be used to produce a variety of mineralogical data. These include, calculated assay, elemental distributions, mineral grade recoveries, density distributions, modal

mineralogy, mineral associations, free surface, phase specific surface area PSSA, mineral liberation data and classified/unclassified images. These can be presented in graphical or tabulated form and it is also possible to compare and group results where required.

4.3.1.7 Sample Preparation Techniques

Inappropriate preparation of a sample can reduce or destroy important information and so sample preparations needs careful attention. The primary purpose of sample preparation is to ensure that the in-situ microstructure and composition is revealed. The ability to observe subtle details in the microstructure and composition depends strongly on the preparation procedure. In this work, all sulphide samples were prepared for SEM analysis by impregnating representative sample batches in epoxy resin. Epoxy-based resins are the most suitable for sample encapsulation/impregnation particularly when the sample is soft, pulverent, cracked or brittle. In order to ensure that voids, pores and cracks are penetrated with epoxy, the resin molds were places inside a vacuum chamber causing the sample to evolve any trapped air. Breaking and restoring the vacuum several times helped to expel all of the trapped air inside the sample and allows the air pressure to force epoxy into the voids and cracks. The lower the viscosity of the resin then the deeper its depth of penetration into the sample. After the sample has had vacuum pressure applied for 10-20 minutes the samples were removed and allowed to cure and permanently harden for at least 24 hours. The samples were then extracted from the mold and prepared for grinding/polishing by removing excess material from the edges of the block using a grinding wheel. A lapping and grinding procedure was then employed to ensure that deformations and surface irregularities are removed and to ensure that the critical surface

is perfectly flat. Initial grinding is performed using successively finer-grained abrasive papers in water on a horizontal grinding wheel. The sample removal rate from the critical surface decreases with decreasing grit size. Once the sample has been ground so as to reveal a good section of particles, a polishing procedure may then be applied. The polishing regime will produce a flat scratch free surface which is commonly mirror like in appearance (depending on the sample lustre). A polished surface is essential for microstructural examinations by secondary or back scattered electron imaging. There are various types of polishing abrasives but in this work a diamond suspension in oil was used from 9μm to 1μm size using polishing cloths attached to a horizontal rotary wheel.

4.3.1.8 Magnetic Property Measurement.

The current methods available for measuring the magnetic properties of materials are well documented (Wasmuth and Unkelbach, 1991; Svoboda and Fujita, 2003). Many methods have been designed specifically for the measurement of magnetic moments. These techniques can be summarised into two categories. Firstly, **force** techniques have been developed to measure the force exerted on a magnetised sample in a magnetic field gradient. The Faraday balance and Alternating Gradient Force Magnetometer (AGM) are popular instrument based on this method. Secondly, instruments which measure the voltage induced by a changing flux using a Hysteresis Meter (HM) or the Vibrating Sample Magnetometer (VSM) are prevalent examples of **inductive** techniques. In this work the changes in magnetisation or magnetic susceptibility of pyrite as a result of heating was determined using a VSM instrument. Its fundamental principal of operation will be discussed here.

The Vibrating Sample Magnetometer is used to measure the magnetic moment of a sample and then subsequently its magnetisation. Most elements posses very weak magnetic properties and are either paramagnetic (very weakly attracted to a magnet) or diamagnetic (very slightly repelled by a magnet). Others such as iron, cobalt, nickel and gadolinium are termed ferromagnetic are strongly attracted by a magnet (at room temperature). In these ferromagnetic elements, each atom behaves as a small magnet as a result of the out-of-balance electron spins (John, 2003). Under unmagnetised conditions, ferromagnetic materials will posses a random oriented domain structure. However, when under the influence of a magnetic field, all the domains tend to align themselves in the direction of that field. The material is now magnetised. If the alignment is permanent (i.e. present after the removal of the field) then the material is said to be magnetically hard. On the other hand, if the material losses the alignment once the field has been removed then the material is said to be magnetically soft and the magnetic domains will revert back to a random orientation. The degree of magnetisation induced on a ferromagnetic material does not increase linearly with increasing magnetic field. This can be seen on a typical magnetisation curve (Path OA) shown in Figure 4.18. The magnetisation induced follows a curved path until magnetic saturation is reached (Point A). When the magnetic field is reduced, then the magnetisation reduces slowly (but still has a positive value when the field has been removed). The degree of magnetisation remaining is termed remanence (Point B_r). To reduce the magnetisation in the sample to zero, a reversal of the applied magnetic field is necessary and it magnitude is equivalent to the value at Point H_c. The value of H_c is termed coercivity. Should the reversal of the field continue

until saturation (Point A´), then the material will be magnetised in the opposite direction. Increasing the magnetising field in the positive direction will then complete the B-H curve shown in Figure 4.18.

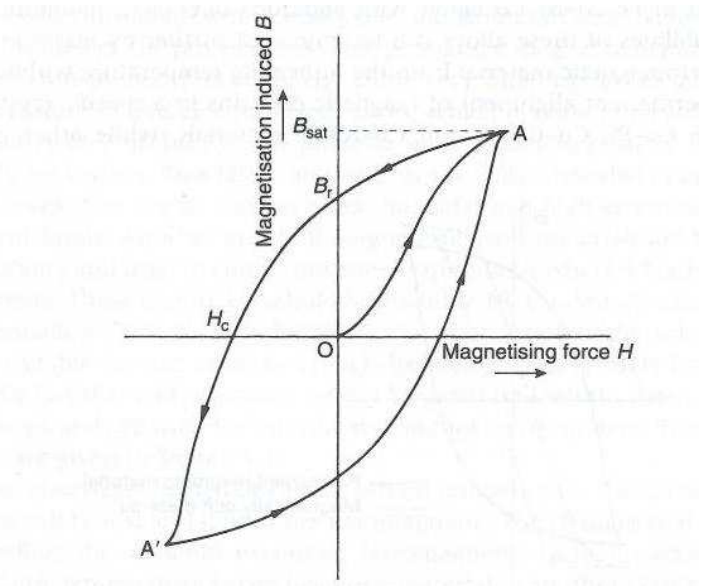

Figure 4.18 The hysteresis loop for a ferromagnetic material.

Materials with high coercivity and remenance (having a "square" hysteresis loop), such as γ-Fe_2O_3, have uses as magnetic recording materials (Waters, et al., 2007).

4.3.1.9 Separation by Magnetic Force – Basic Principles

The practical significance of magnetism (particularly magnetic separation) has been exploited in many mineral processing technologies. Magnetic separation (along with electrostatic separation and froth floatation) is one of the main methods for separation valuable minerals from gangue. The spectrum of applications of magnetic separation technology is staggering, as is the machinery available for various applications (Wet or Dry and eddy-current). The magnetic properties of minerals can be used to calculate separation efficiencies and help to control the final product grade. Therefore, reliable

measurement of the magnetic properties of minerals is essential to the design of future processes. The recovery of the magnetic fraction that can be achieved after processing is not the only factor that should be under consideration. The effect of field strength on the magnetic properties of the material is of equal importance. Since pyrite has been reported to be diamagnetic (Rowson and Rice, 1990) or weakly paramagnetic (Schneider, et al., 2004; Ramaseshan, 1947) the effect of microwave treatment on the magnitude of the magnetisation pre and post-treatment should be monitored. The Vibrating Sample Magnetometer (VSM) can be used for characterising magnetic materials by measuring the **magnetic moment** of a sample as a function of magnetic field strength and temperature and then, in turn, the magnetisation. A schematic diagram of a VSM is shown in Figure 4.19. The VSM instrument, devised by Foner (1956, 1969) represents by far the most common type of magnetometer in use today.

The magnetic moment of a sample is the product of magnetisation of the sample (magnetic moment per unit volume) times the volume of the sample. If a sample is aligned between the poles of an electromagnet and vibrated, then the field lines generated by the sample cut through the detection coils, attached to the poles of the electromagnet (see Figure 4.19), and so allows for the magnetic moment of the sample to be measured. The moment can then be converted into magnetisation using the following expression;

$$\mathrm{M} = \frac{\mu}{\mathrm{V}} \qquad [4.1]$$

Where M, μ and V are the magnetisation (Am^{-1}), the magnetic moment (Am^2) and the volume of the sample (m^3) respectively.

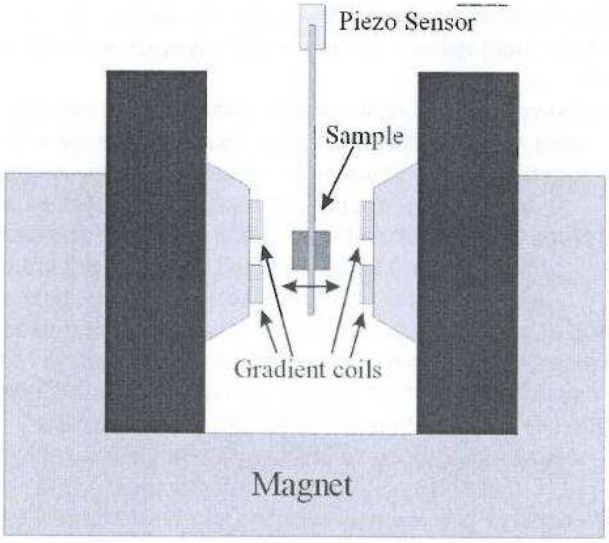

Figure 4.19 Schematic layout of the Vibrating Sample Magnetometer (Speliotis).

It is essential that the material to be measured by the VSM is finely ground and well packed into the sample holder. For this work, pyrite was riffle split using a micro-riffler and each representative sample was carefully weighed. A small amount of sample (~0.01g) was well packed into the sample holder and placed between the detection coils of the instrument. The resulting magnetic properties of the sample were processed using VSM software, where the magnetic susceptibility calculations were performed according to the following equation;

$$\chi = \frac{M}{H} \qquad [4.2]$$

Where χ, M and H are the magnetic susceptibility, the magnetisation (Am^{-1}) and the field strength (Am^{-1}) respectively.

The magnetic field was ramped up to a maximum of 2T and then reduced back over time to zero.

4.3.2 Heating Apparatus.

4.3.2.1 Small Scale Fluidised Bed Microwave Applicator

Small scale fluidised bed experiments were carried out on screened pyrite samples. For the purposes of these experiments, a 1kW single mode microwave cavity applicator was used as shown in Figure 4.20.

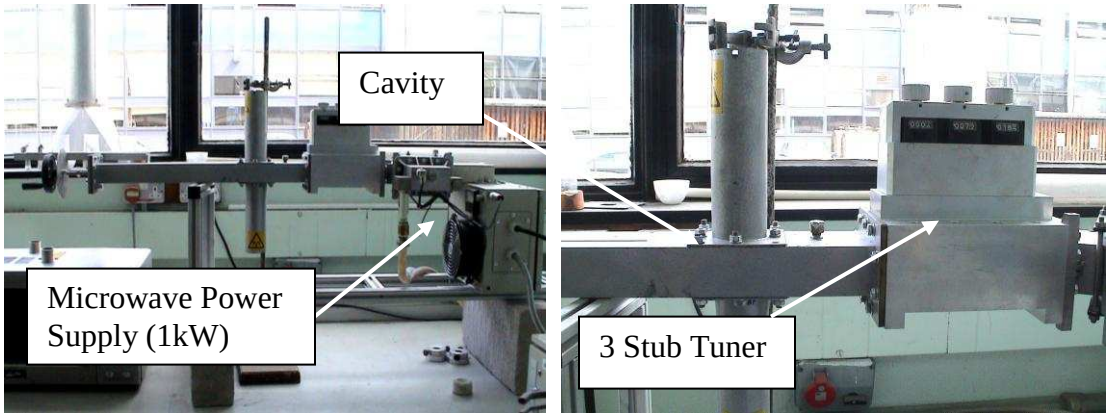

Figure 4.20 Single Mode Microwave Cavity Applicator.

The apparatus was constructed and commissioned by Industrial Microwave Systems Ltd and consists of a WR340 waveguide, 3-stub tuner (for impedance matching and minimisation of reflected power) and 1kW generator operating at 2.45GHz.

Initially the pyrite samples were screened into narrow size fractions of -600+425μm and -38μm and placed, in turn, into a standard elutriation tube (Fisher Scientific). The 10g samples were then semi-fluidised using Oxygen/Nitrogen gas mix to aid the oxidation process and to ensure good agitation within the field. The tube was then placed into the cavity and the gas flow rate adjusted to ensure complete particle entrainment (flow rate is particle size dependant). To maximise power transfer to the sample, the waveguide characteristics were tuned using the stub-tuner device situated along the waveguide. This

was achieved by monitoring and minimising the differential power level between incident power to the cavity and reflected power detected. A schematic diagram representing key elements in the experimental setup is shown in Figure 4.21.

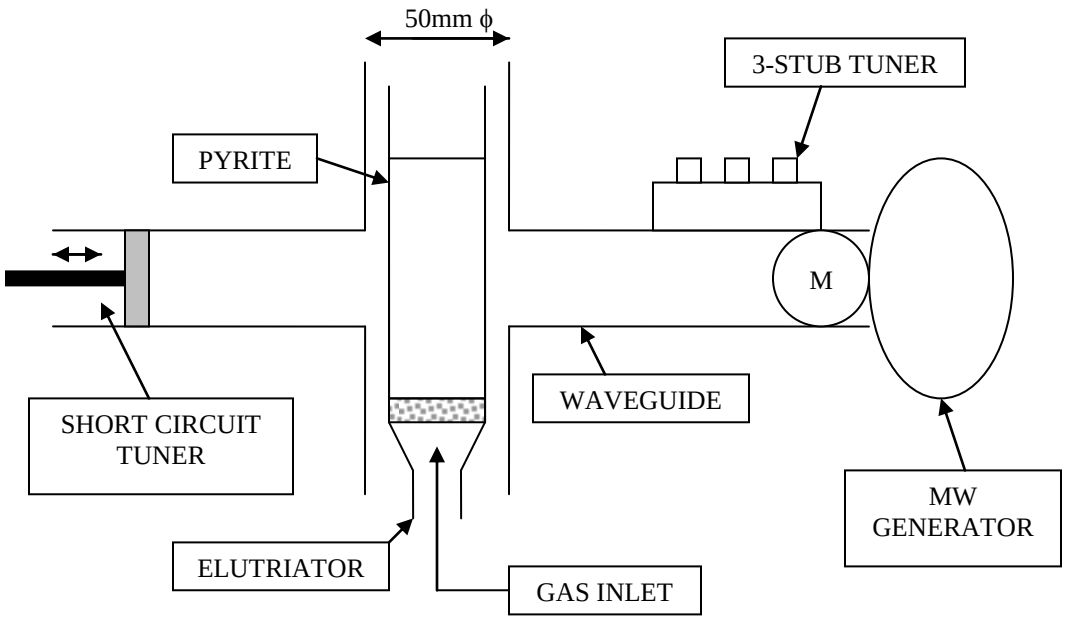

Figure 4.21 Schematic diagram of elutriation experiment using a single mode cavity.

4.4 Experimental Program and Results.

4.4.1 Experimental Objectives.

The experimental objectives of this program of work are to investigate the transformation of pyrite to magnetically enhanced pyrrhotite (and other products) using novel microwave energy methods and conventional heating techniques. This work will monitor the thermal behaviour of pyrite under a controlled temperature/time/atmospheric regime and will seek to establish whether oxidation/desulphurisation and magnetic property alterations are grain size, time or temperature dependent by MLA and VSM analysis

The thermal behaviour of pyrite will be investigated by TGA/DSC methods in both oxidising and inert atmospheric conditions.

4.4.2 Sample Preparation and Screening

This work focuses on two narrow size classes of museum grade pyrite -600+425μm and -53+38μm. The samples were purchased from mineral dealers Gregory, Bottley and Lloyd of London. The samples were roll crushed and screened in preparation for sub-sampling and pre-treatment characterisation. Each sieve charge was then riffle split using a micro-riffler in order to ensure batches were representative of the original bulk product.

4.4.3 Untreated Pyrite Characterisation.

X-ray diffraction (XRD) analysis was performed to inform pre-treatment characterisation of the sample, the results of which are displayed by the diffraction pattern in Figure 4.22(a). The XRD analysis of each untreated size fraction showed no other detectable phases present (within the threshold of sensitivity ~5%vol of sample) and is consistent with standard patterns for FeS_2. (Web Source ICSD Database - Appendix A4).

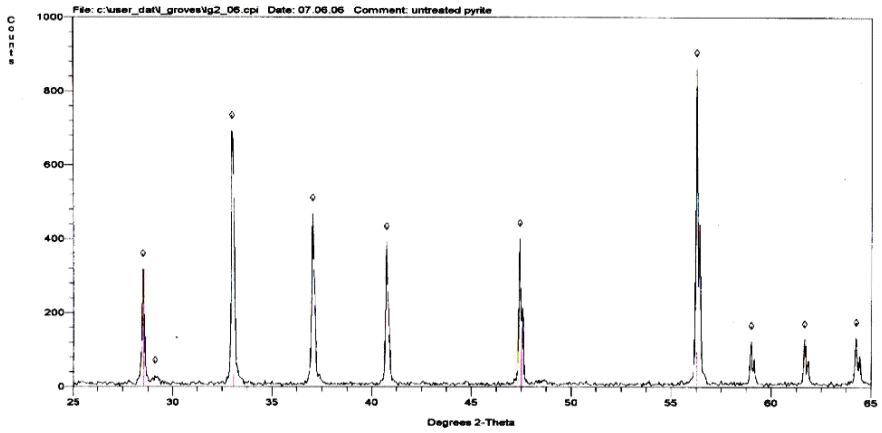

Figure 4.22(a) XRD diffractogram for pure untreated pyrite.

Untreated samples of each size fraction were mounted in epoxy resin molds and prepared for SEM analysis to ensure that each sample was of the highest purity before heat treatment experiments were undertaken. The results displayed in Appendix A4 show histograms of phase specific surface area of each sample expressed as a percentage. It can be seen that the pyrite contains other mineral inclusion which were not included in this analysis. These other inclusions make up only a small percentage of the overall mineralogy and so can be discarded. Some samples show higher purity than others and in that case of the -38μm fraction, a very small amount of pyrrhotite was observed which is considered in this analysis and discussed later. Figure 4.22(b) shows an untreated pyrite grain with characteristic sub-concoidal fracturing and no signs of natural oxidation.

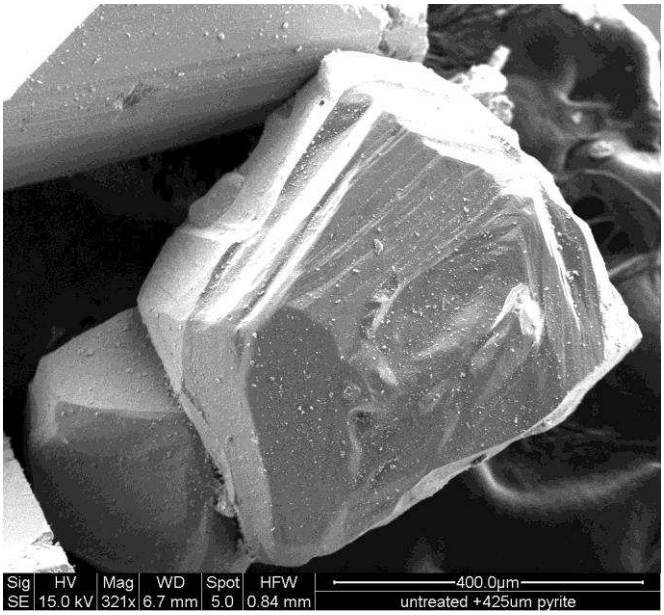

Figure 4.22 (b) Secondary electron image of an untreated -600+425μm pyrite grain.

Magnetic susceptibility data were collected with the use of a vibrating sample magnetometer (VSM). As the sample vibrates in the magnetic field generated by a superconducting magnet, a voltage signal is picked up and is proportional to the magnetic moment of the sample. Knowledge of the sample weight is then used to convert magnetic moment to specific magnetisation. As the magnetic field is ramped to the selected field strength (2T), a graph is generated consisting of data points of magnetisation (M) versus field strength (H). Specific magnetic susceptibility can then be calculated using Eqn. 4.2. Consequently, the specific magnetic susceptibility (χ) is the slope of the VSM-generated curve at any point along the curve. Figure 4.23 and 4.24 display the magnetic susceptibility as a function of field strength for untreated freshly prepared pyrite from each size band.

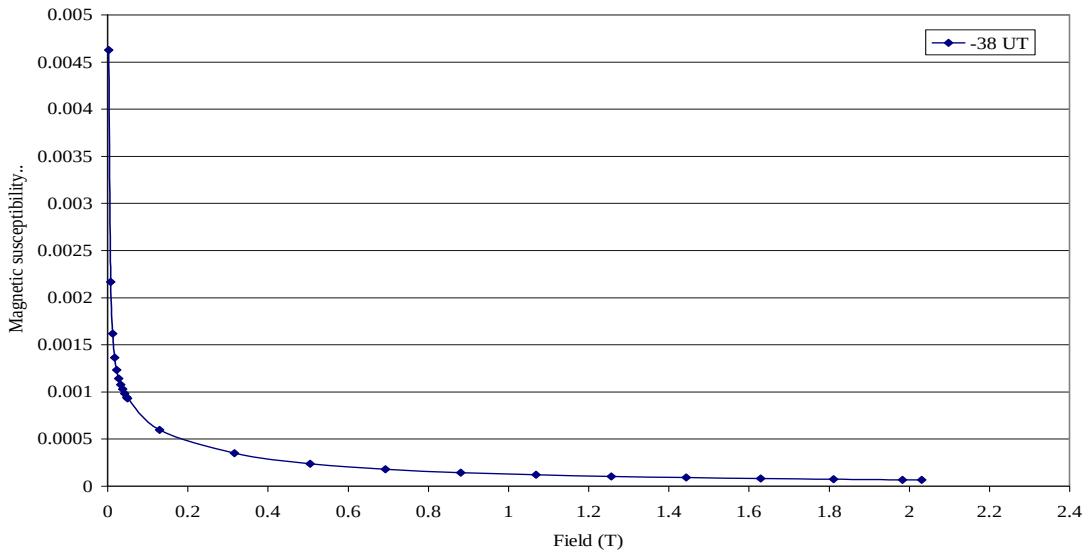

Figure 4.23 Magnetic susceptibility of untreated -38μm pyrite.

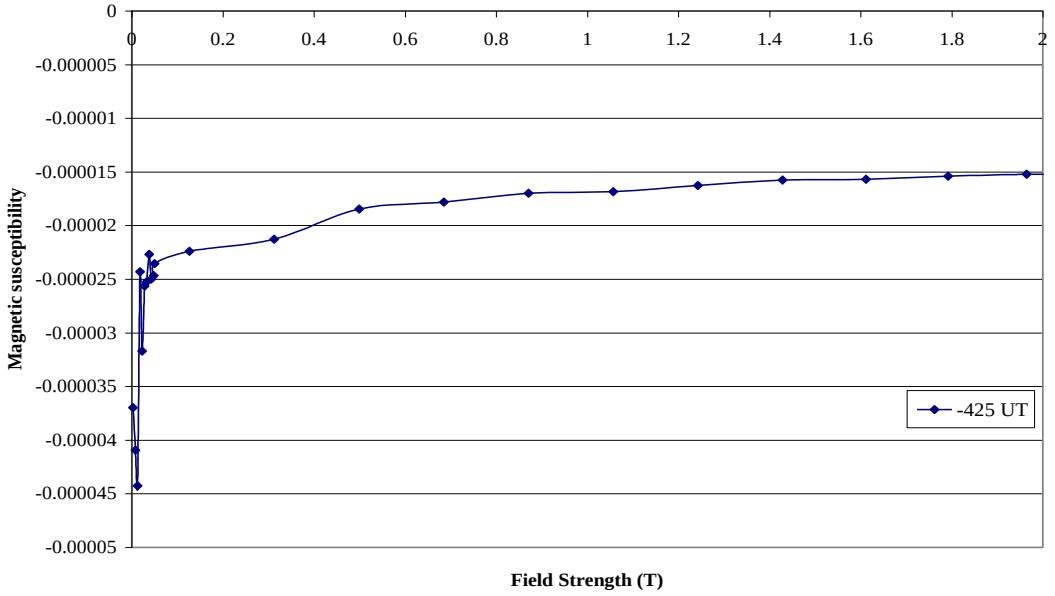

Figure 4.24 Magnetic susceptibility of untreated -425μm pyrite.

The susceptibility curve shown in Figure 4.23 shows a sharp decrease in the susceptibility from the start of the test in the field range of 0 to 2 Tesla. This can be attributed to saturation of small amount of iron or is perhaps as a result of other ferromagnetic inclusions in the sample. After the sample was saturated the susceptibility was near constant throughout the rest of the field sweep. The results displayed in Figure 4.24 are less convincing and shows a diamagnetic response. However, one must consider the scale of the susceptibility axis when making direct comparisons between samples. Conflicting data may be as a consequence of inherent variability in mineral composition, the presence of inclusions and other contaminants or subtle alterations in the experimental procedure and conditions may have affected the results. After initial saturation, once again the susceptibility was near constant throughout the rest of the field sweep. Consequently, both untreated pyrite samples show both paramagnetic and ferromagnetic tendencies. The

ferromagnetic component is likely to be as a result of iron contamination and/or as a result of low-temperature phase transition to monoclinic pyrrhotite which had been detected by SEM analysis previously.

It has been reported by Waters et al., 2007 that industrial magnetic separation processes tend to work in the range on 0.5 to 1 Tesla. They hypothecated that lowering the magnetic field would not necessarily lead to a decrease in recovery in this case and that recovery at low field values is generally the greatest percentage of the total recovery (true for both wet and dry magnetic separation).

4.4.4 Thermal Alteration Monitoring by TGA/DSC in dynamic air.

The thermogravimetic behavior of pyrite in air has been investigated here in order to establish possible temperatures at which phase transformation is taking place. These useful indicators are then used to establish a heating regime for conventional roasting experiments. The samples were monitored in both nitrogen and air in non-isothermal heating atmospheres in order to establish specific temperature indicators where phases transitions are likely to occur. These transitions are manifested in changes in sample percentage weight and heat flux monitoring for exothermic and endothermic reactions. The results of simultaneous TGA and DCS analysis for the oxidative roasting of pyrite in dynamic air (100ml/min) at a constant heating rate of 5°C/min in the temperature range of ambient to 900°C is shown in Figure 4.25 and 4.26 respectively. At a temperature of 250°C the first exothermic peak on the DTA curve occurs with associated mass loss initiated at this temperature. On further heating at 500°C an exothermic peak is evident

with further mass loss. Total mass loss in the sample over the entire temperature range is ~30%. The rate of change in mass loss is determined by dividing the change in weight by the sampling interval $\left[\frac{dw}{dt}\right]$. This is known as the weight loss derivative.

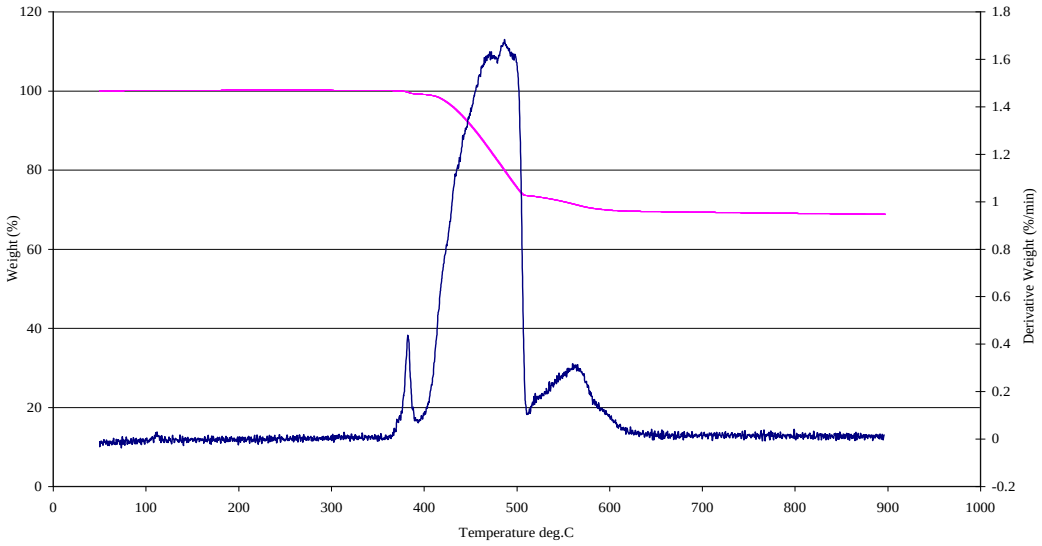

Figure 4.25 TGA/DTA analysis for pyrite in dynamic (100ml/min) air at 5°C/min.

This result shows that the exothermic transformation of pyrite to hematite/magnetite occurs with at least three steps between 250 - 700°C. Knowledge of these critical temperature at which phase transitions are likely to occur are significant for the following reasons:

- The conventional heating regime may be designed such that pyrite samples may be heated to pre-determined temperatures and air quenched to preserve phases.
- Pyrite samples heated through a range of temperatures may be prepared for XRD and MLA characterisation to identify and quantify thermal decomposition products.

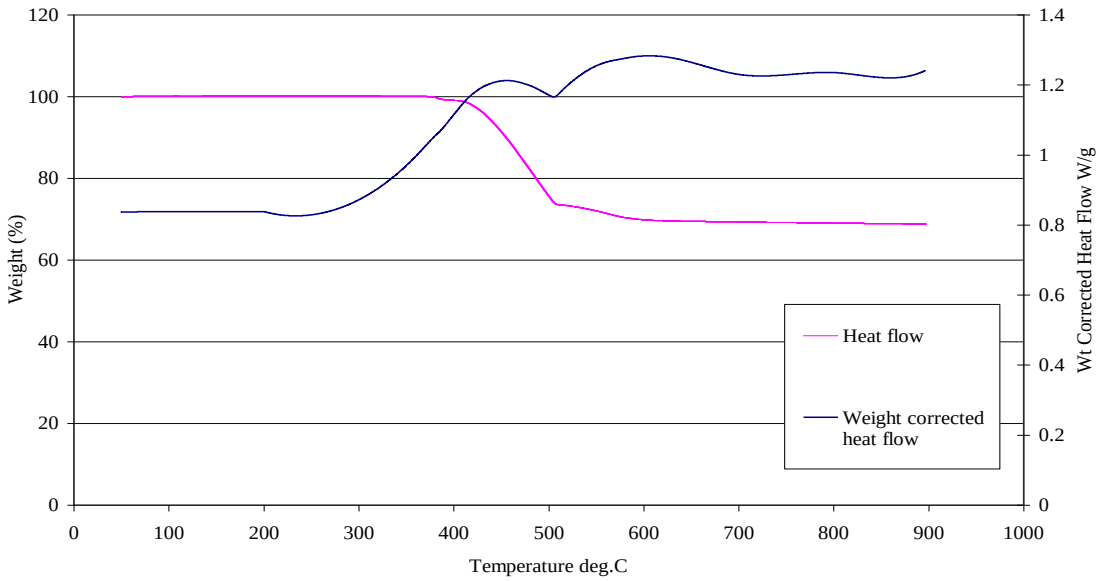

Figure 4.26 DSC analysis for pyrite in dynamic (100ml/min) air at 5°C/min.

From the information displayed by TGA/DSC analysis, one can see that total transformation (complete oxidation) occurs at around 670°C. However, it is important to note here that due to the fact that the only a small sample mass was required for TGA tests (<0.1g) and the sample pans are deep, it is possible that only the particles close to the top surface of the sample were exposed to the air atmosphere. Consequently this may have resulted in incomplete oxidation of the sample if oxygen had not been able to penetrate through the sample to all particles. It was proven very difficult to achieve mono-layered pyrite particles given the geometry of the sample pans. The results presented here are consistent with other reports that the onset decomposition temperature for pyrite is 400°C (Dunn, 1997, Paulik, et al., 1982).

4.4.5 Thermal Alteration Monitoring by TGA/DSC in dynamic nitrogen.

The thermogravimetic behavior of pyrite in nitrogen has been investigated here in order to establish possible temperatures at which phase transformation is taking place. The results of which are displayed in Figures 4.27 and 4.28.

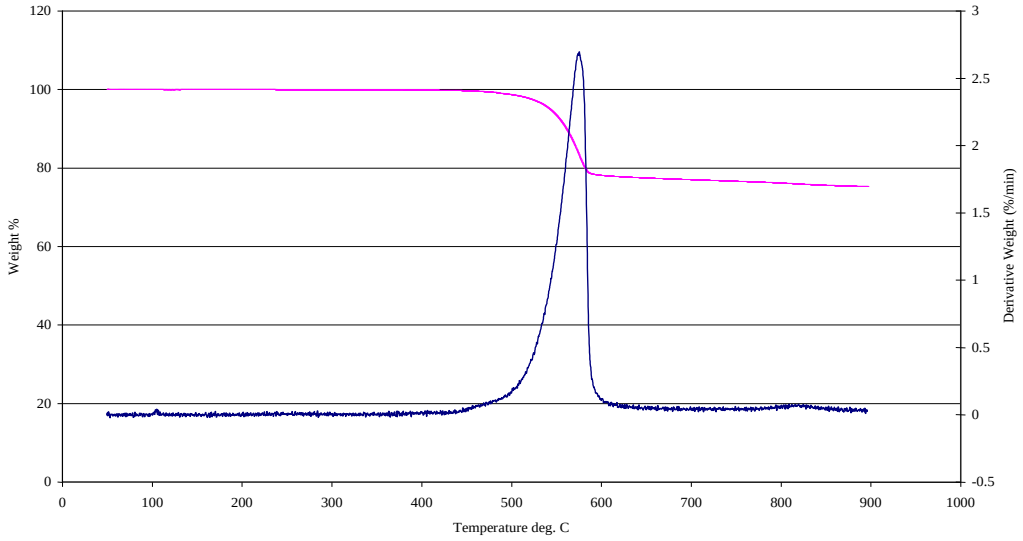

Figure 4.27 TGA analysis for pyrite in dynamic (100ml/min) nitrogen at 5°C/min.

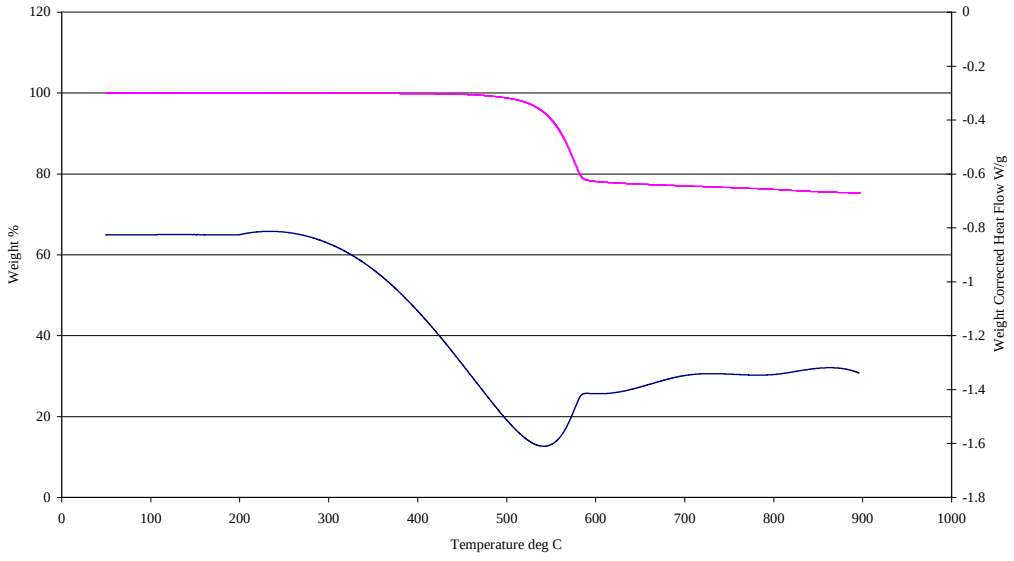

Figure 4.28 DCS analysis for pyrite in dynamic (100ml/min) nitrogen at 5°C/min.

The weight loss profile for pyrite heated in nitrogen is shown in Figure 4.27 and indicates a total mass loss of ~25% over the temperature interval of 50°C (equilibrium) to 900°C. Heating pyrite in an inert atmosphere (in this case nitrogen) can bring about two process these can be summarised as follows;

- Phase transformation (such as an $\alpha \rightarrow \beta$ transition).
- Conversion of one phase to another (through decomposition, liberating sulphurous gases).

In order to establish the nature of the product formed from the results of such thermal events indicated by TGA/DSC analysis, small samples of -38μm pyrite were heated (in both air and nitrogen) to predetermined temperatures (coincident with key thermal events) using a Pyris Perkin-Elmer thermogravimetric instrument. Representative samples <0.1g of pyrite were heated at 5°C/min to temperatures of 450, 460, 470, 480, 490 and 500°C. Each sample was allowed to soak at each temperature for 15 minutes and allowed to cool inside the furnace. The samples were heated in both air and nitrogen gas streams at a flow rate of 100ml/min. After each experiment the samples were removed from the instrument and immediately prepared for SEM analysis. The results of which are shown in Figures 4.29 and 4.30. It can be seen fro Figure 3.26 of pyrite heated in dynamic air that the amount of pyrrhotite formed does not very significantly across the temperature range. Taking into account the existence of small amounts of pyrrhotite in the original untreated sample we can see the majority of pyrrhotite formed here is at a roasting temperature of 460°C. Clearly temperature is the controlling factor in this experiment since all samples have experienced identical heating cycles.

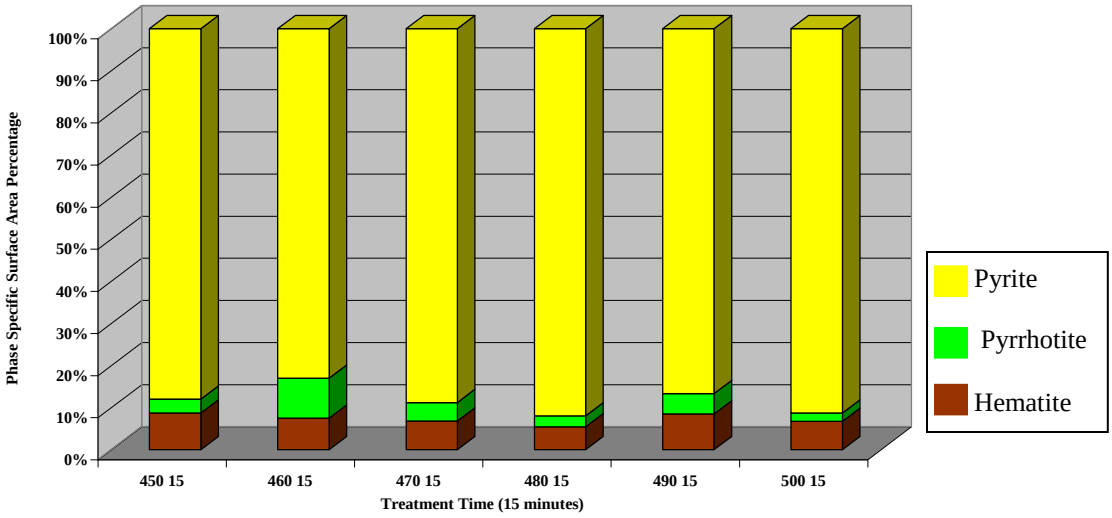

Figure 4.29 Thermogravimetric analysis of -38μm pyrite heated in dynamic air.

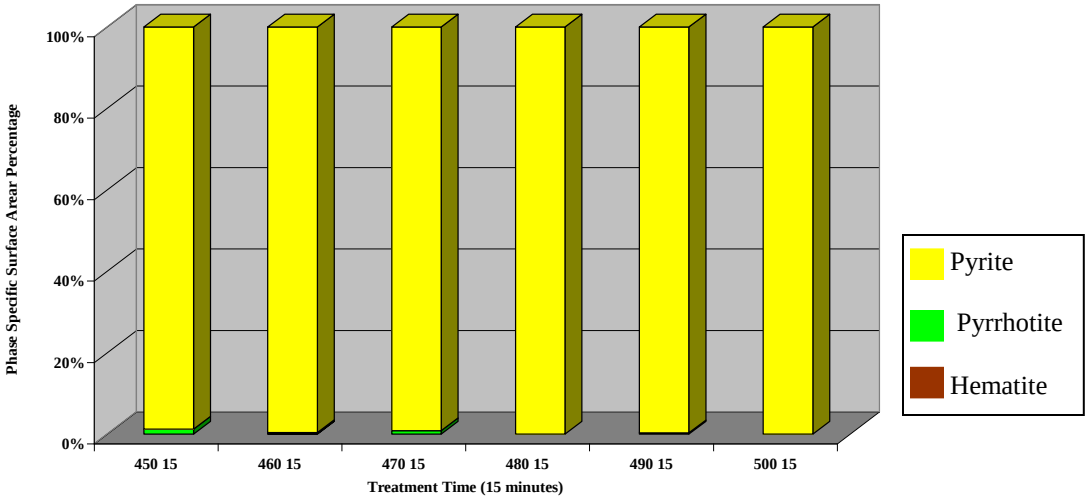

Figure 4.30 Thermogravimetric analysis of -38μm pyrite heated in dynamic nitrogen.

Once again, it is noted here that gas penetration to all particles is unlikely due the geometry of the sample pans and the particle size being tested. Consequently, it is possible that only the surface layer of particles have been affected by oxidation resulting in large amounts of pyrite remaining after treatment. .

The results presented in Figure 4.30 show pyrite heated in a dynamic gas stream. In this case oxidation is prevented and little evidence of phase alteration is found over the experimental temperature range. The small amount of pyrrhotite found here at 450 and 470°C is likely to have been present before heating. One would have expected that some decomposition phase alteration would be present in sample heated to 490 and 500°C given the distinct endothermic reaction and mass loss taking place as illustrated in DSC analysis presented in Figure 4.28. When heated in an inert atmosphere, pyrite will decompose to release sulphur gas and form and iron sulphide of lower sulphur content. According to Hu, et al., 2006, under equilibrium conditions, sulphur content in the formed pyrrhotite (x in the FeS_x) is controlled by temperature. However, if the sulphur gas pressure is high (partial pressure of sulphur gas is lower than equilibrium gas pressure) then sulphurous gas release will be prohibited. A reasonable explanation for the observations found here is that for pyrite heated in an oxidising atmosphere, the conversion rate is controlled by temperature and indicates the occurrence of simultaneous thermal decomposition of pyrite and the oxidation of the formed pyrrhotite given the existence of pyrite, pyrrhotite and hematite. The oxidation here would follow the unreacted core model proposed by Hu, at al., 2006. However, for pyrite heated in inert atmospheres, it is likely that the controlling factor is sulphur gas pressure which may be lower than the corresponding equilibrium pressure and so decomposition by release of sulphur gas is retarded. As such no evidence of pyrrhotite is found as indicated by the results presented in Figure 4.30.

4.4.6 Dielectric Properties of Pure Pyrite - Cavity Perturbation Measurements.

Dielectric measurements were taken on untreated fresh pyrite samples in air using the cavity perturbation technique on a well packed particulate sample. The sample was heated in a conventional tube furnace situated above the cavity, and dielectric measurements were taken from ambient temperature to a maximum of 650°C, at 50°C intervals. The sample was allowed to soak at each temperature increment for 15 minutes before a measurement was taken. Figure 4.31 shows the correlation between temperature and dielectric loss factor. The initial increase in the dielectric loss factor between ambient and ~100°C is due to the presence of moisture in the sample. After which, the water is removed and the loss factor decreases and stabilises until ~400°C.

Figure 3.28 demonstrates clearly that at around 400°C an initial subtle decrease in the loss factor is evident. This is consistent will observations made by TGA/DSC analysis shown in Figures 4.25 and 4.26 at which the onset of oxidation is likely to occur with corresponding mass loss and exothermic thermal anomaly.

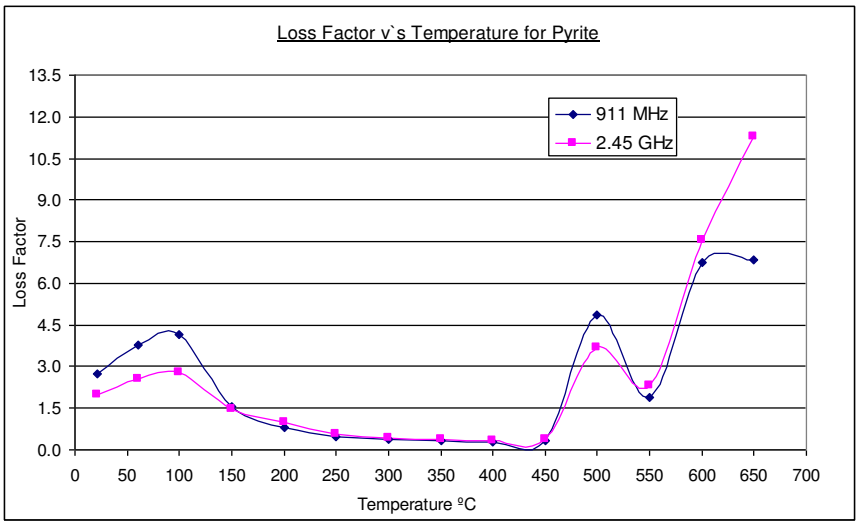

Figure 4.31 Dielectric Loss Factor versus Temperature at 911MHz and 2450MHz.

The loss factor then increases sharply at ~450°C consistent with increased mass loss between 450 and 550°C. It is reasonable to assume that the surface of the sample in contact with the atmosphere inside the tube furnace is experiencing decomposition and oxidation to form pyrrhotite and/or hematite which manifests itself here in the observed increase in the dielectric properties at this point. It is unlikely however, that the entire sample will be oxidised due to the size and shape of the sample holder and the fact that sufficient gas penetration to all tightly packed particles is unlikely. It should also be noted that small changes in volume associated with the decomposition of pyrite through to hematite will also affect the volume of sample to volume of cavity ratio which will also alter the dielectric properties.

4.4.7 Conventional Roasting Experiments

In this experiment, two narrow size fractions, <38µm and -0.6 + 0.425µm, of pyrite were prepared using standard crushing and sieving techniques.

In the first instance, 10g (representative of the bulk) of pyrite of each size fraction was conventionally heated in air using a Carbolite muffle furnace to temperatures of 400, 450, 500 and 600°C. These critical temperatures were selected based on results from TGA/DSC experiments and are coincident with key thermal anomalies. The pyrite samples were arranged in a monolayer on aluminium foil before being placed in the furnace. For each temperature the samples were heated for 60 s, 900 s and 1800 s. The heated products were then allowed to air cool before being prepared for SEM analysis. The samples were mounted in Resin and polished before being carbon coated to eliminate damage to the sample from charges that can built up from the strong

electric currents from the electron beam of the SEM. Samples were also mounted on stub adaptors for 3D particle surface texture observations.

Mineral Liberation Analysis (MLA) software was then used to process Scanning Electron Microscope (SEM) operations, using XBSE measurement for collecting data. The XBSE data collects a series of back-scattered electron images which are particulated and pre-segmented during the measurement process. An X-ray spectrum is collected from each particle which has been identified from the back-scattered electron image. A raw greyscale image is generated and a false coloured image of the particles can be displayed. The mineral identity of each particle is compared to measured mineral data of known spectra to identify mineral species.

Modal mineralogy data can then be generated to provide information about the identity of minerals in the sample, which include mineral proportions on an area % basis.

4.4.8 Results (-600+425µm Particles)

Scanning Electron Microscopy reveals that a significant alteration in the morphology of pyrite grains is evident at temperatures in excess of 450°C for both <38µm and -0.6 + 0.425µm size fractions. Modal mineralogy data for 400°C conventional heating reveals that the percentage area conversion from pyrite to pyrrhotite is small, regardless of roasting time. Figure 4.32 shows a comparison between roasting time with the percentage area of minerals present in the sample.

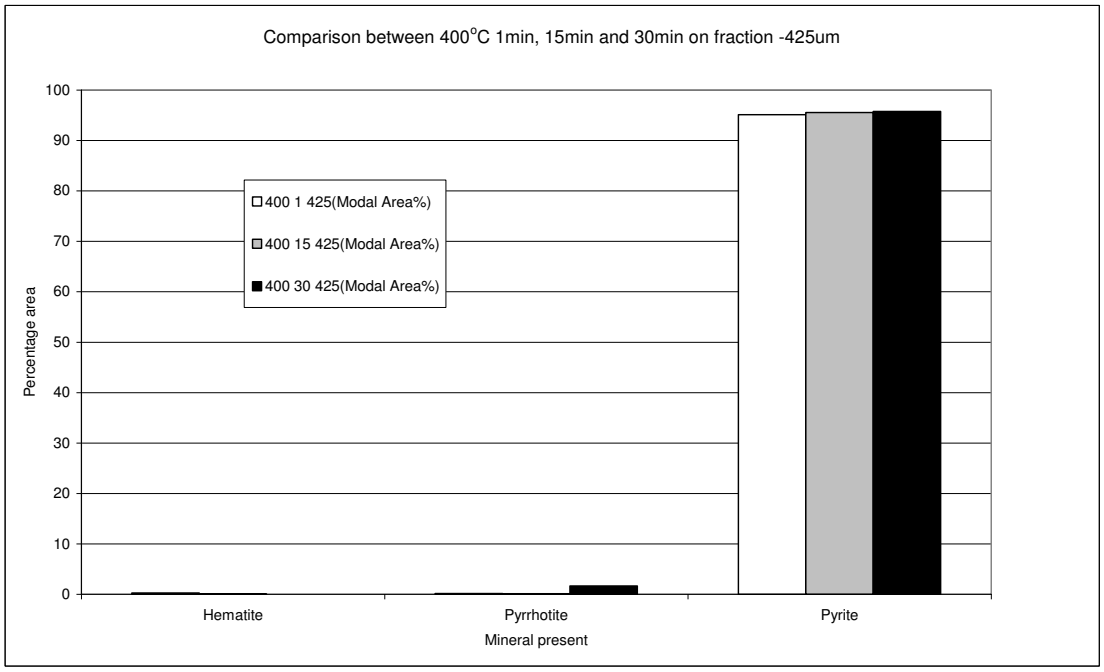

Figure 4.32 Modal area % plot of roasted -0.6+0.425µm pyrite at 400°C.

The Modal mineralogy data for roasting at 450°C and 500°C show the formation of pyrrhotite and hematite in each sample. A small increase in the modal area percentage for pyrrhotite and hematite can be seen at 450°C roasting times of 900 s and 1800 s. The results for roasting at this temperature for only 60 s shows little impact on the formation of a pyrrhotite phase. Figures 4.33 & 4.34 shows a comparison between roasting time with the percentage area of minerals present in the sample at 450°C, 500°C and 600°C respectively.

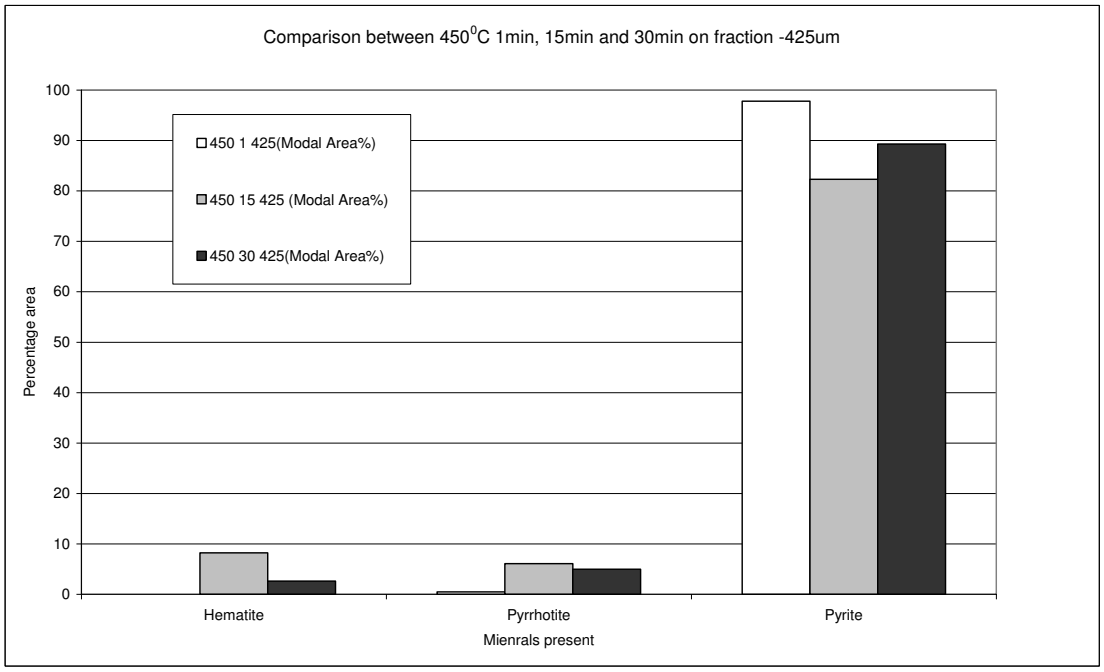

Figure 4.33 Modal area % plot of roasted -0.6+0.425µm pyrite at 450°C.

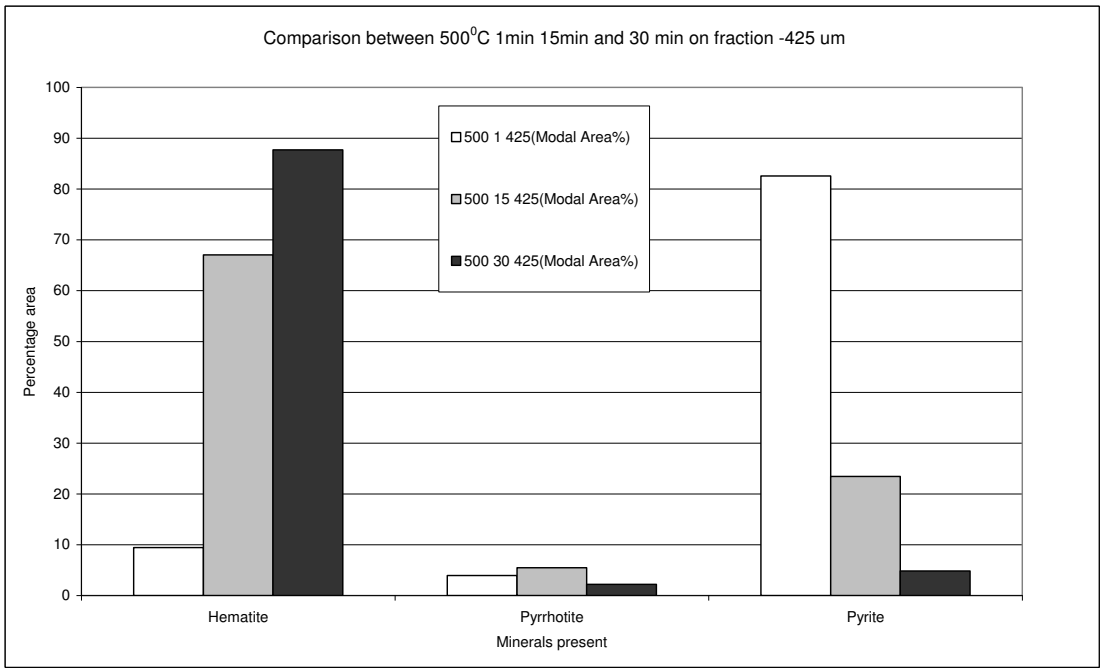

Figure 4.34 Modal area % plot of roasted -0.6+0.425µm pyrite at 500°C.

It is evident from Figure 4.34 that there is a large increase in the modal percentage area of hematite while the formation of pyrrhotite changes little with furnace residence time. Further investigation is needed at temperatures between 450°C and 500°C since roasting at 500°C for 900 s and 1800 s has a detrimental effect on pyrrhotite formation due to the formation large areas of hematite.

In contrast, the results presented in Figure 4.35 for conventional roasting at 600°C, show a significant increase in area for pyrrhotite are after only roasting time 60 s. However, after 900 s and 1800 s in the furnace, almost all pyrite has been oxidised for form hematite.

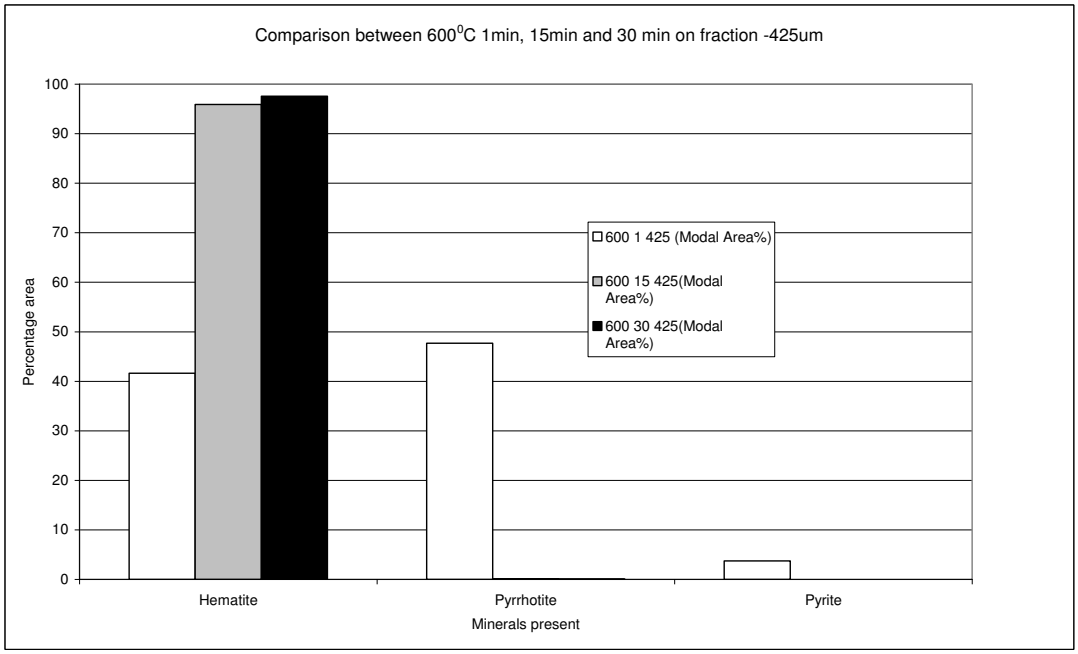

Figure 4.35 Modal area % plot of roasted -0.6+0.425µm pyrite at 600°C.

The secondary electron image of a typical roasted +425 pyrite particle shown in Figure 4.36 is evidence of significant oxidation at a roasting temperature of 600°C for 15 minutes.

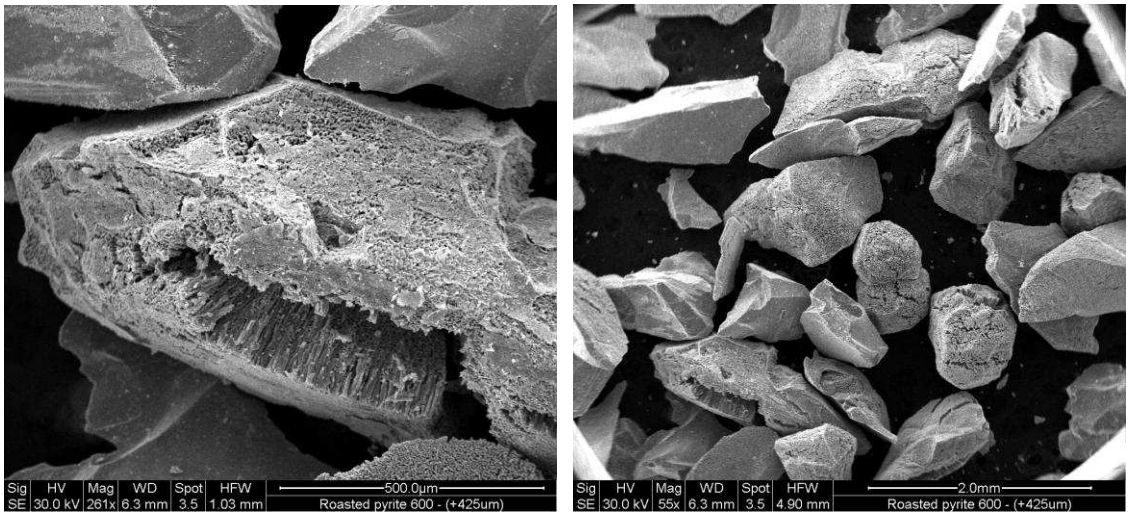

(a) **(b)**

Figure 4.36 (a) Secondary electron images +425µm pyrite particle conventionally roasted for 15 minutes at 600°C. (b) +425µm pyrite particles showing porous texture.

The particle shown in Figure 4.36 shows total oxidation with the grain splitting and swelling. Not all particles appear to have experienced complete oxidation although evidence of surface alterations and porosity is common particularly for particle roasted at the highest temperatures for the longest period of time.

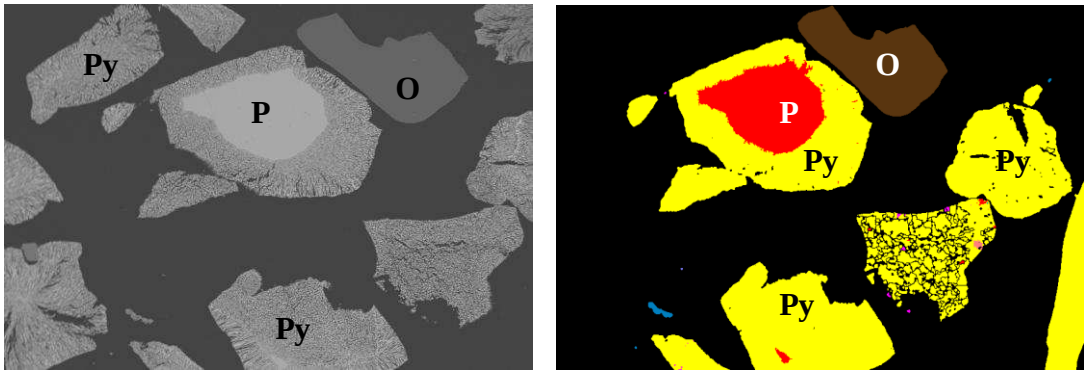

(a) **(b)**

Figure 4.37 (a) BSE image showing pyrite particles +425µm conventionally roasted for 15min. (b) BSE false coloured image of "a"showing areas of pyrite and pyrrhotite formation due to oxidation. (P=Pyrite, Py=Pyrrhotite, O=Other)

The BSE images shown in Figure 4.37 shows clearly that the onset of oxidation starts at the surface of the particle and proceed towards its centre. It can also be seen that not all particles have been completely altered to porous pyrrhotitie with an unreacted pyrite core remaining in some instances. There is some evidence to suggest that pyrite has been transformed by a two step process: the thermal decomposition of the pyrite particle resulting in porous pyrrhotite being the first step, then successive oxidation of pyrrhotite to form hematite. No evidence of magnetite was observed in any samples examined here.

4.4.9 Results (-38µm Particles)

The modal mineral percentage area results for <38µm pyrite particles roasted at 400, 450, 500 and 600°C are presented in Figures 4.38, 4.39, 4.40 and 4.41 respectively.

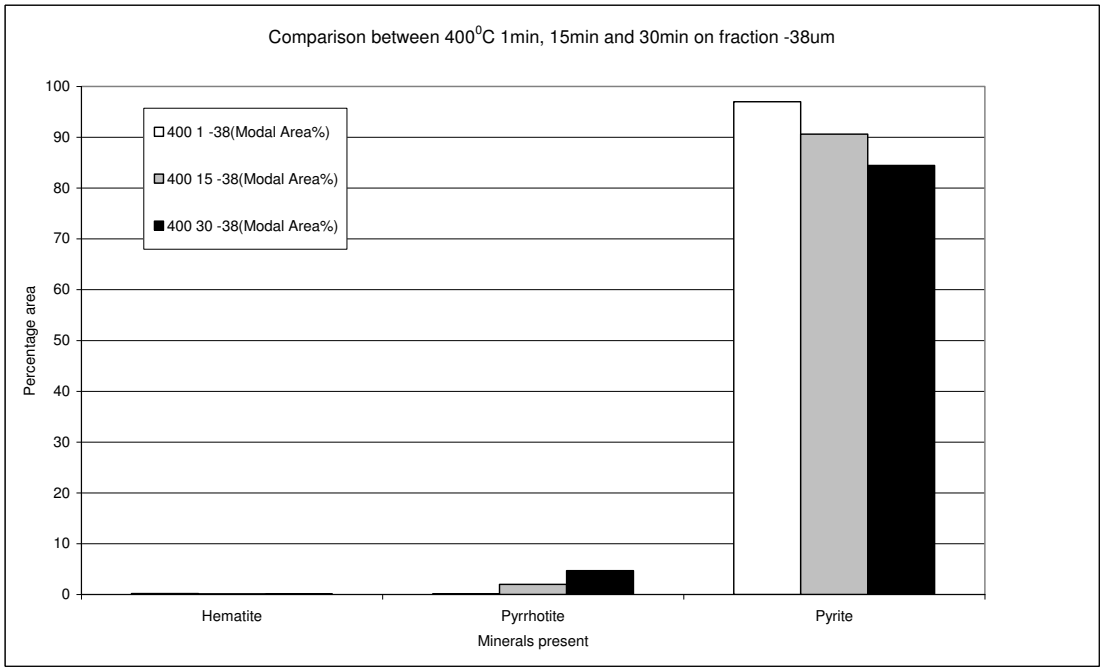

Figure 4.38 Modal area % plot of roasted -38µm pyrite at 400°C.

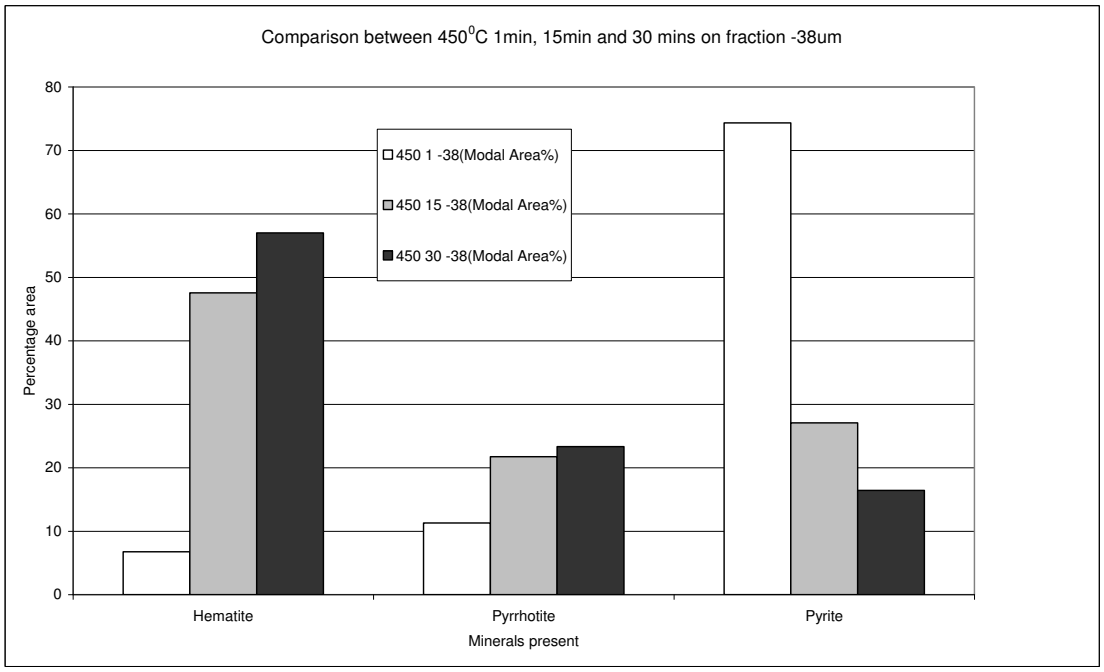

Figure 4.39 Modal area % plot of roasted -38µm pyrite at 450°C.

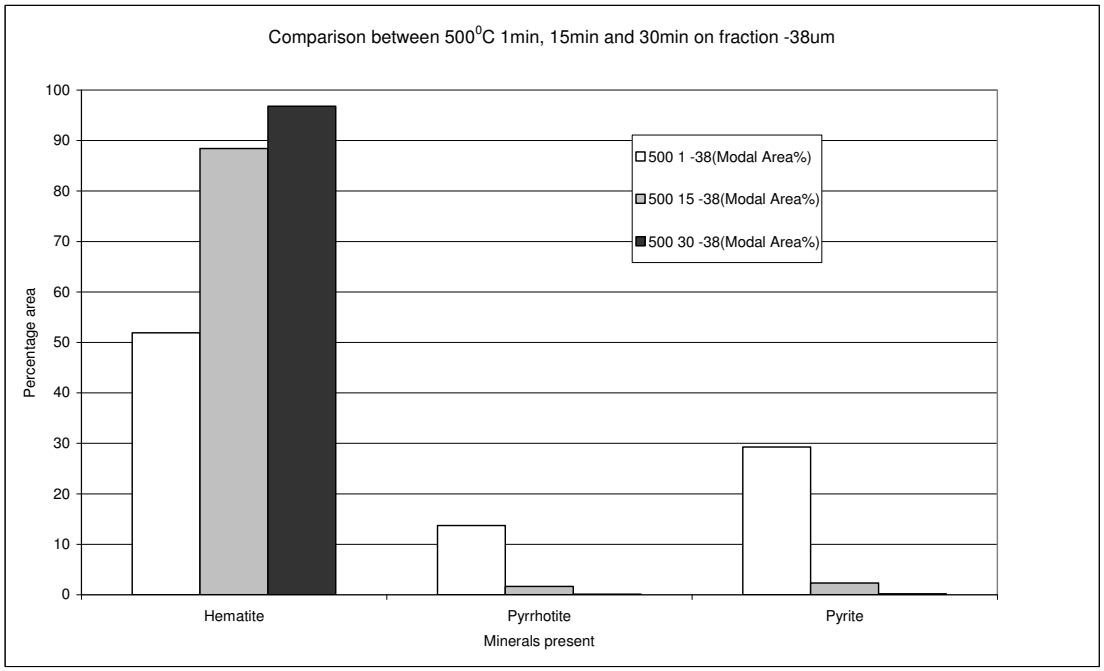

Figure 4.40 Modal area % plot of roasted -38µm pyrite at 500°C.

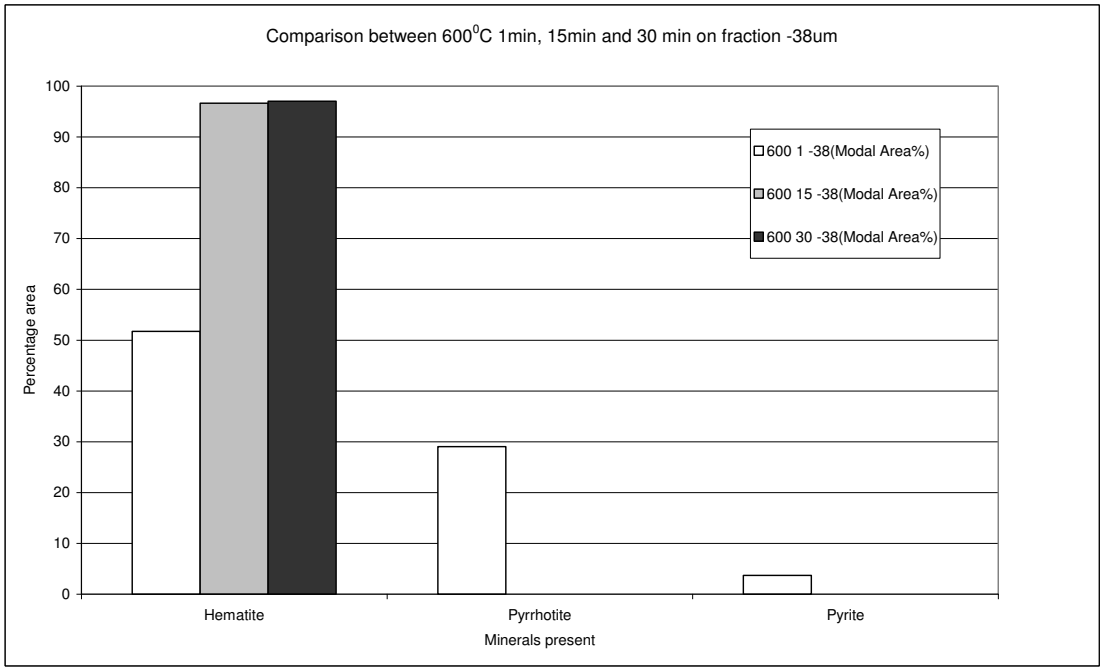

Figure 4.41 Modal area % plot of roasted -38µm pyrite at 600°C.

Modal mineralogy data for 400°C conventional heating reveals that the conversion from pyrite to pyrrhotite is once again insignificant regardless of roasting time for <38µm pyrite particles. The test results for <38µm roasted pyrite at 450°C show promising results with significant amount of pyrrhotite formed. It can be seen that the percentage area of pyrrhotite phase produced upon heating increases with increasing residence time (along with a similar trend from hematite). It is clear from the results shown for roasting at 500°C and 600°C shown in Figure 4.40 and 4.41 respectively that roasting for 900 s and 1800 s, pyrite decomposes completely to hematite. The secondary electron image of a series of typical roasted -38µm pyrite particles shown in Figure 4.42 is evidence of oxidation at a roasting temperature of 400°C for 1 minute.

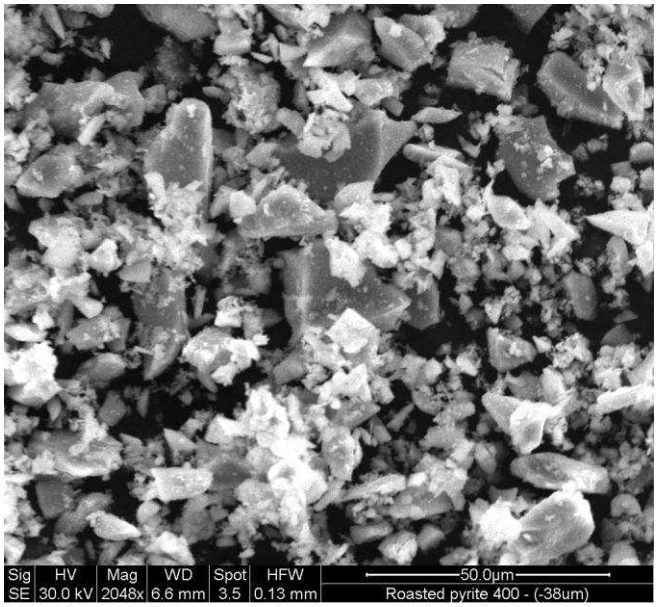

Figure 4.42 (a) Secondary electron images -38µm pyrite particles conventionally roasted for 1 minute at 400°C.

It can be seen that few particles have been affected by heating, with the larger particle remaining largely unaffected. This is consistent with MLA analysis presented in Figure 4.38, which suggests that at 400°C and heating time of 1 minute, no form of oxidation transformation to either pyrrhotite or hematite has been detected. It is clear to see from the results presented here, that it is time and not temperature which is the overriding controlling factor in -38µm pyrite transformation by this method.

4.5 Conventional roasting Magnetic Property Measurement.

The effects of conventional heat treatment (in air) on the magnetic properties of pyrite have been investigated here. The magnetic properties of finely ground (-38µm) pyrite were measured using a Lakeshore 7300 Series Vibrating Sample Magnetometer (VSM). Initially the VSM instrument was calibrated using a Nickel Sphere. Hysteresis loops were gathered for field strengths up to a maximum of 1600kAm^{-1}. Using the TGA/DSC

analysis data in Figure 4.25 and 4.26 respectively, a set of key temperatures at which mass loss and heat flow anomalies indicate the onset of oxidation and other phase transformations were selected. Each pyrite sample was heated using a thermogravimetric Pyris Perkin-Elmer instrument in dynamic air (100ml/min) at a constant heating rate of 5°C/min until the critical temperature is reached. The sample is then allowed to soak at this temperature for 15 minutes until being allowed to cool in air. The critical temperatures selected, coincident with heat flow and mass loss anomalies were 380, 400, 490, 515 and 570°C. Figure 4.43 shows the hysteresis loops in the first quadrant for each experiment.

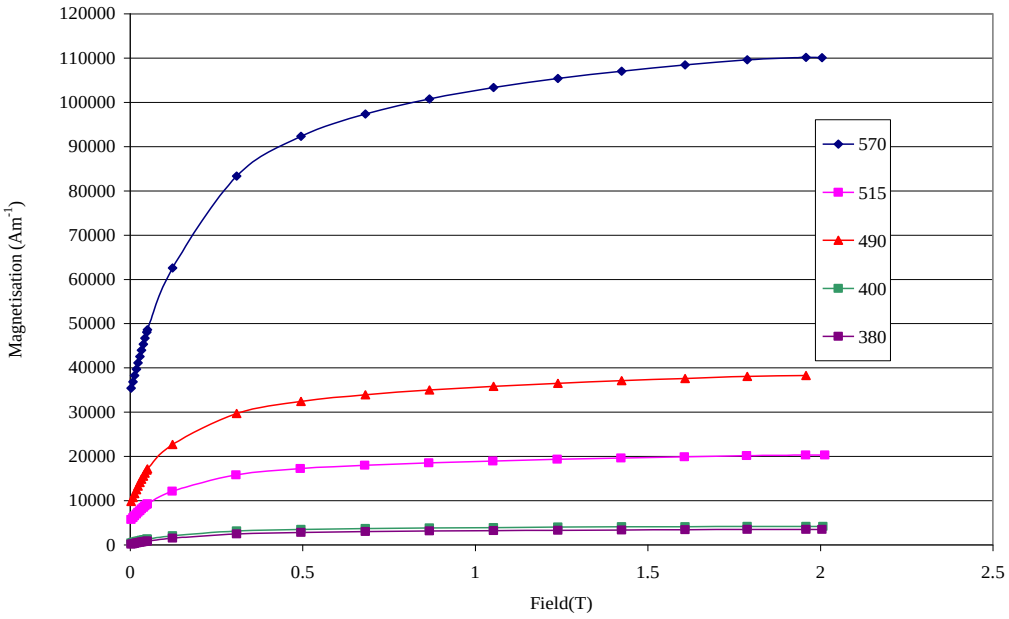

Figure 4.43 Hysteresis curves in the first quadrant for thermally treated pyrite.

The hysteresis curves shown in Figure 4.43 show the effect of temperature on the magnetisation of each treated pyrite sample. It is clear from data presented here that the magnetisation has increased with increasing temperature. The magnitude of the

maximum magnetisation increases considerably from ~2 kAm^{-1} for treatment at 380 and 400°C to over 110 kAm^{-1} for treatment at 570°C. It is likely that this increase in the magnetisation is as a direct result of pyrrhotite formation from oxidation of the sample. This hypothesis is supported by XRD analysis on each sample presented in Appendix A4. Similar results have been report by Waters, et al., 2007 who found that the magnetisation continued to increase with increasing treatment temperature up to 700°C due to the formation of pyrrhotite. The magnetisation then modestly decreased as a result of the formation of antiferrimagnetic hematite at 800°C. The corresponding magnetic susceptibility curves for each sample are shown in Figure 4.44.

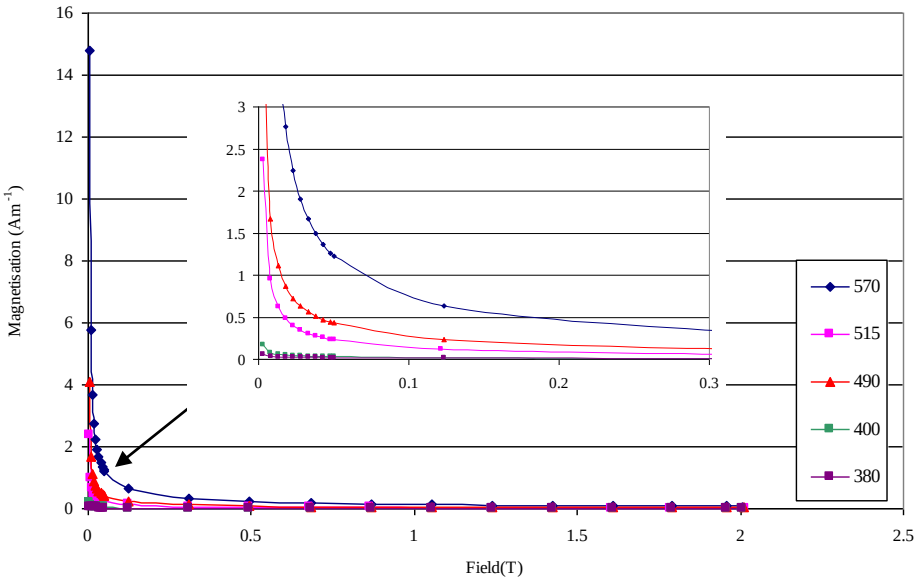

Figure 4.44 Magnetic susceptibility curves for conventionally heated pyrite samples.

The degree of magnetic saturation as indicated in the VSM data presented in Figures 4.43 and 4.44 indicates the degree of ferromagnetism in the sample. It can be seen from the susceptibility curves shown in Figure 4.43 that the initial magnetic susceptibility for the sample treated at 570°C is significantly higher when compared to Untreated, 380 and

400°C. Furthermore, the field strength at which magnetic saturation is achieved increases with increasing temperature.

4.6 Single-mode microwave heating experiments

Small scale fluidised bed experiments were carried out on screened pyrite samples in the narrow size range of -600+425μm and -38μm. In the case of the smaller size fraction, the pyrite was riffle split into three representative 10g batches. The samples were fluidised within a standard elutriation tube with the gas volume flow rate adjusted to ensure stable dynamic flow and complete particle entrainment. The samples were treated for 4, 10 and 15 seconds at full power (1kW). To maximise power transfer to the sample, the waveguide characteristics were tuned using the stub-tuner device situated along the waveguide. After treatment the samples were removed from the microwave apparatus and allowed to cool in air before being prepared for SEM/MLA analysis. The results are presented in Figure 4.45.

4.6.1 Results (-38μm particles)

The results indicate that after 4s treatment time only a small amount of pyrite has been altered to pyrrhotite with no hematite present from MLA investigations. However, after 10s of treatment a significant amount of pyrite has been altered to pyrrhotite and hematite. With increased treatment time it was found that pyrite was oxidised mainly to hematite with some pyrrhotite present in the sample. The overall amount of pyrrhotite produced (on % area basis) had slightly decreased after 10s when compared with the results for 4s treatment. The maximum temperature of the particles during treatment was not measured in these experiments. BSE sample images of each treatment are shown in Figure 4.46(a), 4.46(b) and 4.46(c) respectively.

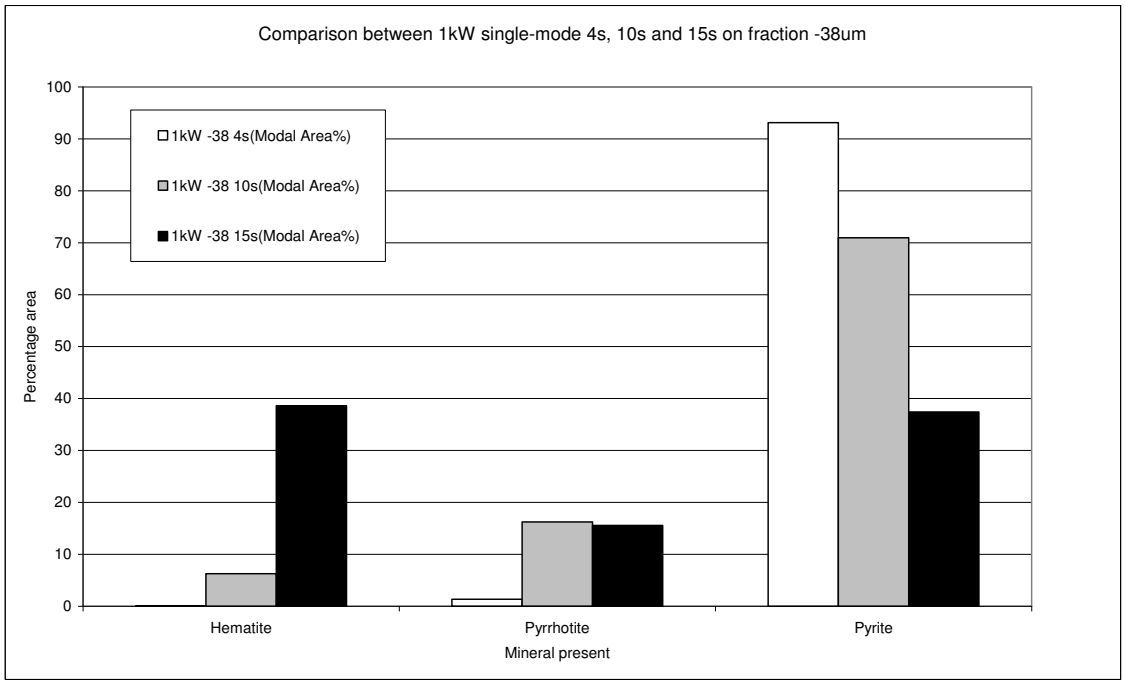

Figure 4.45 Modal area % plot of microwave treated -38µm pyrite particles.

It can be seen in Figure 3.36(a) that the fines show signs of oxidation with the larger particle remaining largely unaffected. The image of the 1kW 10s treatment of the +38µm pyrite in Figure 4.46(b) suggests that particles have combined during treatment to form aggregates. The large particles show some oxidation and are host to small crystals of iron sulphate. Once again there is evidence to suggest that not all particles are affected by microwave heating. Significant oxidation is present after 15 seconds of treatment time. It can be seen in Figure 4.46(c) that aggregates have been formed and large particle exhibit swelling and have a porous surface texture. This expansion and change in surface texture was also evident in conventionally heated samples. The BSE image in Figure 4.47 at high magnification shows the characteristic particle splitting along ridges and porous structure.

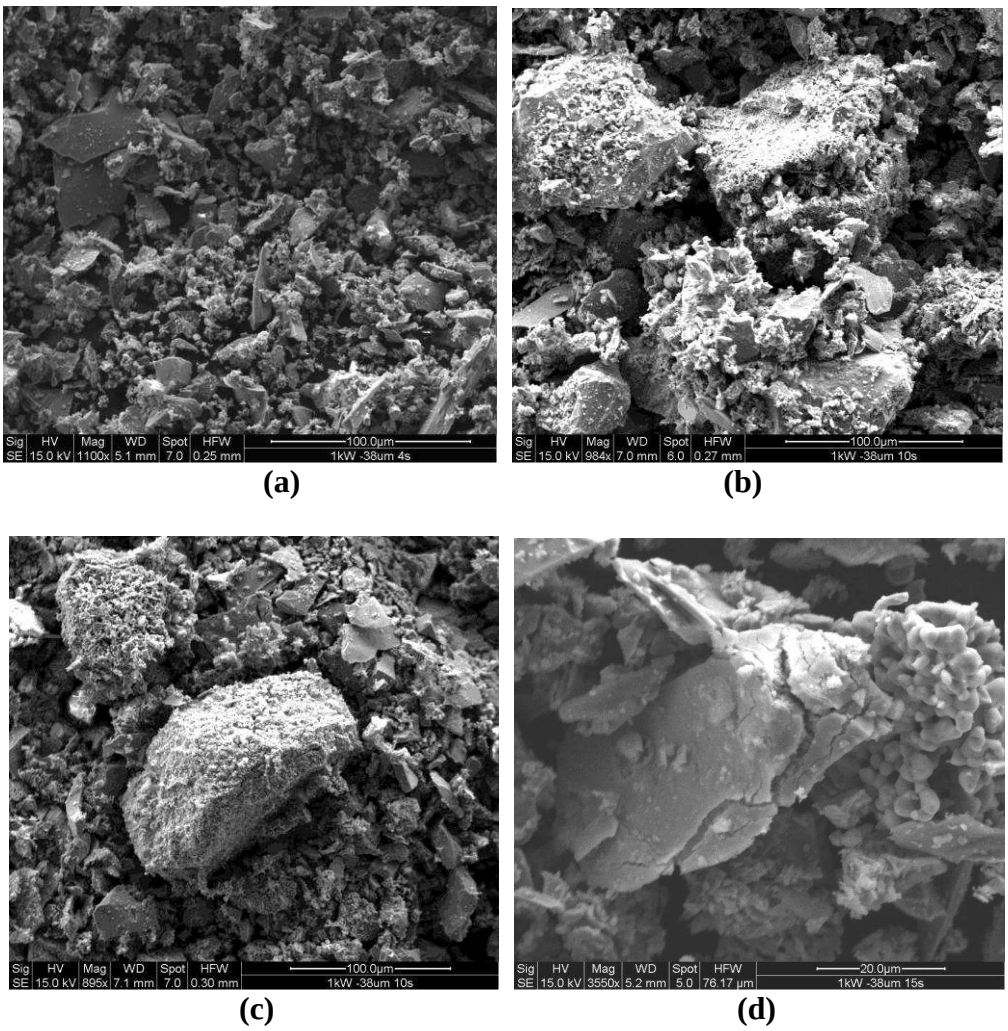

Figure 4.46 BSE images -38 microwave treated pyrite (a) 1kW, 4 sec treatment time (b) 1kW, 10 sec treatment time (c) 1kW, 15 sec treatment time (d) 1kW, 15 sec treatment time (High Mag)

It can be seen in Figure 3.36(a) that the fines show signs of oxidation with the larger particle remaining largely unaffected. The image of the 1kW 10s treatment of the +38µm pyrite in Figure 4.46(b) suggests that particles have combined during treatment to form aggregates. The large particles show some oxidation and are host to small crystals of iron sulphate. Once again there is evidence to suggest that not all particles are affected by microwave heating. Significant oxidation is present after 15 seconds of treatment time. It

can be seen in Figure 4.46(c) that aggregates have been formed and large particle exhibit swelling and have a porous surface texture. This expansion and change in surface texture was also evident in conventionally heated samples. The BSE image in Figure 4.46(d) at high magnification shows the characteristic particle splitting along ridges and porous structure.

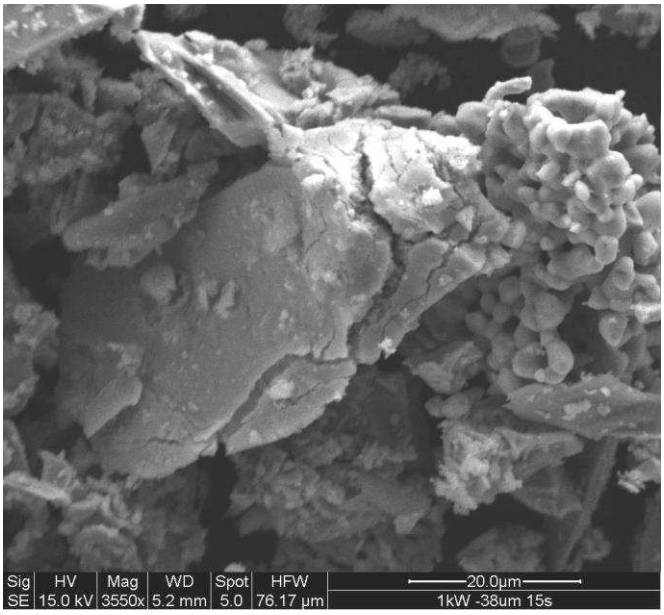

Figure 4.47 High magnification BSE image of -38µm pyrite (1kW, 15 sec treatment).

4.6.2 Results (-600+425µm Particles)

The pyrite was riffle split into two representative 10g batches. The samples were fluidised within a standard elutriation tube with the gas volume flow rate adjusted to ensure stable dynamic flow and complete particle entrainment. The samples were treated for 8.77, 10, 20, 40, 120 and 172 seconds at full power (1kW). To maximise power transfer to the sample, the waveguide characteristics were tuned (for each experiment) using the stub-tuner device situated along the waveguide. In a number of cases, the

experiment was terminated due to significant arcing coupled with high reflected power. Correct tuning of the waveguide is therefore essential in these experiment but extremely difficult maintain a steady reflected power in practice. After treatment the samples were removed from the microwave apparatus and allowed to cool in air before being prepared for SEM/MLA analysis. The results are presented in Figure 4.48.

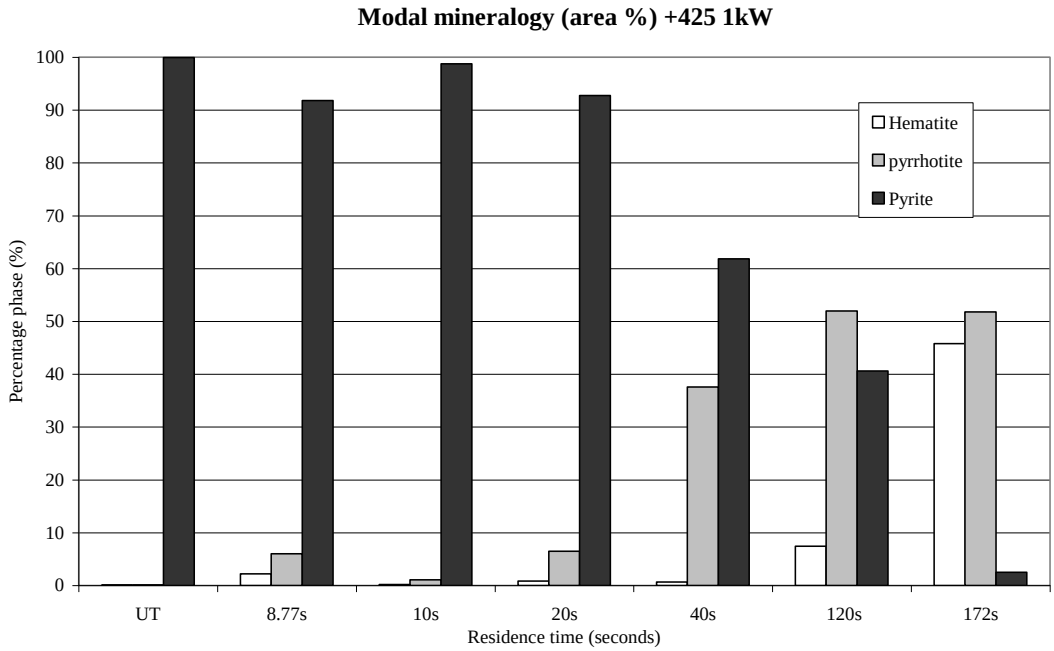

Figure 4.48 Modal area % plot of microwave treated -0.6 + 0.425µm pyrite particles.

The MLA results for untreated (UT) pyrite have been included here for comparison purposes. To some extent it can be seen that the amount of pyrrhotite formation increases with increasing residence time. The anomaly at 10 seconds treatment time is due to difficulties associated with waveguide tuning where reflected power minimisation proved difficult to control. It is noted here that only very small areas of hematite are detected

until 120 and 172 second treatment times, where it can be seen that almost 50% of the sample measured after 172 seconds treatment time consisted of hematite with very little (<5%) pyrite remaining. A selection of BSE images of microwave treated pyrite particles are shown in Figure 4.49.

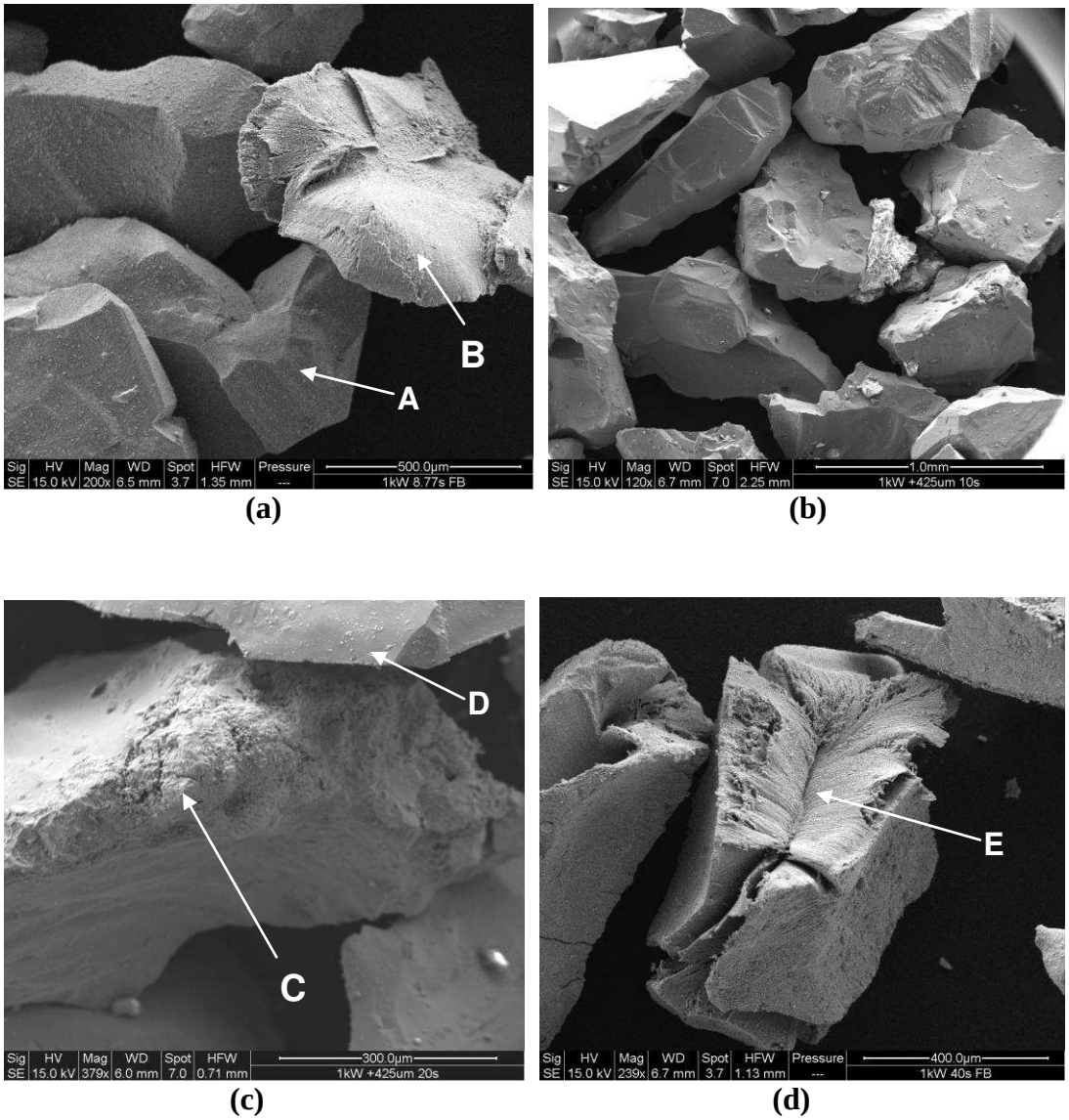

(a) **(b)**

(c) **(d)**

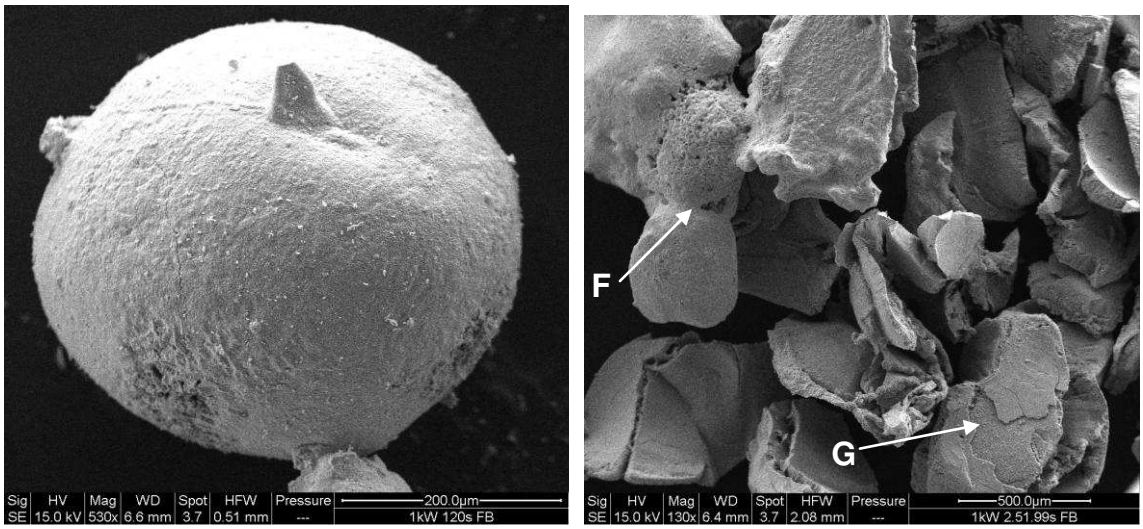

(e) **(f)**

Figure 4.49 BSE images +425µm microwave treated pyrite (a) 1kW, 8.77 sec treatment time, (b) 1kW, 10 sec treatment time, (c) 1kW, 20 sec treatment time, (d) 1kW, 40 sec treatment time,(e) 1kW, 120 sec treatment time, (f) 1kW, 172sec treatment time.

It can be seen in Figure 4.49 (a) that significant oxidation has occurred in particle **B** showing the characteristic porous texture and exfoliation of the surface that has also been observed in conventionally heated particles. However, it is clear that not all particles were affected by microwave heating and most probably microwave coupling was not achieved evenly throughout the sample. This can be seen in particle **A** where the BSE image shows that although fine sulphate particles were identified on its surface, it remains virtually unaffected. The BSE image shown in Figure 4.49(b) indicates that microwave coupling was not successfully achieved in this experiment with the majority of particle showing little sign of oxidation. Figure 4.49(c) shows that significant oxidation has taken place after 20 seconds treatment where oxidation is particularly evident along particle ridges. Particle **C** exhibits the characteristic porous texture. However, once again particle **D** is indicative of uneven heating and shows little sign of

oxidation. As the residence time increases, more particle have chance to couple with the microwave and therefore the yield of both pyrrhotite and hematite increase. The highly magnified image shown in Figure 4.49(d) shows a particle with extensive oxidation. The characteristic swelling and porous texture (similar to that seen in conventionally heated samples) is clear to see at position **E**. It is impossible to conclude that this particle has experienced complete oxidation from the 3D-BSE image. However, upon examination of 2D-BSE images it was shown that the majority of particle has experienced some oxidation with a very small number of particle being unaffected and a number of particle showing an unaffected pyrite core conducive to the shrinking core model proposed by Hu, et al., 2007. After 120 seconds of exposure time at full power the experiments yield over 50% (by area) of pyrrhotite after MLA analysis with <10% hematite and ~ 40% pyrite remaining. Again examination of the MLA data, together with observations of 2D-BSE images, show that uneven heating has taken place in this sample. Some particles show complete oxidation through to hematite, with some showing evidence of pyrrhotite surrounded by hematite and other showing an unaffected pyrite core with a pyrrhotite and hematite surround (typical of the shrinking core model). The image in Figure 4.49(d) shows a particle that has sintered to Fe after 120 seconds treatment time. The image shown in Figure 4.49(d) is not a typical occurrence but shows the extent to which uneven heating and unsuccessful microwave coupling can affect the results in these experiments. After 172 seconds treatment time very little pyrite remains and extensive oxidation the vast majority of particles is evident as seen in Figure 4.48. The BSE image shown in

Figure 4.49(f) shows that some sintering has taken place at position **F** the vast majority of particles show a porous and exfoliating surface texture show at point **G**.

4.7 Microwave heated sample magnetic property measurement (-38μm Particles).

The effects of microwave heating on the magnetic properties of pyrite have been investigated here. The magnetic properties of finely ground (-38μm) pre-treated pyrite were measured using a Lakeshore 7300 Series Vibrating Sample Magnetometer (VSM). Initially the VSM instrument was calibrated using a Nickel Sphere. Hysteresis loops were gathered for field strengths up to a maximum of 1600kAm^{-1}. Figure 4.50 shows the hysteresis loops in the first quadrant for each experiment.

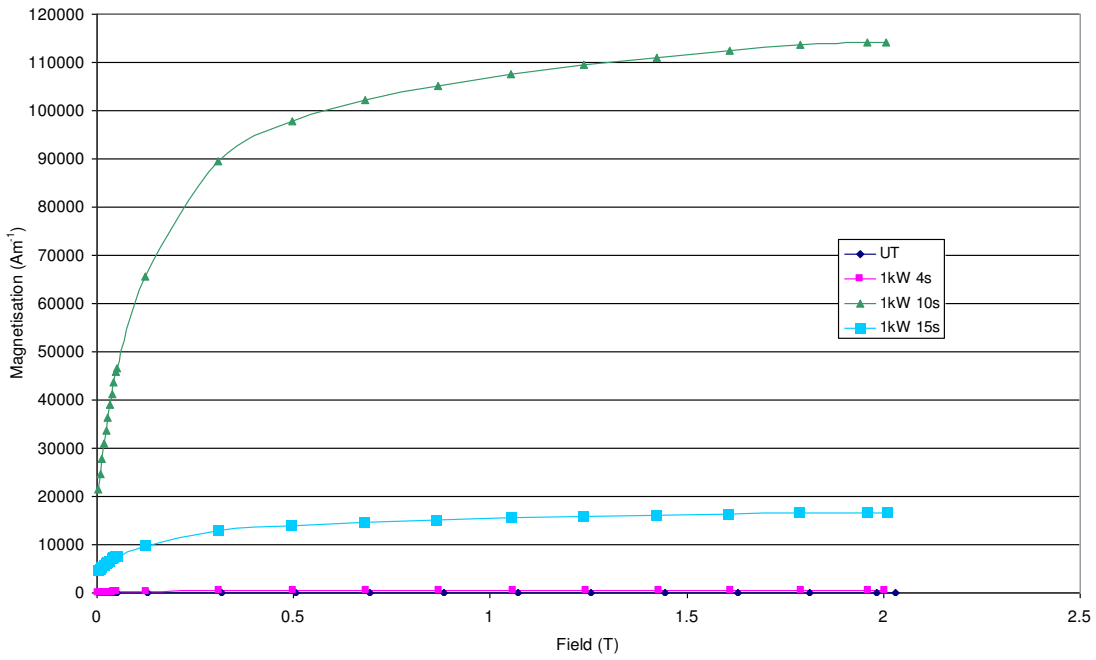

Figure 4.50 Hysteresis curves in the first quadrant for microwave treated -38μm pyrite.

The hysteresis curves shown in Figure 4.50 show the effect of microwave exposure time on the magnetisation of each treated -38μm pyrite sample. The sample treated for 10 seconds shows a greater magnetisation that the sample treated for 15 seconds. This is probably due to the significant amount of hematite produced after 15 seconds and simply the sample was treated for too long which had a detrimental effect on its magnetic properties as a result of the formation of antiferrimagnetic hematite. The amount of pyrrhotite formed after 15 second was less than produced after 10 seconds as seen in Figure 4.50. The magnitude of the maximum magnetisation increases considerably from ~2.5 kAm^{-1} for untreated pyrite to over 110 kAm^{-1} for the treatment time of 10 seconds. It is likely that this increase in the magnetisation is as a direct result of pyrrhotite formation of the sample and therefore shows that controlling treatment time (and thus pyrrhotite formation) is key to successfully increase the magnetic properties of pyrite. It is impractical to measure the temperature of the sample whilst resident in the microwave cavity and so maximum temperature achieved for each experiment cannot be discussed or reported. The corresponding magnetic susceptibility curves for each sample are shown in Figure 4.51. The degree of magnetic saturation as indicated in the VSM data presented in Figures 4.50 and 4.51 indicates the degree of ferromagnetism in the sample. It can be seen from the susceptibility curves shown in Figure 3.41 that the initial magnetic susceptibility for the sample treated for 10 seconds is significantly higher when compared to Untreated, 4 and 15 second treatment time. Furthermore, the field strength at which magnetic saturation is achieved increases with increasing pyrrhotite formation in the sample.

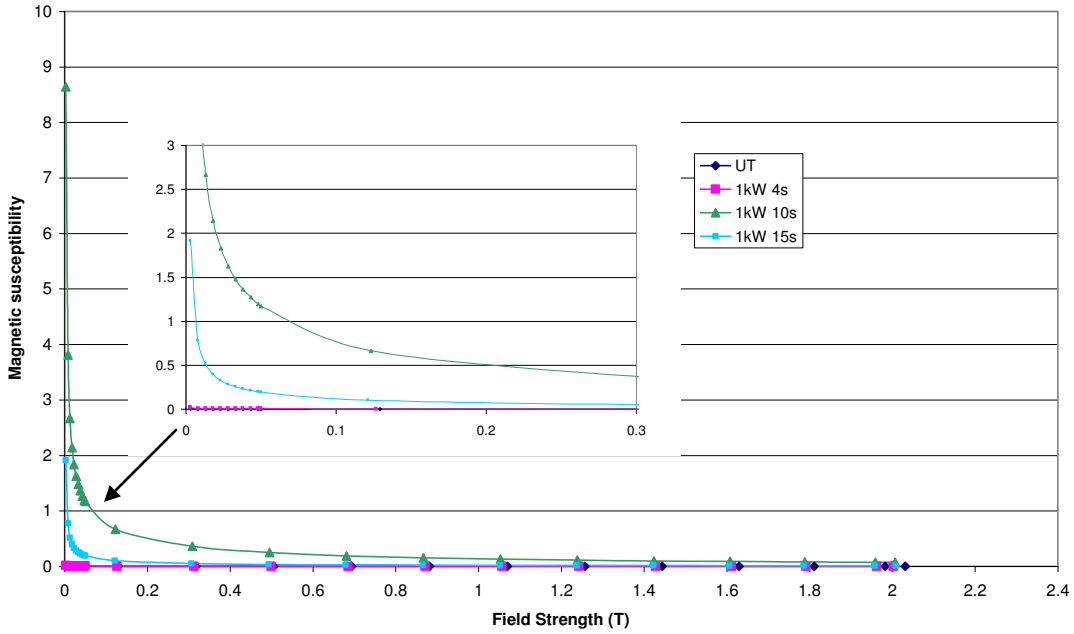

Figure 4.51 Magnetic susceptibility curves for microwave heated -38μm pyrite samples.

4.8 Microwave heated sample magnetic property measurement (+425μm Particles).

The effects of microwave heating on the magnetic properties of pyrite have been investigated here. The magnetic properties of finely ground (+425μm) pre-treated pyrite were measured using a Lakeshore 7300 Series Vibrating Sample Magnetometer (VSM). Three samples were tested after exposure times of 8.77 and 20 seconds. Figure 3.42 shows the hysteresis loops in the first quadrant for each experiment. The hysteresis curves shown in Figure 3.42 show the effect of microwave exposure time on the magnetisation of each treated +425μm pyrite sample. The sample treated for 8.77 seconds shows a slightly larger magnetisation that the sample treated for 20 seconds. It can be seen from the results displayed in Figure 3.38 that the amount of pyrrhotite formed (% area basis) is similar for each experiment with the 8.77 exposure time producing

slightly more hematite. Therefore one would expect that the magnetisation should be higher in the sample treated for 20 seconds, although the difference in magnetic susceptibility is very small as seen in Figure 4.51 The magnetic susceptibility curves for each sample are shown in Figure 4.51.

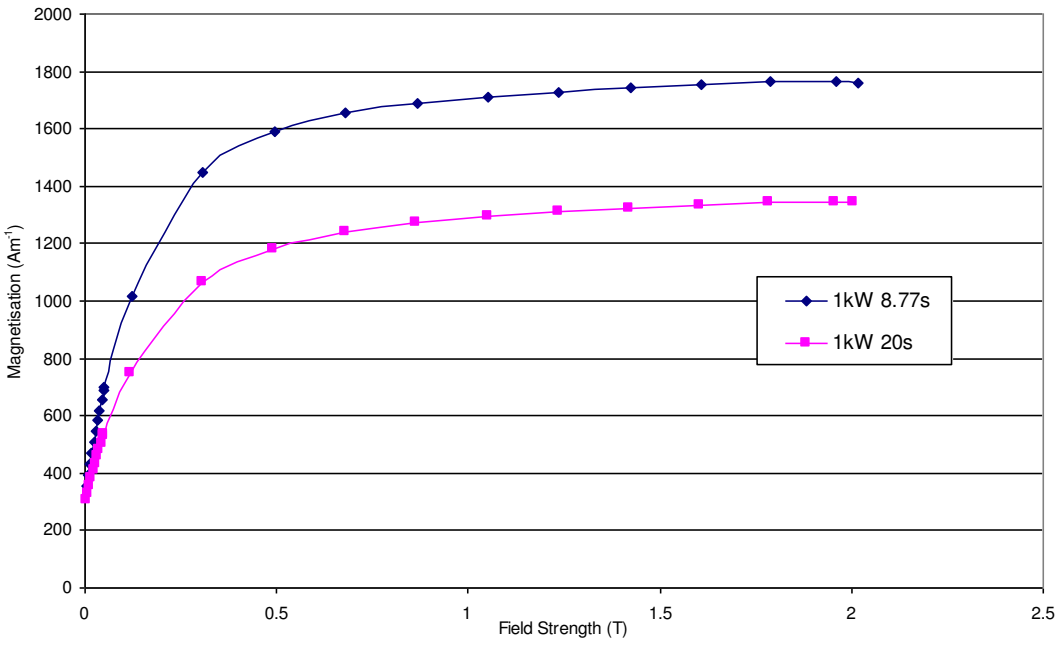

Figure 4.52 Hysteresis curves in the first quadrant for microwave treated -+425µm pyrite.

Given the scale of the magnetic susceptibility axis and that the alteration in magnetic susceptibility is very small for the two experiments tested here, it is necessary for further investigation to be carried out on samples treated for exposure time of 40, 120 and 172 seconds before any conclusion can be drawn as to the effect of microwave exposure time on the magnetic properties of +425µm pyrite.

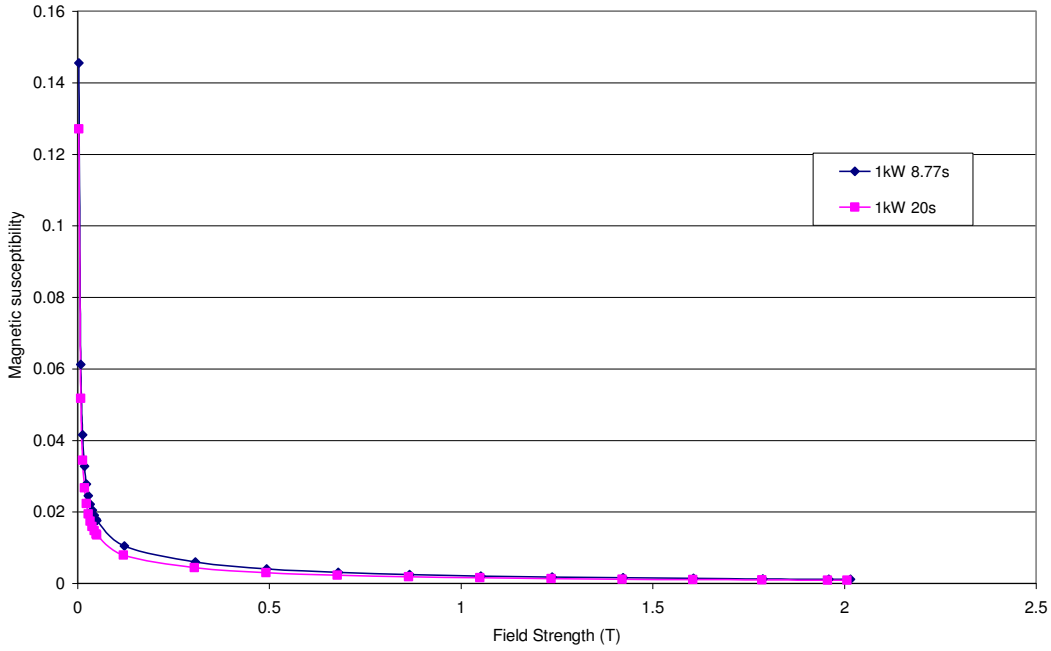

Figure 4.53 Magnetic susceptibility curves for microwave heated +425μm pyrite samples.

4.9 Discussion

It is clear from the analysis of previous published work and the work presented here that the thermal transformation of pyrite either by oxidation or desulphurisation is a complex process and will be controlled by a number of mechanisms. It has been shown that the whole process is governed by atmospheric gas pressure, temperature, particle size and the method of heat application. This study has demonstrated that, in practice, these mechanisms are difficult to control and measure. An obvious example of this is the fact that the temperature of the fluidised particles inside the single-mode microwave cavity could not be measured to a reasonable degree of accuracy and therefore the conclusions as to the key controlling transformation mechanisms in this case are not concrete. The experimental variables in the microwave experiments were the applicator design (mono or multi-mode applicators), power level and the residence time of the particle within the microwave cavity. The results for the 1kW single-mode microwave experiments for -38μm particle and +425μm particles are shown in Figure 4.54 and 4.55 respectively.

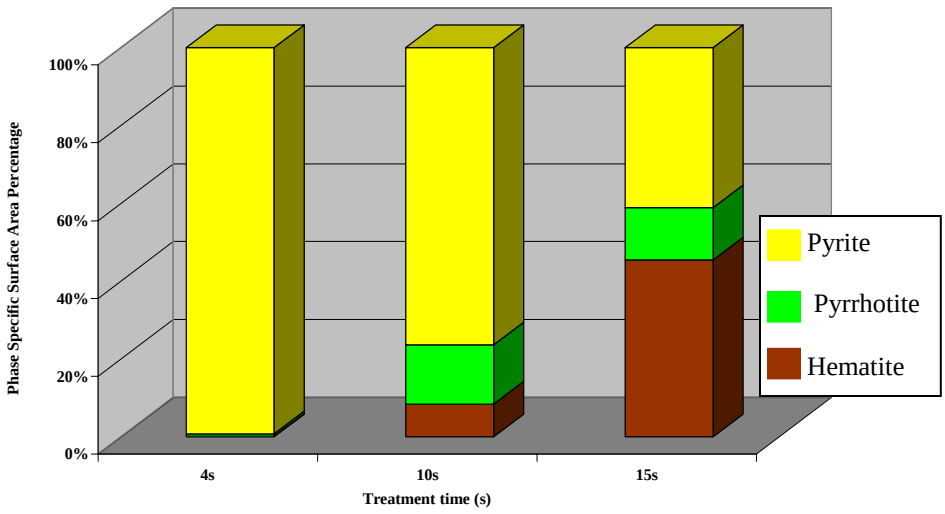

Figure 4.54 1kW single-mode fluidised bed microwave experiments for -38μm pyrite particles.

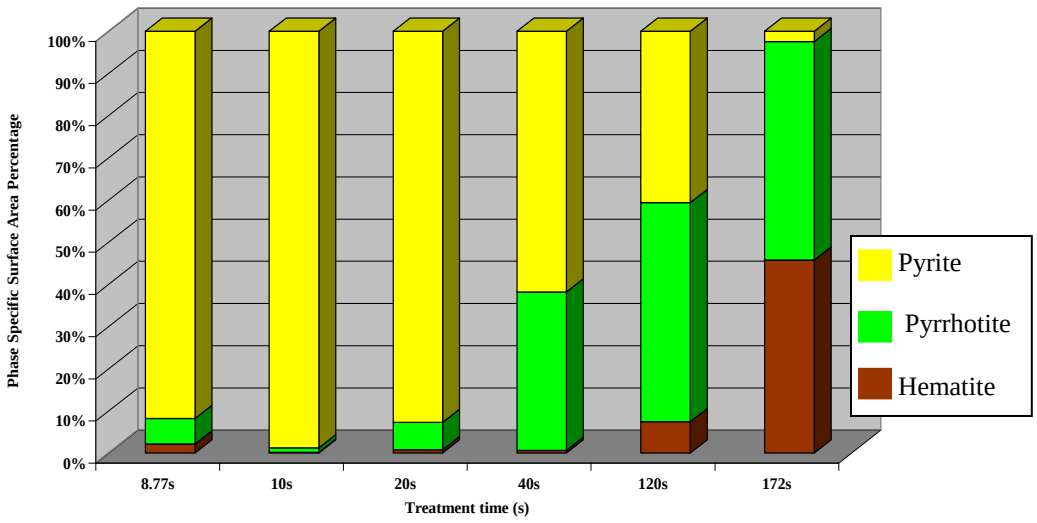

Figure 4.55 1kW single-mode fluidised bed microwave experiments for +425μm pyrite particles.

The results from MLA analysis shown in Figure 4.54 for -38μm particles show that microwave treatment for only 4 seconds had little effect on its oxidation. Difficulties with reflected power control and microwave coupling with the particle have had an effect on the results here. After 10 seconds treatment time ~20% of the pyrite has been converted to pyrrhotite with some hematite present also. With longer treatment time the fraction of pyrrhotite produced is reduced and hematite is formed. Although temperature is not quantifiable in these experiments, it is reasonable to assume that as treatment time increases the particle temperature is also likely to increase. Observations of the treated particles by SEM/MLA analysis show that in some cases pyrite has been directly oxidised to hematite. In other cases pyrrhotite has been formed as an intermediate with the particle showing characteristic shrinking core effects. It is possible that the nature of the phases formed during this process is as a result of two effects. Firstly the particle

couples with the microwaves early in the experiment and heats rapidly. In this case, heating rates and temperature are high, oxygen diffusion through the gas layer is not prohibited (since the particles are fluidised) and complete direct oxidation of the particle occurs. On the other hand, it is reasonable to assume that not all particle with couple with the microwaves at the same time. In this case, heating time is shorter, particle maximum temperature is lower and intermediates such as pyrrhotite are able to be formed. As sulphur burns at the surface of the particle the resulting pyrrhotite becomes porous (pathways for gas ejection) allowing oxygen diffusion into the particle and the pyrrhotite is oxidised further through to hematite. In some cases particles couple with the microwaves late in the process and so are not completely oxidised by this method. In this case the inner core of the particle remains unaltered. The results in Figure 4.54 suggest that temperature is the controlling factor in the transformation and long microwave exposure time will not necessarily result in an increased pyrrhotite yield. Overexposure to microwaves, coupled with high heating rates will favour hematite formation which can adversely affect the magnetic properties of the sample (production of antiferrimagnetic hematite). The magnetic property results shown in Figure 4.50 support this theory whereby the sample treated for 15 seconds exhibited a significantly lower magnetisation than the sample treated for 10 seconds. This is almost certainly as a result of antiferrimagnetic hematite formation. No evidence was found of magnetite formation in the treated product in this experiment which, according to Hu, et al., 2007 is formed as a result of oxygen deficiency at the reaction front (caused by fast reaction rates or slow oxygen diffusion).

The result for the microwave heating experiment on +425μm pyrite is shown in Figure 4.54 for comparison. The results again suggest that pyrrhotite formation is time/temperature dependent and that heating the sample for prolonged periods of time will result in hematite formation which will have a detrimental effect on the magnetic properties of the final product. SEM/MLA measurements and observations of treated +425μm sample show irregular heating characteristics with some particles heavily oxidised, others partially oxidised and some unaffected by microwave heating. These are typical results due to the nature of the experiments and the obvious problems associated with the particles coupling with microwaves. Assuming that the particles which exhibit extreme oxidation are those which coupled early in the experiment, it is clear that microwave coupling proved to be problematic in these experiments. The results displayed after 10 seconds treatment should be discarded due cavity tuning difficulties and the fact that reflected power could not be adequately minimised. The magnetic property results for microwave treated +425μm pyrite are inconclusive. The VSM tests were carried out on two samples of similar composition in terms of pyrrhotite content. As a result the differences between the magnetisation and magnetic susceptibility of each sample, as shown in Figure 4.52 and 4.53 respectively, are small (although modestly improved from untreated results). Further work is required here to include the magnetic property measurement of all samples in the experimental regime so that accurate conclusions can be draw as to the extent of the improvement in the magnetic properties as a result of microwave treatment time. The fact that magnetite was not identified in any of the microwave experiments presented in this work suggests that in both -38μm and +425μm

experiments oxygen diffusion to the reaction front was not prohibited either by means of unfavourable sulphur gas partial pressure or by pore blocking effects at the particle surface. It can be seen from the dielectric properties versus temperature results displayed in Figure 4.31 that the dielectric properties alter at the point at which the onset of pyrite oxidation is likely to occur. Changes in the loss factor of pyrite are observed once phase transformation has started to take place affecting its susceptibility to be heated by microwave energy. During the experiments it was noted that once some particles had coupled with the microwaves the effect would be that the heating rate became uncontrollable and in some cases the experiment was halted.

The SEM/MLA data presented for pyrite heated during thermogravimetric analysis proved unreliable. The result presented in Figure 4.29 for pyrite heated in air show no particular trend with respect to pyrrhotite or hematite formation. The temperatures selected for heating to take place were informed from a TGA/DSC trace where a likely phase transition coincided with heat flow and mass loss anomalies. The standard alumina sample pans used in these experiments were narrow and deep. As such good gas exchange between the particle and the atmosphere could not be achieved (apart from particles close to the surface). In an ideal situation, large open sample pans should be used so that a thin layer of particle (a few particles deep) can be achieved. The results presented in Figure 4.30 for pyrite heated in a nitrogen atmosphere show that little (if any) transformation has taken place at the experimental temperatures. This is inconsistent with TGA/DSC traces where clear anomalies associated with phase transitions can be observed. It is likely that the temperature range chosen for the TGA experiments in inert

atmospheres are set to low and more investigative work is necessary at elevated temperatures. The results at 450°C and 470°C show some evidence of pyrrhotite formation. However, a small amount of pyrrhotite was reported in the untreated samples and so it is impossible to conclude that these were formed due to thermal effects.

The SEM/MLA results for conventionally heated -38μm are presented in Figure 4.56 for comparison.

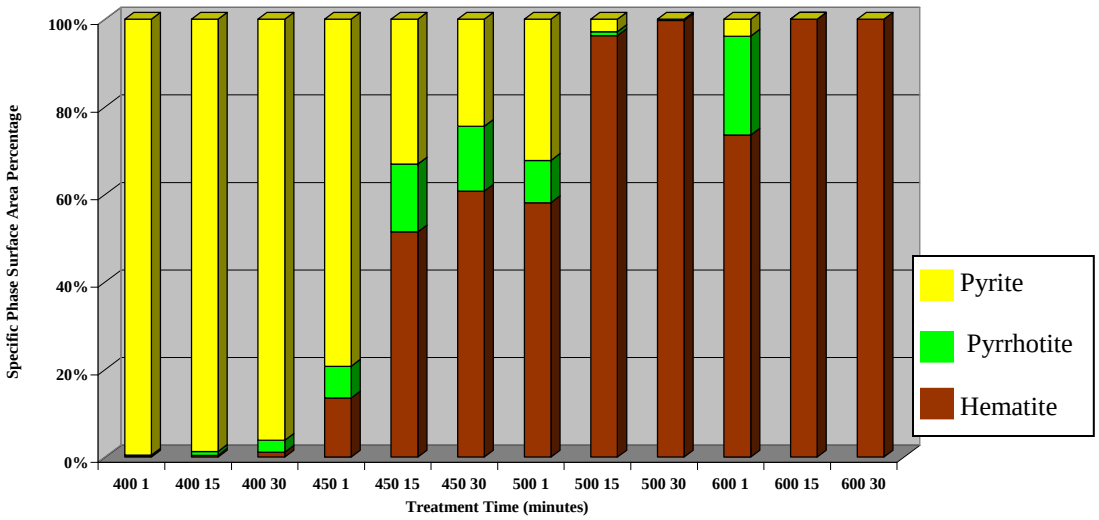

Figure 4.56 Conventional heating experiments for -38μm pyrite particles in static air.

It can be seen from the results presented Figure 4.56 that pyrrhotite formation by heating with conventional means is difficult control. The controlling factors here are likely to be temperature, heating rate and atmospheric gas conditions. In all cases the muffle furnace was pre-heated to the desired experimental temperature and the mono-layer of particles was placed inside the furnace once the critical temperature was achieved. The samples heated to 400°C show a modest increase in the pyrrhotite formation with increased heating time, although little evidence of oxidation can be seen for the heating time of 60

seconds. As the temperature is increased further to 450°C the formation of hematite becomes significant. Increased residence time only serves to increase hematite formation for all temperature including 500 and 600°C. At 600°C, pyrrhotite was only formed after 60 seconds treatment time with 15 and 30 minutes producing only hematite and complete oxidation of all particles.

Along with the microwaved samples, magnetite was not observed in any of the results presented for conventionally heated -38μm pyrite. At high temperature and high heating rates for prolonged periods the pyrite will oxidise directly to form a hematite outer layer. If oxygen diffusion to the reaction front is prohibited (oxygen consumed before it reaches the reaction front) then decomposition of the pyrite will occur producing pyrrhotite.(as if in an inert atmosphere). This process will prevail until pyrite is completely decomposed allowing oxygen to penetrate through to the reaction front. The pyrrhotite formed will then successively decompose through to hematite. This will result in the formation of pyrrhotite as an intermediate. The SEM/MLA results for conventionally heated +425μm are presented in Figure 4.57 for comparison. The results presented in Figure 4.56 show that for particles heated at 400°C, no oxidation has taken place even after 30 minutes residence time within the furnace. These results indicate that particle surface area to volume ratio has a direct effect on the oxidation of the larger particles. In comparison, the -38μm particles have a much higher surface area to volume ratio and will require a lower activation energy than that required for the larger particles. If this is the case, then grain size is a major controlling factor in these experiments. It can be seen that for both particle sizes, treatment at 600°C for 60 seconds yield the greatest percentage of pyrrhotite.

For both experiments, pyrrhotite was found to be abundant as an intermediate due to the decomposition of pyrite from sulphur diffusion outwards (as opposed to oxygen diffusion inwards). The combination of short residence times and high heating rates resulted in the reaction being incomplete even for the -38μm particle experiments.

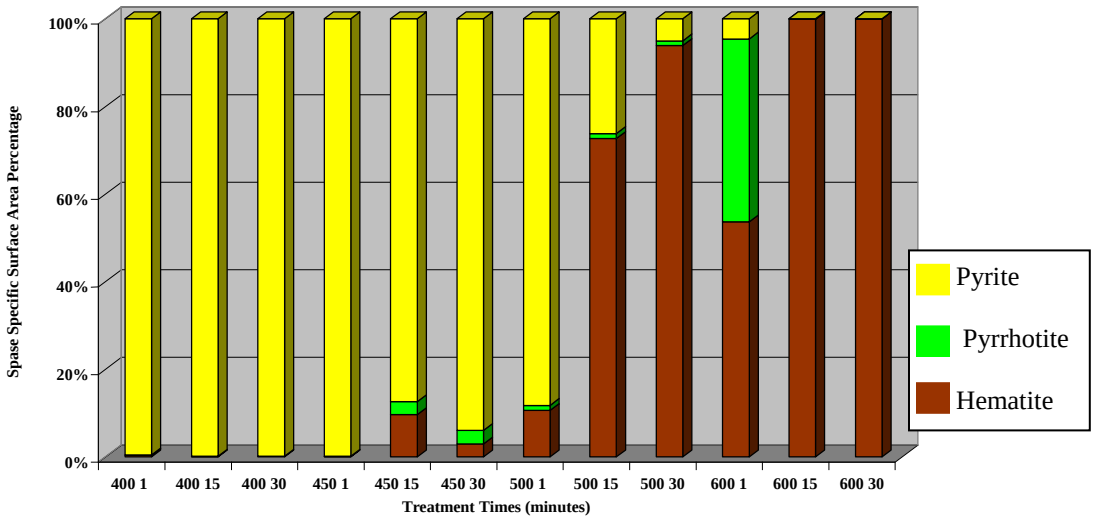

Figure 4.57 Conventional heating experiments for +425μm pyrite particles in static air.

Sample magnetisation and magnetic susceptibility curves for conventionally heated pyrite are shown in Figure 4.43 and 4.44 respectively. Generally, the magnetic properties of pyrite are improved with heating. The results indicate that for temperatures up to 400°C the magnetic properties have not improved when compared to untreated samples. These results are consistent with the MLA date presented in Figure 4.29 which show little pyrrhotite formation up to 400°C (regardless of heating duration).

This is consistent with XRD data (Appendix A4) at 380°C and 400°C which shows a high purity pyrite trace. As the temperature increases the magnetic properties increase but are dependant on pyrrhotite formation. Figure 4.43 and 4.44 show that the magnetic properties of 570°C much improved by order of magnitude when compared to untreated sample data. It would also appear that 490°C shows a greater magnetic susceptibility than 515°C, likely to be as a result of a larger percentage of pyrrhotite formed in this case. The existence of pyrrhotite is shown in XRD (Appendix A4) data for 490°C and 570°C experiments but is qualitative and not quantitative data.

4.10 Conclusion

Exposure of pyrite to both microwave heating and conventional heating methods improves its magnetic properties due to phase changes on the surface of the mineral particles. SEM/MLA has proven to be powerful tool in observing these phase changes. In order to increase the magnetic susceptibility of pyrite the formation of monoclinic pyrrhotite in necessary and in some cases has been successfully formed by both microwave and conventional heating methods (which has been identified by XRD analysis). Generally speaking, the magnetic properties of conventionally heated samples increased with increasing temperature although finite temperature control has proven to be problematic in this case. The conditions favourable for the formation of monoclinic pyrrhotite, in conventionally heated experiments, depend upon a number of key factors. These are, temperature, particle size and atmospheric gas pressure. In some cases overheating can have a detrimental affect on the magnetic properties of pyrite due to the formation of hematite (oxidation of pyrrhotite). Conventionally heated samples show the highest magnetic susceptibility in these experiments. This is partly because conventional heating allows for a more controlled and uniform heating process. The results observed from microwave heating experiments have shown that this method of heating is not a uniform process and temperature measurement of the sample is difficult. As a result of this, not all particles were treated for the same amount of time, with some coupling with microwaves early in the experiment and other left unaffected. Pyrite is a semi-conductor and heats initially by ohmic conduction. As a result, pyrite will readily heat within a microwave field if matched correctly.

The characteristic shrinking core model proposed by Hu, et al., 2007 has been observed in both microwave and conventionally heated samples. In a number of cases, grains from conventional and microwave treatment show an unreacted pyrite and pyrrhotite formed as an intermediate. An example of this is shown in Figure 4.57.

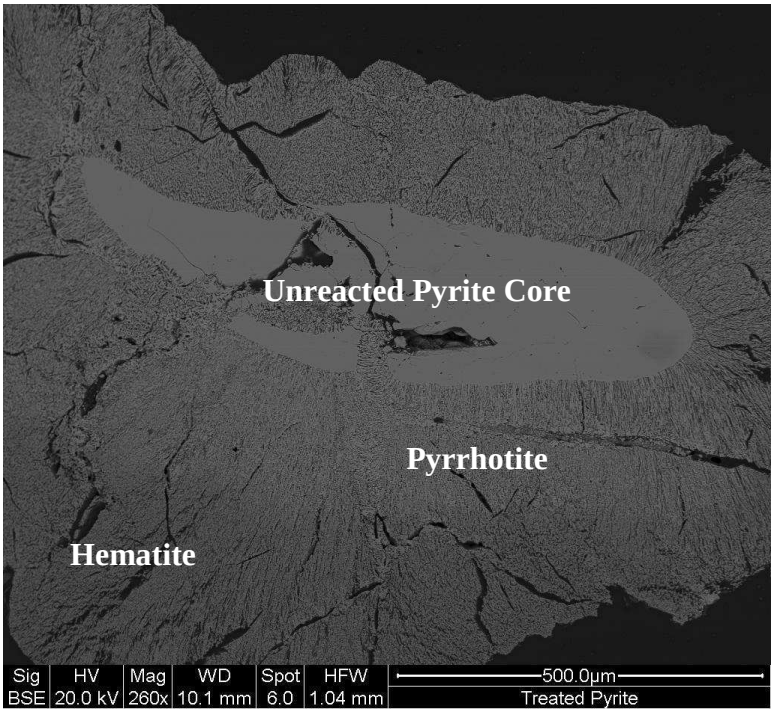

Figure 4.57 conventionally heated -600+425µm 500°C 15 minutes (2D back scattered image –BSE)

Chapter 5 - The Influence of Heterogeneity on the Dielectric Properties of Coal

5.1 Introduction

Understanding the fundamental mechanisms through which coal heats using microwave energy is critical to this research. The dielectric properties of any material govern its heating behaviour in the presence of a microwave field. Dielectric properties can vary significantly with composition, frequency, temperature and density (Salsman 1991; Nelson 1988). In order to fulfil any process requirements and to optimise any conditions at which to apply the microwave energy, a detailed knowledge of the dielectric permittivity (in particular dielectric constant [ε`] and the dielectric loss factor [ε"]) are essential. Specifically, these properties quantify the capacitive and conductive components of the dielectric permittivity.

An investigation into dielectric properties of a variety of coals is presented here. Since coal is a highly heterogeneous material formed via complex geological and chemical processes, it can be very difficult to characterise. Coals from a metamorphic series which range from peat, through lignite (brown coal), sub-bituminous, bituminous and anthracite exhibit very different chemical and physical characteristics as a result of geological deposition, diagenesis or biochemical coalification.

Previous studies concerning the dielectric properties of coal are, on the whole, rather general and superficial. This is because in most cases, little concern is given to the effects of surface moisture, mineral matter, maceral composition or other structural parameters

such as carbon aromaticity, all of which can significantly influence dielectric response. This study reports the dielectric property data for 10 different coal samples selected on the basis of varying rank (carbon structure), chemical and physical properties. In dielectric analysis, coal cannot simply be regarded as a mixture of two components (moisture and carbon), but must be considered to be a complex aggregate of organic and inorganic constituents as well as water. Therefore, in order to evaluate any dependence of dielectric property on coal rank, surface moisture and any inorganic impurities were removed from each sample via a drying and two-stage demineralisation process. These pre-measurement stages serve to eliminate the need to employ cumbersome and complex multi-phase dielectric mixture equations and therefore the need to identify the dielectric property of each continuous phase separately. Previous work by Marland *et al.,* 2001 on the dielectric properties of UK coals and UK power-station blends have shown that electric permittivity decreases with coal rank as a direct result of increasing moisture levels associated with low rank coals. Furthermore, it was suggested that the relative real permittivity of coal is greater than most mineral matter, with the exception of pyrite, which may increase the bulk coal permittivity if present in sufficient quantities. However, the proximate analysis characteristics for the suite of UK high volatile bituminous coals used in these experiments demonstrated that mineral matter content and mineral composition were extremely varied across the experimental range and obviously, the moisture content for each coal was also varied. Using volatile matter content as a rank indicator, Marland *et al* concluded that the dielectric properties of coal were dependant

on rank, with moisture content being the controlling factor. Moreover, the dielectric properties calculated on a mineral matter free basis (calculated using mixture equations) were markedly different when compared to the dielectric properties of each sample on an "as-received" basis. Differences in carbon structure and carbon aromaticity across the rank range and its effect on the dielectric properties were not discussed by the authors. The work reported in this Chapter extends previous work carried out by others by looking at the dielectric properties of 12 different coals. In the first instance, a procedure is outlined for determining the complex permittivity components of the solid material of known densities from those properties of pulverised samples measured over a range of bulk densities. Properties of the solid will be estimated from extrapolation functions of the dielectric constant and loss factor that are related to the bulk density of the air-particle mixture. Examples of this technique are given for two UK coals, namely Daw Mill and Welbeck. Secondly, the dielectric properties of coal as a function of rank/carbon content will be investigated. To minimise the influence of mineral matter and moisture on the measured dielectric properties, each sample will be chemically demineralised and dried to produce dry, mineral-free coal for each test. A constant sample bulk density will be observed in each case to minimise the effect of density variations when measuring dielectric properties across the range of experiments. The reflectance of the vitrinite maceral for each coal will be used as a rank indicator and the carbon structure of each coal will be measured by 13C NMR analysis.

Dielectric measurements were performed on pulverised samples using the cavity perturbation technique at 912MHz and 2470MHz and at ambient temperature. The cavity perturbation technique is particularly useful for measuring small powdered samples.
In particular, proximate analysis, mineral and maceral composition and the fundamental structure of coal with a view to electron mobility will be considered, including existing work on the microwave heating of carbonaceous materials.

5.2 Coal Structure

5.2.1 The Molecular Structure of Coal

The molecular structure configuration of coal is determined to a large extent on the complex progression of coal through a digenesis or coalification process. Coal is chemically heterogeneous and is composed principally of two basic classes of material: organic carbonaceous material or *macerals* and inorganic crystalline material or *minerals*. The carbonaceous material forms the combustible part of the coal and is characterised by three maceral groups: *vitrinite, liptinite and inertinite* (a detailed description of these macerals is given in Chapter 2).
The problem with ascertaining and describing the molecular structure of the organic part of coal is that it is not structurally dependant on a single molecule but a complex mixture of molecules which vary according to the type of coal under consideration. The relative magnitude or severity of the conditions in the coalification process leads to increasing *coal rank*. For most purposes, coal can be arranged in `rank order` from peat through to meta-anthracite and fundamentally, coal rank increases with increasing carbon content. Many physical and chemical properties vary with rank (see Chapter 2) but the basic

information concerning ideas of the structure of coal can be found in van Krevelen`s 'Coal' (1961). This piece of work along with a variety of other investigations (Lowrey 1963, Crelling, 1989, Stach, 1982, Tingey and Morrey, 1973) has regrettably not produced a coherent understanding of the molecular structure of coal. The complexity and heterogeneity of coal presents a significant challenge when comparing different coals.. Indeed, given the diversity of coals, the variety of their starting material and the geological conditions upon within they were formed, it would be very surprising if a molecular model which described the whole range of coals were proposed. However, this does not suggest that one should discount or ignore this work and much of it has illustrated rather than clarified the lack of understanding of the structure of coal. The conclusions drawn from van Krevelen on the molecular structure of coal are a useful overview and are summarised here:

- Coal is strongly aromatic with aromaticity increasing more or less steadily with rank.
- Coal has a polymeric structure.
- Coal has a non-uniform structure and high molecular weight.

Crelling, 1989 describes coal as a three dimentional cross-linked polymeric network consisting of carbon, hydrogen, oxygen and lesser amounts of nitrogen and sulphur. Figure 5.1 shows a two-dimensional representation of what the structure of a molecule of bituminous coal might consist of (Crelling, 1989).

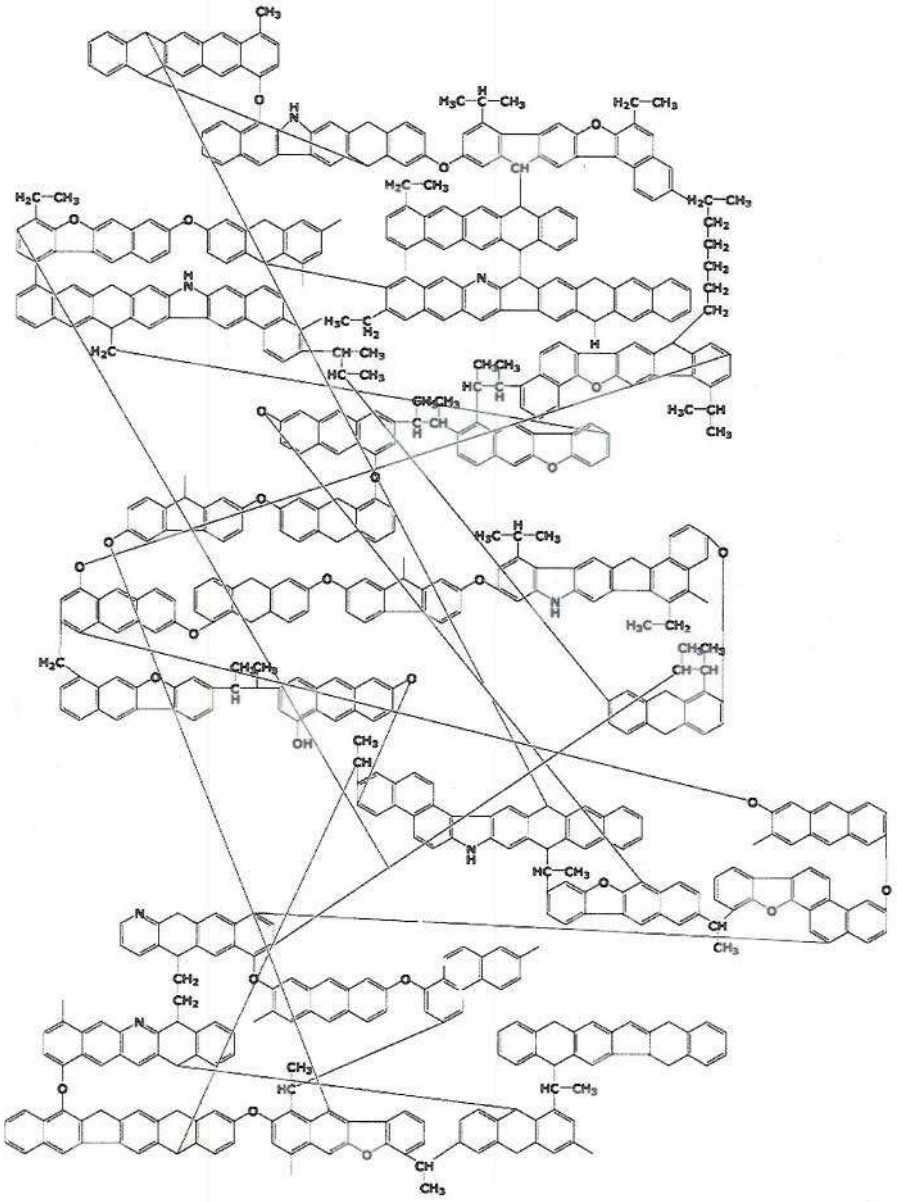

Figure 5.1 2-D representation of a molecule of bituminous coal (Crelling, 1989).

A structural comparison of coals of various ranks reveals the following (Web Ref: 1 2005).

- Lignite coal consists largely of single aromatic rings extensively substituted with oxygen functional groups (~1 oxygen per 3 to 4 carbons). The cross links between the ring is almost exclusively hydrogen bonds with a few aliphatic links
- Sub-bituminous coals contain mostly single rings with oxygen functional groups on almost all rings (~1 oxygen per 5 to 6 carbons). Both hydrogen and oxygen provide bridging structures, in addition to a few aliphatic links (Crelling 1989).
- The bituminous coal category is broad. As rank increases there is a significant increase in the amount of ring systems with a greatly reduced number of oxygen functional groups (~ 1 oxygen per 20 carbon atoms – high rank bituminous). With increasing rank, the nature of the cross links gradually decreases from a mixture of aliphatic and aromatic links, to almost exclusively aromatic bridges (van Krevelen 1993).
- Anthracitic coals have a high aromaticity and are graphitic in nature with multiple ring systems. Functional groups are rare (~ 1 oxygen per 100 carbons). The nature of cross linking is almost entirely direct aromatic-aromatic links.

Figures 5.2 & 5.3 overleaf show the structural molecular models of low rank and high rank coals respectively (van Krevelen 1993).

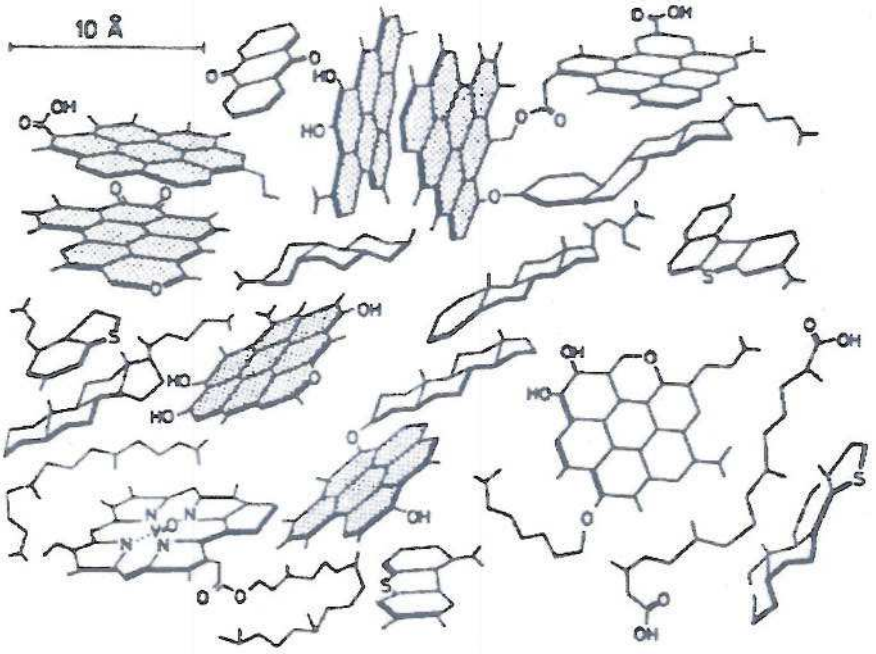

Figure 5.2 – Structural model of relatively low rank coal (van Krevelen 1993).

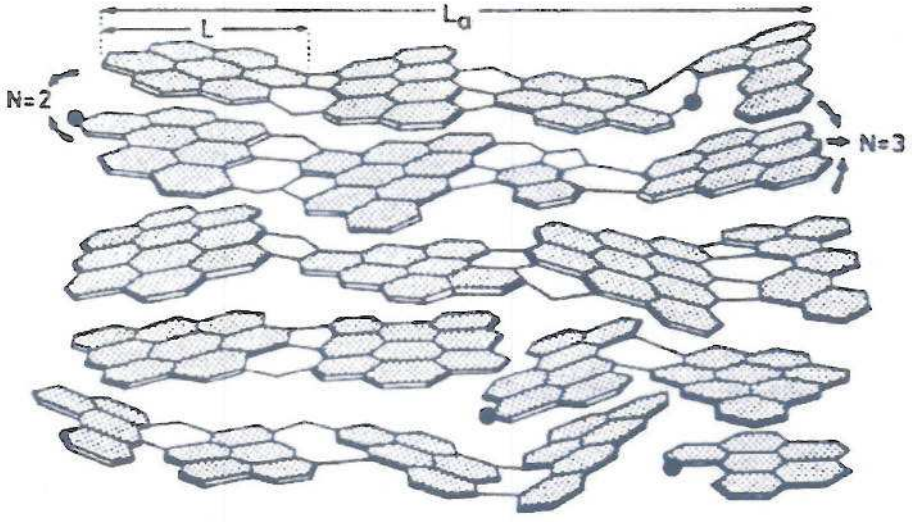

Figure 5.3 – Structural model of relatively high rank coal (van Krevelen 1993).

5.2.2 Carbon Aromaticity – Solid state NMR

It is well understood that, on the whole, coal is considered to be strongly aromatic (van Krevelen 1993). In recent years $^{13}C._{NMR}$ has been used to obtain structural information on carbon types present in carbonaceous materials such as coal, cokes and other coal derivatives (Maroto-Valer *et al.*, 1996 & 1998, Snape *et al.*, 1989, Solum *et al.*, 1989, Franz *et al.*, 1992). Furthermore, it is generally accepted that $^{13}C._{NMR}$ and SPE (Single-pulse excitation) are reliable techniques to obtain aromaticities and other structural parameters in coal (Maroto-Valer *et al.*, 1997). Cross polarisation (CP) and single-pulse excitation are established reliable techniques for producing ^{13}C spectra on carbonaceous materials (Snape *et al.*, 1989, Love *et al.*, 1992, Sfihi *et al.*, 1988). Carbon aromaticities for a series of 15 coal samples were obtained by solid state $^{13}C._{NMR}$ using the quantitative single-pulse excitation (SPE) technique (Maroto-Valer *et al.*, 1997). In this study, a linear correlation between the aromaticity of bituminous coal (in the range 0.73-0.91) and its atomic H/C ration was evident. Reliable and accurate information on the fundamental structure of carbonaceous material and particularly coal (in context with this study) can dominate its potential for microwave heating. This is because as ordering within the material increases, the number of π-bond electrons also increases. This is particularly true for highly aromatic materials where electron mobility and free charge per unit volume will influence the dielectric properties of the material significantly. In this study, solid state ^{13}C spectra were obtained using a Brucker DSX200 instrument equipped with a

double-bearing probe for cross-polarisation and magnetic angle spinning (MAS). The resonance frequency ^{13}C was 50MHz and the sample was spun at the magic angle with a speed of 60kHz. Typically 20.000 scans were accumulated with high power ^{1}H decoupling. The contact time was 3.0ms for CP and the relaxation delay was 1.5s. Dipolar dephasing experiments were carried out using a dephasing period of 50μs. All spectra in this work was collected at ambient temperature and processed with a line-broadening factor of 50Hz. Figure 5.4 shows a typical $^{13}C._{NMR}$ spectra and integral for La Jagua Coal (83%C) generated using cross polarisation.

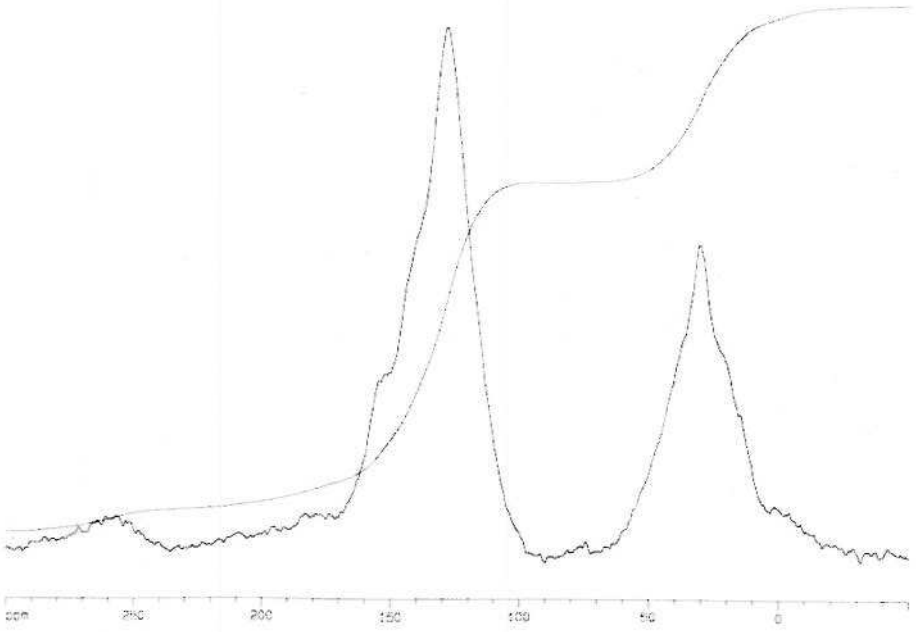

Figure 5.4 $^{13}C._{NMR}$ spectra for La Jagua Coal sample.

As can be seen in Figure 4.12 there are two clear peaks. The aliphatic carbons generate a peak centred between 0-45ppm and aromatic structures generate a peak centred around 124ppm (Marota-Valer *et al.*, 1998, Andresen *et al.*, 1998). The integral curve can be used to interpret the aromaticity of the sample under examination.

Table 5.1 shows the rank and aromaticity values of a series of selected coals.

Coal Type	Aromaticity (5%)	Rank (VR)
Hambach	50.8	0.29
Betts Lane	77.1	0.98
Tilmanstone	91.7	1.51
Cynheidre	97.5	3.45
Lea Hall	73.2	0.55
Pittsburgh	70.2	0.73
Baddersley	69.7	0.55
La Jagua	63.5	0.52
Reitspruit	70.2	0.81
Goedehoop	72.6	0.77

Table 5.1 Aromaticity of selected coals generated by $^{13}C._{NMR}$ analysis.

Essentially, as coal rank increases, aromaticity increases significantly. Furthermore, aromaticity is seen to be effectively proportional to dielectric loss factor (ε"). It is therefore evident that as aromaticity and hence carbon ordering increases, loss factor increases. This well defined relationship can be seen in Figure 5.5 which illustrates the relationship between carbon aromaticity and dielectric loss factor (cavity perturbation techniques).

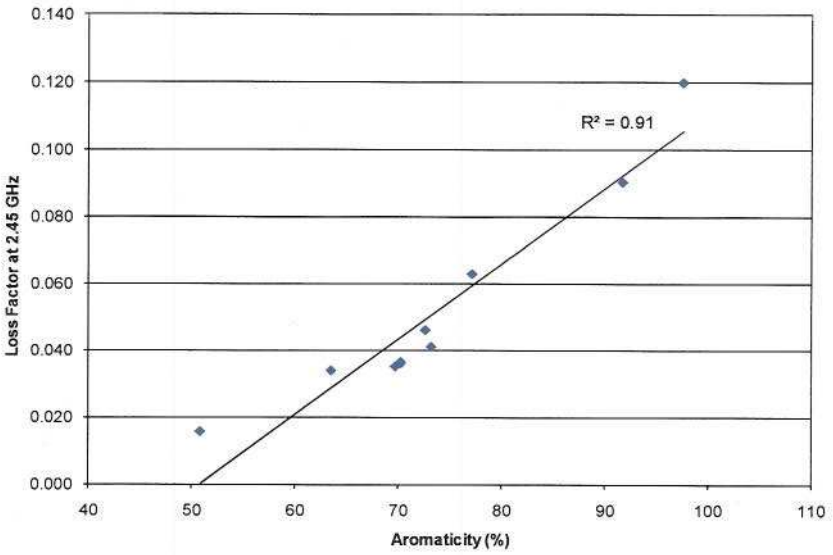

Figure 5.5 Relationship between coal aromaticity and loss factor.

5.2.3 Structural variations within coal macerals.

In 1978 studies of $^{13}C._{NMR}$ spectra for individual macerals in coal were investigated (Retcofsky and VanderHart, 1979). The macerals were separated from a West Virginia HVA bituminous coal (85.8%C) and the calculated carbon aromaticity values were – vitrinite 85% - exinite 66% - fusinite ~96%. The results indicated that the aromaticity increases in the order **liptinite (exinite) < vitrinite < inertinite.** The results of this study can be seen in the spectra presented in Figure 5.6. The vitrinite and semifusinite fractions contained 3-6 and 9 to over 15 aromatic rings, respectively.

In 1998 Maroto-Valer *et al.*, undertook a quantitative $^{13}C._{NMR}$ study of structural variations within vitrinite and inertinite maceral groups derived from a semifusinite-rich bituminous coal. Each fraction with purities over 90% were obtained by density gradient

centrifugation. As expected, the aromaticities of the vitrinite fractions were significantly lower than those of the semifusinite ones.

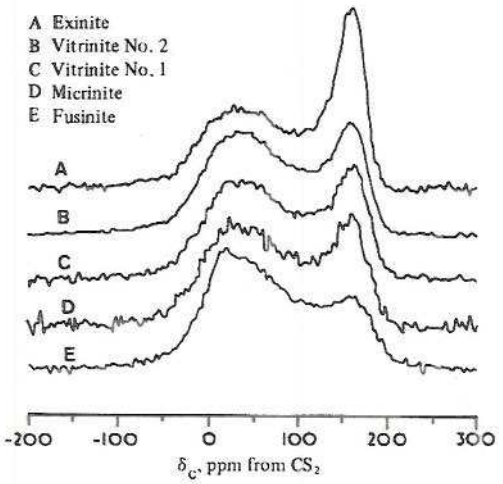

Figure 5.6 Magnetic resonance spectra of macerals West Viginia bituminous coal. (Retcofsky and VanderHart, 1978)

5.3 Dielectric Properties Measurements

5.3.1 The Resonant Cavity Perturbation Technique.

The technique used for measuring of the dielectric properties of materials using a TM_{0n0} axially symmetric Cavity is described in Section 2.7. This type of measurement technique is most suitable for measuring the complex permittivity of a small pulverent or granular samples at frequencies between 50MHz and 3GHz (depending on the cavity dimensions) and at elevated temperatures of up to 1400°C. The system has the advantage of allowing the sample shape, volume and density to be easily controlled. For the empty cavity used in this study, the measured frequencies are 912 MHz and 2.47GHz or resonant modes n=2 and n=5, respectively. These frequencies are of particular interest since all

microwave systems used for experimental testing operate at 2.45GHz and many industrial systems described in Chapter 2, operate at 915MHz. A schematic layout of the dielectric measuring equipment is shown in Figure 2.7.

5.3.2 Density Dependence on the Dielectric Properties of Particulates.

The relationship between density and dielectric properties can be used to estimate the dielectric properties of a solid medium from measurements on pulverised powdered samples, particularly when solid samples cannot be obtained or when measurements on solid materials is not convenient. The density of powdered samples must be considered and accounted for when using the dielectric properties of particulate materials. The density dependence of the dielectric properties can also be used for the determination of density. The influence of a dielectric depends on the amount of mass interacting with the electromagnetic field, therefore, the mass per unit volume or density, will have an effect on the dielectric properties. This is of course particularly notable and problematic when measurements are made on particulate dielectrics such as pulverised or granular materials. Bulk density variations can interfere with dielectric measurements and introduce inaccuracies particularly when dielectric property comparison studies are performed. The use of a resonant cylindrical cavity (cavity perturbation) is the most desirable technique for measuring the dielectric properties of particulate materials. Relationships between the dielectric constants and loss factors of pulversied materials and the bulk density of these materials are discussed in this work, and data illustrating the relationships are presented. The analysis presented here developed by S.O Nelson 1983,

indicates that linear relationships can be developed between functions of the dielectric properties of particulate materials and their densities.

Firstly, recall the relative complex permittivity as $\varepsilon_r = \varepsilon_r' - j\varepsilon_r''$, where ε_r' and ε_r'' are the dielectric constant and loss factor respectively.

From previous work, Kent *et al.*, 1977, developed fundamental relationships, that both ε_r' and ε_r'' should be quadratic functions of the density of the particulate material. Therefore,

$$\varepsilon_r' = a\rho^2 + b\rho + 1 \tag{5.1}$$

Further,

$$\varepsilon_r'' = c\rho^2 + d\rho + 0 \tag{5.2}$$

where ρ is the air-particle mixture density and a, b, c and d are unique constants calculated for a particulate material. The dielectric constant ε_r' and the loss factor ε_r'' have values of 1 and 0 respectively. (Note that for air alone the complex permittivity may be written as $\varepsilon_r = 1 - j0$ and hence $\rho = 0$).

It was noted by Klein *et al.*, 1981, that the relationship between the square root of the dielectric constant $\sqrt{\varepsilon_r'}$ and the density on the composite air-particle mixture was linear. Therefore based on his observations this linear relationship may be written as

$$\sqrt{\varepsilon_r'} = m\rho + c \tag{5.3}$$

where m is a constant for a given material and also the slope of the straight line of the graph $\sqrt{\varepsilon_r'}$ against density. From the quadratic relationship Eqn. (5.1) the intercept $c = 1$. Thus if the relationship at (5.1) holds true, one can estimate the dielectric constant at all densities including that of the solid material from only one measurement of the dielectric

constant of a particular material at one density, where the intercept would be $\left(\rho = 0, \sqrt{\varepsilon_r'} = 1\right)$.

Manipulation of Eqn. (5.2) reveals that $\sqrt{\varepsilon_r''}$ does not vary linearly with density. However, completing the square for (5.2) reveals,

$$\sqrt{\varepsilon_r'' + \frac{d^2}{4c}} = \sqrt{c\rho} + \sqrt{\frac{d^2}{4c}} \text{ or } \sqrt{\varepsilon_r'' + e} = \sqrt{c\rho} + \sqrt{e} \qquad (5.4)$$

where $e = \frac{d^2}{42}$

Thus, a linear relationship involving ε_r'' and density can be observed. However a single measurement for the evaluation of ε_r'' will not suffice since the constant e must be determined. A minimum of two measurements will be sufficient for the determination of the loss factor at any density, although as more measurements are taken the accurate evaluation of the slope term for both dielectric constant and loss factor will become more precise.

Work presented by Krasewski *et al.,* 1988, on air-particle mixtures is consistent with (5.1) and (5.3) where

$$\varepsilon_r' = \left[\sqrt{\varepsilon_{r1}'} + v_2\left(\sqrt{\varepsilon_{r2}'} - \sqrt{\varepsilon_{r1}'}\right)\right]^2 \qquad (5.5)$$

where subscripts 1 and 2 refer to materials 1 and 2 in the mixture (i.e. perhaps a air-coal mixture) and v_2 is the volume fraction of the space occupied by material 2 or the solid

phase. However, v_2 is equivalent to $\frac{\rho}{\rho_2}$ where ρ is the total bulk density of the material under examination and ρ_2 is the density of the solid material.

Then (5.5) can be rewritten as

$$\varepsilon_r' = \left[1 + \frac{\rho}{\rho_2}\left(\sqrt{\varepsilon_{r2}'} - 1\right)\right]^2 \tag{5.6}$$

Now, taking the root of (5.6), we have

$$\sqrt{\varepsilon_r'} = \frac{\sqrt{\varepsilon_{r2}'} - 1}{\rho_2}\rho + 1 \text{ which is equivalent to (5.3) where, } m = \frac{\left(\sqrt{\varepsilon_{r2}'} - 1\right)}{\rho_2} \tag{5.7}$$

Since $v_1 + v_2 = 1$ for a two phase mixture then (5.5) may be written

$$\varepsilon_r' = \left[(1 - v_2)\left(\varepsilon_{r1}'\right)^{1/2} + v_2\left(\varepsilon_{r2}'\right)^{1/2}\right]^2 = \left[v_1\left(\varepsilon_{r1}'\right)^{1/2} + v_2\left(\varepsilon_{r2}'\right)^{1/2}\right]^2 \tag{5.8}$$

This suggests that simply the square roots of the dielectric constants are additive when taken in proportion to their respective volume fractions.

Nelson and You *et al*, 1981, also studied several two component mixture equation, the most successful identified were derived by Landau and Lifshitz and by Looyenga, whereby the cubic roots of the dielectric constants were additive in proportion with their respective volume fractions.

Thus,

$$\varepsilon_r' = \left[v_1\left(\varepsilon_{r1}'\right)^{1/3} + v_2\left(\varepsilon_{r2}'\right)^{1/3}\right]^3 \tag{5.9}$$

From the general mass, volume and density relationship (5.9) may be expressed in terms of respective sample mass and density fraction,

$$\varepsilon_r^{`} = \left[ \frac{\rho}{\rho_1} m_1 \left(\varepsilon_{r1}^{`}\right)^{1/3} + \frac{\rho}{\rho_2} m_2 \left(\varepsilon_{r2}^{`}\right)^{1/3} \right]^3 \tag{5.10}$$

where m_1 and m_2 are the mass fraction of material 1 and that of material 2, respectively. In the same way, subscripts 1 and 2 refer to material 1 and material 2.

For example, ρ_1 simple refers to the density of material 1, where ρ is given by ,

$$\rho = \frac{\rho_1 \rho_2}{\rho_2 + (\rho_1 - \rho_2) m_2} \tag{5.11}$$

To satisfy the basic assumptions of air-particle mixtures we can write Eqn. 5.9 as

$$\sqrt[3]{\varepsilon_r^{`}} = \frac{\sqrt[3]{\varepsilon_r^{`}} - 1}{\rho_2} \rho + 1 = m\rho + 1 \tag{5.12}$$

5.3.2.1 Sample Preparation Data Acquisition

In order to examine the relationships between dielectric constants and density described above, data was collected to include measurements taken on`as-received` pulverised (<38μm) coal samples representative of the bulk. The dielectric constant ($\varepsilon`_r$) and the dielectric loss factor ($\varepsilon"_r$), the real and imaginery parts, respectively, of two UK derived coal samples were measured. Dielectric measurements were taken using the resonant cavity perturbation technique at room temperature on each material and repeated five times at each frequency of interest, namely 912MHz and 2.47GHz. The dielectric property measurements were taken at five different bulk densities, which were achieved by tapping the base of the glass sample holder with its axis in the vertical orientation. This technique helped to ensure that the sample packing density was uniform along the

length of the sample. The solid density of each sample was determined using an air comparison pycnometer and the samples were allowed to air dry for 48hrs before testing commenced. To ensure experimental consistency, a constant sample volume for each test was observed consistent with perturbation theory and satisfying Eqn`s 2.5 & 2.6 . Properties of the solid are obtained by extrapolation of functions of the dielectric constant and loss factor that are mathematically related to the bulk density of the air--particle mixture.Table 5.2 below shows the Proximate and Ultimate analysis for Welbeck and Daw Mill coal on an as-received basis.

		WELBECK	DAW MILL
PROXIMATE			
MOISTURE	%	6.1	3.56
ASH	%	4.4	6.1
VOLATILE MATTER	%	35.7	34.02
FIXED CARBON	%	53.8	56.32
ULTIMATE			
HYDROGEN	%	4.96	-
CARBON	%	76	-
NITROGEN	%	1.9	-
SULPHUR	%	1.39	-
OXYGEN	%	15.75	-

Table 5.2 Proximate and Ultimate analysis for WelBeck and Daw Mill Coal

It was previously shown that, for an air and pulverized particle mixture, the square root (Eqn. 5.7) and cubic root (Eqn.5.12) of the dielectric constant is linear with the density ρ, of the air-particle mixture (Nelson and Stetson *et al.,* 1976).

Also the square root of $(\varepsilon_r^{"} + e)$, where e is a small constant, is linear with density.

Furthermore, Kent *et al.,* 1977 has shown that both the dielectric constant $\varepsilon_r^{'}$ and dielectric loss $\varepsilon_r^{"}$ can be expressed as quadratic functions of the air-particle density (Eqn.

5.1 and 5.2 respectively). The coefficients a, b , c and d are constants for the specific material under examination at a given frequency. The intercept in Eqn. 5.7 and 5.12 for the square root and cubic root relationships respectively is unity, since the dielectric constant at $\rho = 0$ (i.e. no particles) is 1. For the measurement data on ε_r' for the pulversied coal samples, a linear regression analysis was performed and calculated according to Eqn. 5.7 and 5.12 and is shown on a plots of $\sqrt{\varepsilon_r'}$, ρ and $\sqrt[3]{\varepsilon_r'}$, ρ shown in Figure 5.7 and 5.8 respectively. The data point (0,1) is included in the regression, this the intercept for both the square root and cube root models is essentially 1. The linear relationships of $\sqrt{\varepsilon_r'}$, ρ and $\sqrt[3]{\varepsilon_r'}$, ρ permit the estimation of the dielectric constant of the solid material, providing ρ for the solid is known and then solving for ε_r' by linear extrapolation.

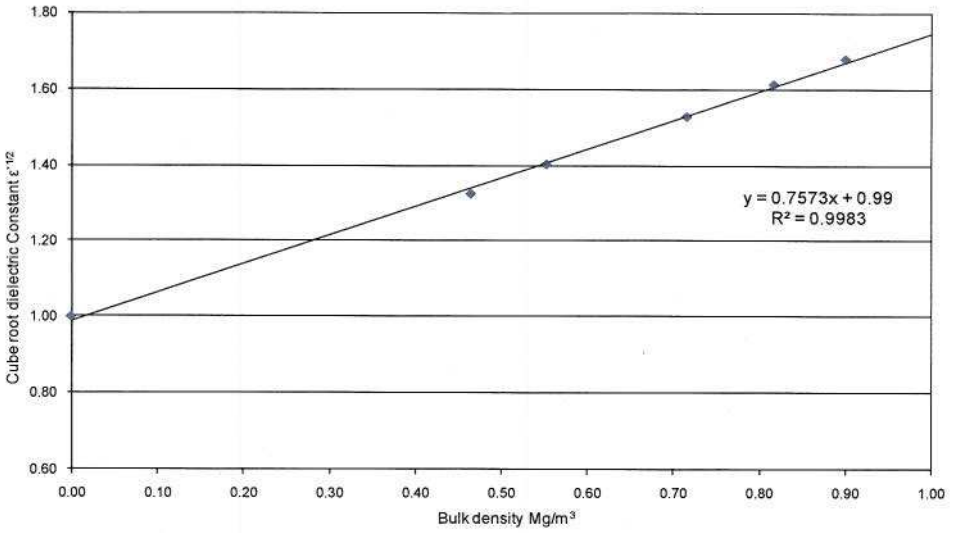

Figure 5.7 Linear regression analysis of the Square root of the dielectric constant for pulverised Welbeck coal sample and their bulk densities at 912MHz and 20°C.

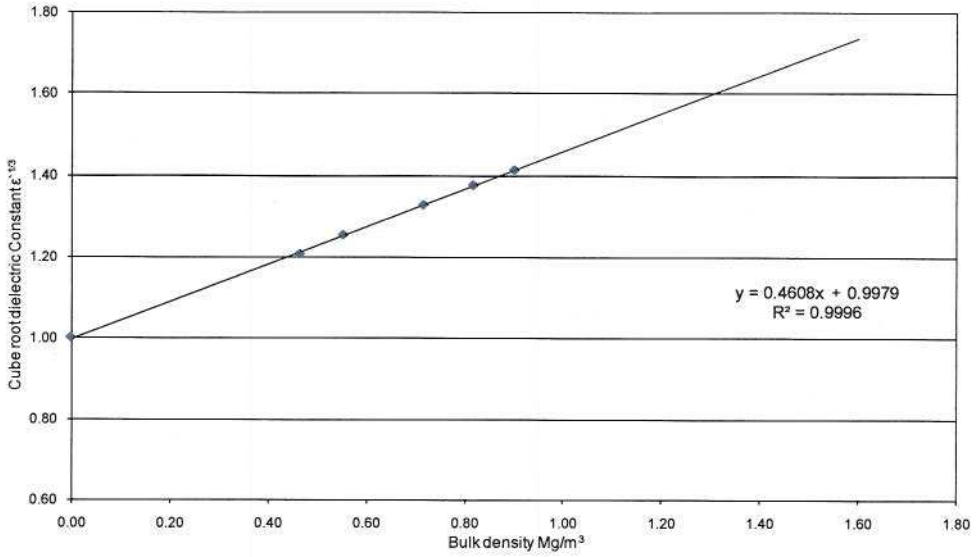

Figure 5.8 Linear regression analysis of the Cube root of the dielectric constant for pulverised Welbeck coal sample and their bulk densities at 912MHz and 20°C.

It is also possible, with reference to Eqn. 5.1, to estimate the dielectric constant ε_r' by quadratic or polynomial regression analysis. The second order relationship of ε_r' , ρ is shown in Figure 5.9. As before, the data point (0,1) is included when $\rho = 0$. From this data, the coefficients of the quadratic expression in Eqn.5.1 are found and thus an estimation of the dielectric constant of the solid material is possible.

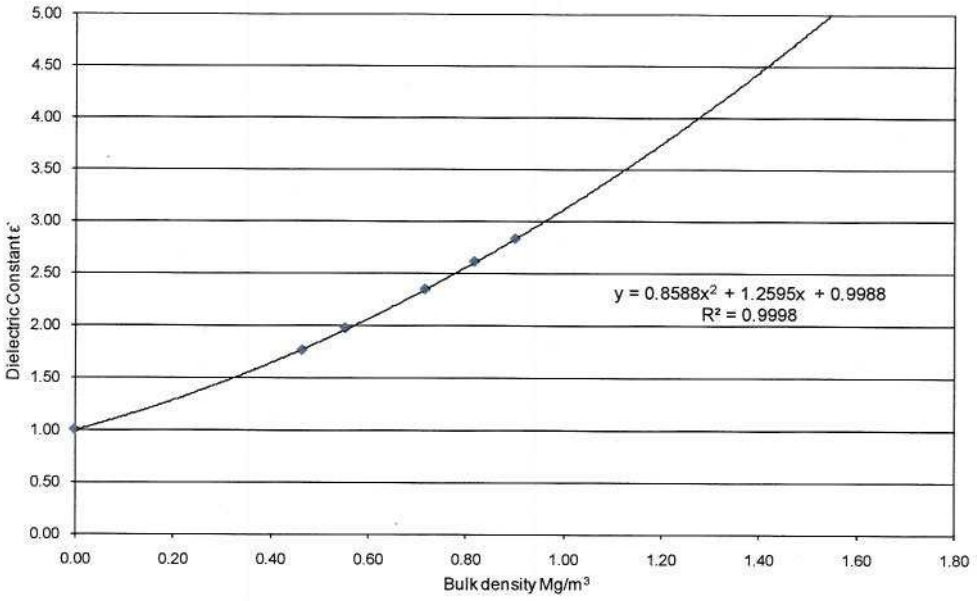

Figure 5.9 Quadratic relationship between the dielectric constant of pulverised Welbeck coal sample and their bulk densities at 912MHz and 20°C.

The use of the linear relationship for the estimation of the dielectric loss factor $\varepsilon_r^{"}$ requires a calculation for the constant `e` in the linear regression model $(\varepsilon_r^{"} + e)_{,} \rho$. However, the value of the constant `e` can only be calculated after first determining `c` and `d` of Eqn. 5.2 by second order polynomial or quadratic regression analysis. A second order polynomial regression line for the dielectric loss factor of a pulverised Welbeck coal sample at 912MHz and 20°C is shown in Figure 5.9.

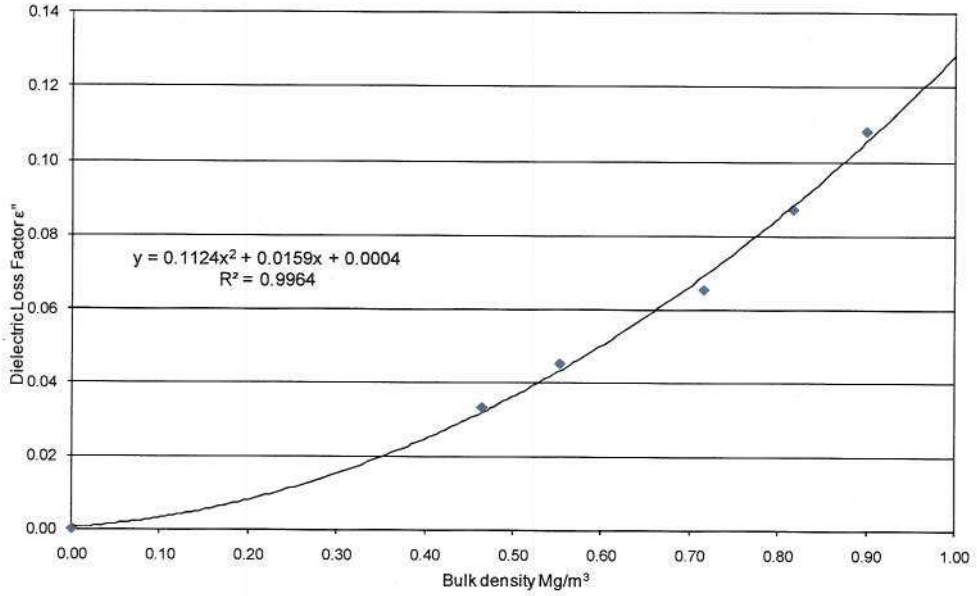

Figure 5.10 Second order regression analysis of the dielectric loss factor for a pulverised Welbeck coal sample and their bulk densities at 912MHz and 20°C.

The point (0,0) has been included in the analysis since that for air alone, the complex permittivity may be written as $\varepsilon_r = 1 - j0$ with $\rho = 0$. This inclusion is necessary to ensure that the intercept is small (essentially zero). The resulting second order trend line expression generated by this data will yield the quadratic coefficients `c` and `d` from Eqn. 5.2. Once the coefficients are know, the constant `e` may be calculated for $(\varepsilon_r^{"} + e)$ and this an estimate for the loss factor of the solid material may be calculated by linear regression analysis of $(\varepsilon_r^{"} + e)^{1/2}$ vs. ρ . The linearity of the square root of the dielectric loss factor with density is shown in Figure 5.11.

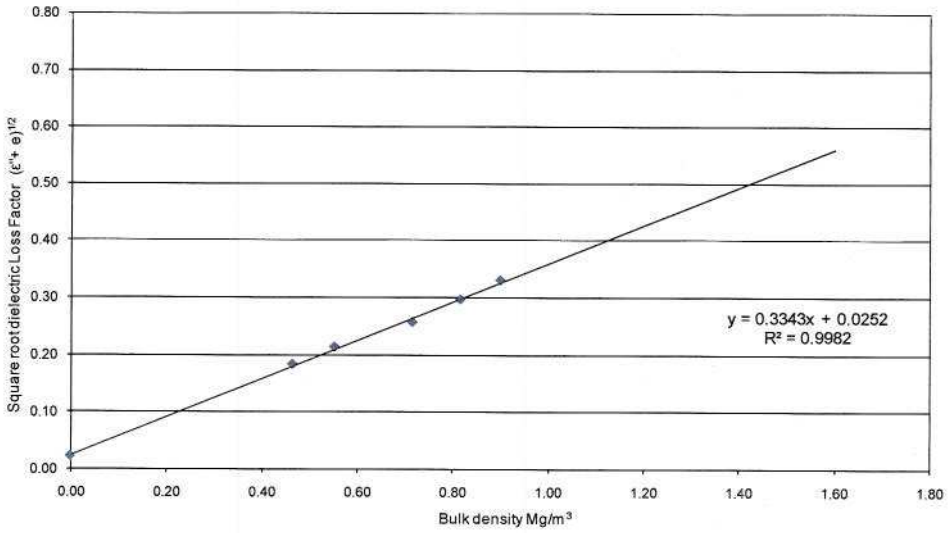

Figure 5.11 Linear regression analysis of the Square roots of the dielectric Loss Factor for pulverised Welbeck coal sample and their bulk densities at 912MHz.

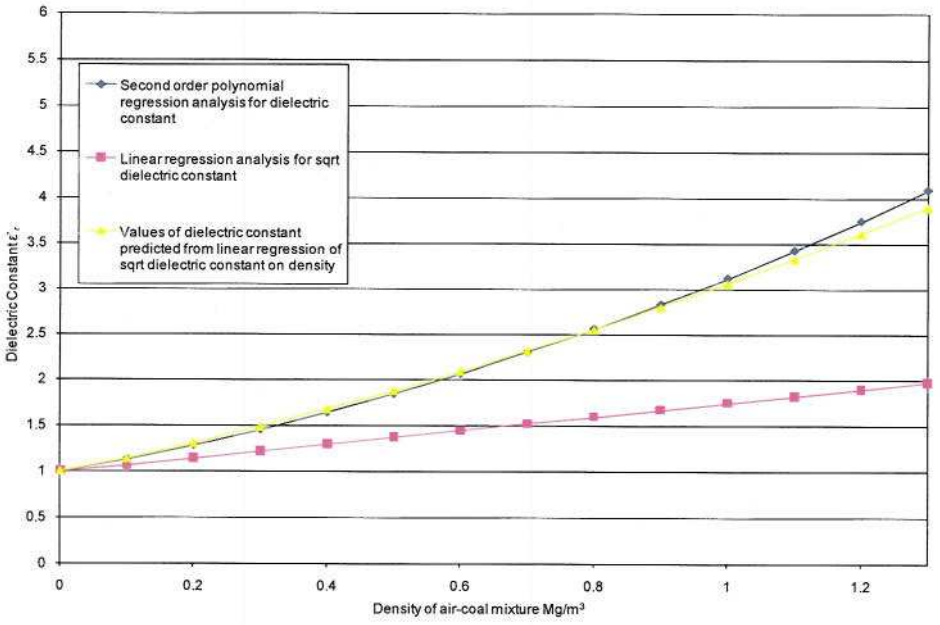

Figure 5.12 Density dependence of the dielectric constant $\varepsilon`_r$ and $(\varepsilon`_r)^{½}$ for Welbeck coal at 912MHz and 20°C

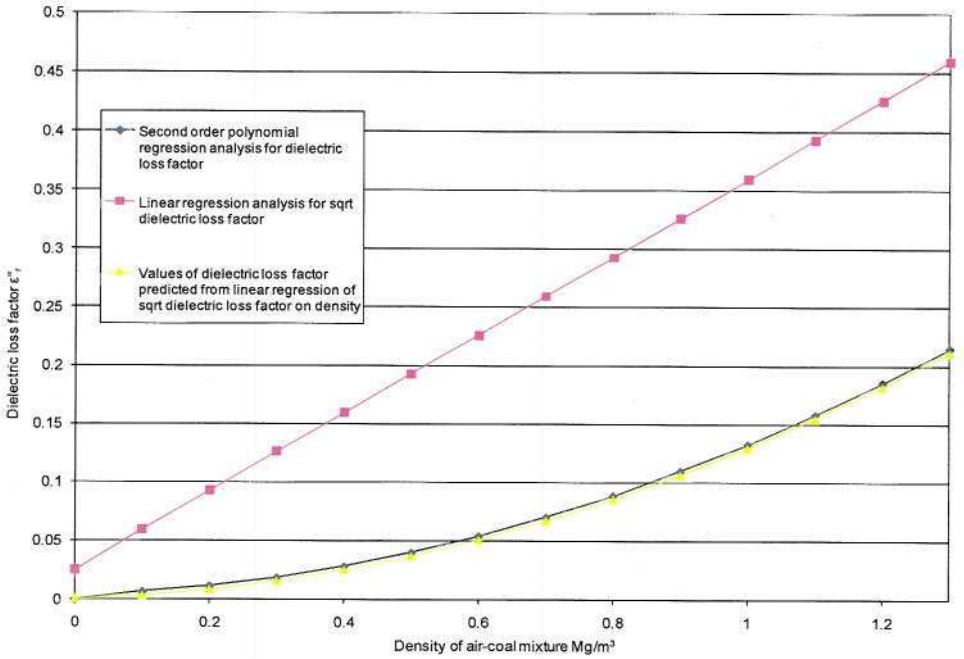

Figure 5.13 Density dependence of the dielectric Loss Factor ε''_r and $(\varepsilon''_r)^{1/2}$ for Welbeck coal at 912MHz and 20°C

Figures 5.12 and 5.13 illustrate the experimental points for measured values of $\varepsilon_r^{'}$ and $\varepsilon_r^{''}$ respectively, through a range of densities for pulverised Welbeck coal samples at 911MHz. The solid curves through experimental points $\left(\rho,\varepsilon_r^{'}\right)$ and $\left(\rho,\varepsilon_r^{''}\right)$ were obtained by second order polynomial regression analysis of the form $\varepsilon_r^{'} = a\rho^2 + b\rho + 1$ and $\varepsilon_r^{''} = c\rho^2 + d\rho + 0$ with (0,1) and (0,0) intercept coordinates used for the calculations for dielectric constant and dielectric loss factor respectively (see Figures 5.17 and 5.18). Also shown in Figures 5.12 and 5.13 is the linear regression analysis for $\left(\rho,\sqrt{\varepsilon_r^{'}}\right)$and $\left(\rho,\sqrt{\varepsilon_r^{''}+e}\right)$, with (0,1) and (0,0) intercept coordinates again included for the calculations of dielectric constant and dielectric loss factor respectively, providing values for the

coefficients consistent with $\sqrt{\varepsilon_r'} = b\rho + c$ and $\sqrt{\varepsilon_r'' + e} = b\rho + c$ (see Figures 5.7 and 5.11).

In the same way, measurements were taken for Welbeck coal samples at 2.45GHz at 20°C and for Daw Mill coal samples at frequencies of 912MHz and 2.45GHz, and estimates for the dielectric constants and dielectric loss factors were obtained. The graphical data for these experiments is shown in Appendix 5.

5.3.2.2 Regression analysis coefficients and comparison

Table 5.3 illustrates the coefficients of the regression equations for the dielectric constants ε_r' of the particulate materials against increasing bulk density ρ, by means of the relationships given in Eqns. 5.1, 5.3 and 5.12 consistent with the Kraszewski and Landau-Lifshitz and Looyenga mixture predictions, respectively.

Coefficients of empirical equations relating the dielectric constant (ε_r') and density (ρ) of particulate materials

		Well Beck Coal		Daw Mill Coal	
Regression model	Constant	911 MHz	2.45GHz	911 MHz	2.45GHz
$\varepsilon'_r = a\rho^2 + b\rho + c$	c	0.9980	0.9995	1.0065	1.0019
with (0,1) intercept	b	1.2595	1.0421	1.2325	1.1023
	a	0.8588	0.4962	1.6352	0.8619
	R^2	0.9998	0.9926	0.9947	0.9992
$(\varepsilon'_r)^{1/2} = b\rho + c$	c	0.9900	0.9944	0.9863	0.9924
with (0,1) intercept	b	0.7573	0.5881	0.9054	0.6889
	R^2	0.9983	0.9928	0.9906	0.9973
$(\varepsilon'_r)^{1/2} = b\rho + c$	c	0.9515	0.9728	0.9308	0.9619
without (0,1) intercept	b	0.8102	0.6178	0.9993	0.7405
	R^2	0.9996	0.9770	0.9793	0.9966
$(\varepsilon'_r)^{1/3} = b\rho + c$	c	0.9979	0.9991	0.9953	0.9975
with (0,1) intercept	b	0.4608	0.3642	0.5524	0.4282
	R^2	0.9996	0.9938	0.9937	0.9989
$(\varepsilon'_r)^{1/3} = b\rho + c$	c	0.9897	0.9954	0.9762	0.9876
without (0,1) intercept	b	0.4721	0.3692	0.5847	0.4450
	R^2	0.9994	0.9763	0.9807	0.9975

Table 5.3 Coefficients of empirical relationships for dielectric constant ε_r'.

The equations relating to predictions for dielectric loss factor are presented in Table 5.4. The results presented here are for both quadratic and linear regression models consistent with Eqn 5.2 and Eqn 5.4 respectively.

Coefficients of empirical equations relating the dielectric loss factor (ε_r") and density (ρ) of particulate materials

		Well Beck Coal		Daw Mill Coal	
Regression model	Constant	911 MHz	2.45GHz	911 MHz	2.45GHz
$\varepsilon''_r = a\rho^2 + b\rho + c$	c	0.0040	0.0002	0.0007	0.0003
with (0,0) intercept	b	0.0159	0.0348	0.0161	0.0342
	a	0.1124	0.0418	0.2044	0.0775
	R^2	0.9964	0.9973	0.9923	0.9965
$(\varepsilon''_r + e)^{1/2} = b\rho + c$	e	0.0006	0.0072	0.0003	0.0038
with $(0,e^{1/2})$ intercept	c	0.0252	0.0859	0.0207	0.0628
	b	0.3343	0.2041	0.4497	0.2775
	R^2	0.9982	0.9982	0.9940	0.9978
$(\varepsilon''_r + e)^{1/2} = b\rho + c$	c	0.0310	0.0891	0.0325	0.0682
without $(0,e^{1/2})$ intercept	b	0.3264	0.1997	0.4297	0.2682
	R^2	0.9932	0.9930	0.9758	0.9917

Table 5.4 Coefficients of empirical relationships for dielectric Loss Factor ε_r".

Table 5.5 below shows the predictions for dielectric constant and loss factor made by each regression model investigated here. Each model predicts the dielectric property of a solid material based on measurements from air-particulates samples.

Estimated dielectric properties of solid materials from measurements on air and particulate materials

			Estimated dielectric constant ε'_r					Estimated Loss Factor $\varepsilon''r$		
			Best-fit	$(\varepsilon'_r)^{1/2} = b\rho + c$		$(\varepsilon'_r)^{1/3} = b\rho + c$		Best-fit	$(\varepsilon''_r + e)^{1/2} = b\rho + c$	
Material	Density Mg/m^3	Frequency (GHz)	quadratic curve	with intercept	without intercept	with intercept	without intercept	quadratic curve	with intercept	without intercept
Well Beck Coal	1.276	0.9110	4.0867	3.8986	4.0191	4.0725	4.1224	0.2146	0.2114	0.2073
		2.4500	3.1928	3.0938	3.1540	3.1779	3.2114	0.1161	0.1234	0.1216
Daw Mill Coal	1.347	0.9110	5.3722	4.6800	4.9724	5.0303	5.2346	0.3671	0.3664	0.3494
		2.4500	3.8915	3.5644	3.7039	3.7539	3.8411	0.1757	0.1794	0.1738

Table 5.5 Predictions for Dielectric Constant and Loss Factor for solid coal material based on measurement on air-particulate samples.

5.3.2.3 Dielectric Constants of Heterogeneous Mixtures

In a review of the dielectric properties of heterogeneous mixtures conducted by Van Beek 1965, a number of equations for the prediction of solid material dielectric constants were discussed. A series of theoretical models were presented including formulae developed by Bruggeman, 1935, Böttcher 1952, Maxwell-Garnet and Rayleigh. Each formula has different origins and will be discussed in brief here. In this report, each model has been evaluated using dielectric measurements taken on particulate mixtures using the cavity perturbation technique.

The Bruggeman equation was evaluated using measurements on powdered coal samples, namely those of Daw Mill and Well Beck.

The Bruggeman mixture equation states,

$$1-v_2 = \frac{\varepsilon_2^{`} - \varepsilon^{`}}{\varepsilon_2^{`} - \varepsilon_1^{`}} \left(\frac{\varepsilon_1^{`}}{\varepsilon^{`}} \right)^{1/3} \tag{5.13}$$

Where,

$\varepsilon^{`}$ is the dielectric constant of the mixture

$\varepsilon_1^{`}$ is the dielectric constant of the continuous phase (usually air $\varepsilon_1^{`} = 1$)

$\varepsilon_2^{`}$ is the dielectric constant of the discrete phase (coal)

v_2 is the volume fraction of the discrete solid phase (coal)

N.B This notation has been adopted throughout the mixture analysis unless otherwise stated.

A curve can then be plotted of permittivity ε' against a predicted volume fraction of the discrete phase. Using the Bruggeman equation with values substituted for ε_1' and ε_2', where $\varepsilon_1' = 1$ for air and ε_2' is equal to the solid material permittivity at the corresponding frequency e.g. $\varepsilon_2' = 4.94$ for Daw Mill coal at 911 MHz and 25°C. The measured values of ε_2' were plotted from experimental data and compared to the prediction made by Bruggeman with Eqn. 5.13. An example of the Bruggeman model is shown in Figure 5.14.

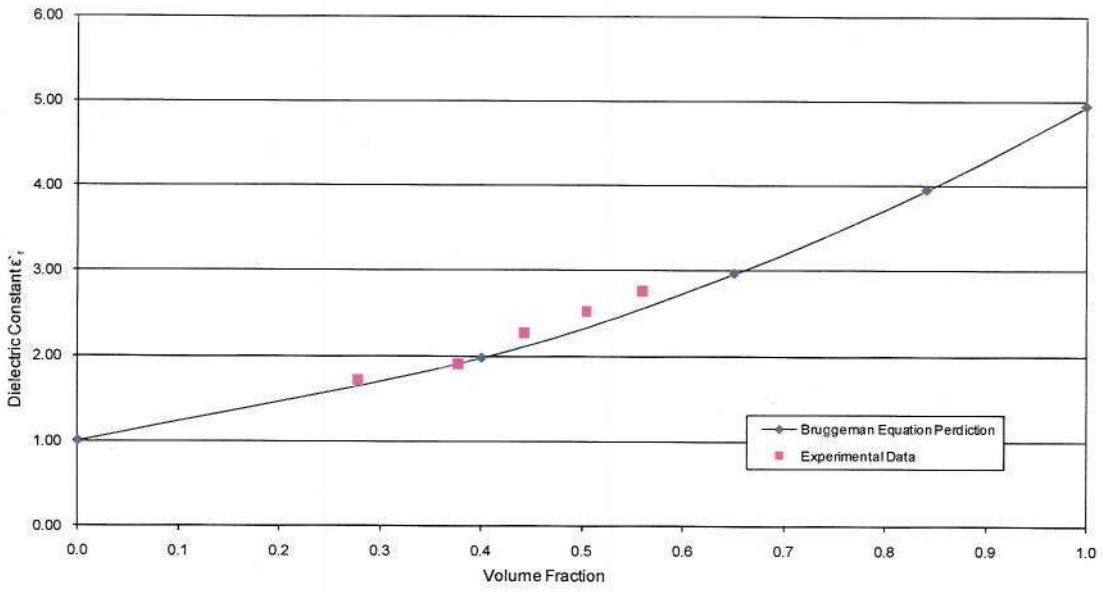

Figure 5.14 Prediction of the Dielectric Constant of Heterogeneous Mixtures according to the Bruggeman model. Experimental Data taken for Daw Mill coal at 911MHz.

The Rayleigh equation was evaluated, again using measurements on powdered Daw Mill coal samples,

The Rayleigh mixture equation states,

$$\frac{\varepsilon' - \varepsilon_1'}{\varepsilon' + 2\varepsilon_1'} = v_2 \frac{\varepsilon_2' - \varepsilon_1'}{2\varepsilon' + \varepsilon_2'} \tag{5.14}$$

This formula was derived for a cubical array of spheres in a medium. Approximations have been made however, to simplify this case including $\bar{\varepsilon}_1 = \varepsilon_1'$ (where $\bar{\varepsilon}_1$ is the permittivity value for the continuous phase that is `seen` by the discrete particles). This is said to true when the concentration of the dispersed phase is low. For more concentrated mixtures, the approximation $\bar{\varepsilon}_1 = \varepsilon'$ can be used to alter the equation to,

$$\frac{\varepsilon' - \varepsilon_1'}{3\varepsilon'} = v_2 \frac{\varepsilon_2' - \varepsilon_1'}{2\varepsilon' + \varepsilon_2'} \tag{5.15}$$

In this case it is necessary to solve Rayleigh`s equation (5.14) for ε_2' (the dielectric constant of the discrete phase). Which re-arranged gives,

$$\frac{\varepsilon_1' - 2k\varepsilon_2'}{v_2 - k} = \varepsilon_2' \quad \text{Where, } k = \frac{\varepsilon' - \varepsilon_1'}{\varepsilon' + 2\varepsilon_1'} \text{ i.e. L.H.S of Eqn. 5.14} \tag{5.16}$$

The volume fraction component of ε_2' can be described by,

$v = \dfrac{v_2}{v_1 + v_2}$ where v is the *total volume fraction* and v_1 is the volume taken by air

and,

$v_2 = \dfrac{v_2}{v_1}$ is the *volume ratio*

The measured values of $\varepsilon_2^{'}$ were plotted from experimental data and compared to the prediction made by Rayleigh with Eqn. 5.16. This data can be seen in Figure 5.15.

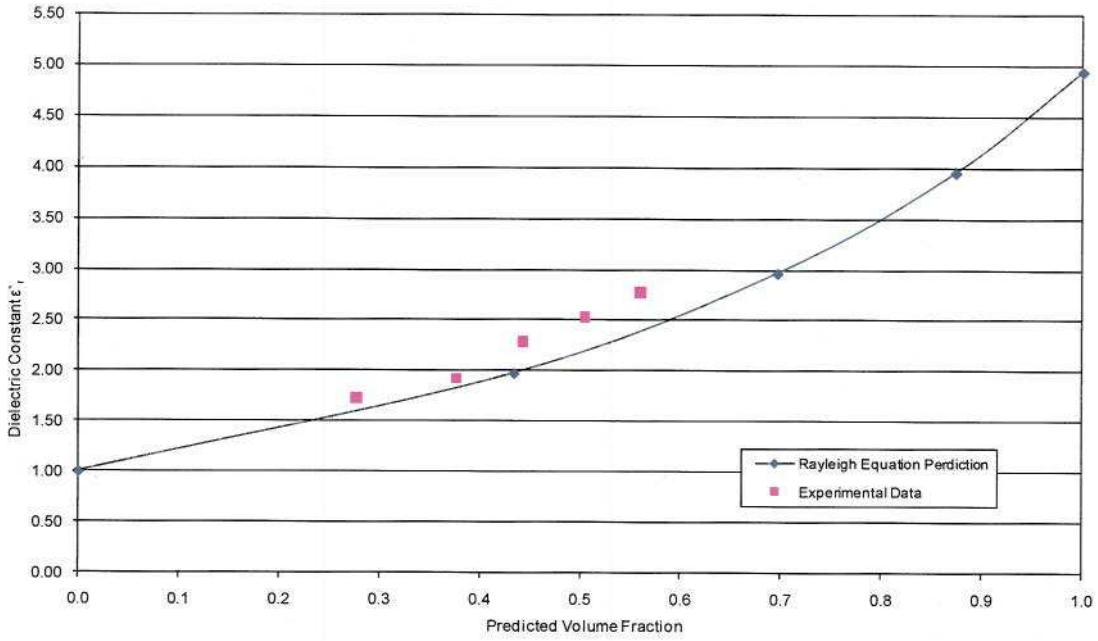

Figure 5.15 Prediction of the Dielectric Constant of Heterogeneous Mixtures according to the Rayleigh model. Experimental Data taken for Daw Mill coal at 911MHz.

The Böttcher equation is now evaluated, using measurements on powdered coal samples, The Böttcher equation,

$$v_2 = \frac{\left(\varepsilon^{'} - \varepsilon_1^{'}\right)\left(2\varepsilon^{'} + \varepsilon_2^{'}\right)}{3\varepsilon^{'}\left(\varepsilon_2^{'} - \varepsilon_1^{'}\right)} \qquad (5.17)$$

It can be seen that the Böttcher equation is similar to the Bruggeman equation in that the dielectric constant of the second phase (coal) must be known for the predictions to be made. Therefore, the Nelson values predicted for the solid phases were used for the purposes of these evaluations.

The measured values of $\varepsilon_2^{'}$ were plotted from experimental data and compared to the prediction made by Böttcher with Eqn. 5.17.

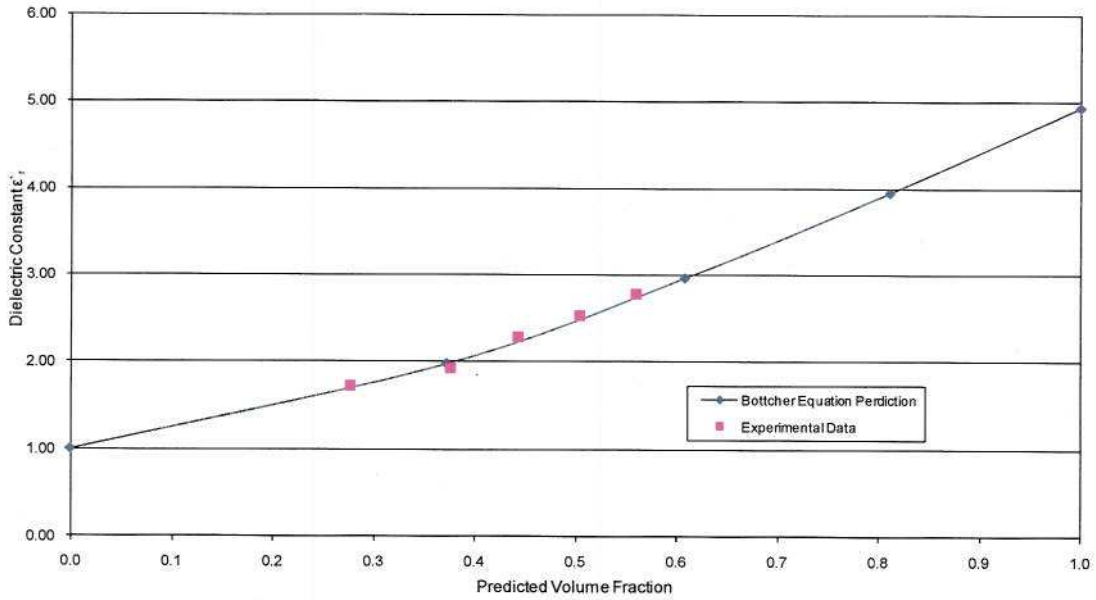

Figure 5.16 Prediction of the Dielectric Constant of Heterogeneous Mixtures according to the Böttcher model. Experimental Data taken for Daw Mill coal at 911MHz.

Other common theories to describe the dielectric permittivity of a heterogeneous mixture are described by the Maxwell-Garnet theory. Maxwell-Garnet theory is derived based on the polarisation induced by an externally applied, uniform electric field on isolated spherical inclusions within a host material. Depending on whether air or coal is considered as the host (major phase), two expressions for the permittivity of the composite mixture $\varepsilon^{'}$ as a function of the relative density of coal are developed.

When coal is considered as the major phase, we have:

$$\varepsilon' = \frac{\varepsilon_2'\left(\varepsilon_1'(3-2\rho)+2\rho\varepsilon_2'\right)}{\left(\rho\varepsilon_1'+\varepsilon_2'(3-\rho)\right)} \tag{5.18}$$

and when air is considered as the major phase, we have

$$\varepsilon' = \frac{\varepsilon_1'\left(\varepsilon_2'(1+2\rho)+2\varepsilon_1'(1-\rho)\right)}{\left(\varepsilon_2'(1-\rho)+\varepsilon_1'(2+\rho)\right)} \tag{5.19}$$

In this case it is considered that coal is the host material (major phase). Then using Eqn. 5.18 the Maxwell-Garnet expression can be used to predict the dielectric constant of the mixture as a function of the relative density. Figure 5.17 illustrates the comparison between the predictions of the Maxwell-Garnet equation with measured experimental data. In this case, note that the dielectric constant ε` for both experimental data and those made by the Maxwell model prediction are plotted against relative density ρ for comparison which is consistent with Eqn. 5.18

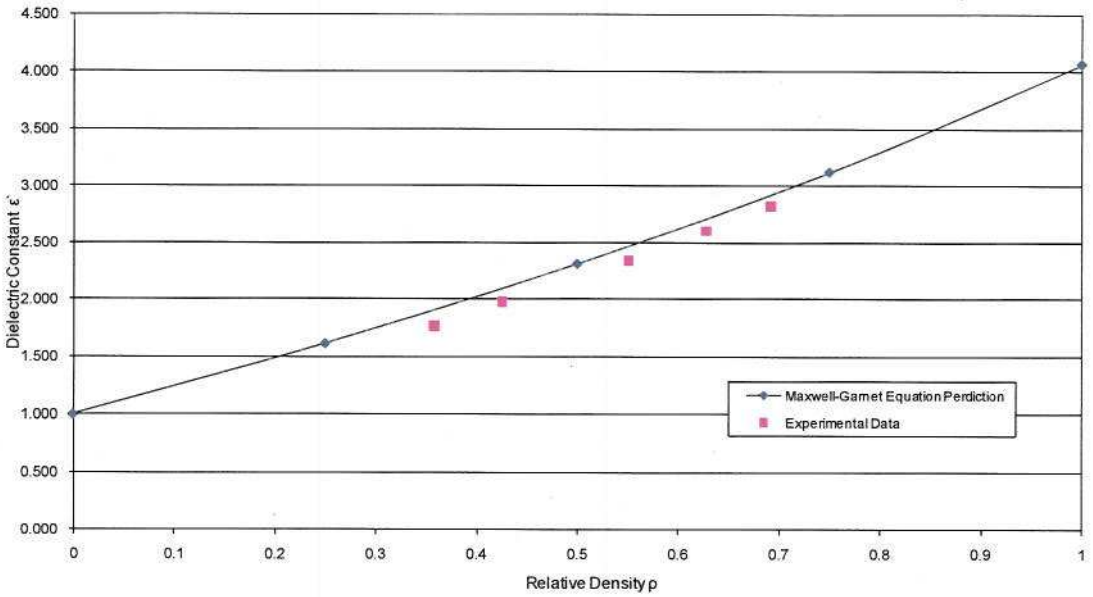

Figure 5.17 Prediction of the Dielectric Constant of Heterogeneous Mixtures according to the Maxwell-Garnet model. Experimental Data taken for Daw Mill coal at 911MHz.

5.3.3 Characterisation of Coal and its Relationship with Dielectric Properties

A consensus of the aromaticity values reported in Table 5.1 would be that there appears to be a definite increase with rank. The values reported in this work range from ~50% for low rank lignite, 60-80% for sub-bituminous and bituminous coals to nearly 100% for anthracite. This is consistent with other investigations (Dodds 2007; Whitehurst 1978). It has been shown that high aromaticity, electron mobility and free charge, will influence a materials dielectric property appreciably (Dodds 2007). Coal rank has been described in section 2.1.4.2, but it is important to note that rank is not a simple continuous progression and therefore will not produce a linear trend when rank parameters are plotted against each other. Another coal rank parameter, useful from a chemical point of view, is its carbon content. Making an accurate prediction on the dielectric properties of coal, based on a rank parameter alone, can be misleading and problematic. The composition and character of each coal must be considered and determined firstly by the nature and makeup of the original organic and inorganic accumulation and secondly by the degree of coalification. Therefore, maceral composition and mineral content will be highly influential on dielectric property data. Furthermore, it has also been demonstrated in this work that sample preparation for dielectric measurement, in particular packing density, sample volume and moisture content, will also have influence on the data presented. Previous studies on the aromaticity of coals have either limited themselves to the effects of rank or to differences between macerals (Carr and Williams, 1990). The general conclusion is that aromaticity and rank increase simultaneously although not necessarily linearly. These studies have shown that that aromaticity of coal and of coal macerals increases with maturity as

measured by vitrinite reflectance. However, it was evident that the aromaticity-reflectance relationship obtained for vitrinites differed significantly to that obtained from liptinites. The aromaticity – reflectance relationships were due to the processes occurring during coalification or maturation. Carr and Williamson explained that upon maturation , the vitrinte maceral will initially lose oxygenated components from its structure with the result that isolated polycyclic aromatic rings are formed. As a result of this formation, a large increase in aromaticity is evident but will not produce a significant increase in the reflectance of vitrinite. Furthermore, these aromatic rings are only rarely formed during the initial stages of coalification, but above a reflectance level of $R_{vi} = 0.7\%$, these rings are readily formed in the structure. Above a vitrinite reflectance level of $R_{vi} = 3\%$, hydrocarbon generation from vitrinite largely ceases, as aromatic carbon formation is replaced by the fusion of the polycyclic rings to produce aromatic sheets. Whilst the aromaticity will continue to increase slowly after $R_{vi} = 3\%$, vitrinite reflectance continues to increase rapidly. This study contains the analysis data of 10 coals obtained from different sources. The aim is to determine the effect of coal maturation or rank, maceral properties and aromaticity on its dielectric properties.

5.3.3.1 The Effect of Moisture Content on Dielectric Properties.

Dielectric properties in general vary significantly with material composition, frequency, temperature and density (Meredith 1998, Pickles *et al.*, 2005, von Hippel 1954). The moisture content of a material can have great effect on measured dielectric properties and is particularly significant for low-loss materials. This is because water has a relatively

high dielectric constant and loss factor of 77 and 13 respectively at 2.45GHz. It is, in fact, possible to determine the moisture content of a material from its dielectric properties alone (Trabelsi *et al.*, 1999). The effect of moisture content on the dielectric properties of some common minerals associated with coal is demonstrated in Table 5.6. The dielectric properties were measured on pulverised samples <38μm using the cavity perturbation technique for each material both on an "as-received" (a.r) basis and after furnace drying (dry) for 4hrs in a nitrogen atmosphere at 105°C. The density dependence of the dielectric properties for each material was taken into account when preparing each sample for measurement. A constant sample volume and packing density in each case was therefore observed.

Mineral Type	*Fire Clay*	*Ball Clay*	*Silica Sand*	*Silica (Pure)*	*China Clay*	*Red Terracotta Clay*
ε_r' (a.r)	2.909	1.967	2.530	2.125	1.767	2.41
ε_r' (dry)	2.526	1.754	2.476	2.121	1.645	2.07
ε_r'' (a.r)	0.375	0.076	0.011	0.005	0.039	0.24
ε_r'' (dry)	0.158	0.007	0.009	0.003	0.004	0.06

Table 5.6 Dielectric Properties of some common coal associated minerals.

Table 5.6 demonstrates that the presence of water in the sample has the effect of increasing the microwave absorbing properties of the material. On a "dry" basis (upon the removal of surface water), both the dielectric constant and loss factor are reduced significantly.

5.3.3.2 The Effect of Rank on Dielectric Properties of coal.

Fundamentally, coal rank increases with increasing carbon content. Furthermore, as rank increases, moisture content, volatile matter content and oxygen and hydrogen content decrease, conversely calorific value increases with increasing rank. However, maceral composition and mineral composition/content are unrelated to rank. Each maceral may vary significantly according to the type of coal under examination. This fact can be extremely problematic when trying to make a credible evaluation of its dielectric properties, or more importantly, making a comparison from one coal to another. Clearly, any variation in moisture content and it subsequent effect on dielectric properties can be minimised, provided that the samples have undergone a drying regime to remove surface moisture (inherent moisture may still remain after heating at 105°C). The data presented Table 5.1 and Figure 5.13 proves that dielectric loss factor is related to coal aromaticity and that aromaticity is related to carbon content across a range of coals. The dielectric properties of UK coals and UK power station blends were investigated by Marland *et al.*, 2001. Measurements on pulverized coal samples were performed using the cavity perturbation technique. The dielectric measurements which performed at ambient temperatures up to 180°C showed that upon surface moisture removal, both the dielectric constant and loss factor decreased significantly. The work concluded that moisture content was the dominant factor affecting the dielectric properties although no specific trend was evident when comparing the dielectric constant or loss factor with coal rank on a dry basis.

Moreover, volatile matter content rather that vitrinite reflectance was used as a rank indicator. Maceral and mineral composition were measured by Marland *et al.,* 2001 but were not removed from the coal, which is one possible explanation as to why significant variations in dielectric properties were evident across the rank range but with no specific trend evident. On a simplistic level, it is probable that mineral composition/content and maceral composition for each coal are masking any possible rank effect.

The presence of mineral matter in coal when performing dielectric measurements is clearly problematic if comparisons with rank (or any other parameter) are to be meaningful. Mineral matter, in particular pyrite, place huge limitations on any dielectric property investigation on coal. Measurements made on dry mineral-free coal would therefore be beneficial and serve to eliminate the effect of these impurities on the results obtained.

5.3.4 Characterisation and specification of a series of world coals.

A series of UK and world coals were selected for this study. The coals were chosen to reflect a variety of petrographic types and ranks and were sourced from The British Coal Utilisation Research Association (BCURA).

5.3.4.1 Proximate Analysis

Proximate analysis for each coal was carried out using a Pyris 1 Perkin Elmer thermogravimetric analyser, under standard conditions according to BS1016-3. Each

sample was finely ground to minimise size effects and then a sample of 10-20mg was heated in Nitrogen at 35ml/min from ambient temperature to 120°C at 50°C/min and allowed to soak at 120°C for 5 minutes. The sample was then heated from 120°C to 920°C at 50°C/min and held at 920°C for 5 minutes. The input gas to the furnace was then switched to air at 40ml/min and the sample was allowed to cool to 820°C. The sample is then held at this temperature for a further 20 minutes.

The "as-received" proximate analysis for the suite of coals used in this work is given in Table 5.7.

Coal Type	% Moisture	% Ash	% Volatiles	% Fixed Carbon	% Volatiles d.a.f
Hambach	8.3	3.4	59.4	29.0	67.2
Tilmanstome	0.7	5.3	15.9	78.0	17.0
Cynheidre	1.3	22.5	6.5	69.7	8.5
Lea Hall	2.9	2.6	40.7	53.8	43.1
Pittsburgh	1.7	4.4	58.2	35.7	38.0
Baddersley	2.5	3.3	40.4	53.7	43.0
La Jagua	1.7	6.9	39.6	51.8	43.3
Reitspruit	1.4	8.7	36.4	53.5	40.5
Geodehoop	1.0	14.2	28.0	56.7	33.0
Betts Lane	0.5	8.3	21.9	69.3	24.0

Table 5.7 Proximate Analysis of all coal sample (on a wt% as received basis)

5.3.4.2 Rank Analysis (Vitrinite Reflectance)

The petrographic properties of the vitrinite maceral in coal change uniformly with increasing rank and in reflected light, the reflectance of vitrinite increases progressively. The coal samples were prepared into a standard block using liquid resin mixed with methyl-ethlyl-ketone (50% w/w). Each block was then ground and polished and then examined under a polarised-light microscope with 32x magnification oil immersion objective and 10x magnification eyepiece. The reflectance R_{vi} is then calculated as the

percentage of normal incident light that is reflected from a polished vitrinite surface. Details of the sample preparation and measurement procedure are detailed in Section 2.4.1.2. Other information can be found from British Standard BS6127, 1995. Figure 5.18 shows the histogram distributions for a number of coals of varying rank, illustrating a progressive increase in average vitrinite reflectance as rank increases.

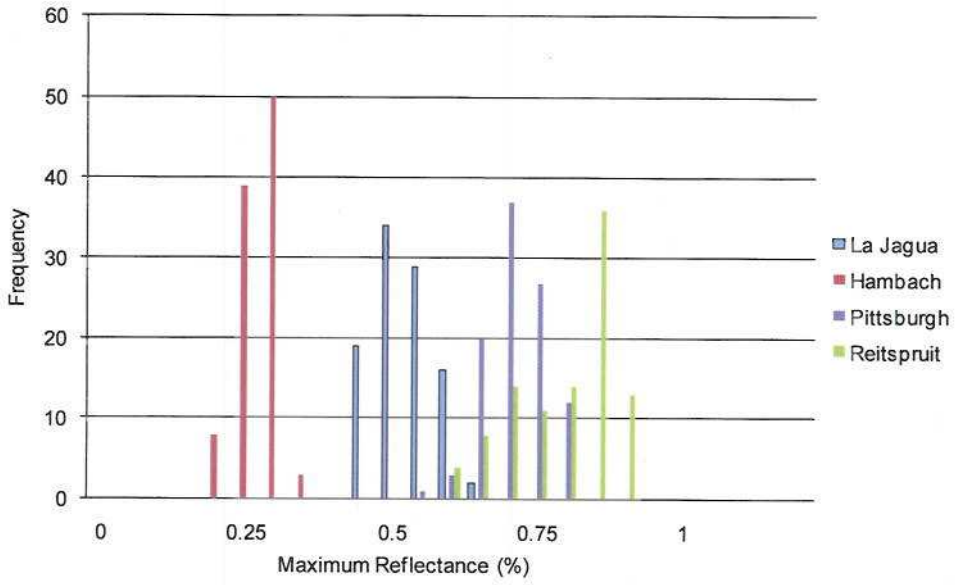

Figure 5.18 A Reflectance Histogram for a range of coals showing a difference in rank.

The results of rank analysis on each coal sample are shown in Table 5.8.

Coal Type	R_{vi}
Hambach	0.29
Tilmanstome	1.35
Cynheidre	3.46
Lea Hall	0.55
Pittsburgh	0.73
Baddersley	0.55
La Jagua	0.54
Reitspruit	0.81
Geodehoop	0.77
Betts Lane	0.98

Table 5.8 Rank Analysis based on Random Vitrinite Reflectance (as-received basis).

5.3.4.3 Maceral Analysis

The maceral distribution in each coal is reported here using a grey-scale reflectogram generated by an automated image analysis technique developed by the University of Nottingham (Lester *et al.*, 1994, Cloke *et al.*, 1995). A detailed description of this technique and the data interpretation is outlined in Section 2.4.1.1. A Leitz Ortholux II POL-BK microscope was used for all petrographic investigations using a 32x magnification oil-immersion lens and non-fluorescing oil from Leitz. The reflectance of a whole coal sample was measured using the image analysis procedure and technique described by Lester *et al.*, 2003. Figure 5.19 shows a series of typical reflectance histogram profiles for all the maceral groups from varying rank coals from this study. From this data maceral proportions can be calculated and are shown in Table 5.9.

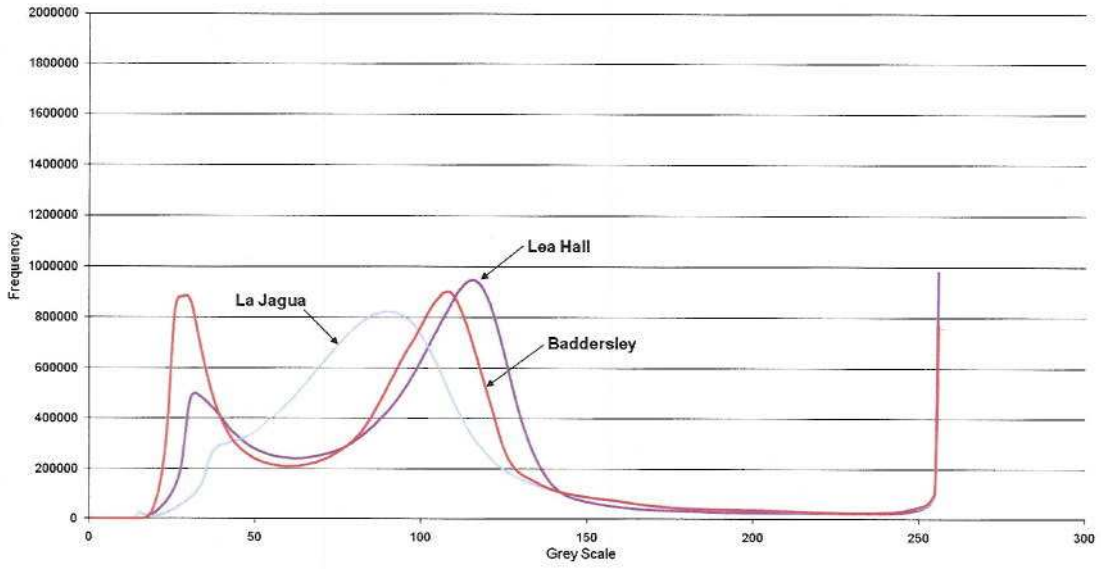

Figure 5.19 Full maceral histogram profiles for three selected coals on an as received basis (background resin removed).

Coal Type	Vitrinite	Liptinite	Inertinite
Hambach	82	17	1
Tilmanstome	89	0	11
Cynheidre	96	0	4
Lea Hall	76	13	11
Pittsburgh	89	1	10
Baddersley	75	10	15
La Jagua	83	1	16
Reitspruit	70	3	27
Geodehoop	66	3	31
Betts Lane	92	4	4

Table 5.9 Petrographic analysis information for the coals (results are on a vol% mineral matter free basis).

5.3.4.4 Demineralisation using HF and ferric ions

The presence of mineral matter and in particular pyrite in coal can affect its dielectric properties significantly as discussed previously. The problem of ascertaining the dielectric properties of the organic carbonaceous phase of the coal structure lies in the fact that the mineral content and composition of coal can vary widely for different coals and so comparisons of the dielectric properties from one coal to another, without consideration of its inorganic composition and water content can be misleading. The removal of mineral matter has been practiced for several decades (Crawford, 1951; Meyers, 1973 & 1981, Steel *et al.*, 2004, Zhiheng and Steel, 2007). These studies have shown that it is possible to dissolve minerals using leaching liquors and waste solution regeneration schemes to produce coal of significantly reduced ash content. The University of Nottingham has been developing a two-stage leaching process using low concentration aqueous hydrofluoric acid (HF) to remove mainly Al and Si mineral followed by second leach by Ferric ions (Fe^{3+}) which are able to oxidise pyrite (without oxidising the organic coal structure)(Meyers, 1973) and dissolve insoluble fluorides

formed during the HF leaching stage (Zhiheng and Steel, 2007). Each coal sample (See Table 4.10) was demineralised using the two-stage chemical leaching process outlined by Zhiheng and Steel, 2007. The ash content before and after leaching was measured to ensure that ~0.5%wt (dry basis) remained. The calorific value of each sample was measured after chemical demineralisation using an IKA C5000 calorimeter, which, in each case, suggested no oxidation had occurred to the carbonaceous matrix of the coal. After the two-stage leaching process was complete, the coal samples were allowed to air dry naturally for 24hrs in a fume cupboard. The samples were then transferred to a drying oven set at a temperature of 105°C for a further 3hrs. Once the drying process was complete the samples were stored in a glass desiccator.

The ash content (%wt - db) for each coal before and after chemical leaching is summarised in Table 5.10.

Coal	Country	C (wt%, daf)	Raw coal ash, (wt%, db)	HF treated coal ash, (wt%, db)	HF/Fe^{3+} treated coal ash, (wt%, db)	Ash removal by HF, %	Ash removal by HF/Fe^{3+}, %
Hambach	GER	67.5	4.50	4.50	1.06	0.00	76.44
Tilmanstone	UK	92.4	5.44	0.73	0.31	86.58	94.30
Cynheidre	UK	95.2	1.83	0.27	0.08	85.25	95.63
Lea Hall	UK	81.1	3.28	1.56	0.56	52.44	82.93
Pittsburgh No. 8	USA	84.6	11.46	1.53	0.48	86.65	95.81
Baddesley	UK	80.5	4.28	1.66	0.48	61.21	88.79
La Jagua	COL	82.6	2.20	0.48	0.30	78.18	86.36
Reitspruit	SA	83.6	12.88	1.33	0.31	89.67	97.59
Geodehoop	SA	85.5	13.68	5.20	0.57	61.99	95.83
Betts Lane	UK	90.0	8.54	4.29	1.27	49.77	85.13

Table 5.10 Ash contents of each coal sample before and after demineralisation. UK – United Kingdom, GER – Germany, USA - United States of America, COL – Columbia, SA – South Africa.

Once the samples had been oven dried, they were ready for dielectric measurement using the cavity perturbation technique. This is a well suited technique for measurements of powdered material and does not require a smooth surface as is the case when using the coaxial line technique (Hutcheon *et al.,* 1992). A detailed measurement technique is described earlier in Section 4.3.1.

It can be seen in Table 5.10 that the mineral extraction efficiency depends strongly on the type of coal but the extract yield for most coals in this study is high, with only Geodehoop (0.57%), Betts Lane (1.27%) and Hambach (1.06%) showing a treated ash content of greater than 0.5%wt (dry basis) after a single chemical leach treatment.

5.3.4.5 Dielectric Properties of Demineralised Coal

Table 4.11 shows the dielectric properties for each coal sample. Measurements were taken on an "as-received", "de-Ashed" and "de-Ashed (dry)" basis for comparison. The values are the average of five readings, all of which lie within the acceptable levels of accuracy of 5% to 10% for dielectric constant and loss factor respectively (Hutcheon *et al.,* 1992). It can be seen that the dielectric loss factor ε" for coal is relatively low across all experiments indicating that the material is a relatively poor microwave heater. The loss factor for double distilled water (ε") is 5.2 and 13 at frequencies of 912MHz and 2.47GHz respectively. The relationship between the dielectric properties of coal and its carbon content or rank is a complex one. Changes in carbon structure associated with increasing

coal rank should, in principle, be represented by a change in its dielectric property. Increased ordering within the carbon structure as rank progresses should lead to an increase in the dielectric properties of coal as a result of increased electron mobility as suggested by literature and this experimental investigation. However, inclusions of other phases within the coal structure, namely moisture and mineral matter (and in particular pyrite), may obscure any relationships which might otherwise be developed. Minimising the effect of these responsive phases is therefore of significant value to this investigation, if direct comparisons from one coal to another across the rank range are to be reported. In this experimental investigation, the effect of coal mineral matter (including pyrite) and surface moisture on its dielectric property has been minimised as far as possible by a two stage leaching (HF/Fe^{+3} demineralisation) and further drying treatment as described earlier. Furthermore, the relationship between sample bulk density and its dielectric properties, as discussed in section 5.3.2, was accounted for by ensuring a constant sample volume and packing density across all cavity perturbation measurements. A histogram profile for the dielectric loss factor of coal on an "as-received", "de-ashed" and "de-ashed (dry)" basis is shown in Figure 5.28 for a measurement frequency of 2.47GHz. The value of loss factor in all coal samples decreases (in some cases dramatically) after drying i.e. after the final drying stage from "de-ashed" to "de-ashed (dry)". Such a significant drop is explained by the removal of water in the oven drying process ($\varepsilon''=13$ at 2.47GHz), considering that the total loss-factor of a multi-component material is due to the volume fractions of individual

components. The significant decrease in dielectric loss factor upon drying for low rank coals is explained by a relatively high "as-received" moisture content (8.3%M for Hambach coal) as can be seen in the proximate analysis Table 5.7.

Figure 5.28 appears to show no correlation between dielectric loss factor (ε") and rank on an "as-received" basis. Clearly, the contribution of water and the fact that each sample contains differing amounts of mineral matter may be disguising any trend that may have otherwise been evident as a result of structural ordering within the carbon matrix as rank progresses. In the case of low rank Hambach coal, the presence of both moisture and mineral matter on an "as-received " basis have increased its dielectric loss factor when compared to measurements taken on a "de-ashed (dry)" basis. This is also true for Baddersley, Lea Hall and La-Jagua coals. These are low to medium rank coals when compared to the remaining coals as can been seen from the rank analysis data shown in Table 5.8. The dielectric loss factor at 2.47GHz for Hambach coal on a "de-ashed (dry)" basis is ε"=0.016 which is a significant drop from ε"=0.038 on an "as-received" basis. This reduction is explained by the fact the Hambach coal is a low rank lignite coal with a less ordered carbon structure than any other coal used in these experiments. The data presented here would suggest that the measurement of dielectric loss factor for low rank coals on an "as-received" basis are an over estimation due to the contribution of both mineral matter and moisture. Conversely, for higher rank coals (C>85% [wt] and R_{Vi}>0.7%) the dielectric loss factors on an "as-received" basis are lower than those after "de-ashing" and moisture removal. This is true for Pittsburgh #8, Geodehoop, Betts Lane, Tilmanstone and Cynheidre coals. When comparing the dielectric loss factors for the coal

samples above one can suggest the following: In all cases the dielectric loss factor at 2.47GHz and 912MHz increases after mineral matter removal. This suggests that the loss factor of the samples on an "as-received" basis is suppressed by the contribution made by the mineral matter inclusions in the matrix. Moreover, in all cases the dielectric loss factors after demineralisation and drying is higher than those measured on an "as-received" basis. The dielectric loss factor decreases upon moisture removal from all the samples tested. Such a tendency is clearly related to the fact that these are high rank coals and consequently exhibit higher ordered carbon structures promoting an increase in electron mobility across the aromatic matrix. Aromaticity of the carbon structure of coal increases significantly with rank and is seen to be directly proportional to the dielectric loss factor. This relationship can be observed in Figure 5.21 and Table 5.1.

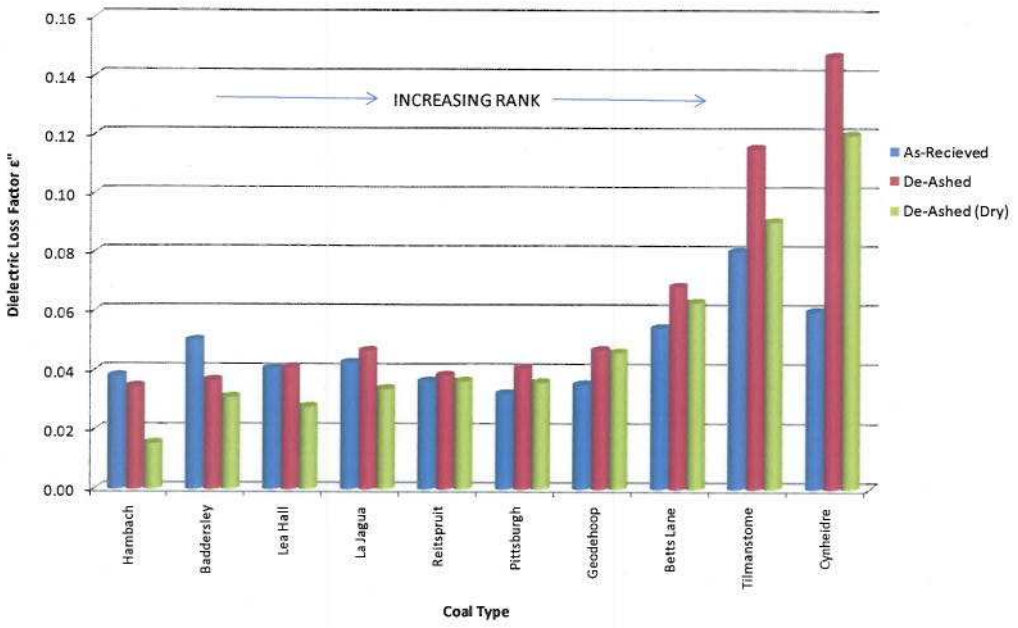

Figure 5.20 Histogram profile for the dielectric properties of De-Ashed (dry) coal samples. Measurement on as-received and De-Ashed basis are included for comparison

The results shown in Figure 5.5 for dielectric loss factor at 2.47GHz vs carbon aromaticity agree with the expected correlation, in that coal carbon aromaticity increases steadily with rank. However, this relationship is only observed once the contributions from mineral matter inclusions and water have been minimised. Furthermore, a relationship is observed for dielectric loss factor at 2.47GHz ("de-ashed (dry)" basis) vs Random Average Vitrinite Reflectance R_{vi}. This relationship is shown in Figure 5.29. The linear relationship presented in Figure 4.29 is a legitimate one considering the rank range of the materials under examination. Dodds, 2006 studied the relationship of dielectric loss factor and vitrinite reflectance for a number of coal and coke samples. An exponential relationship of loss factor against vitrinite reflectance was examined and proposed, however in the experiments reported by Dodds, 2006, the rank range was from ~0.8 to ~8%. This evidence also suggested that a dramatic increase in electron mobility had occurred across the coal/coke matrix as carbon aromaticity increased.

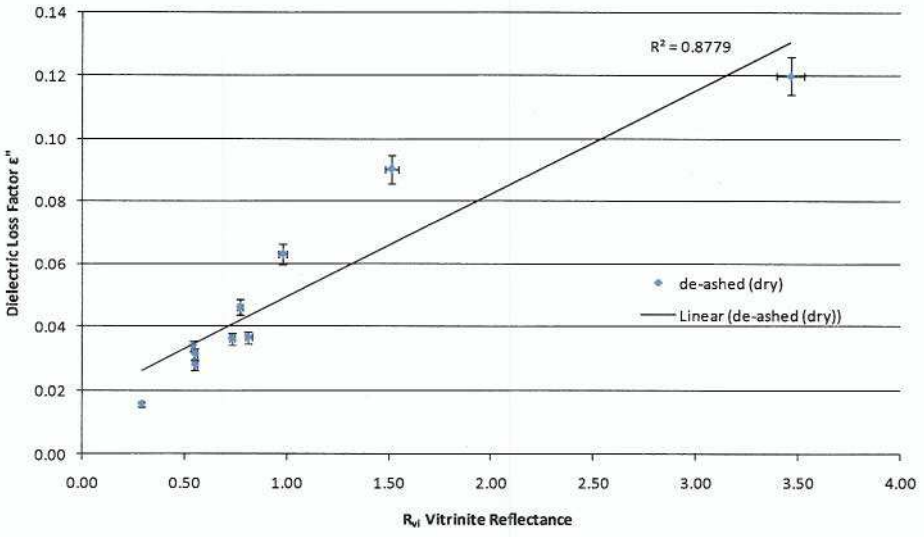

Figure 5.21 Relationship between Dielectric Loss Factor measured at 2.45GHz and Random Average Vitrinite Reflectance (from oil immersion microscopy) R_{vi}.

Although the relationship presented in Figure 5.21 is a reasonable one, it does not provide a clear indication of the point of changing reflectance, at which a dramatic increase in electron mobility and hence a dramatic increase in dielectric loss factor occurs.

One possible explanation for the scatter shown in Figure 5.21 may still be the presence of some mineral matter and inherent moisture remaining in the sample after leaching and oven drying. The ash content after HF/Fe^{3+} leaching is shown in Table 5.10.

	As.Recieved					
	@ 912 MHz			@ 2470 MHz		
COAL	ε'	ε''	tanδ	ε'	ε''	tanδ
Hambach	2.354	0.040	0.017	2.337	0.038	0.016
Baddersley	2.485	0.047	0.019	2.465	0.050	0.020
Lea Hall	2.738	0.047	0.017	2.738	0.041	0.015
La Jagua	2.354	0.047	0.020	2.338	0.043	0.018
Reitspruit	2.353	0.043	0.018	2.345	0.037	0.016
Pittsburgh	2.083	0.030	0.014	2.044	0.032	0.016
Geodehoop	2.421	0.039	0.016	2.410	0.035	0.015
Betts Lane	2.357	0.066	0.028	2.324	0.054	0.023
Tilmanstome	2.616	0.088	0.033	2.606	0.080	0.031
Cynheidre	2.799	0.081	0.029	2.766	0.060	0.022
	DE-ASHED					
	@ 912 MHz			@ 2470 MHz		
COAL	ε'	ε''	tanδ	ε'	ε''	tanδ
Hambach	1.994	0.037	0.019	1.988	0.035	0.018
Baddersley	2.370	0.036	0.015	2.340	0.037	0.016
Lea Hall	2.232	0.039	0.017	2.210	0.041	0.019
La Jagua	2.375	0.042	0.018	2.374	0.047	0.020
Reitspruit	2.398	0.042	0.017	2.377	0.038	0.016
Pittsburgh	2.442	0.039	0.016	2.429	0.041	0.017
Geodehoop	2.468	0.035	0.014	2.350	0.047	0.013
Betts Lane	2.317	0.055	0.024	2.302	0.068	0.021
Tilmanstome	2.550	0.129	0.050	2.387	0.115	0.048
Cynheidre	2.821	0.198	0.070	2.768	0.147	0.053
	DE-ASHED (dry)					
	@ 912 MHz			@ 2470 MHz		
COAL	ε'	ε''	tanδ	ε'	ε''	tanδ
Hambach	1.955	0.029	0.015	1.923	0.016	0.008
Baddersley	2.192	0.038	0.017	2.161	0.031	0.014
Lea Hall	2.348	0.030	0.013	2.339	0.028	0.012
La Jagua	2.185	0.041	0.019	2.161	0.034	0.016
Reitspruit	2.201	0.042	0.019	2.181	0.037	0.017
Pittsburgh	2.104	0.034	0.016	2.090	0.036	0.017
Geodehoop	2.425	0.045	0.019	2.389	0.046	0.019
Betts Lane	2.373	0.075	0.032	2.324	0.063	0.027
Tilmanstome	1.883	0.107	0.057	1.909	0.090	0.047
Cynheidre	2.801	0.161	0.057	2.761	0.120	0.044

Table 5.11 Dielectric properties for coal on an "as-received", "de-ashed" and "de-ashed (dry)" basis at 912MHz and 2.47GHz.

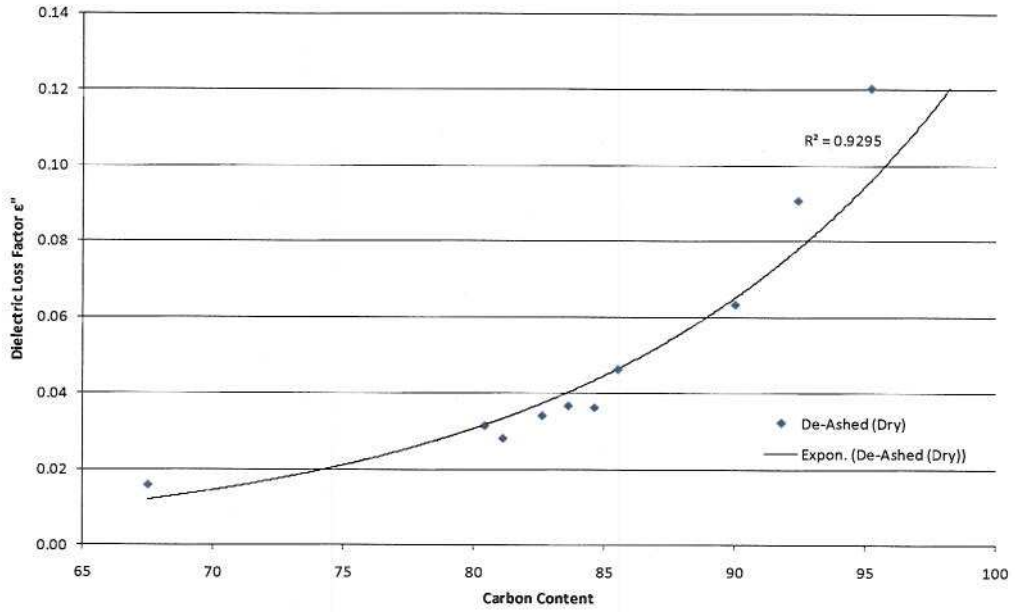

Figure 5.22 Relationship between Dielectric Loss Factor measured at 2.45GHz and Carbon Content for all coal samples on a De-Ashed dry basis.

Figure 5.22 shows that a near exponential relationship exists between coal carbon content (d.a.f) and loss factor measured at 2.45GHz. This relationship is only evident once mineral matter and surface moisture has been minimised by HF/Fe^{+3} leaching and oven drying.

5.4 Discussion

The difficulty in maintaining uniform bulk densities and sample volume is a major source of error when dielectric measurements are made on particulate materials using the cavity perturbation technique. The investigation presented in this work into the dependence of the dielectric properties of pulverised coal upon its density is important for a number of reasons. It has been shown that the density dependence is a complicating factor and must be accounted for if direct comparisons are to be made from one material to another. If other factors remain constant, density dependence of the dielectric properties are useful for measurement of moisture content and density. Moreover, this work has shown to be useful in estimating the dielectric properties of solid material from measurements on granular or pulverised material, particularly when solid material cannot be obtained or when measurement of the solid is not convenient. It is mainly for the latter reason that a number of mixture formulae for the permittivity of heterogeneous systems have been examined in this work. Some of these and other formulae were compared by Nelson, 1983 and Kraszewski and Kulinski, 1976 for predicting the permittivities of two-phase mixtures. Based on observation made in this work and by other similar investigations the following observations are made.

(1) The linearity of the $\sqrt{\varepsilon_r'}$ with ρ and $\sqrt[3]{\varepsilon_r'}$ with ρ relationships provide the means for estimating the dielectric constant ε_r' of an air-particle mixture at any density, including that of the solid material, by using the measurement of the dielectric constant ε_r' at a known density and the $\left(\rho = 0, \varepsilon_r' = 1\right)$ intercept.

(2) The linearity of $\sqrt{\varepsilon_r'}$ and $\sqrt[3]{\varepsilon_r'}$ with ρ are consistent with published dielectric formulae that requires the addition of the weighted square roots and cube roots, weighted in terms of volume or density-mass fractions, of the dielectric constants of the constituents of the mixture.

(3) For the dielectric loss factor ε_r'', linearity can be expected between $\sqrt{\varepsilon_r'' + e}$ and ρ, where e depend on the specific material under examination.

(4) Thus, the linear relationship between $\sqrt{\varepsilon_r'' + e}$ and ρ, enables a reliable estimation of ε_r'' at any density. However, for more accurate estimations there is a necessity to take measurements of ε_r'' at several densities for accurate determination of the constant e and the slope of the straight line.

(5) The quadratic relationships for both ε_r' and ε_r'' seem to be valid in this application and compares well with the other linear regression models presented in this work.

The lines of best fit through the experimental data, as determined by the least-squares calculation, cannot be expected to provide reliable predictions very far outside the range of experimental data. For this reason, it is not surprising to find some, albeit small, disagreement between least-squares and linear regression predictions of the solid material (calculated from air-comparison Pycnometer experiments). It is only when extrapolation is over a relatively short range that least-squares predictions for the solid material dielectric properties can be relied upon.

The relationship between the structural variations within coal and their dielectric properties is a relatively new field of investigation. The natural heterogeneity of coal will mean that comparisons of their dielectric properties from one coal to another are at best tenuous unless all sources of error can be minimised or eliminated. The density dependence of dielectric properties on particulate material has already been shown to be a source of considerable error if experimental sample bulk density continuity is not observed. Accurate predictions on the dielectric properties of coal based on rank alone can be misleading. Variations in moisture content, inorganic inclusions (inc. pyrite) have been shown to influence the dielectric properties of coal significantly.

An important first step in the analysis of the dielectric properties of coal is to be able to assess the structural nature of each sample. Solid state C^{13}_{NMR} spectra for each sample were examined and used to interpret carbon aromaticities for each sample which are shown in Table 5.1. Furthermore, the optical properties of the vitrinite maceral in each sample were used as an indicator of rank which is also shown in Table 5.1. This data shows that, essentially, as coal rank increases, carbon aromaticity increases significantly as expected. Therefore, it is not inconceivable to expect a relationship between coal rank and its dielectric properties. However, experimental data for the dielectric properties of coal in this series, measured on an `as-received` basis did not reflect these assumptions. No correlation between dielectric loss factor and rank or permittivity and rank is evident. Interference from moisture and gangue inclusions (mineral matter content and composition), present in varying quantities, depending on the type of coal under

examination, were responsible for these unreliable results. Changes in the dielectric properties of coal as a result of pyrolysis (degree of oxidation) are noted here but are not relevant in these experiments. The dielectric anisotropy phenomenon of coal, as discussed by Tonkonogov and Veksler, 1968 is noted but is again not relevant in the experiments since all measurements were taken of pulverized material.

Chapter 6 - The effect of microwave energy upon the decomposition of pyrite in coal.

6.1 Introduction

Future challenges for "clean coal technologies" are substantial because coal offers an abundant widely spread fossil fuel resource for our world. The growing energy demands of developing countries coupled with the demand for significant reductions in greenhouse gas emissions mean that now, more than ever, "clean coal technologies" are at the forefront of all future energy policies (Beér, 2007). The emission controls on CO_2 ,NO_X, SO_X and particulate matter together with fluidised bed combustion (FBC), integrated gasification combined cycle (IGCC) etc. are all key pathways and each will play a significant role in new generating capacity. Coal is still and will continue to be the most widely used fossil fuel in the mix of primary fuels used to generate electricity for the foreseeable future. However, coal combustion produces structurally more pollutants than other fossil fuels since it contains mainly carbon (producing CO_2) and sulphur in the form of pyrite/marcasite (SO_x is the resulting product) as reactive components. Moreover, coal is not a uniform source of fuel due the extreme variability in its composition. This will of course make standardisation of advanced cleaning technologies difficult with any solution being "fuel type/source" sensitive.

Control of SO_2 emissions is stringent all over the world and has produced some regional initiatives to reduce these emissions. These include the use of adsorbants such as hydrated lime reacting with siliceous materials such as fly ash and metal oxides such as

Copper Oxide/Cerium Oxide which have been employed to absorb SO_2 from the combustion flue gas stream (Flue Gas Desulphurisation - FGD). This technology is discussed in detail in Section 3.7.1. There are however, some limitations to these emissions reduction processes. Firstly the adsorbents can be difficult to regenerate and where regeneration is possible the process is extremely energy intensive. Secondly, the process produces a huge amount of secondary waste which has little commercial value. The cost of current SO_x reduction technologies, such as FGD plants, represent a significant proportion of the total cost of a modern coal fired power plant.

In most coals, sulphides in the form of pyrite and to a lesser extent marcasite are largely responsible for the SO_x emissions from coal combustion. The occurrence, abundance and associations of these sulphides will vary significantly from source to source. As well as post combustion technologies to tackle SO_x emissions, there are technologies currently in use for the physical cleaning of coal prior to combustion. Although these are predominantly used for mineral matter removal (low ash product), some sulphur may be rejected but the proportion that is intimately associated with the organic portion of the matrix will not be removed. The main separation process for removing sulphide minerals from their associated gangue is by froth flotation or electrostatic separation techniques (described Section in 3.7.3). The separation of fine particles from coal in an attempt to remove sulphur bearing phases is a considerable challenge which has received much attention. Some of these pre-combustion cleaning technologies which include washing (Liu, 1982) and density separation have been in use since the 1970`s. Others, such as

chemical leaching and selective microwave heating, are more recent areas of research. A review of these technologies is outlined in Section 3.8.

There have been numerous investigations into the desulphurisation of coal by magnetic separation (Rowson et al., 1990; Butcher et al., 1996; Bluhm et al., 1995; Rowson & Rice, 1995). To facilitate the removal of pyrite from coal by magnetic separation various techniques have been employed to increase its magnetic susceptibility. One means of improving the magnetic properties of pyrite is the use of microwave energy to selectively heat the pyritic phase altering its surface chemistry and possibly inducing a phase alteration to increase its magnetic properties thereby making magnetic separation a more efficient process (Waters et al., 2007). The mechanisms proposed for the decomposition and oxidation of pyrite by microwave and conventional heating are discussed in Chapter 4. Specifically, the magnetic properties of iron sulphides have been discussed in Section 3.2.2.3 and it has shown that pyrite (FeS_2) and hexagonal pyrrhotite (Fe_9S_{10}) are weakly paramagnetic at ambient temperatures and will exhibit magnetisation only when in the presence of a magnetic field. However, Greigite (Fe_3S_4) and monoclinic pyrrhotite (Fe_7S_8) exhibit ferromagnetic tendencies and are able to carry magnetisation. The current published literature in this area is reviewed in Section 3.8.3. Exposure of pyrite to microwave energy has been shown to improve the recovery of pyrite when magnetically separated using both wet and dry techniques (Waters et al., 2007). However, whilst the magnetic recovery increased corresponding with changes in the magnetisation of the material, observation of favourable pyritic phase

alterations remains inconclusive. Several recent studies have investigated the application of low power microwave radiation to improve the magnetic properties of both museum grade pyrite samples and in-situ coal derived pyrite in an effort to improve recovery by magnetic separation (Waters et al., 2007, Uslu & Atalay 2003; Kingman et al., 2000+; Rowson & Kelly 1995; Bluhm et al., 1986; Xia & Pickles 1999Kingman & Rowson 1998, Rowson & Rice, 1990). Almost all of the above work was carried out at low microwave power levels <1900W for small samples <0.5kg with consequently low power densities (kW/m^3). Higher power densities were not achieved due to the use of low power low efficiency microwave sources found in most domestic kitchens. As a result of these limitations, exposure times in the order of minutes were necessary to achieve any significant effects. It is unlikely that long residence times are economically or practically viable, especially if the coal is being treated whilst in the process passing from the storage hopper to the separator, for example.

In Chapter 4, it has been shown that exposure of pure pyrite to both microwave heating and conventional heating methods improve its magnetic properties due to phase changes on the surface of the mineral particles. These phase changes and associated increases in magnetic properties were observed using SEM/MLA , XRD and VSM (Vibrating Sample Magnetometer) analysis respectively. It is however, of particular interest to further explore and understand the nature of the effects of microwave heating on the conversion of in-situ pyrite in coal by SEM/MLA evaluation after treatment.

This chapter extends previous work by others by assessing quantitatively the influence of higher applied microwave power levels on the conversion of pyrite in coal whilst also monitoring how petrographic and proximate characteristics change as a result of high power microwave exposure, with respect to burnout and potential burnout problems.

6.2 Experimental Investigation

6.2.1 Coal Specification

Bituminous Kentucky coal was used in this investigation and riffle split into 8 sets of ~1kg batches. Kentucky coal was chosen for this scientific study because of its high sulphur content and in particular high pyritic sulphur content >12%. The proximate and petrographic analysis of Kentucky coal is shown in Table 6.1(a) and 6.1(b) respectively. Proximate analysis was performed on an `as-received` basis using a Pyris 1 Perkin-Elmer thermogravimetric analyser according to BS1016-3 and petrographic characterisation was carried using an automated image analysis method during oil immersion microscopy on polished sample mounts (Lester et al., 2002). Rank analysis based on reflected light measurements on polished vitrinite was performed according to (BS 6127, 1995) and the result is shown in Table 6.1(c). The full details for Rank analysis measurements based on vitrinite reflectance are outlined in Section 3.4.1.2 of this report. Analysis of Sulphur forms for Kentucky coal were conducted by TES-Bretby coal and commodity laboratory, Burton-upon-Trent in accordance with (BS 1016-11) and are shown in Table 6.1(d). The estimated dielectric properties of Kentucky coal at frequencies of 911MHz and 2.45GHz

based on regression relationships with bulk density are shown in Table 6.1(e). The density dependence of the dielectric properties of properties of pulverised coal is described in Section 5.3.2.

					dry, ash free basis		
Coal Type	*% Moisture*	*% Ash*	*% Volatiles*	*% Fixed Carbon*	*% Volatiles*	*% Fixed Carbon*	*Fuel Ratio*
Kentucky	2.8	26.2	37.8	33.3	53.1	46.9	0.88

Table 6.1(a) Proximate analysis of Kentucky coal (on wt% as-received basis).

Coal Type	*% Vitrinite*	*% Liptinite*	*% Semifusinite*	*% Fusinite*	*% Pyrite*	*% Mineral*
Kentucky	87.2	4.8	2	1.6	4	0.4

Table 6.1(b) Petrographic analysis for Kentucky coal (vol% basis)

Coal Type	R_{vi}
Kentucky	0.70

Table 6.1(c) Rank analysis of Kentucky coal based on Random Vitrinite reflectance measurements (as-received basis).

Coal Type	*% Pyritic Sulphur*	*% Sulphate Sulphur*	*% Organic Sulphur*
Kentucky	12.28 (78%)	0.64 (4%)	2.83 (17%)

Table 6.1(d) Forms of Sulphur for Kentucky coal (Analysis on as-received basis) (Percentage distribution of toal sulphur shown in brackets)
TES-Bretby – Coal and Commodity Testing Laboratory – Burton-upon-Trent.

Estimated dielectric properties of solid materials from measurements on air and particulate materials

			Estimated dielectric constant ε'_r					Estimated Loss Factor $\varepsilon''r$		
			Best-fit	$(\varepsilon'_r)^{1/2} = bp + c$		$(\varepsilon'_r)^{1/3} = bp + c$		Best-fit	$(\varepsilon''_r + e)^{1/2} = bp + c$	
Material	Density Mg/m^3	Frequency (GHz)	quadratic curve	with intercept	without intercept	with intercept	without intercept	quadratic curve	with intercept	without intercept
Kentucky Coal	1.32	0.9110	4.0960	3.7200	4.0220	3.8280	4.0770	0.2781	0.2610	0.2775
		2.4500	3.8020	3.5030	3.7390	3.6980	3.7850	0.3048	0.2908	0.3031

Table 6.1(e) Estimated Dielectric properties of as-received, air dried pulverized Kentucky Coal.

6.2.2 Microwave Equipment

Microwaves were generated using a 3–15kW variable power generator operating at 2.45GHz. All tests were carried out in a multimodal cavity connected via a rectangular WR 430 waveguide and E-H plane automatic tuner as shown in Figure 6.1. The generator, E-H tuner and applicator cavity were manufactured and supplied by Sairem, France. The E-H plane automatic tuner was employed for impedance matching of the generator and waveguide to that of the applicator and its load. This ensures the maximum absorbance of microwave energy by the load. Unless impedance is matched then it is impossible to transfer all of the forward microwave power into the load being heated (Kingman et al., 2004). For each multimode test the samples were placed in a 5-litre capacity Pyrex beaker and the generator set to the required forward power level. The dimensions of the cavity were 460x430x640mm and the loaded beaker was placed in the centre of a rotating turntable inside the cavity.

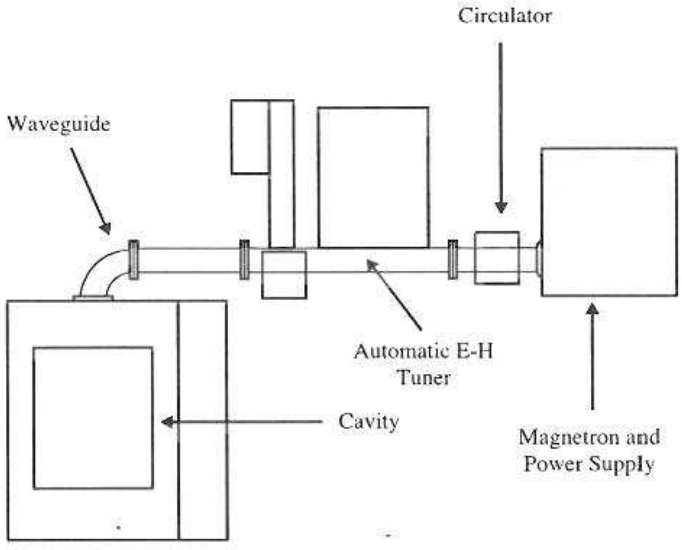

Figure 6.1 Schematic view of microwave generator, waveguide and cavity apparatus (Kingman et al., 2004).

For all tests, an attempt was made to keep the mass of the sample consistent (~1kg) and the position of the load inside the cavity identical. Whilst the fundamental dielectric properties of coal mean that it can be difficult to heat in a microwave field (the organic portion of coal is essentially transparent to microwaves) it does contain components with higher dielectric loss in its complex matrix (moisture, pyrite and other mineral inclusions). Therefore, the use of low power microwave sources is unlikely to heat the bulk load to reach sufficient temperatures for pyrite decomposition/transformation, even when heated for extended periods. There is however, evidence in literature to suggest that these difficulties can be overcome when sufficient initial power input is possible, even allowing the coal to be rapidly heated to a devolatilisation stage and event ignition (Kanilo et al., 2003; Lester et al., 2006; Marland et al., 2000).

6.2.3 Experimental Method

Seven samples of run-of-mine Kentucky coal were carefully sampled to ensure they were representative of the bulk material and six were treated at an applied power level of 8kW for 5, 10, 15, 20, 25 and 30 seconds respectively in the multimodal microwave cavity. A further seventh test at an applied power level of 15kW for 20 seconds was also completed under the same experimental setup conditions. In all tests, the samples were treated in air and no attempt was made to measure bulk temperature. Any volatiles released were extracted through a vacuum fume hood surrounding the microwave cavity. After microwave treatment, each sample batch was sized on a $\sqrt{2}$ series sieve nest and then a selection of individual size fraction was chosen to be analysed separately.

6.2.4 Post Treatment Analysis Techniques

6.2.4.1 Petrographic Characterisation

Image analysis for petrographic characterisation was carried out using the KS400 v3.1 software supplied by Imaging Associates Ltd and a Zeiss Axiocam Colour digital camera using PCI interface card.

6.2.4.2 Sample Preparation

Samples of treated material along with initial coal were prepared for examination under polarised light and SEM analysis. Loose particulate as well as cross sectional images were obtained by SEM analysis. The samples for polarised reflected light observation were prepared by embedding a representative sample in resin prior to being ground and polished using a Struers Tegrapol polisher. Once the samples are dry-sieved the separate size fractions are riffled to produce the requisite amount to prepare block mounts. This was undertaken using a small box riffle or micro-riffle where the weight requirement is lower. Generally for the 30mm mounts, 1.5 to 2g of coal per mount was required. The micro-riffled fractions are placed in 30mm diameter polythene mounting cups. Fractions incorporating significantly liberated pyrite are prone to segregation due to the large density differences between the pyrite and the coal. Care was therefore taken to ensure homogenisation of the sample within the mount. Struers ‘epofix’ epoxy resin was carefully added to the mounting cup to the desired fill level, and vacuum impregnation is undertaken in a Struers ‘Epovac’. This procedure involves subjecting the mount to a controlled vacuum in order to remove the air from between the coal particles. On re-pressurising to atmospheric pressure the epoxy was forced into the void spaces,

effectively enveloping the particles. The mounts were cured for a minimum of 12 hours at ambient temperature, after which the solid mount was removed from the mounting cup. The samples for SEM analysis were prepared by embedding the coal in ~30mm diameter carnauba wax mounts. The solidified sample block was then carefully ground, polished and lapped to a fine finish exposing a representative cross section of particles. Each wax block was then coated with a conductive carbon layer applied by vacuum evaporation method. Carbon coating is undertaken in a JEOL carbon evaporator, which imparts an even coating of carbon of thickness of approximately 20-50nm. The use of carnauba wax as the mounting media is critical when observations of coal are made using SEM/BSE methods as it provides a sufficient contrast in backscatter coefficient between the mounting medium and the coal particles to allow the coal particles to be measured. Accurate measurement requires that the particle cross sections for each size fraction are statistically representative of the bulk sample, and this necessitates careful sampling and mounting procedures, as well as measurement of a sufficient number of particles. It is therefore important that a sufficient number of particles are measured to obtain statistically relevant data (Cloke, et al., (1995). The smaller size fractions (<150µm) necessitate only one 30mm diameter mount to fulfill the required statistic, but larger size fractions require multiple mounts.

6.2.4.3 Mineral Liberation Analysis

The mineral liberation analyser at Nottingham comprises an FEI Quanta 600 scanning electron microscope with a large chamber to accommodate a computer-controlled stage and sample holder carousel taking up to 14x30mm dia. polished thick section mounts as

shown in Figure 6.2. Mineral characterisation utilises signals from a backscattered electron (BSE) detector and an EDAX X-ray detector with Genesis 4000 software.

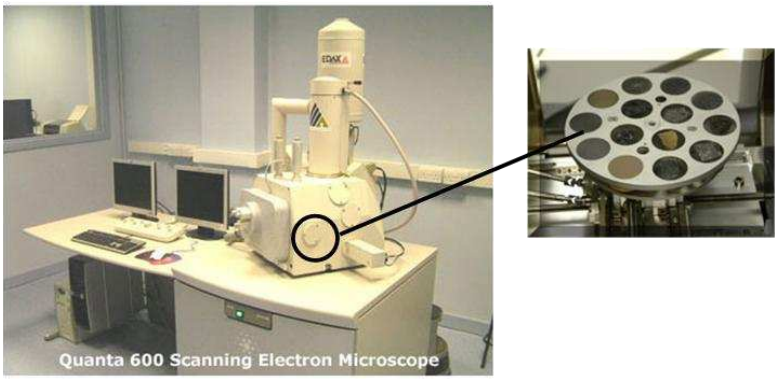

Figure 6.2 Mineral Liberation Analyser – SEM sample holder carousel.

The MLA measurement process involves automated collection of BSE and EDX signals from sequential frames, with image processing to identify particle boundaries and mineral segments. For each frame this involves the following steps:

- **BSE Image Capture**

  For characterisation and quantification studies each frame incorporates a number of coal particles, and for textural evaluation this will incorporate an area of a large particle. The SEM magnification and screen resolution are selected to show appropriate level of textural detail, and to elucidate the boundaries of touching particles. BSE Image brightness and contrast is set via standards to ensure consistency. The greyscale (based on 8 bits per pixel) has 256 shades, defined from 0 to 255. For MLA analysis the background greyscale low, in this case epoxy, is set at ~15 and the greyscale high is set at ~250 using either a gold, copper or nickel standard, depending in the brightness of minerals in the ore.

Atomic number is the main factor determining grey level contrast in BSE images. The phase with the highest weighted mean atomic number with has the highest BSE coefficient and therefore the highest grey level and thus will appear brightest in the BSE image.

- **On-Line BSE Image Processing**

  This involves background extraction and coal/gangue mineral/pyrite segmentation. A greyscale threshold is allotted to remove the carnauba wax 'background'. Greyscale variations within coal particles reflect the distribution of mineral phases because the intensity of the BSE signal is proportional to mean atomic number, and the BSE image is segmented accordingly to show the spatial distribution of minerals. For liberation studies, each measurement frame undergoes an automated deagglomeration sequence, in which contacting particles are separated using image processing routines. This is described further in Section 3.3.2.4. The polished surface will present two-dimensional particle cross sections of all sizes up to the maximum for the given size fraction.

- **X-ray Spectra Collection**

  Spectra are collected for each mineral segment to enable classification, undertaken by off-line processing subsequent to measurement. Quantitative electron microprobe analysis is usually carried out on flat well polished specimens using a focused beam at normal incidence. Figure 6.3 shows the X-ray ionisation volume in a TEM (Transmission Electron Microscopy) sample compared with the equivalent volume for an SEM sample. Normally, SEM

samples are thick enough for the focused probe to be contained within the sample, i.e. complete absorption of the primary beam. This causes the beam to spread within the material and leads to a number of different phenomena that affect the analytical treatment of raw X-ray counts obtained from the material. These include atomic number (Z), absorption (A) and fluorescence (F) effects, which are dealt with by applying matrix corrections. The incident beam energy, material density and take off angle therefore have a profound effect on X-ray intensity and quantitative results in the SEM. Where two or more minerals cannot be

distinguished by the BSE grey-level (this is the case for many gangue minerals with similar mean atomic number), multiple X–ray spectra are collected per segment, in a square grid array of operator-programmed spacing. Collection of these arrays is triggered via specified grey level ranges, or by specified X-ray spectra. Grain based X-ray mapping (GXMAP) mode was used in this investigation using a threshold BSE coefficient trigger for pyrite/pyrrhotite grains. X-ray mapping of the whole image including coal and gangue minerals (excluding pyrite and its decomposition products) would be an extremely time consuming process. A comprehensive X-ray mapping for each pyrite grain identified by using the threshold technique can cut measurement and processing time for each frame significantly. A mineral standards library was collect from a range of samples to ensure the correct identification of key phrases.

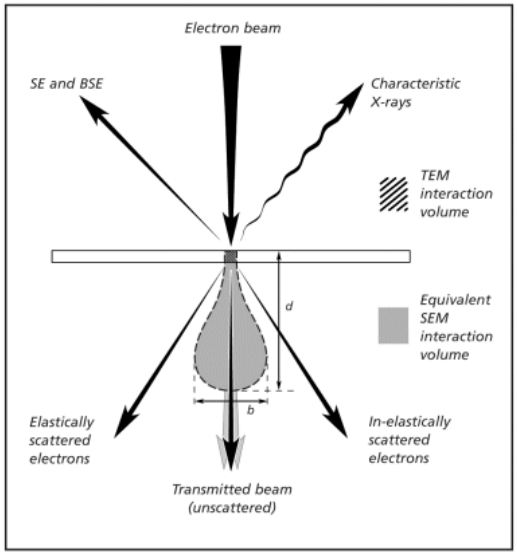

Figure 6.3 Electron beam – Specimen interactions (Oxford Instruments, 2010).

- **Sequential Frame Measurement**

  The MLA software controls the movement of the SEM stage so that sequential BSE image frames can be captured and processed automatically, to cover either the whole area of the polished section or a predetermined area. The resulting measurement file is a series of frames of grey-level segmented particles or areas, with one or more X–ray spectra associated with each segment.

- **Processing the measured Data – Classified Image Generation**

  The measurement file is processed to classify segments using the associated X-ray spectra. This process uses a reference standards file incorporating characteristic X-ray spectra for all phases identified within the coal. The process of classification involves automatic pattern matching of the measurement spectra with those of the reference standards. The majority of the reference spectra are collected by the operator prior to processing of measurement files, but mineral

segments returned as ‘unknown’ by the off-line processing can be subsequently located and identified, the relevant X-ray spectra included into the spectral reference file and the measurement file re-classified. The result of classification is a set of image files in which the phases are identified by different colours. For textural examinations of large particles in which the particle measurement includes a large number of frames, these frames can be merged together to form a composite classified image of the particle. A schematic showing the steps in generation of classified images is shown in Figure 5.4.

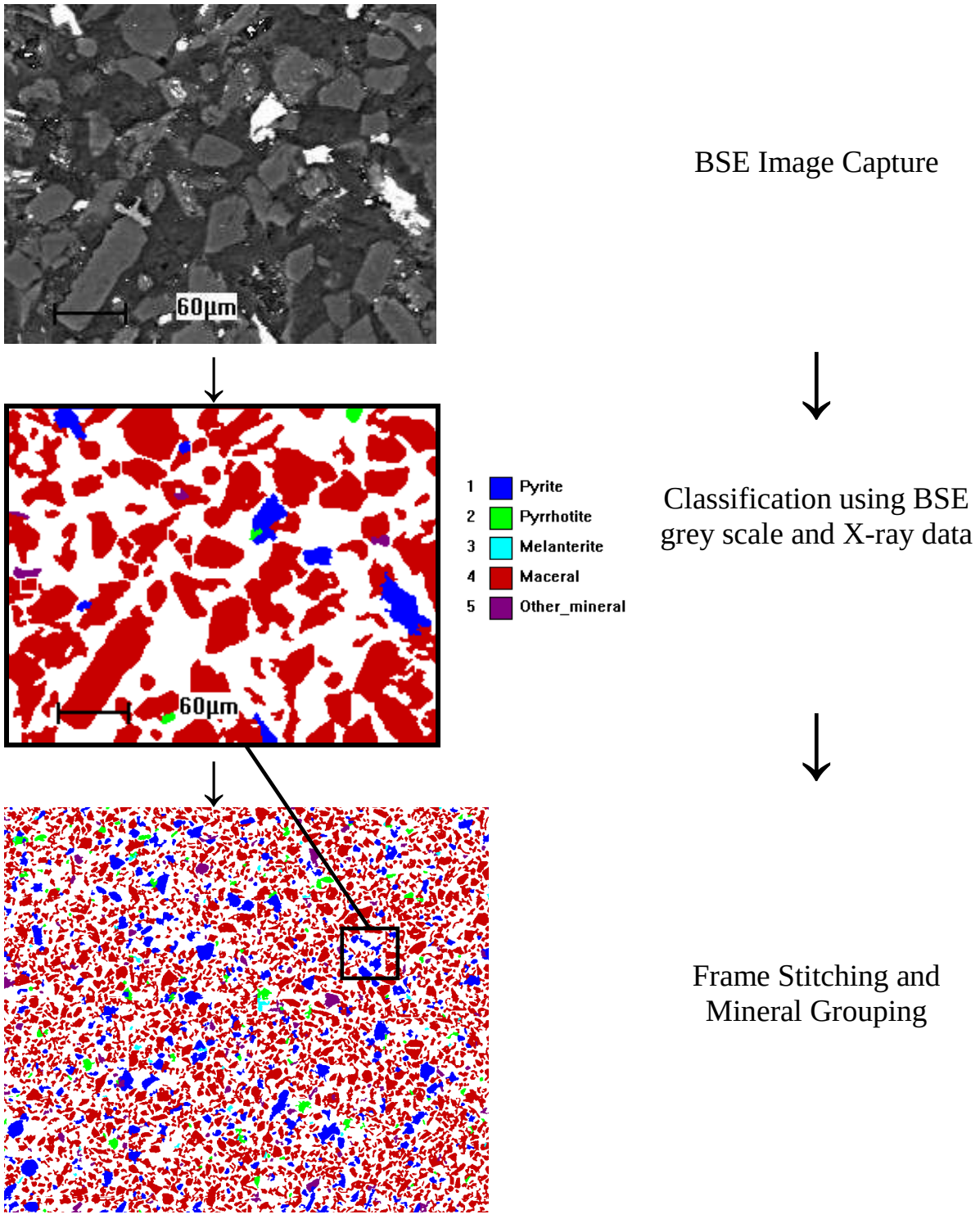

Figure 6.4 a schematic showing the key steps in generating a classified image.

The classified images can be processed by the MLA software to quantify relevant mineralogical parameters. This software does not have the capability to correct stereologically so the quantities relate to the two-dimensional image. Some parameters require the input of compositional or density data. This information is generally extracted from a database in the MLA software, but in the case of less common minerals, data can be taken from the literature or web sources.

6.2.4.4 X-ray Mapping and Topographical Considerations

Generally, it is recommended that quantitative X-ray analysis requires a homogeneous "thick" (to the radiation) sample with a flat polished surface. The roughness of a fractured or sawn surface affects the back scattered electron images and the X-ray analyses adversely. Ideally, specimen preparation involves using epoxy-impregnated polished sections which are smooth, scratch free, giving low relief and good epoxy penetration into the particles to support the microstructure. Under the light reflectance optical microscope characterisation is based on association and light reflectance intensity. It is reliant on the interaction of light with the sample and the ability of the human eye and brain to discriminate textures. Discrimination by SEM is based on the interaction of a high energy electron beam and the sample. Since SEM discrimination is electron based and the optical microscope is light based, it is very difficult if not impossible to identify individual macerals by SEM measurements. Furthermore, when using epoxy resin blocks to support the microstructure of coal it is difficult to distinguish between maceral and the epoxy "background" using BSE intensity (the average atomic number and therefore BSE intensity of maceral is close to that of the epoxy mounting medium).One solution to this

problem is to use carnauba wax as the mounting medium, which then enables the wax, coal matrix and mineral components to be distinguished from each other by BSE intensity (Creelman and Ward, 1996; van Alphen, 2006, Straszheim and Markuszewski, 1990). The disadvantage of using carnauba wax as the mounting medium is that sufficient impregnation into the pores of the specimen to support the microstructure is difficult to achieve. As a result, mechanical preparation such as polishing can cause fracturing, pitting, microcracking and plucking of coal grains from the host wax which in turn effects surface flatness and particle relief. This can make "real" features of the microstructure difficult to identify. Moreover, carnauba wax will be abraded at a different rate to pyrite due to their different hardness and so some topographical difference is inevitable. Quantitative X-ray microanalysis is normally carried out on flat and polished specimens at normal incidence as shown in Figure 6.3. However, if these conditions are not satisfied, the accuracy may suffer. A tilted specimen changes both the X-ray take off angle and the angle of electron incidence. Furthermore, when analysing particles, the position of the electron beam and the detector relative to the irregular particle surface can have a profound effect on the degree of absorption. Figure 6.5 demonstrates how the results are affected by loss of X-ray intensity owing to the irregular angle of beam incidence. The BSE image of a museum grade pyrite specimen shown in Figure 6.5(a) was mounted and glued on a 'stub' (10mm diameter aluminium disc with a spigot stage attachment) supported on a thin carbon film which gives minimal X-ray background. X-ray spectra were collected at strategic positions across the particle surface to exploit the irregular surface planes that will affect X-ray absorption. The five X-ray collections

positions are shown in Figure 6.5(a) along with corresponding X-ray spectra shown in Figures 6.5(b), 6.5(c), 6.5(d), 6.5(e) and 6.5(f) respectively. Peak positions are characteristic of a particular element and intensity (height) is a function of its relative abundance. Therefore, phase identifications are made by examination of peak positions and relative intensities. In addition, X-ray spectra were collected from different positions across the surface of a flat polished specimen of pyrite, shown in Figure 6.6(a) from the same source are shown in Figures 6.6(b), 6.6(c), 6.6(d), 6.6(e) and 6.6(f) respectively. The XRD diffractogram for the pyrite sample is shown in Figure 6.7 and is consistent with standard patterns for FeS_2. This demonstrates that incident beam energy and take off angle can have a profound effect on X-ray intensity and quantitative results in the SEM. This potential source of error is particularly significant when poor BSE level contrast results in two phases not being segmented and hence delineation of phase boundaries is impossible (i.e. associated pyrite and pyrrhotite phases). Therefore, to accurately discriminate between pyrite and its decomposition products formed as a result of microwave treatment (i.e. deviations from stoichiometric FeS_2) X-ray mapping of the whole sulphide grain is necessary to resolve the phase boundaries. This will involve applying GXMAP analysis to all sulphide phases identified within the coal matrix to discriminate between possible sulphide phases that cannot be segmented by BSE grey level alone. Figure 6.8 illustrates the advantages of selective mapping of phases over traditional point X-ray analysis for the example of particle containing pyrite and pyrrhotite.

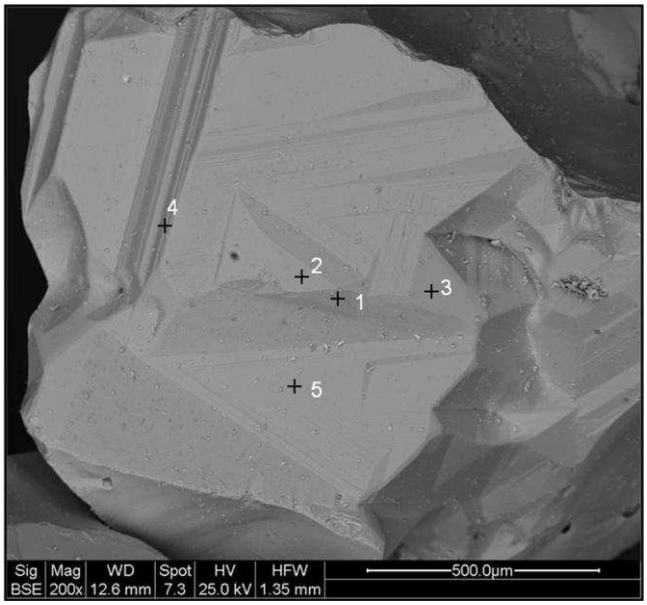

Figure 6.5(a) BSE Image of a single 'stub' mounted Pyrite Grain showing X-ray Spectra Measurement Points.

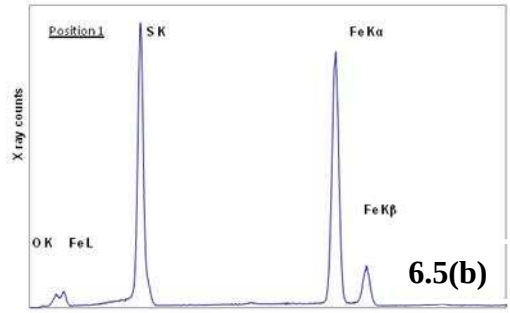

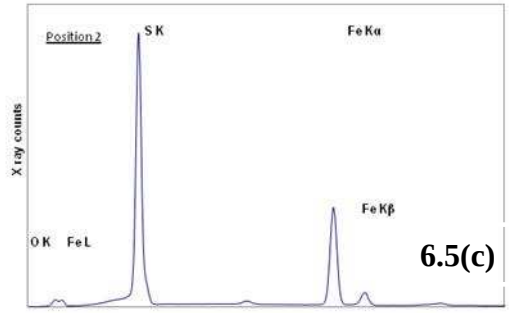

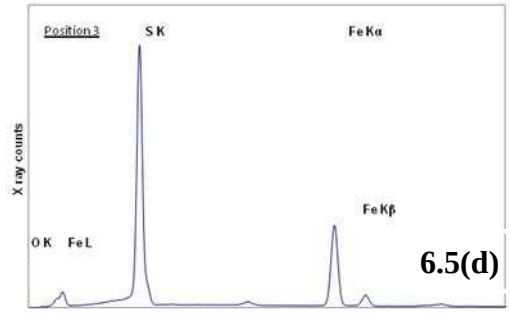

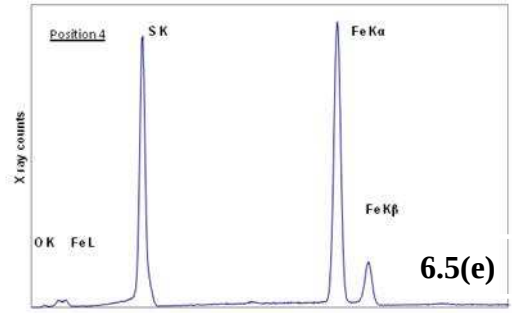

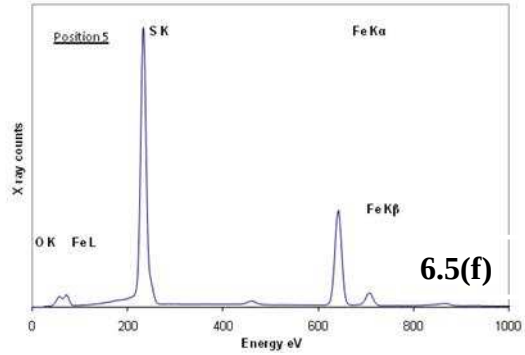

Impingement of the beam electrons (primary electrons) can eject inner shell electrons from the target (sample) atoms. These ejected electrons are called secondary electrons. When this happens electrons from the next energy shell drop back to fill the position, with emission of an X-ray quantum, the energy of which is characteristic of the precise atom and transition. The X-ray detector counts the X-rays, measures their energies and the software produces a graph of number of X-rays per energy channel - i.e. the X -ray spectrum. However the number of X-rays reaching the detector are not

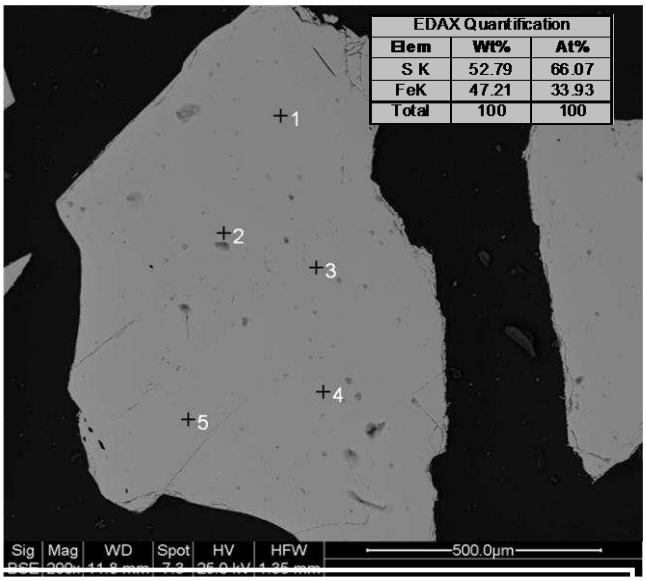

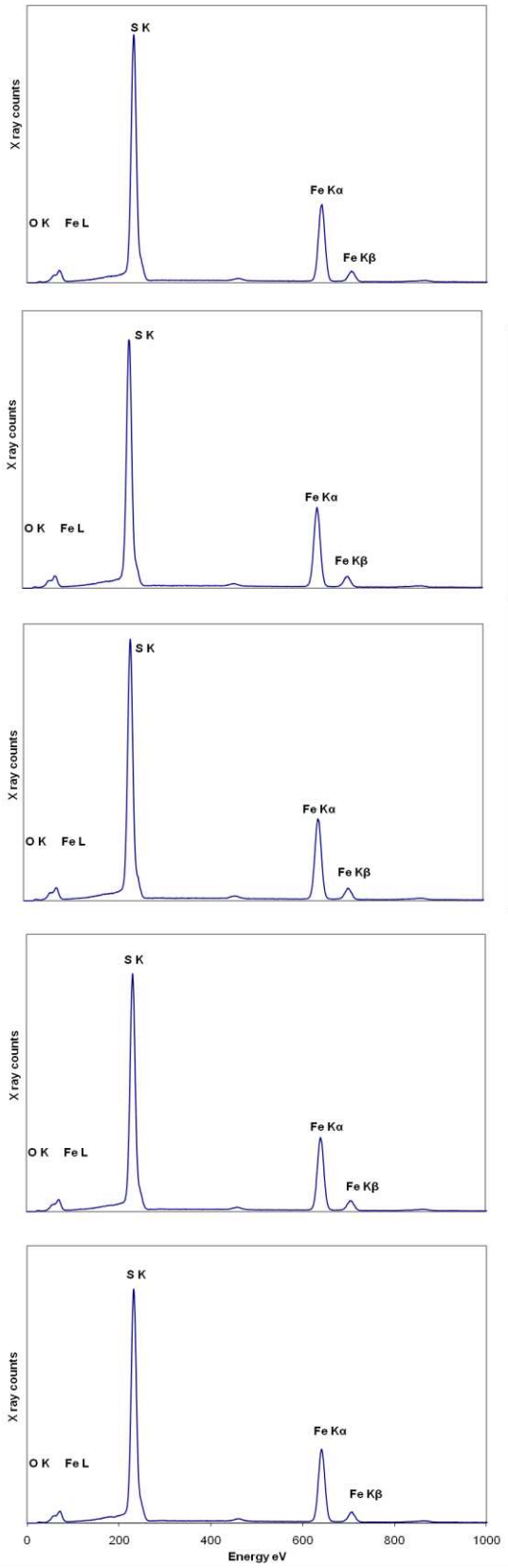

Figure 6.6(a) BSE Image of a single polished Pyrite Grain showing X-ray Spectra Measurement Points (Inset; EDAX Quantification).

the number of the constituent atoms (in this case Fe and S in the ratio 1:2) and are affected by atomic number, absorption of X-rays as they travel through the material and Fluorescence.

The calculation that produces quantitative analysis relies on knowledge of the precise geometry between the primary beam, the sample and the X-ray detector.

In the case of non-planar surfaces it is the absorption factor which is the concerning issue. A key factor is that the 'lighter' (lower energy) X-rays are attenuated more quickly than the 'heavier'

Rough surfaces effectively mean altering the absorption paths, thus the difference in absorption between lighter (S) and heavier (Fe) X-rays will vary.

Generally this will be seen as a decrease in peak height of Sulphur, resulting in spectra which look more like pyrrhotite than pyrite as shown in Figure 6.8.

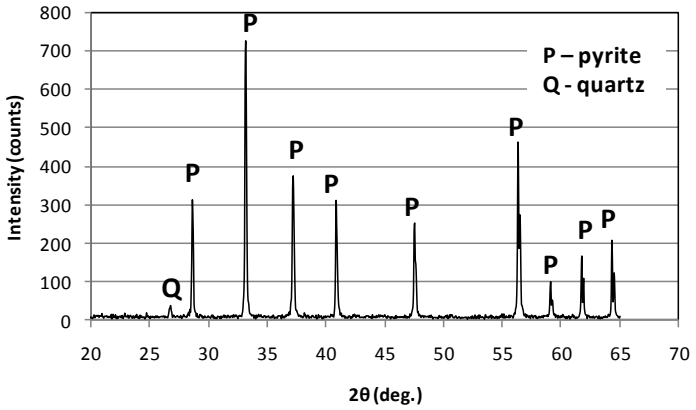

Figure 6.7 XRD Diffractogram for Pure Pyrite Sample Shown in Fig. 6.5 & 6.6.

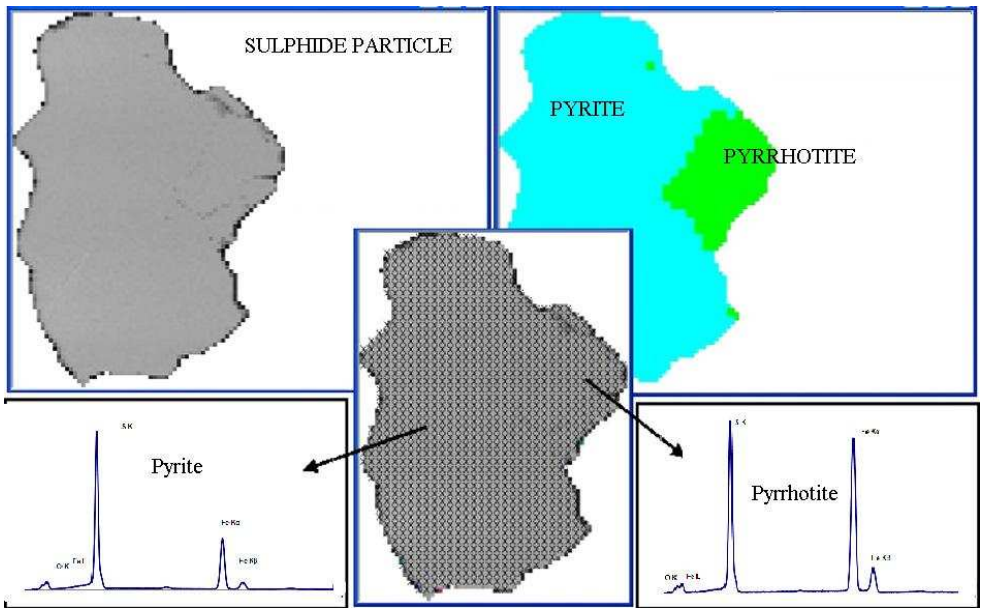

Figure 6.8 X-ray map of a sulphide particle containing both pyrite and pyrrhotite phases (Adapted; Fandrich et al., 2007).

In this investigation, grain based X-ray mapping analysis (GXMAP) is employed where phase boundaries cannot be segmented on BSE grey level as is the case with pyrite – pyrrhotite transitions. This ensures that only the grains of interest are mapped which reduces measurement time. This technique imposes a grid over the particle of interest, as shown in Figure 6.8, and X-ray spectra are collected at each grid interval to generate a comprehensive mineral map. X-ray spectra are compared to a mineral standards library which was set up from strategic measurements from the specimen. Building the standards library directly from the specimen to be measured ensures that the measurement conditions at that moment are reflected in the standards (such as beam energy - keV) and will also provide an elemental character that better reflects the chemistry of the specimen. Spectra identification will then involve an error based search for the measured spectra in the standards library to find the most probable fit.

6.2.4.5 MLA Data Acquisition and Presentation

The examination, processing and presentation of quantitative mineralogical data generated by the MLA software are performed on'DataView' software. Pixel data is combined with elemental compositions and densities of each identified mineral to produce a variety of data including, modal mineralogy, calculated assay, elemental and mineral grade recoveries, particle and mineral grain size distributions, elemental distributions, particle density distributions, mineral associations and locking, phase specific surface are (PSSA) and mineral liberation by free surface.

Phase identification of the coal constituents of sizes -38, 53, 150 and 425µm (from √2 sieve nest), was determined by SEM/EDAX analysis through BSE images, examples of which are shown in Figure 6.9. These size fractions were chosen to represent a range of particle sizes and to study the influence of particle size on the transformation of pyrite to pyrrhotite.

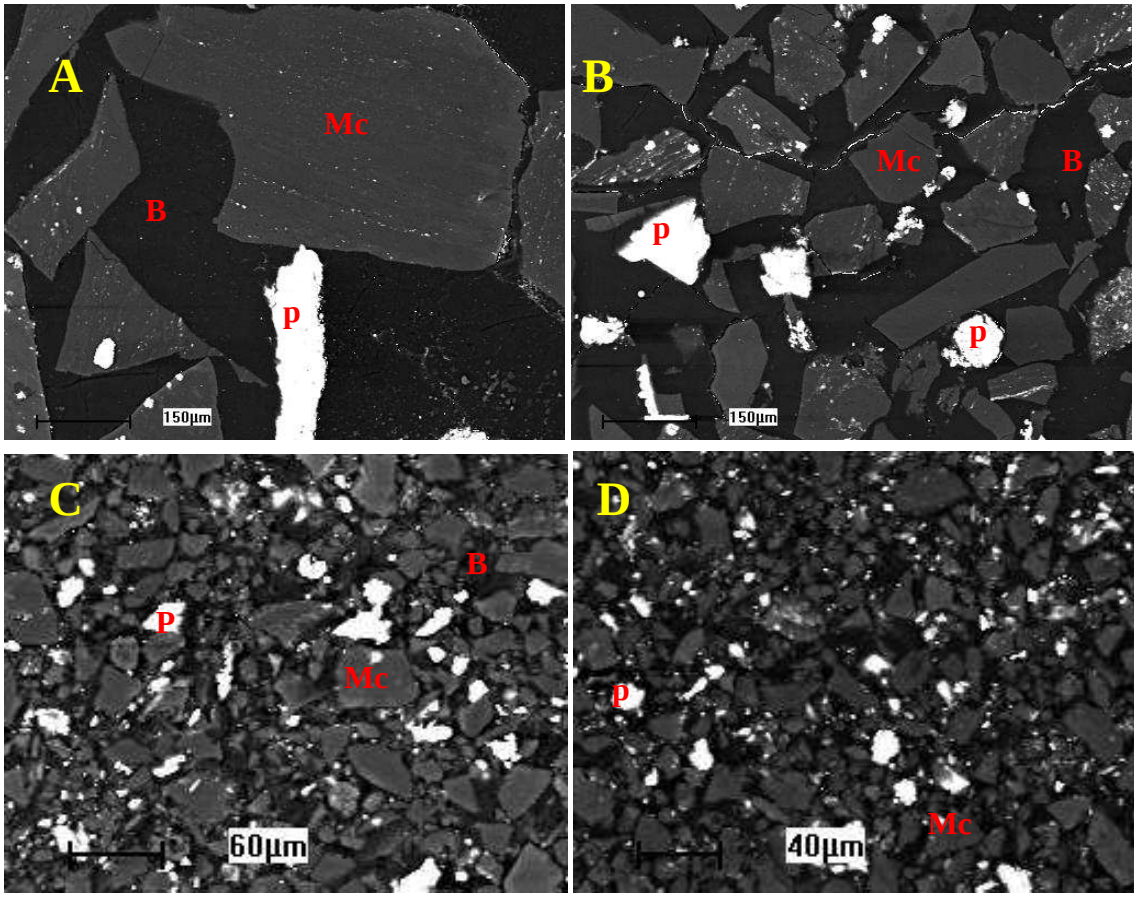

Figure 6.9 SEM/BSE Images of untreated Kentucky coal showing predominantly, maceral (Mc), pyrite (P) and carnauba wax (background) (B). [A = -425+300µm, B = -150+106µm, C = -53+38µm, D = -38µm].

The size range of pyrite grains in the run-of-mine Kentucky coal samples is large, ranging from up to 350µm in diameter to smaller than 5µm in diameter occurring in a

variety of forms (1) disseminated crystals and irregular aggregates of various size and shapes, (2) individual framboids or nodules intimately associated with macerals, (3) narrow veins. From careful observations, small pyrite grains are predominantly enclosed in the organic portion of the coal matrix.

The major mineral phases identified by EDAX analysis through BSE images are shown in Table 6.2.

Mineral	*Density*	*Empirical Formula*	*Al (%)*	*Fe (%)*	*H (%)*	*O (%)*	*S (%)*	Si (%)
Pyrite	5.0	FeS_2	-	46.5	-	-	53.5	-
Pyrrhotite	4.6	FeS	-	63.5	-	-	36.5	-
Melanterite	1.9	$FeSO_4(7H_2O)$	-	20.1	5.1	63.3	11.5	-
Maceral	1.3	C	-	-	-	-	-	-
Other_mineral	2.6	$Al_2Si_2O_5$ $(OH)_4$	20.9	-	1.6	55.8	-	21.8

Table 6.2 Composition of major mineral phases identified by EDAX (%wt).

Mineral constituents that were present in minor amounts (less than 2%) are grouped as 'Other-Mineral' (Aluminium Silicate Hydroxide) and the organic carbonaceous portion of each particle grouped as 'maceral'. Differentiation between macerals was not possible by EDAX analysis for reasons described in 6.2.4.5. It is speculated that melanterite, which is intimately associated with pyrite, has an artificial origin formed during weathering of Fe sulphides i.e. pyrite (Vassilev and Vassileva, 1996).

6.3 Results

6.3.1 Post Microwave Treatment Thermal Analysis

Bulk coal is generally a poor microwave absorber which can be attributed to its dielectric properties and in particular, a low loss factor of approximately ε_r" = 0.03.

Bulk coal can therefore be considered to be essentially transparent to electromagnetic waves. As a result, microwaves have an excellent penetration depth into the coal particles. However, water (or inherent moisture content) has a high loss factor compared to most materials of approximately 12 at 25°C and 2.45GHz (Meredith, 1997). This means that water (along with other lossy phases such as pyrite) will selectively and rapidly heat compared to the organic coal matrix. This will inevitably lead to a rapid increase in the bulk temperature of the coal if sufficient power is maintained for a period of time that allows heat transfer by conduction. Microwave heating may therefore lead to pyrolysis or thermal oxidation which is undesirable from a process point of view such as injection into the boiler and burnout for example.

The thermal characterisation of coal is of vital importance and will show whether microwave heating significantly affects the burnout of the coal. The proximate composition after treatment will give a very basic guide to burnout which is a key parameter when buying combustion coals (Su et al., 2001).

Proximate analysis was performed on each coal sample as described in Section 6.2.2. The intrinsic reactivity of each sample was also measured using a non-isothermal TGA program. Each coal sample was finely ground and 10-20mg was heated in air to 300°C at 50°C min^{-1} and then to 900°C at 10°C min^{-1}. The temperature at which weight loss reached a maximum value was measured (dW/dt = max). This is known as the sample 'peak temperature' (PT). The temperature at which burnout falls below 1% min^{-1} (wt basis) was also measured and is known as the sample 'burnout temperature' (BT) (Unsworth et al., 1991). The proximate analysis of microwave treated coal is shown in

Table 6.3 (Proximate analysis for untreated control sample is included here for comparison). The peak temperatures (PT) and burnout temperatures (BT) are given in Table 6.4. (PT and BT for the untreated control sample are included here for comparison).

					dry, ash free basis		
Treatment	*% Moisture*	*% Ash*	*% Volatiles*	*% Fixed Carbon*	*% Volatiles*	*% Fixed Carbon*	*Fuel Ratio*
Untreated	2.8	26.2	37.8	33.3	53.1	46.9	0.88
5sec @ 8kW	2.8	26.8	37.3	33.1	53.0	47.0	0.89
10sec @ 8kW	2.2	26.4	35.4	36.0	49.5	50.5	1.02
15sec @ 8kW	2.4	21.0	37.1	39.6	48.4	51.6	1.07
20sec @ 8KW	2.0	24.3	35.3	38.4	47.9	52.1	1.09
25sec @ 8kW	1.8	22.2	35.6	40.4	46.8	53.2	1.14
30sec @ 8kW	1.4	30.8	31.0	36.8	45.8	54.2	1.18
15sec @ 15kW	1.1	29.8	25.5	43.6	37.0	63.0	1.71

Table 6.3 Proximate analysis for microwave treated Kentucky Coal (%wt).

Treatment	*Peak Temperature (°C)*	*Burnout Temperature (°C)*
Untreated	481	743
5sec @ 8kW	535	730
10sec @ 8kW	482	748
15sec @ 8kW	481	739
20sec @ 8KW	484	737
25sec @ 8kW	492	749
30sec @ 8kW	487	824
15sec @ 15kW	488	853

Table 6.4 PT and BT for microwave treated Kentucky Coal.

6.3.1.1 Fuel Ratio

After microwave treatment for longer residence times and higher power settings (higher energy input), volatiles were released resulting in a loss in volatile matter from the coal matrix. This trend is reported in Figure 6.10. Displacement of volatiles prior to combustion is undesirable since it is likely to adversely affect the degree of burnout and

flame stability (Lester and Kingman, 2004). The fuel ratio (Fixed Carbon [FC]/Volatile Matter [VM]) shows an increase with increasing residence time and forward power demonstrating that volatiles were lost in measurable amounts during microwave exposure. The fuel ratio for each coal sample is reported in Table 6.5. A loss of a significant proportion of volatiles during pre-treatment can be problematic because volatiles released prior to combustion might present an explosion hazard (Xiumin et al., 2001).

Treatment	*Energy Input (kWh)*	*Fuel Ratio*
Untreated	0.0	0.88
5sec @ 8kW	11.1	0.89
10sec @ 8kW	22.2	1.02
15sec @ 8kW	33.3	1.07
20sec @ 8KW	44.4	1.09
25sec @ 8kW	55.6	1.14
30sec @ 8kW	66.7	1.18
15sec @ 15kW	83.3	1.71

Table 6.5 Fuel Ratio for microwave treated Kentucky Coal (prox. FC/VM)

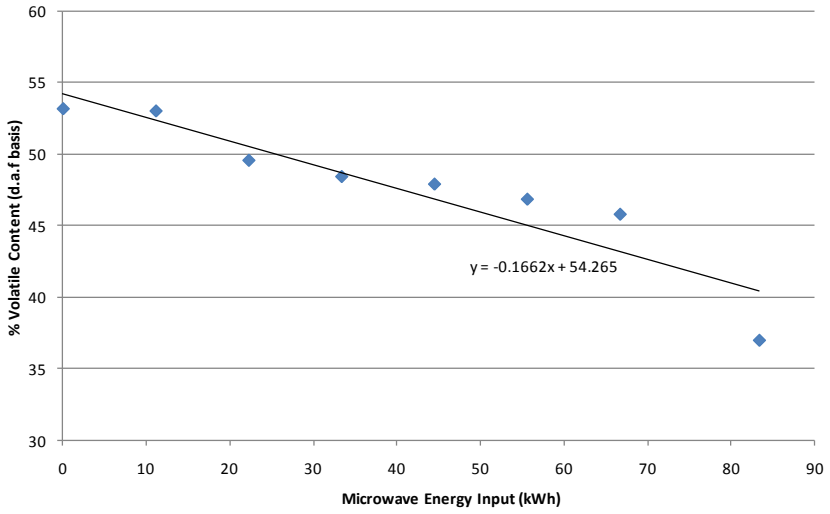

Figure 6.10 Volatile matter Content profile for Microwave treated Kentucky Coal. Data reported on a dry, ash free basis.

The trend reported in Figure 6.10 show that there is a marginal decrease in volatile matter up to 30 seconds treatment time at 8kW forward power level with a further significant displacement in volatile matter (d.a.f) after 20 seconds treatment time at 15kW forward power level. The implication of this is that the organic coal matrix has been heated to temperatures (probably local to lossy phases) in excess of 300°C which has caused devolatilisation. There is evidence in literature that suggests that coal can be heated rapidly using microwave energy (>1000°C) provided that there is sufficient energy input (Kanilo et al., 2003). Further microwave heating, with sufficient residence time and power input can eventually produce coke (Lester et al., 2006).

6.3.1.2 Moisture Content

After each treatment and at all power settings, condensation could be seen inside the glass beaker sample holder. Generally speaking, the amount of visible condensate (on a qualitative basis) increased both with increasing residence time and forward power level. These observations are consistent with proximate data reported in Table 6.3. For example, the moisture content of the sample treated for 20 seconds @ 15kW forward power has been reduced by ~60% when compared to the moisture content in the untreated sample. However, it is interesting to note from Table 6.3 that there is no sign of moisture loss at 8kW forward power level for a residence times of 5, 10 and 15 seconds. Moisture removal from the sample as a result of its change in phase to steam is therefore unlikely during relatively short treatment time. Given the relatively low dielectric loss factor of the coal organic matrix (compared to other inclusions such as pyrite and moisture) the bulk material is not likely to heat up significantly during short exposure

times. Moreover, it is assumed that moisture migration through the coal structure takes place as a result of several liquid/gas phase changes and therefore significant removal of inherent moisture may require prolonged treatment time at sufficiently high power levels. This is consistent with other work published by Lester and Kingman, 2003 where it was noted that high forward power (15kW) and short exposure times (0.1 sec) had little effect on moisture content within each sample. Furthermore, Marland et al., 2001 noted that the moisture content of coal was not significantly affected (not reduced more than 50%) despite spending 8 minutes in a low power (650W) multimode cavity. This is because low power results in low heating rates and in the case of coal, a slower release of water from the particle matrix.

6.3.2 Optical Properties – Vitrinite Reflectance

Prolonged microwave heating of coal will inevitably lead to some degree of oxidation. Depending on the degree of oxidation, maceral proportions and their reflectance may alter significantly. Since maceral reflectance can influence burnout (Phong-Anant et al., 1989) it is essential to monitor reflectance changes (detectable in vitrinite) as a result of microwave heating. The Vitrinite reflectance data for each microwave treated coal sample is reported in Table 6.6. Vitrinite reflectance for untreated coal is shown for comparison.

		Microwave Energy Input kWh						
	untreated	11.1	22.2	33.3	44.4	55.6	66.7	83.3
average	0.57	0.58	0.56	0.61	0.70	0.71	0.78	0.71
minimum	0.45	0.45	0.43	0.31	0.60	0.52	0.55	0.50
maximum	0.70	0.70	0.70	0.79	0.80	0.99	0.97	0.91
std. Dev.	0.057	0.052	0.056	0.064	0.039	0.089	0.085	0.08

Table 6.6 Vitrinite Reflectance for microwave treated Kentucky Coal (%R_{Vi}).

Figure 6.11 shows the reflectance histogram profiles for untreated and treated (20 sec @ 15kW) Kentucky coal samples. Table 6.6 and Figures 6.11, 6.12 and 6.13 clearly show an increase in reflectance of vitrinite as a result of microwave treatment compared to measurements made on the untreated coal sample. It can be seen from the reflectance data shown in Table 6.6 shows that microwave residence time is the key factor affecting vitrinite reflectance. This implies that the structural arrangement of carbon is changing resulting in progressive graphitisation, macerals are being oxidised through microwave pre-treatment, which in turn negatively affects its pyrolysis and burnout performance. Changes in structural ordering have also been shown to affect the dielectric properties of the material (as outlined in Chapter 5) essentially controlling the possibility of electron mobility across carbon sheets.

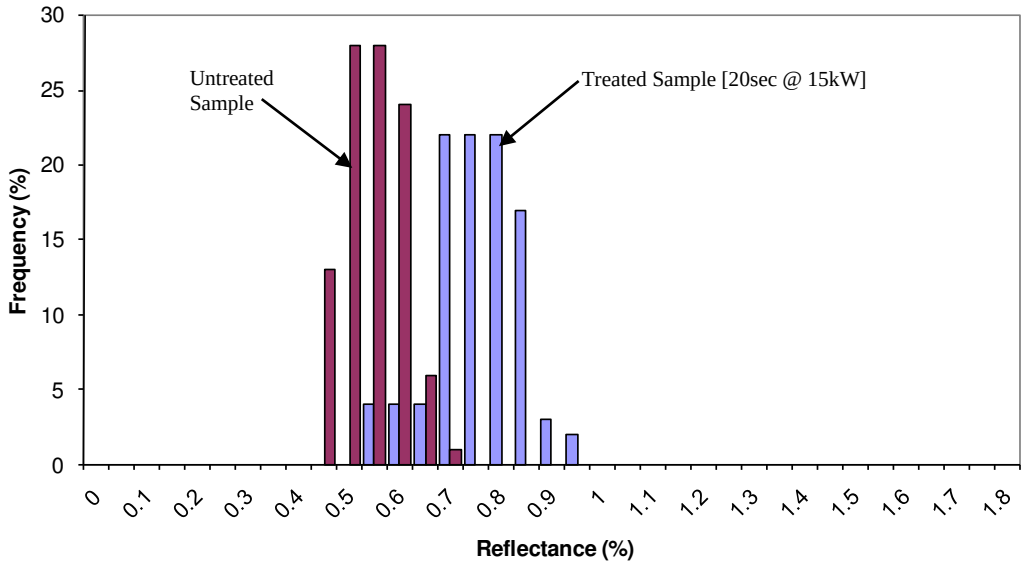

Figure 6.11 A reflectance histogram for untreated and microwave treated Kentucky coal.

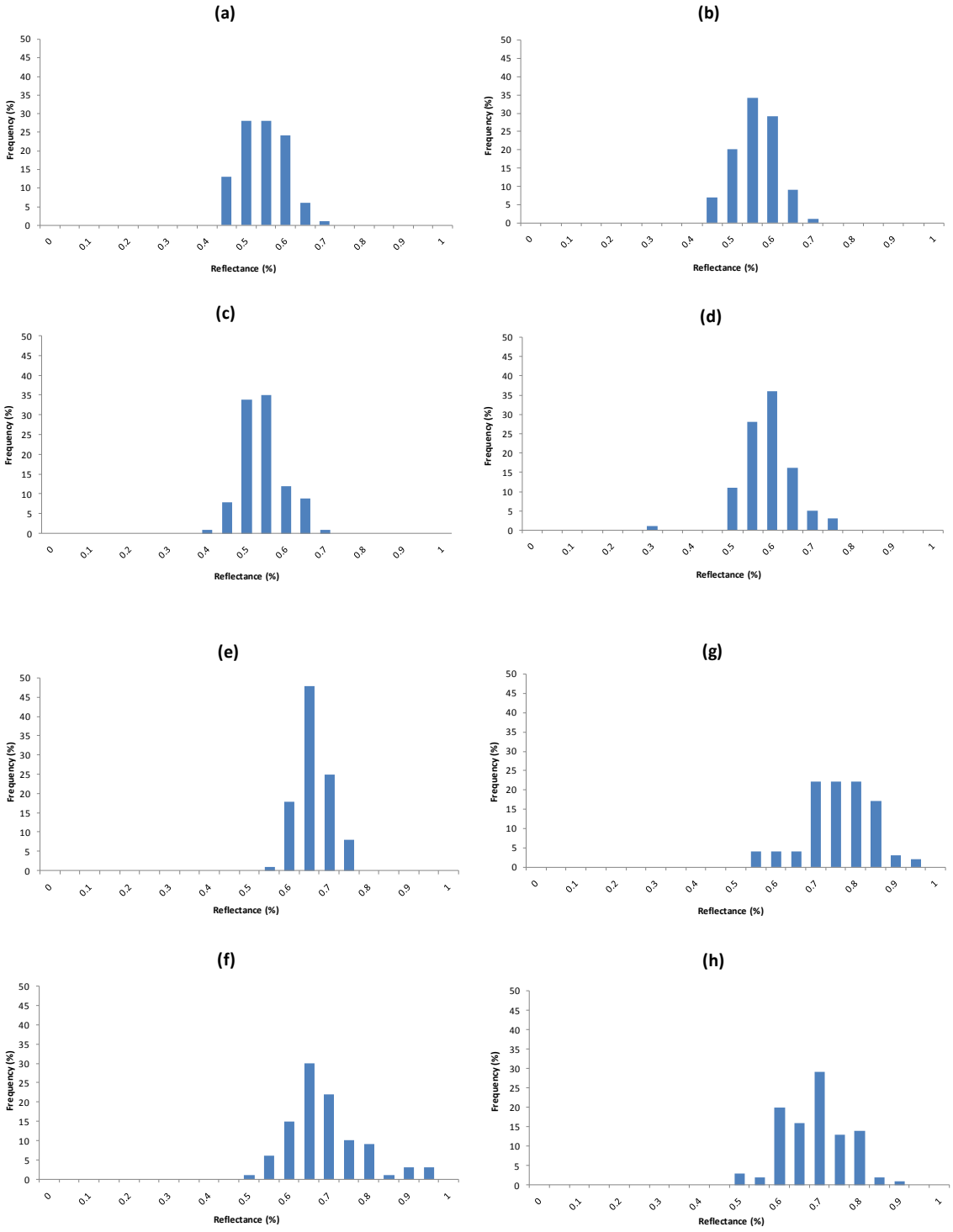

Figure 6.12 Kentucky Coal Vitrinite Reflectance Profiles (a) Untreated, (b) 8kW 5s, (c) 8kW 10s, (d) 8kW 15s, (e) 8kW 20s, (f) 8kW 25s, (g) 8kW 30s, (h) 15kW 30s

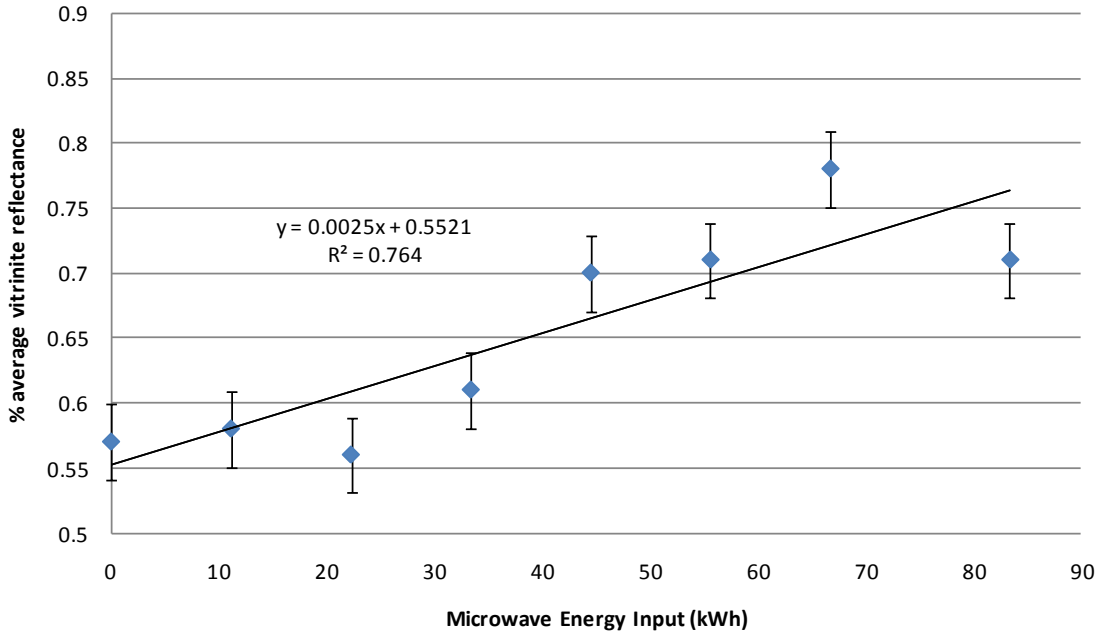

Figure 6.13 Plot of % average vitrinite reflectance against microwave energy input.

6.3.3 SEM study of pyrite / pyrrhotite transformation.

The principal objective of this work is to evaluate the effect of high power microwave heating on the transformation of coal derived pyrite to form pyrrhotite. The SEM measurement process, data acquisition and presentation have all been outlined previously in Section 6.2.5.3. As discussed previously, topographical relief and discontinuities in the specimen surface cannot be avoided and so ultimately a degree of misclassification by X-ray analysis is likely if not inevitable using the sample preparation techniques described in Section 6.2.5.2. Figure 6.14 shows the percentage of pyrite transformation to pyrrhotite v`s microwave energy input (kWh). The results show a positive correlation between pyrrhotite formation and microwave energy input. For the reasons outlined in detail in Section 6.2.5.4 there is evidently a degree of misclassification caused

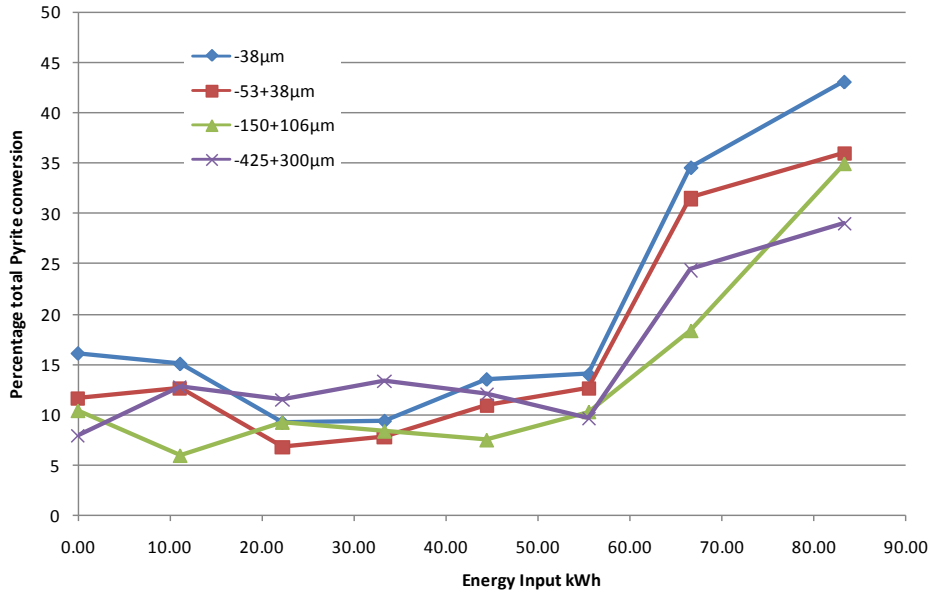

Figure 6.14 Percentage total pyrite conversion (% modal area) to pyrrhotite v`s microwave energy input (kWh).

by topographical discontinuities on the surface of the measure specimens. This has yielded the results displayed in Figure 6.14 which report an apparent existence of pyrrhotite in the untreated control sample. However, from careful and extensive qualitative X-ray investigations of a number of untreated samples across each size range the existence of a pyrrhotite phase was not found. This is also supported by XRD analysis performed on pyrite taken from an untreated -150+106µm coal sample. The XRD diffractograms shown in Figure 6.15 show that there is no evidence of pyrrhotite peaks in the untreated sample. Whilst these results cannot be interpreted quantitatively, the XRD trace taken from the treated sample (-150+106µm 15kW 20s) exhibit the major pyrrhotite peaks. Moreover, the apparent classification of pyrrhotite in each untreated sample was coincident with X-ray measurements taken over non-planer surface areas or at the edges

of pyrite particles where polishing relief was unavoidable. The implication is that there is no evidence of pyrrhotite phases in the original untreated coal and that therefore a degree of experimental error is to be expected using this method of sample preparation and EDAX measurements for this kind of material. Furthermore, 5,10,15 and 20 seconds of heating at 8kW forward power appears to leave the pyrite phases within the coal unaffected by microwave heating and the amount of pyrrhotite identified by X-ray mapping is within experimental error caused by topographical relations with X-ray spectra matching and can be discounted. However, at 25 and 30 seconds of heating at a power level of 8kW and more significantly at 20 seconds heating at 15kW power level respectively, particles showing complete transformation to pyrrhotite were evident. The results, however, show a degree of non uniformity of heating with some pyrite particles showing complete transformation to pyrrhotite while others remain apparently unaffected.

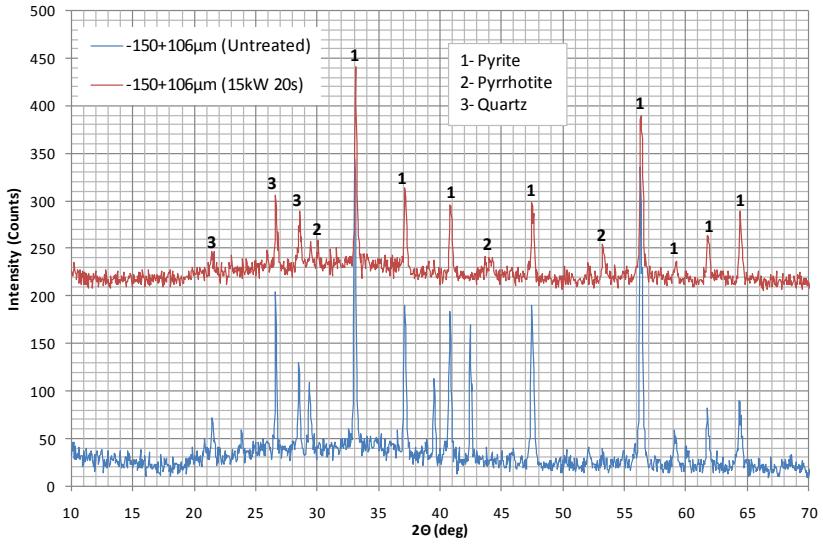

Figure 6.15 XRD Diffractogram for density separated pyrite taken from untreated and treated Kentucky coal samples.

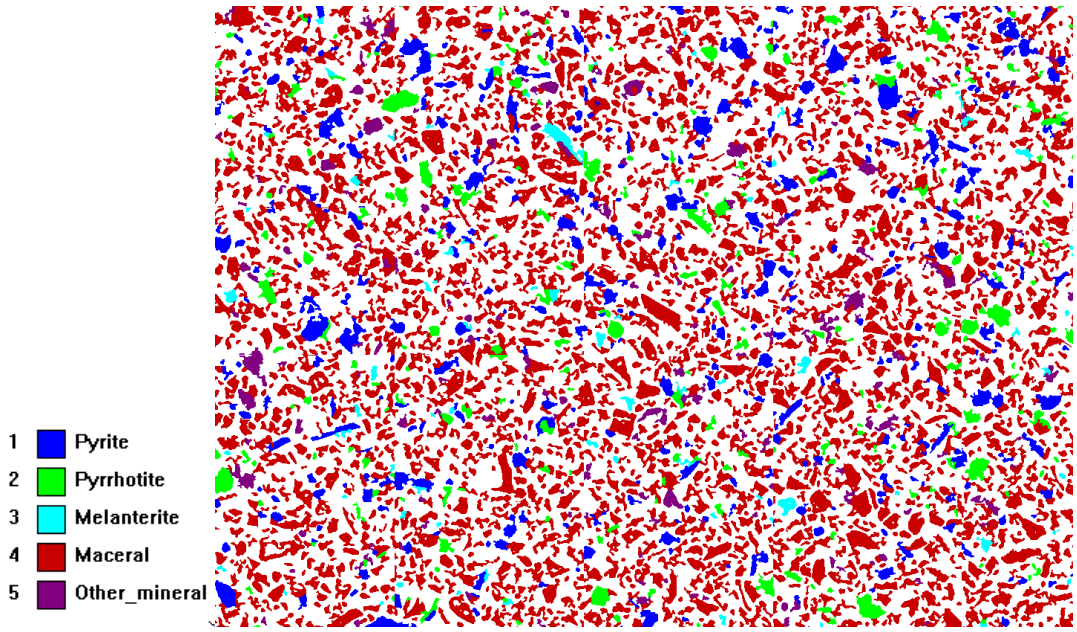

Figure 6.16 (a) Showing non-uniformity of heating and pyrite to pyrrhotite transformation in Kentucky Coal (-38µm, 20sec at 15kW).

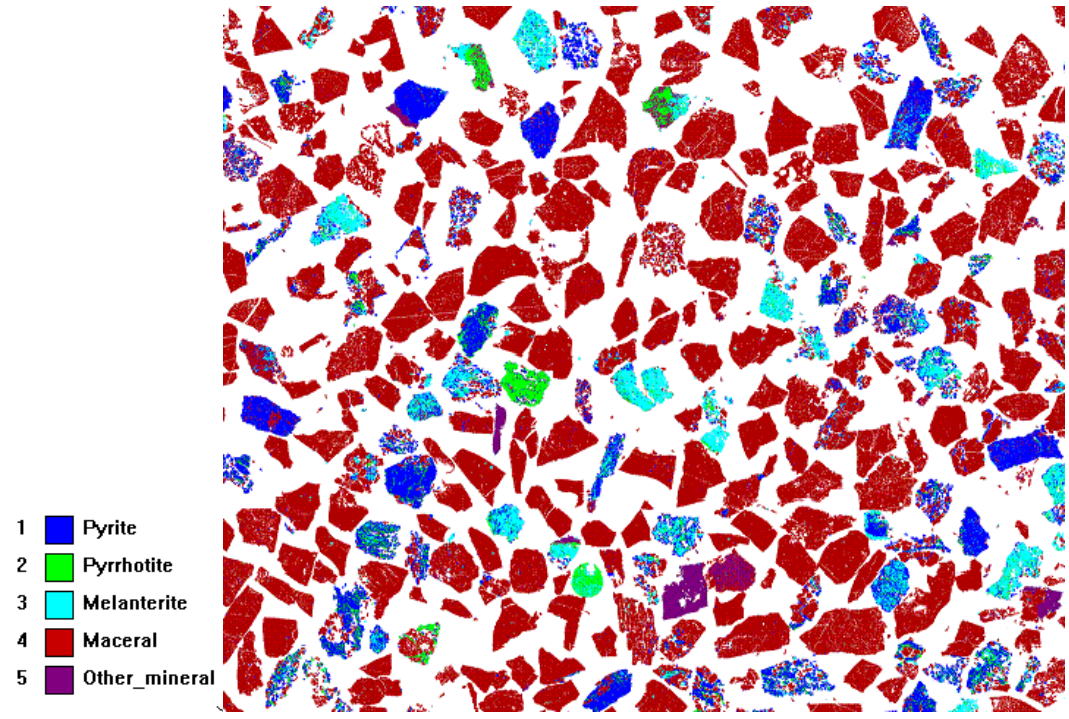

Figure 6.16 (b) Showing non-uniformity of heating and pyrite to pyrrhotite transformation in Kentucky Coal (-425+300µm, 30sec at 8kW).

Figure 6.16 is an example classified image showing the non-uniformity of heating of the pyrite particles which are typical across all size fractions. It is also clear that it is not just liberated particles that are transformed to pyrrhotite but also those intimately associated with the organic matrix are also affected. Whilst the results observed in Figure 6.14 and typically Figure 6.16 demonstrates microwave heating of pyrite in coal is not a uniform process, it is clear that higher power density (volumetric absorption of microwave energy, W/m^3) has significant effect on pyrrhotite formation. Unfortunately, higher power densities and associated heating rates for prolonged periods can result in a change in the petrographic and proximate characteristics of the coal, adversely affecting burnout negating any possible advantages for desulphurisation.

6.4 Discussion

The data from this study proves that pyrite in Kentucky coal can be heated by microwave energy to form pyrrhotite. On the basis of the tests carried out, transformation from pyrite to pyrrhotite is feasible with sufficient power densities and/or exposure times. The results reported from this work are particularly significant as they show for the first time that microwave treatment of coal can achieve significant increases in pyrite transformation to magnetically enhanced pyrrhotite. However, these achievements are at the expense of undesirable changes to the coal structure. From the SEM/MLA investigations presented here, the coal sample treated for 20 seconds at 15kW forward power level show that between 20% and 30% (across all size fractions measured) of the original pyrite phase has been transformed to pyrrhotite. These are potentially highly significant amounts. The changes in the proximate character of the microwave treated coals, where pyrite to pyrrhotite formation is most successful (i.e. 30 seconds at 8kW and 20 seconds at 15kW), imply that reactivity (burnout) is adversely affected by microwave treatment, with the severity of the changes dependant on both exposure time and power density. At 8kW forward power for exposure times of 5, 10, 15, 20 & 25 seconds, minimal changes in peak and burnout temperatures are reported, whilst treatment for 30 seconds at 8kW and 20 seconds at 15kW show more marked change. The peak temperature (PT) and burnout temperatures (BT) shown in Table 6.4 are generated from a TGA profile for each treated sample including untreated an untreated control sample for comparison. The peak intensities (dW/dt = max) and positions appear to be relatively similar for exposure times of 5, 10, 15, 20 & 25 seconds at 8kW when compared to the

untreated control sample. However, the PT and BT show a tendency to increase with microwave treatment for 30 seconds at 8kW and 20 seconds at 15kW. This is almost certainly as a result, particularly in the case of BT values, of the production of small amount of charred material, which is less reactive during heating. This is supported by increases in the reflectance of vitrinite maceral for these exposure times and power settings reported in Table 6.6. Heating a coal is likely to increase the values for PT and BT which may then also mean a reduction in its reactivity. It is also clear that increases in microwave exposure time and power setting correspond to increasing PT and BT values. Oxidation of coal by microwave heating of coal particles will occur through one of two mechanisms (or a combination of both) – either exposure to high temperatures (>300°C) for a relatively short period of time or a lower temperature (100-300°C) for a longer periods. The residence time in the microwave field is probably the most significant factor in adversely affecting the coal structure in these tests. The principal heating mechanism within the coal matrix during microwave exposure is through the rapid heating of moisture together with microwave coupling to other lossy phases such as pyrite. The results in Table 6.3 show that although it is possible to gasify the moisture in the coal and reduce the moisture content (%wt basis), driving steam through the pores of the particle, it does not readily liberate the majority of moisture inside the particle in these tests. Whilst any measurement of moisture content reductions after microwave treatment is not a particularly significant factor in this investigation, it demonstrates that with prolonged exposure to microwave energy, the bulk temperature of the coal is likely to increase rapidly, through standard conduction heat transfer paths, for as long as moisture is

present in the structure. The second mechanism through which oxidation of coal will occur is due to the microwave coupling of pyrite (and other lossy inclusions) which heats more rapidly than coal. This rapid heating means that potentially the temperature of the pyrite particle will reach well in excess of 300°C in a very short period of time. Moreover, if the pyrite particle being heated is intimately associated with the organic matrix then inevitably local devolatilisation of the surrounding carbon matrix will occur equating to a reduction in the volatile matter content of the sample. Applying higher powers for short residence times are most likely to achieve pyrite phase alterations whilst preserving the proximate character of the bulk material. It has been shown that extended treatment times can produce significant changes in the reactivity of the sample (Lester and Kingman, 2003). Short exposure times of coal in the microwave cavity will potentially keep the heating of the coal matrix to a minimum which will consequently reduce the risk of devolatilisation.

An assessment of the mechanisms of pyrite transformation in inert and oxygen containing atmospheres at elevated temperature based on a literature review are outlined in Section 4.2. The transformation of pyrite to pyrrhotite by microwave heating has been shown to be problematic for two key reasons. Firstly, electromagnetic heating of pyrite is not a uniform process in terms of temperature control of the particle (coupled with difficulties in temperature measurement of the bulk charge). Under equilibrium conditions, the composition of pyrrhotite from pyrite decomposition is controlled by temperature (Hu et

al., 2005). Secondly it has been demonstrated in this work, and in previous monomodal microwave heating experiments reported in Section 4.3, that microwave coupling with pyrite can be difficult to achieve. The result is that not all pyrite particles are treated for the same amount of time, with some coupling early in the experiment and heats rapidly and others left apparently unaffected for the duration of their exposure to microwaves. The non-uniformity of heating pyrite particles in coal is shown in Figure 6.14. A model of the decomposition and oxidation of pyrite by conventional heating methods presented by Hu, et al., 2005 implies that the decomposition of pyrite to pyrrhotite will follow an unreacted core model controlled by gas layer diffusion depending on the reaction conditions. The direct oxidation process is controlled by temperature and chemical reaction with the inward diffusion of oxygen to form porous pyrrhotite with further successive oxidation of the formed pyrrhotite as the reaction continues. This proposed unreacted core model is observed by SEM/MLA analysis in the experimental work reported in Section 4.3 for both conventionally heated and microwave heated samples even though temperature measurement was impossible in the latter case. In the case of microwave heated pyrite particles, exposure time has been shown to be a controlling factor in the oxidation of pyrite to form pyrrhotite and other reaction products such as hematite (See Section 4.9, Figure 4.54). Whilst it is reasonable to assume that as exposure time increases, particle temperature is also likely to increase the temperature control of the particles and microwave coupling with the target present significant difficulties. Previously it has be shown with observations by SEM/MLA that pyrite can be oxidised directly to hematite (suggesting oxygen diffusion through the surface gas layer is not

prohibited), with other particles showing pyrrhotite formed as an intermediated in the transformation from *pyrite → pyrrhotite → hematite*. However, the study of the transformation of pyrite in inert and oxygen containing atmospheres is highly relevant because, in some situations, it is part of the whole transformation process of pyrite in oxygen containing atmospheres. The microwave heating of pyrite in coal presented in this work does not exhibit the same transformation mechanisms as those observed in Section 4.3. The transformation of pyrite to form pyrrhotite is positively affected by exposure time in the microwave field and power density. This evidence is reported in Figure 6.13 which shows significant increases in pyrrhotite only after microwave treatment for 30 seconds at 8kW and 20 seconds at 15kW. Furthermore, whilst not all particles have been affected by exposure in the microwave field, those that have, show complete decomposition to pyrrhotite. A reasonable explanation for these observations is that pyrite to pyrrhotite conversion rate is significantly influenced by temperature and also heating rate, with reaction rates increasing exponentially with temperature (Hu et al., 2005). Since there was no evidence of the formation of iron oxides, as shown in Figure 6.15 it is reasonable to assume that the mechanism for transformation proceeds as for an inert atmosphere model. The precise sulphur content in the formed pyrrhotite (x in FeS_x) was not measured by X-ray analysis since topographical issues related to spectra differentiation and matching were insurmountable. It is therefore highly probable that transformation products with sulphur content between pyrrhotite and troilite (FeS and $Fe_{1-x}S$) exist in all treated samples. However, it has been shown by others that sulphur content in the transformed pyrrhotite is determined by temperature as shown in Figure 4.2

(Hu, et al., 2005). The thermal decomposition of pyrite to pyrrhotite (or other polytypes) did not follow the unreacted core model described in Section 4.3 or that presented by Hu et al., 2005). It is postulated that the thermal decomposition of pyrite in coal by microwave energy will is controlled by heating rate and temperature, providing that sufficient conditions (high power densities, short exposure) mean that thermal decomposition by the inward diffusion of oxygen is prohibited (due to sulphur gas consumption during its diffusion to the particle surface) which allows transformation through a multi-step sequential process *pyrite* → *pyrrhotite* → *troilite* → *iron* to proceed.

6.5 Conclusions

A particular challenge for microwave assisted coal desulphurisation is the optimisation of electromagnetic energy to maximise coupling with the disseminated pyritic phase and to allow sufficient and selective heating (and subsequent transformation to magnetically enhanced pyrrhotite) to take place, whilst minimising changes in the proximate composition of the bulk material. Previous research utilising lower power microwave systems for the pre-treatment of coal has shown that direct magnetic separation does not significantly reduce the pyritic sulphur content of coal. This suggests that any increases in magnetic properties by low-power microwave energy are not sufficient to enhance the removal of pyrite by magnetic separation. The new approach presented in this work utilising microwave systems operating at industrially relevant power levels and residence times is a significant step change in this field. Furthermore, this is the first time in-situ observations have been made on the preferential transformation of pyrite in coal by microwave heating whilst also monitoring the burnout performance of the treated product. The initial experiments presented here appear to show some very positive results. Multimodal microwave heating has a considerable effect on the transformation of pyrite to form pyrrhotite after relatively short exposure times of 8kW and 15kW forward power. Using 8kW of microwave power, pyrrhotite was formed only after 25 seconds exposure time. The pyrrhotite yield increased further with increasing residence times and power levels. The experiments undertaken for shorter exposure times (<20s) did not produce

significant quantities of pyrrhotite after corrections were made for topographical errors encountered with SEM/MLA observations. The implication is that either the disseminated pyrite particles did not couple with microwaves and therefore no preferential heating took place or that the bulk material did not reach the required temperature >300°C for pyrite decomposition to take place. Furthermore, the proximate composition of the coal did not change significantly until the treatment time reached >20s at 8kW where upon the reactivity of the coal was negatively affected. This implies is that the burnout propensity of the coal could be negatively affected. The microwave residence time inside the cavity is probably the most significant factor affecting burnout.

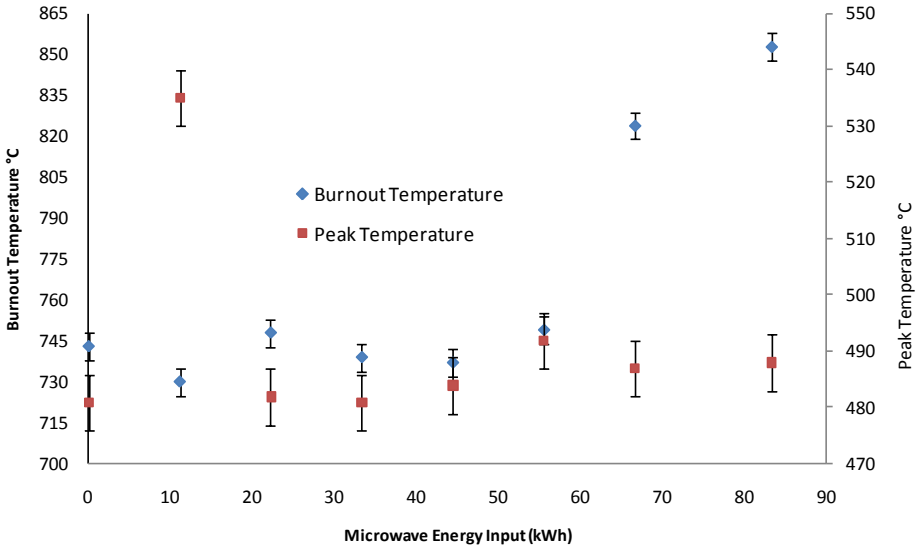

Figure 6.17 Burnout Temperature V`s Microwave Energy Input.

Although no attempt was made to measure the bulk temperature of the coal sample during microwave heating, it is expected that bulk temperature increases with increasing

residence time as moisture is mobilised and volatiles are expelled. It is also possible that the rapid heating of the pyrite particle will impact the surrounding coal matrix producing small amounts of charred material local to the pyrite particle. A plot of Burnout ans Peak Temperature versus microwave energy input is shown in Figure 6.17. The data presented in Figure 6.16 together with that presented in Figure 6.14 show that whilst it is essential to have maximum energy input to allow pyrite transformation to pyrrhotite, residence time should be minimised so as to reduce the negative effects of material burnout associated with prolonged treatment time and high bulk temperatures.

The decomposition of coal derived pyrite by microwave energy does not follow the unreacted core model proposed for convention heating experiments reported in Chapter 4. Whilst the initial investigation presented here suggests that the pyrite particles are transformed directly to pyrrhotite and that the experimental conditions do not favour iron oxide formation, more work is needed to investigate the decomposition mechanisms through which in-situ coal derived pyrite is transformed.

At present, a non-optimised multimodal cavity operating at non-optimised power settings has been shown to transform pyrite in coal to pyrrhotite at the expense of reductions in the reactivity and burnout performance of the material. Changes to the proximate composition of the coal may be minimised by using high power, short pulse microwave technology whereby shorter exposure time would become feasible and the microwave energy requirement reduced further. The uneven electric field distribution with the

multimode cavity may exacerbate difficulties with minimising reflected power and charge coupling over such short exposure times. The importance of a targeted high strength electric field to achieve high heating rates and therefore economic throughputs should be investigates further with the use of single mode applicators operating at industrially relevant frequencies and power levels.

Further work is needed to improve the sample preparation technique for SEM/MLA observations of coal in carnauba wax mounts to minimise pyrite/pyrrhotite misclassification from X-ray spectra matching as a result of surface topography. Work in this area is continuing.

Chapter 7 – Conclusions and Further Work

7.1 Conclusions

The work reported in this thesis has shown that high power (>3kW) microwave treatment of coal can induce phase alterations in organically bound pyrite to enhance its magnetic susceptibility and therefore to potentially aid the sulphur-coal separation process by magnetic recovery. Although there is a significant body of published work which considers the heating of such materials, there has been little attention given to understanding the fundamental mechanisms through which coal and its associated pyrite content heat in an applied microwave field. This is a clear gap in the current state of the art.

A detailed review of the literature in this field has shown that some carbonaceous materials contain a level of bonding in their complex structure in which exists a free charge with the ability to move along the aromatic lattice. It has been shown that less well ordered structures can be considered to be relatively microwave transparent with higher ordered structures able to be readily heated in a microwave field. The relationship between coal rank and the aromaticity of its complex carbonaceous structure has been used to underpin an investigation into the fundamental mechanisms through which coal heats in a microwave field. Measurements of the dielectric properties of different coals of varying rank using the resonant cavity perturbation technique have proven that a clear

correlation exists between dielectric loss factor and the degree of structural ordering. For the first time a new and fundamental relationship between coal rank and dielectric loss factor is reported.

This study has shown that exposure of pyrite to both conventional and microwave heating methods enhanced its magnetic properties as a result of phase alterations at the particle surface, quantified by SEM/MLA and Vibrating Sample Magnetometer (VSM). Conventionally heated pyrite samples showed the highest magnetic susceptibility increases, probably due to difficulties surrounding the temperature control associated with microwave heating. From a review of the literature in this field and by SEM observations made for each sample test in this work, a general pyrite transformation model as a result of microwave heating is proposed.

Several recent studies have investigated the application of low power (600W) microwave energy to improve the magnetic properties of both museum grade pyrite samples and in-situ coal derived pyrite in an effort to improve recovery by magnetic separation through favourable thermally induced phase alterations. Almost all of this previous work was carried out at low microwave power levels with consequently low power densities in the FeS_2 phase. Higher power densities could not be achieved due to the use of low power low efficiency microwave sources found in most domestic kitchens. As a result of these limitations, exposure times in the order of minutes were necessary to achieve any significant temperature increases. The study presented in this thesis extends the previous work by others in assessing quantitatively the influence of higher applied microwave power levels on the conversion of pyrite in coal. It was demonstrated that with sufficient

power and residence time, the conversion of pyrite to pyrrhotite is achievable using microwave heating. The amount of pyrrhotite formed as a result of microwave exposure varies with microwave residence time and forward power level. Comparisons of change in the iron sulphide species in the coal was made between microwave treated and untreated material. Using a multimode microwave cavity it was found that significant amounts of pyrrhotite were formed in 20s when using 15kW of microwave power. Treatment at lower power levels in this type of cavity was found to be less effective. The overall effect of treatment on the calorific value and proximate character of the coal was minimal.

7.1.1 Decomposition & Oxidation of Pyrite by Conventional and Microwave Heating.

Initially, an assessment of the mechanisms of pyrite transformation in inert and oxygen containing atmospheres at elevated temperatures was conducted based on a detailed review of literature. Whilst most of the literature relates to the conventional furnace heating of pyrite, little attention has been given to the affect of its transformation mechanisms by heating in an applied microwave field. It has been shown in this work and by others that with careful control of temperature and atmospheric conditions pyrite may be decomposed to magnetically enhance pyrrhotite. However, the temperatures required to produce favourable pyrite decomposition products by conventional heating in air (> 400°C) mean that the pre-treatment of coal bound pyrite is not practically viable due to adverse changes in the proximate character and burnout performance of the coal. The hypothesis that microwave heating can induce similar favourable pyrite transformation

phases to improve its recovery, as demonstrated in conventional heating trials, has been investigated and quantified by SEM/MLA and VSM analysis.

This study considered the treatment of museum grade pyrite particles by both conventional (muffle furnace & TGA chamber) and single mode 1kW fluidised bed microwave heating and used SEM/MLA (Scanning Electron Microscopy) and VSM (Vibrating Sample Magnetometer) to identify and quantify the transformation products and corresponding magnetic properties respectively. In order to significantly increase the magnetic susceptibility of pyrite by thermal decomposition, the formation of monoclinic pyrrhotite is necessary. XRD (X-ray diffraction) analysis has been identified in both conventionally heated samples and those treated by in a microwave field. Generally speaking, the magnetic properties of the conventionally heated (in air) pyrite samples increased with increasing temperature. Although finite temperature control has proven to be problematic in the conventional trials, the formation of pyrrhotite was dependant on a number of key factors. These are particle size and temperature. Overheating of the pyrite particles had a detrimental effect on its magnetic properties due the formation of hematite, probably as a result of the subsequent oxidation of an intermediate pyrrhotite formation at the surface.

The conventionally heated samples showed the largest increase in magnetic properties speculated to be due to conventional heating offering a more controlled and uniform heating process. The results observed after the treatment of pyrite in a single mode microwave applicator were less reliable. This method of heating has not been shown to be a uniform process with temperature measurement of the fluidised particulate material

inside the cavity an insurmountable obstacle. Furthermore, it was observed by SEM/MLA investigations that not all particles were affected by the microwave treatment and, moreover, those that were affected, were not all affected to the same degree. It is therefore reasonable to assume that not all particles will couple with the electric field at the same time in this type of applicator. The implication is that there will be a difference in the relative heating time between particles and therefore a uniform and controlled exposure to permit favourable transformation conditions is difficult to achieve. The characteristic shrinking core model which was proposed by Hu et al., 2007 was observed in both conventionally heated and microwave treated samples.

7.1.2 The Influence of Heterogeneity on the Dielectric Properties of Coal.

The dielectric properties of a material govern its behaviour in the presence of an electromagnetic field. Knowledge of the key dielectric properties are essential for effective cavity design and to ensure a realistic prediction of power loss density
In order to fully understand the relationship between a carbonaceous material structure and its dielectric properties, the fundamental mechanisms by which carbonaceous materials heat in an applied electromagnetic field were considered. The hypothesis that dielectric permittivity (and therefore microwave heating response) relates to carbon structural ordering in coal has been quantified using the resonant cavity perturbation technique and ^{13}C NMR. This study has identified two key issues to consider which have been shown to have a profound effect on dielectric property measurements taken using the cavity perturbation technique. Firstly, the dependence of sample bulk densities on

their dielectric properties has been considered. It has been shown through extensive dielectric property measurements taken on two UK coal samples, several fundamental relationships exist which relates the sample material bulk density during resonant cavity measurements to both dielectric constant and dielectric loss factor. These relationships provide a means of estimating the dielectric constant and dielectric loss factor at any bulk density, including that of the solid material from a series of measurements across a range of two-phase (air-coal) mixtures. Secondly, the natural heterogeneity of coal together with the variability in its maturation, moisture content and principal inorganic inclusions have made the comparison of their dielectric properties, from one coal sample to another, futile. This work has shown that without the proper consideration of the impact of coal rank, mineral matter content and moisture content on their dielectric properties, comparisons between coals are difficult to make. Consequently, the problem of ascertaining the dielectric property of the organic carbonaceous phases of a coal structure lies in the fact that mineral matter content and its composition, together with the coal moisture content can vary widely from coal to coal. Inorganic inclusions and moisture have been shown to obscure any relationships between rank (or structural order) and dielectric property which might have otherwise been observed. A new experimental method is introduced to minimise these effects by using a two-stage demineralisation regime (HF followed by Fe^{3+}), a drying stage to remove surface moisture, followed by a bulk density controlled dielectric property

measurement. The theory that the structural order of the coal matrix is related to its dielectric property and therefore its microwave heating response has been quantified for the first time in this work. This study included a wide range of coals from very different geological conditions and of differing degrees of digenesis or rank to test the hypothesis. The quantitative measurement of structural ordering, made by ^{13}C NMR spectra analysis has shown that essentially, as coal rank increases, the aromaticity of its carbon structure increases. As the structural ordering increases, the level of free charge (per unit volume) increases together with electron mobility which results in an increase in dielectric loss factor. Dielectric property measurements made on a series of dry, demineralised (de-ashed (dry)) coals with varying rank between 0.29-3.46%, have demonstrated that a direct relationship exists between carbon aromaticity and dielectric loss factor. This thesis has demonstrated the feasibility of rapid dielectric property measurement, through the systematic experimental approach reported and the relationships developed, can be used to predict coal rank, carbon content and carbon aromaticity.

7.1.3 The effect of microwave energy upon the decomposition of pyrite in coal.

It has been shown that it is possible to decompose pyrite in coal to form pyrrhotite using high power (<3kW) microwave energy in a microwave applicator. The effectiveness of microwave heating to induce favourable pyritic phase alterations has

shown to be dependent on applied microwave power and exposure time (temperature dependant). This thesis has demonstrated the feasibility of this process through the systematic use of proximate characterisation and SEM/MLA investigations. The SEM/MLA investigation made, post microwave treatment, are particularly significant because they show for the first time the nature of thermally transformed pyrite which is intimately associated with a coal matrix. It has been categorically shown that process control is an important are of consideration in the optimisation of this process. Whilst the bulk coal temperature was not measured in these microwave heating tests, its regulation is of vital importance to prevent any adverse effects on its proximate character and to minimise burnout by keeping microwave exposure times short and therefore bulk temperatures are minimised. SEM/MLA analysis post treatment of the coal has shown that microwave heating at 8kW power level for relatively short exposure times (<20s) had minimal effects of pyrite decomposition. It is postulated that the likely reason for this is due to difficulties with the coupling of the electromagnetic energy with the pyrite particles disseminated through the coal. There was not sufficient time left in the project to optimise the multimode cavity to the specific requirements for this process. Furthermore, the proximate character of the coal was not significantly affected by exposure times less than 20 seconds at a power level of 8kW. This implies that the bulk temperature of the coal remained low (<100ºC) and that no significant displacement of volatiles occurred. With increase exposure time and power level (i.e. 8kW >20s and 15kW 20s) significant areas pyrite was decomposed to pyrrhotite confirmed by SEM observations an

characterised by X-ray analysis. Unfortunately, this increase in pyrrhotite formation as a result of increased exposure time and microwave power level adversely affected the theoretical burnout performance of the coal. Thermogravimetric analysis, post microwave treatment, showed that volatile matter had been displace from the coal reducing from 53.1%wt (untreated control sample) to 37%wt (15kW 20 seconds microwave treatment) on a dry ash free basis. This work suggests that probably the most significant factor affecting both pyrrhotite formation and reductions in burnout performance of the coal is microwave exposure time. Process control to balance the two opposing effects of pyrrhotite formation and burnout performance respectively will require a re-appraisal of the technology suitable for the delivery of electromagnetic energy to the product. It has been shown by others that the low power (<600W) multimode microwave treatment of coal to aid desulphurisation requires processing times in the order of minutes rather than seconds.

Extended periods of exposure will inevitably lead in increasing bulk temperatures and therefore will negatively affect the proximate character of the coal. It is for these reasons that the transfer of energy should be conducted in the shortest possible time, which will inevitably require an industrially relevant microwave applicator design to influence the material feed orientation with respect to the electric field distribution and overall heating efficiency. With the careful control of process parameters, high energy transfer to the pyrite phase can be maximised and bulk temperatures can be minimised and therefore favourable economic throughputs can be realised. The importance of a targeted higher electric field to achieve high heating rates in

short exposure times, may be achieved by employing single mode applicators where the field pattern inside the cavity is relatively well defined ensuring rapid intense heating in the area of maximum electric field. Optimisation of the key process requirement identified in this work may provide a major alternative to, or compliment, existing technologies for sulphur control such as, triboelectric separation, flue gas desulphurisation and froth flotation.

7.2 Recommended Further Work

The investigations into the dielectric properties of coal have demonstrated a correlation between structural ordering and dielectric loss factor. The natural future progression of this work is to investigate a range of materials which represent a progression in structural ordering and graphitisation. This may include semi-cokes and graphitised chars which may lie in the region between coal and coke. The use of analysis techniques to quantify aromaticity (^{13}C NMR) together with rapid dielectric property measurement using the resonant cavity perturbation technique marks a significant stage in the validation the model presented in this work.

The future developments in the microwave heating of coal to initiate phase alterations in the in-situ pyrite phase, present a clear and focused challenge as a result of the preliminary work outlined in this thesis.

Effective process control would be necessary to maximise phase transitions from pyrite to magnetically enhanced pyrrhotite whilst maintaining the proximate composition of the bulk material post treatment. The use of numerical electromagnetic simulation techniques in order to accurately optimise cavity design, microwave feed locations, electric field patterns and overall heating efficient would allow for a more targeted and controlled process. This optimisation stage would be critical before any operation at scale is attempted. A monomode cavity design is needed that supports a well defined and high electric field maximising the impact on the pyrite phase. Accurate temperature measurement would be necessary if higher power levels to be used. Higher power levels

would reduce residence times and improve the efficient delivery of power and selective heating of the pyritic phase in coal.

The use of SEM/MLA analysis to quantify the effects of microwave treatment on the thermal decomposition of pyrite has been shown to be an immensely useful tool. This is the first time that microwave treated coal, embedded in a carnauba wax mounting medium, has been analysed by this method with focus on the thermal alterations of the pyrite phase.

There were found to be some significant disadvantages when using carnauba wax to support the microstructure of coal. Mechanical preparation techniques used to grind and polish each sample have been problematic due to the plucking of coal and pyrite particles from the relatively soft wax supporting matrix. It has been shown that pitting, cracking, plucking and scratches can influence the accuracy of quantitative X-ray microanalysis. More work is needed to improve these preparation techniques.

REFERENCES

Abraitis P. K., Pattrick R.A.D, Vaughan D.J, (2004). Variations in the compositional, textural and electrical properties of natural pyrite: a review.
International Journal of Mineral Processing, Volume 74, Issues 1-4, 19 November 2004, Pages 41-59

Abdul A, Srivastava S.K, Haque R, (1992). Chemical desulphurization of high sulphur coals.
Fuel, Volume 71, Issue 7, July 1992, Pages 835-839

Al-Harahsheh M, Kingman S.W, Bradshaw S, (2006). Scale up possibilities for microwave leaching of chalcopyrite in ferric sulphate.
International Journal of Mineral Processing, Volume 80, Issues 2-4, September 2006, Pages 198-204

Al-Harahsheh M, Kingman S.W, (2007). The influence of microwaves on the leaching of sphalerite in ferric chloride.
Chemical Engineering and Processing: Process Intensification, Volume 46, Issue 10, October 2007, Pages 883-888

Al-Harahsheh M, Kingman S.W, Saeid A, Robinson J, Dimitrakis G, Alnawafleh H, (2009). Dielectric properties of Jordanian oil shales
Fuel Processing Technology, Volume 90, Issue 10, October 2009, Pages 1259-1264

Ali A.Y, S.M. Bradshaw, (2009). Quantifying damage around grain boundaries in microwave treated ores
Chemical Engineering and Processing: Process Intensification, Volume 48, Issues 11-12, November 2009, Pages 1566-1573

Allen R.M, Carling R.W, VanderSande J.B, (1986). Microstructural changes in coal during low temperature ashing.
Fuel, Volume 65, Issue 3, March 1986, Pages 321-326

de Alwis A. A. P, Fryer P.J, (1990). The use of direct resistance heating in the food industry
Journal of Food Engineering, Volume 11, Issue 1, 1990, Pages 3-27

Appleton T.J, Colder R.I, Kingman S.W, Lowndes I.S, Read A.G, (2005). Microwave technology for energy-efficient processing of waste.
Applied Energy, Volume 81, Issue 1, May 2005, Pages 85-113

Arai M, Binner J.G.P, Cross T.E, (1995). Use of Mixture Equations for Estimating complex Permittivities from Measurements on Porous or Powdered Ceramic Specimens.
Japanese Journal of Applied Physics, Volume 31, Issue 1, September 1995, Pages 6463-6467

Arai S., Fukushima T, Morimoto T, Tojyo E, Tokuda N, Yoshizawa M, Hattori T, (1989). Development of a split coaxial RFQ at INS
Nuclear Instruments and Methods in Physics Research Section A: Accelerators, Spectrometers, Detectors and Associated Equipment, Volume 278, Issue 1, 15 May 1989, Pages 236-240

Asif M., Muneer T, (2007). Energy supply, its demand and security issues for developed and emerging economies. Renewable and Sustainable Energy Reviews, Volume 11, Issue 7, September 2007, Pages 1388-1413

ASTM D388 - 05 Standard Classification of Coals by Rank

Barker W.W, Parks T.C, (1986). The thermodynamic properties of pyrrhotite and pyrite: A re-evaluation
Geochimica et Cosmochimica Acta, Volume 50, Issue 10, October 1986, Pages 2185-2194

Barranco R.M, (2001) The characterisation and combustion of South American Coals, PhD thesis, University of Nottingham UK.

Barranco R.M, Cloke M, Lester E, (2003). Prediction of the burnout performance of some South American coals using a drop-tube furnace★
Fuel, Volume 82, Issues 15-17, October-December 2003, Pages 1893-1899

Bazayanc G.V, (1999). Energ. Elektrif. (Kiev) 1999, Volume 189, Issue 2

Becker U, Munz A.W, Lennie A.R, Thornton G, Vaughan D.J, (1997). The atomic and electronic structure of the (001) surface of monoclinic pyrrhotite (Fe_7S_8) as studied using STM, LEED and quantum mechanical calculations
Surface Science, Volume 389, Issues 1-3, 6 November 1997, Pages 66-87

Beér J.M, (2007). High efficiency electric power generation: The environmental role.
Progress in Energy and Combustion Science, Volume 33, Issue 2, April 2007, Pages 107-134

Belzile N, Chen Y.W, Cai M, Li Y, (2004). A review on pyrrhotite oxidation.
Journal of Geochemical Exploration, Volume 84, Issue 2, September 2004, Pages 65-76

Björkman A, (2001). Projects on coal characterization.
Fuel, Volume 80, Issue 2, January 2001, Pages 155-166

Boon M, Heijnen J.J, (1998). Chemical oxidation kinetics of pyrite in bioleaching processes
Hydrometallurgy, Volume 48, Issue 1, March 1998, Pages 27-41

Borah D, Baruah M.K, Haque I, (2001). Oxidation of high sulphur coal. Part 2.
Desulphurisation of organic sulphur by hydrogen peroxide in presence of metal ions.
Fuel, Volume 80, Issue 10, August 2001, Pages 1475-1488

Boyabat N, Özer A.K, Bayrakçeken S, Gülaboğlu M. Ş., (2004). Thermal decomposition of pyrite in the nitrogen atmosphere.
Fuel Processing Technology, Volume 85, Issues 2-3, 15 February 2004, Pages 179-188

British Geological Survey, (2010). Mineral Profile – Coal.
www.MineralsUK.com

BS 1016-106: (1996 & 1997) Methods for analysis and testing of coal and coke, British Standard

Butcher D.A and Rowson N.A (1995). IChemE Research Event (1995), p. 580

Callister W.D, (1999). Materials Science and Engineering – An Introduction
Fifth Edition, John Wiley & Sons, Inc., USA

Campbell P. E, McMullan J.T, Williams B.C, (2002). Concept for a competitive coal fired integrated gasification combined cycle power plant
Fuel, Volume 79, Issue 9, July 2000, Pages 1031-1040

Chaplin G, Pugsley T, (2005). Application of electrical capacitance tomography to the fluidized bed drying of pharmaceutical granule
Chemical Engineering Science, Volume 60, Issue 24, December 2005, Pages 7022-*7033*

Cloke M, Lester E, (1994). Characterization of coals for combustion using petrographic analysis: a review
Fuel, Volume 73, Issue 3, March 1994, Pages 315-320

Cloke M, Lester E, Gibb W, (1997). Characterization of coal with respect to carbon burnout in p.f.-fired boilers
Fuel, Volume 76, Issue 13, October 1997, Pages 1257-1267

Cloke M, Lester E, Belghazi A, (2002). Characterisation of the properties of size fractions from ten world coals and their chars produced in a drop-tube furnace
Fuel, Volume 81, Issue 5, March 2002, Pages 699-708

Cloke M, Gilfillan A, Lester E, (1997). The characterization of coals and density separated coal fractions using FTIR and manual and automated petrographic analysis
Fuel, Volume 76, Issue 13, October 1997, Pages 1289-1296

Cloke M, Lester E, Belghazi A, (2002). Characterisation of the properties of size fractions from ten world coals and their chars produced in a drop-tube furnace
Fuel, Volume 81, Issue 5, March 2002, Pages 699-708

Cloke M , Lester E, Allen M, Miles N.J, (1995). Automated maceral analysis using fluorescence microscopy and image analysis
Fuel, Volume 74, Issue 5, May 1995, Pages 659-669

Cloke M, Lester E, Allen M, Miles N.J, (1995). Repeatability of maceral analysis using image analysis systems
Fuel, Volume 74, Issue 5, May 1995, Pages 654-658

Cole David A, Simmons G.W, Herman R.G, Klier K, Nagy I.C, (1987). Transformations of iron minerals during coal oxidation
Fuel, Volume 66, Issue 9, September 1987, Pages 1240-1248

Crelling J.C, Kruge M.A, (1998). Petrographic and chemical properties of carboniferous resinite from the Herrin No. 6 coal seam Original Research Article
International Journal of Coal Geology, Volume 37, Issues 1-2, September 1998, Pages 55-71

Černý J, Sýkorová I, Maxa D, Weishauptová Z, Šebor G, Blažek J, (1997). Relationship between properties and conversions of North Bohemian coals during coal/oil coprocessing
Fuel Processing Technology, Volume 50, Issues 2-3, February 1997, Pages 235-247

Dai S, Deyi R, Yuegang T, Longyi S, Shengsheng L, (2002). Distribution, isotopic variation and origin of sulfur in coals in the Wuda coalfield, Inner Mongolia, China
International Journal of Coal Geology, Volume 51, Issue 4, September 2002, Pages 237-250

DEFRA, (2008). Air Quality Strategy for England, Scotland, Wales and Northern Ireland. Department for Environment, Food and Rural Affairs,

Dunn J. G, Chamberlain A.C, (1997). The recovery of gold from refractory arsenopyrite concentrates by pyrolysis-oxidation
Minerals Engineering, Volume 10, Issue 9, September 1997, Pages 919-928

Elsamak G, Altunta§ Özta§ N, Yürüm Y, (2003). Chemical desulfurization of Turkish Cayirhan lignite with HI using microwave and thermal energy★
Fuel, Volume 82, Issue 5, 1 March 2003, Pages 531-537

Evans N.G. (1995). The Dielectric Properties of Ceramics at 2.45GHz and Their Influence on Microwave Firing, PhD Thesis
Staffordshire University, UK, School of Engineering & Advanced Technology

Fanslow G, Hou C, Bluhm D, Markuszewski R, (1988). Journal of Microwave Power and Electromagnetic Energy 22 (1988), p. 211.

Fegley Jr. B, Lodders K, Treiman A.H, Klingelhöfer G, (1995). The Rate of Pyrite Decomposition on the Surface of Venus
Icarus, Volume 115, Issue 1, May 1995, Pages 159-180

Ferrando A.C, Andrés J.M, Membrado L, (1995). Coal desulphurization with hydroiodic acid and microwaves
Coal Science and Technology, Volume 24, 1995, Pages 1729-1732

Finkelstein N. P., (1997). The activation of sulphide minerals for flotation: a review International Journal of Mineral Processing, Volume 52, Issues 2-3, December 1997, Pages 81-120

Fletcher P, Stephenson T, Judd S, (1994). The use of an applied electric field for the filtration of particles from a low conductivity aqueous suspension
Chemical Engineering Science, Volume 49, Issue 14, July 1994, Pages 2371-2378

Gilfillan A, Lester E, Cloke M, Snape C, (1999). The structure and reactivity of density separated coal fractions
Fuel, Volume 78, Issue 14, November 1999, Pages 1639-1644

Goodarzi F, Snowdon L, Gentzis T, Pearson D, (1994).
Petrological and chemical characteristics of liptinite-rich coals from Alberta, Canada
Marine and Petroleum Geology, Volume 11, Issue 3, June 1994, Pages 307-319

Graus W.H.J, Worrell E, (2007). Effects of SO_2 and NO_x control on energy-efficiency power generation. Energy Policy, Volume 35, Issue 7, July 2007, Pages 3898-3908

Gupta D. C., (1999). Environmental aspects of selected trace elements associated with coal and natural waters of Pench Valley coalfield of India and their impact on human health
International Journal of Coal Geology, Volume 40, Issues 2-3, June 1999, Pages 133-149

Gupta S, Mohan K, Prasad R, Gupta S, Kansal A, (1998). Solid waste management in India: options and opportunities
Resources, Conservation and Recycling, Volume 24, Issue 2, November 1998, Pages 137-154

Haas J, Tamura M, Weber R, (2001). Characterisation of coal blends for pulverised fuel combustion
Fuel, Volume 80, Issue 9, July 2001, Pages 1317-1323

Hamlyn M.G, (1991). Microwave Sintering of Ceramics, PhD Thesis
Staffordshire Polytechnic, UK, Department of Electrical and Electronic Engineering.

Han T.J, Huang H.U, Huang W, (2006). Solvothermal synthesis and magnetic properties of pyrite $Co_{1-x}Fe_xS_2$ with various morphologies
Materials Letters, Volume 60, Issue 15, July 2006, Pages 1805-1808

Hao L, Gibbs B.M, (1998). Reduction of N_2O emissions from a coal-fired circulating fluidized-bed combustor by secondary fuel injection
Symposium (International) on Combustion, Volume 27, Issue 2, 1998, Pages 3077-3083

Harmer J. R, Callcott T.G, Maeder M, Smith B.E, (2001). A rapid coal characterisation analysis by low-resolution NMR spectroscopy and partial least-squares regression
Fuel, Volume 80, Issue 9, July 2001, Pages 1341-1349

Hart N.A. (2004). The Development of a Combined Microwave and Electric Radiant Heating System for Processing Ceramics, PhD Thesis
Staffordshire University, UK, School of Engineering & Advanced Technology

Hayashi J, Oku K, Kusakabe K, Morooka S, (1990). The role of microwave irradiation in coal desulphurization with molten caustics Original Research Article
Fuel, Volume 69, Issue 6, June 1990, Pages 739-742

Hayvanovych V. Pysh'yev S, (2003). Desulfurization of Low-Rank Coal with High Sulfur Content is the First Stage of Coal Burning at Heat Electric Stations. Energy Fuels, 2003, Volume 17, Issue 5, Pages 1186–1190

Helble J.J, Srinivasachar S, Boni A.A, (1990). Factors influencing the transformation of minerals during pulverized coal combustion
Progress in Energy and Combustion Science, Volume 16, Issue 4, 1990, Pages 267-279

Hong Y, Fegley Jr. B, (1998). The sulfur vapor pressure over pyrite on the surface of Venus Planetary and Space Science, Volume 46, Issues 6-7, June-July 1998, Pages 683-690

Hower J.C, Ban H, Schaefer J.L, Stencel J.M, (1997). Maceral/microlithotype partitioning through triboelectrostatic dry coal cleaning
International Journal of Coal Geology, Volume 34, Issues 3-4, December 1997, Pages 277-286

Hower J.C, Eble C.F, (1996). Introduction: Geology and petrology of Appalachian coals. International Journal of Coal Geology, Volume 31, Issues 1-4, November 1996, Pages 1-2

Hu G, Dam-Johansen K, Wedel S, Hansen J.P, (2006). Decomposition and oxidation of pyrite
Progress in Energy and Combustion Science, Volume 32, Issue 3, 2006, Pages 295-314

Hu H, Chen Q, Yin Z, Zhang P, (2003). Thermal behaviors of mechanically activated pyrites by thermogravimetry (TG)
Thermochimica Acta, Volume 398, Issues 1-2, 5 March 2003, Pages 233-240

Hu H, Chen Q, Yin Z, Zhang P, Zou J, Che H, (2002). Study on the kinetics of thermal decomposition of mechanically activated pyrites
Thermochimica Acta, Volume 389, Issues 1-2, 1 July 2002, Pages 79-83

Huang J. H, Rowson N.A, (2002). Hydrometallurgical decomposition of pyrite and marcasite in a microwave field
Hydrometallurgy, Volume 64, Issue 3, June 2002, Pages 169-179

Huang J. H, Rowson N.A, (2001). Heating characteristics and decomposition of pyrite and marcasite in a microwave field
Minerals Engineering, Volume 14, Issue 9, September 2001, Pages 1113-1117

Huang J. H., Rowson N.A, (2002). Hydrometallurgical decomposition of pyrite and marcasite in a microwave field
Hydrometallurgy, Volume 64, Issue 3, June 2002, Pages 169-179

Huffman G P, Huggins F.E, Levasseur A.A, Chow O, Srinivasachar S, Mehta A.K, (1989). Investigation of the transformations of pyrite in a drop-tube furnace
Fuel, Volume 68, Issue 4, April 1989, Pages 485-490

Huggins F.E, (2002). Overview of analytical methods for inorganic constituents in coal
International Journal of Coal Geology, Volume 50, Issues 1-4, May 2002, Pages 169-214

Hutton A.C, Graham U.M, Hower J. C, Rathbone R.F, Robl T.L, (1996). Petrography of pyrolysis and pyrolysis-steam retorted residues from the alpha torbanite and the alpha cannel coal Original Research Article
Organic Geochemistry, Volume 24, Issue 2, February 1996, Pages 219-226

ICTIS/TR15, IEA Coal Research, London, 1981

Jagadeesh M.S, Seehra M.S, (1980). Electrical resistivity and band gap of marcasite (FeS_2)Physics Letters A, Volume 80, Issue 1, 10 November 1980, Pages 59-61

Jaworek A, Krupa A, Czech T, (2007). Modern electrostatic devices and methods for exhaust gas cleaning: A brief review
Journal of Electrostatics, Volume 65, Issue 3, March 2007, Pages 133-155

Jelinowska A, Tucholka P, Badaut-Trauth D, (1999). Magnetic mineral variations of South Caspian Sea sediments at laminae scale
Physics and Chemistry of the Earth, Part A: Solid Earth and Geodesy, Volume 24, Issue 9, 1999, Pages 823-828

Jerz J.K, Rimstidt J.D, (2004). Pyrite oxidation in moist air
Geochimica et Cosmochimica Acta, Volume 68, Issue 4, 15 February 2004, Pages 701-714
Jones D.A., Kingman S.W, Whittles D.N, Lowndes I.S, (2007). The influence of microwave energy delivery method on strength reduction in ore samples
Chemical Engineering and Processing, Volume 46, Issue 4, April 2007, Pages 291-299

Jones D. A, Lelyveld T.P, Mavrofidis S.D, Kingman S.W, Miles N.J, (2002). Microwave heating applications in environmental engineering—a review
Resources, Conservation and Recycling, Volume 34, Issue 2, January 2002, Pages 75-90

Jones D.A, Kingman S.W, Whittles D.N, Lowndes I.S, (2005). Understanding microwave assisted breakage
Minerals Engineering, Volume 18, Issue 7, June 2005, Pages 659-669

Kelly R. M, Rowson N.A, (2002). Microwave reduction of oxidised ilmenite concentrates
Minerals Engineering, Volume 8, Issue 11, November 1995, Pages 1427-1438

Kingman S. W, Rowson N.A, (1998). Microwave treatment of minerals-a review
Minerals Engineering, Volume 11, Issue 11, November 1998, Pages 1081-1087

Kingman S.W, Vorster W, Rowson N.A, (2000). The influence of mineralogy on microwave assisted grinding
Minerals Engineering, Volume 13, Issue 3, March 2000, Pages 313-327

Kingman S.W, Jackson K, Bradshaw S.M, Rowson N.A, Greenwood R, (2004). An investigation into the influence of microwave treatment on mineral ore comminution
Powder Technology, Volume 146, Issue 3, 8 September 2004, Pages 176-184

Kingman S.W, Vorster W, Rowson N.A, (2000). The influence of mineralogy on microwave assisted grinding
Minerals Engineering, Volume 13, Issue 3, March 2000, Pages 313-327

Klein N, Schuster M, Vitusevich S, Winter M, Yi H.R, (2001). Novel dielectric resonator structures for future microwave communication systems
Journal of the European Ceramic Society, Volume 21, Issue 15, 2001, Pages 2687-2691

Kraszewski A.W, Nelson S.O, You T.S, (1991). Moisture content determination in single corn kernels by microwave resonator techniques
Journal of Agricultural Engineering Research, Volume 48, January-April 1991, Pages 77-87

Kraszewski A.W, Nelson S.O, (1989). Composite model of the complex permittivity of cereal grain
Journal of Agricultural Engineering Research, Volume 43, May-August 1989, Pages 211-219

Kusakabe K, Morooka S, Aso S, (1988). Chemical coal cleaning with molten alkali hydroxides in the presence of microwave radiation
Fuel Processing Technology, Volume 19, Issue 3, October 1988, Pages 235-242

Lambert Jr. J M, Simkovich G, Walker Jr P.L, (1980). Production of pyrrhotites by pyrite reduction
Fuel, Volume 59, Issue 10, October 1980, Pages 687-690.
Lester E, Kingman S.W, Dodds C, Patrick J, (2006). The potential for rapid coke making using microwave energy
Fuel, Volume 85, Issues 14-15, October 2006, Pages 2057-2063

Lester E, Kingman S.W, (2004). The effect of microwave pre-heating on five different coals
Fuel, Volume 83, Issues 14-15, October 2004, Pages 1941-1947

Lester E, Kingman S.W, Dodds C, (2005). Increased coal grindability as a result of microwave pretreatment at economic energy inputs
Fuel, Volume 84, Issue 4, March 2005, Pages 423-427

Lester E, Cloke M, (1999). The characterisation of coals and their respective chars formed at 1300°C in a drop tube furnace
Fuel, Volume 78, Issue 14, November 1999, Pages 1645-1658

Lester E, Watts D, Cloke M, (2002). A novel automated image analysis method for maceral analysis
Fuel, Volume 81, Issue 17, December 2002, Pages 2209-2217

Lester E, Allen M, Cloke M, Miles N.J, (1993). Image analysis techniques for petrographic analysis
Fuel Processing Technology, Volume 36, Issues 1-3, December 1993, Pages 17-24

Lester E, Cloke M, Miles N.J, (1993). The effect of operating conditions on char produced in a drop-tube furnace
Fuel Processing Technology, Volume 36, Issues 1-3, December 1993, Pages 101-108

Levy J.M, Chan L.K, Sarofim A.F, Beér J.M, (1981). NO/char reactions at pulverized coal flame conditions
Symposium (International) on Combustion, Volume 18, Issue 1, 1981, Pages 111-120

Liu X, (1986). The application of and prospects for fluidized-bed combustion technology in coal-mining areas in China
Energy, Volume 11, Issues 11-12, November-December 1986, Pages 1209-1214

Love G.D, Snape C.E, Jarvis M.C, (1998). Comparison of leaf and stem cell-wall components in barley straw by solid-state ^{13}C NMR
Phytochemistry, Volume 49, Issue 5, 5 November 1998, Pages 1191-1194

Lowry, H.H, (1963). Chemistry of Coal Utilization. Supplementary Volume, Wiley, New York. ISBN 0471024945

Mardon S M, Hower J.C, (2004). Impact of coal properties on coal combustion by-product quality: examples from a Kentucky power plant
International Journal of Coal Geology, Volume 59, Issues 3-4, 10 August 2004, Pages 153-169

Marland S, Merchant A, Rowson N.A, (2001). Dielectric properties of coal
Fuel, Volume 80, Issue 13, October 2001, Pages 1839-1849

Marland S, Han B, Merchant A, Rowson N.A, (2000). The effect of microwave radiation on coal grindability
Fuel, Volume 79, Issue 11, September 2000, Pages 1283-1288

Maroto-Valer M.M, Andrésen J.M, Snape C.E, (1998). In situ ^{1}H NMR study of the fluidity enhancement for a bituminous coal by coal tar pitch and a hydrogen-donor liquefaction residue
Fuel, Volume 77, Issues 9-10, July-August 1998, Pages 921-926

Maxwell E, Kelland D.R, Jacobs I.S, Levinson L.M, (1982). Magnetic separation and thermo-magneto-chemical properties of coal liquefaction mineral participates Original Research Article
Fuel, Volume 61, Issue 4, April 1982, Pages 369-376

McIlveen-Wright D.R., Huang Y, Rezvani S, Wang Y, (2007). A technical and environmental analysis of co-combustion of coal and biomass in fluidised bed technologies
Fuel, Volume 86, Issue 14, September 2007, Pages 2032-2042

Menezes R R., Souto P. M, Kiminami R, (2007). Microwave hybrid fast sintering of porcelain bodies
Journal of Materials Processing Technology, Volume 190, Issues 1-3, 23 July 2007, Pages 223-229

Meredith R.J., (1998). Engineers` Handbook of Industrial Microwave Heating.
The Institution of Electrical Engineers, London

Metaxas A.C., Meredith R.J, (1983). Industrial Microwave Heating
The Institution of Electrical Engineers, London

Metaxas A.C., Binner J.P.G, (1989). Microwave Processing of Ceramics
Advanced Ceramic Processing and Technology, Pages 285-367

Mikhlin Y.L, Romanchenko A.S, Asanov I.P, (2006). Oxidation of arsenopyrite and deposition of gold on the oxidized surfaces: A scanning probe microscopy, tunnelling spectroscopy and XPS study
Geochimica et Cosmochimica Acta, Volume 70, Issue 19, 1 October 2006, Pages 4874-4888

Nanthakumar B, Pickles C.A, Kelebek S, (2007). Microwave pre-treatment of a double refractory gold ore
Minerals Engineering, Volume 20, Issue 11, September 2007, Pages 1109-1119

Nelson S.O , Stetson L.E, (1976). Frequency and moisture dependence of the dielectric properties of hard red winter wheat
Journal of Agricultural Engineering Research, Volume 21, Issue 2, June 1976, Pages 181-192

Nelson S.O, (1994). Measurement of microwave dielectric properties of particulate materials
Journal of Food Engineering, Volume 21, Issue 3, 1994, Pages 365-384

Nott K.P, Hall L.D, (1999). Advances in temperature validation of foods
Trends in Food Science & Technology, Volume 10, Issue 11, November 1999, Pages 366-374

OECD, (2010). Coal Information - IEA Online Database.
Organisation for Economic Co-Operation and Development
http://www.oecd.org/document/5/0,3343,en_21571361_33915056_39151365_1_1_1_1,00.html

O'Brien G, Jenkins , Esterle J, Beath H, (2003). Coal characterisation by automated coal petrography
Fuel, Volume 82, Issue 9, June 2003, Pages 1067-1073

Ogawa M, Yoshida N, (2005). Nitrous oxide emission from the burning of agricultural residue
Atmospheric Environment, Volume 39, Issue 19, June 2005, Pages 3421-3429

Olubambi P.A, Potgieter J.H, Hwang J.Y, Ndlovu S, (2007). Influence of microwave heating on the processing and dissolution behaviour of low-grade complex sulphide ores
Hydrometallurgy, Volume 89, Issues 1-2, September 2007, Pages 127-135

Olubambi P.A, Ndlovu S, Potgieter J.H, Borode J.O, (2007). Effects of ore mineralogy on the microbial leaching of low grade complex sulphide ores
Hydrometallurgy, Volume 86, Issues 1-2, April 2007, Pages 96-104

Peters C, Thompson R, (1998). Magnetic identification of selected natural iron oxides and sulphides
Journal of Magnetism and Magnetic Materials, Volume 183, Issue 3, 20 March 1998, Pages 365-374

Petersen H.I, (2006). The petroleum generation potential and effective oil window of humic coals related to coal composition and age Original Research Article
International Journal of Coal Geology, Volume 67, Issue 4, 3 July 2006, Pages 221-248

Pickles C.A, (2009). Microwaves in extractive metallurgy: Part 2 – A review of applications
Minerals Engineering, Volume 22, Issue 13, October 2009, Pages 1112-1118

Pilar G, Adanez J, de Diego L.F, García-Labiano F, Cabanillas A, (2004). Circulating fluidised bed co-combustion of coal and biomass
Fuel, Volume 83, Issue 3, February 2004, Pages 277-286

Prasad M.S, Mensah-Biney R, Pizarro R.S, (1991). Modern trends in gold processing — overview
Minerals Engineering, Volume 4, Issue 12, 1991, Pages 1257-1277

Radojevic M, (1998). Reduction of nitrogen oxides in flue gases
Environmental Pollution, Volume 102, Issue 1, Supplement 1, 1998, Pages 685-689

Raichur A. M, Wang X.H, Parekh B.K, (2000). Quantifying pyrite surface oxidation kinetics by contact angle measurements
Colloids and Surfaces A: Physicochemical and Engineering Aspects, Volume 167, Issue 3, 15 July 2000, Pages 245-251

Remeysen K, Swennen R, (2006). Beam hardening artifact reduction in microfocus computed tomography for improved quantitative coal characterization
International Journal of Coal Geology, Volume 67, Issues 1-2, 3 May 2006, Pages 101-111

Retcofsky H.L, VanderHart D.L, (1978). ^{13}C---^{1}H Cross-polarization nuclear magnetic resonance spectra of macerals from coal Original Research Article
Fuel, Volume 57, Issue 7, July 1978, Pages 421-423

Rimstidt D.J, Vaughan D.J, (2003). Pyrite oxidation: a state-of-the-art assessment of the reaction mechanism
Geochimica et Cosmochimica Acta, Volume 67, Issue 5, March 2003, Pages 873-880

Robinson J.P, Kingman S.W, Snape C.E, Barranco R, Shang H, Bradley M.S.A, Bradshaw S.M, (2009). Remediation of oil-contaminated drill cuttings using continuous microwave heating
Chemical Engineering Journal, Volume 152, Issues 2-3, 15 October 2009, Pages 458-463

Robinson J.P, Kingman S.W, Snape C.E, Bradshaw S.M, Bradley M.S.A, Shang H, Barranco R, (2010). Scale-up and design of a continuous microwave treatment system for the processing of oil-contaminated drill cuttings
Chemical Engineering Research and Design, Volume 88, Issue 2, February 2010, Pages 146-154

Robinson J.P, Kingman S.W, Snape C.E, Shang H, Barranco R, Saeid A, (2009). Separation of polyaromatic hydrocarbons from contaminated soils using microwave heating
Separation and Purification Technology, Volume 69, Issue 3, 15 October 2009, Pages 249-254

Rosso K.M, Becker U, (1990). Proximity effects on semiconducting mineral surfaces II: : Distance dependence of indirect interactions
Geochimica et Cosmochimica Acta, Volume 67, Issue 5, March 2003, Pages 941-953

Rowson N.A, Rice N.M, (1990). Magnetic enhancement of pyrite by caustic microwave treatment
Minerals Engineering, Volume 3, Issues 3-4, 1990, Pages 355-361

Rowson N.A, Rice N.M, (1990). Desulphurisation of coal using low power microwave energy
Minerals Engineering, Volume 3, Issues 3-4, 1990, Pages 363-368

Rowson N.A. (1986). Coal desulphurisation by Microwave Energy, PhD Thesis
University of Leeds, UK

Sengupta A.N, (2002). An assessment of grindability index of coal
Fuel Processing Technology, Volume 76, Issue 1, 20 April 2002, Pages 1-10

Serway R.A (1996). Physics for Scientists and Engineers,
Fifth Edition, John Wiley & Sons, Inc., USA

Sfihi H, Legrand A.P, Doussot J, Guy A, (1996). Solid-state ^{13}C NMR study of β-cyclodextrin/substituted aromatic ketone complexes: evidence for two kinds of complexation of the guest molecules Original Research Article

Colloids and Surfaces A: Physicochemical and Engineering Aspects, Volume 115, 30 August 1996, Pages 115-126

Shang H, Snape C.E, Kingman S.W, Robinson J.P, (2006). Microwave treatment of oil-contaminated North Sea drill cuttings in a high power multimode cavity
Separation and Purification Technology, Volume 49, Issue 1, 1 April 2006, Pages 84-90

Shuey R.T., (1976). Semiconductor Ore Minerals (Developments in Economic Geology 4) Elsevier, Amsterdam

Smart J.P, Morgan D.J, (1994). The effectiveness of multi-fuel reburning in an internally fuel-staged burner for NO_x reduction
Fuel, Volume 73, Issue 9, September 1994, Pages 1437-1442

Solum M.S, Pugmire R.J, Jagtoyen M, Derbyshire F, (1995). Evolution of carbon structure in chemically activated wood Original Research Article
Carbon, Volume 33, Issue 9, 1995, Pages 1247-1254

Speight J.G, Moschopedis S.E, (1986). The co-processing of coal with heavy feedstocks
Fuel Processing Technology, Volume 13, Issue 3, August 1986, Pages 215-232

Speight J.G, (1986). Handbook of Coal Analysis
Wiley and Sons, New York

Speliotis D.E, (1999). Magnetic recording beyond the first 100 Years
Journal of Magnetism and Magnetic Materials, Volume 193, Issues 1-3, March 1999, Pages 29-35

Srinivasachar S, Boni A.A, (1989). A kinetic model for pyrite transformations in a combustion environment
Fuel, Volume 68, Issue 7, July 1989, Pages 829-836

Srinivasachar S, Helble J.J, Boni A.A, (1990). Mineral behavior during coal combustion 1. Pyrite transformations
Progress in Energy and Combustion Science, Volume 16, Issue 4, 1990, Pages 281-292

Stach E, (1982). Textbook of Coal Petrography, 2nd Edition, ISBN 3443390684

Suelves I, Moliner R, Lázaro M.J, (2000). Synergetic effects in the co-pyrolysis of coal and petroleum residues: influences of coal mineral matter and petroleum residue mass ratio.
Journal of Analytical and Applied Pyrolysis, Volume 55, Issue 1, May 2000, Pages 29-41

Swain M.J, James S.J, Swain M.V.L, (2008). Effect of power output reduction of domestic microwave ovens after continuous (intermittent) use on food temperature after reheating
Journal of Food Engineering, Volume 87, Issue 1, July 2008, Pages 11-15

ten Brink H.M, Eenkhoorn S, Hamburg G, (1996). A fundamental investigation of the flame kinetics of coal pyrite
Fuel, Volume 75, Issue 8, June 1996, Pages 945-951

Thomasson J, Coin C, Kahraman H, Fredericks P.M, (2000). Attenuated total reflectance infrared microspectroscopy of coal
Fuel, Volume 79, Issue 6, May 2000, Pages 685-691

Thomas L, (1992) Handbook of Practical Coal Geology: John Wiley & Sons, Chichester, 338 pp. ISBN 0471935573

Toulmin III P, Barton Jr. P.B, (1964). A thermodynamic study of pyrite and pyrrhotite
Geochimica et Cosmochimica Acta, Volume 28, Issue 5, May 1964, Pages 641-671

Uhlig I , Szargan R, Nesbitt H.W, Laajalehto K, (2001). Surface states and reactivity of pyrite and marcasite
Applied Surface Science, Volume 179, Issues 1-4, 16 July 2001, Pages 222-229

Uslu T, Atalay Ü, Arol A.I, (2003). Effect of microwave heating on magnetic separation of pyrite
Colloids and Surfaces A: Physicochemical and Engineering Aspects, Volume 225, Issues 1-3, 15 September 2003, Pages 161-167

Uslu T, Atalay Ü, (2004). Microwave heating of coal for enhanced magnetic removal of pyrite,
Fuel Processing Technology, Volume 85, Issue 1, 15 January 2004, Pages 21-29

van Geet M, Swennen R, David P, (2001). Quantitative coal characterisation by means of microfocus X-ray computer tomography, colour image analysis and back-scattered scanning electron microscopy
International Journal of Coal Geology, Volume 46, Issue 1, March 2001, Pages 11-25

van Krevelen D.W. (1993). Coal : Typology – Physics – Chemistry - Constitution
3rd Revised Edition, Amsterdam, The Netherlands, Elsevier Science Publishers

Vassilev S.V, Vassileva C.G, (1996). Occurrence, abundance and origin of minerals in coals and coal ashes
Fuel Processing Technology, Volume 48, Issue 2, August 1996, Pages 85-106

Vassilev S.V, Vassileva C.G, (1998). Comparative chemical and mineral characterization of some Bulgarian coals
Fuel Processing Technology, Volume 55, Issue 1, April 1998, Pages 55-69

Vaughan D. J, Becker U, Wright K, (1997). Sulphide mineral surfaces: theory and experiment
International Journal of Mineral Processing, Volume 51, Issues 1-4, October 1997, Pages 1-14

Velázquez-Martí B, Gracia-López C, Plaza-Gonzalez P.J, (2005). Determination of Dielectric Properties of Agricultural Soil
Biosystems Engineering, Volume 91, Issue 1, May 2005, Pages 119-125

von Hippel A. (1954). Dielectric Materials and Applications
Technology Press of M.I.T, Wiley and Sons, New York

Vorster W, Rowson N.A, Kingman S.W, (2001). The effect of microwave radiation upon the processing of Neves Corvo copper ore
International Journal of Mineral Processing, Volume 63, Issue 1, June 2001, Pages 29-44

Vuthaluru H.B, (1999). Remediation of ash problems in pulverised coal-fired boilers
Fuel, Volume 78, Issue 15, December 1999, Pages 1789-1803

Vuthaluru H.B, Zhang D, Linjewile T.M, (2000). Behaviour of inorganic constituents and ash characteristics during fluidised-bed combustion of several Australian low-rank coals
Fuel Processing Technology, Volume 67, Issue 3, 1 September 2000, Pages 165-176

Wang H, Bigham J.M, Tuovinen O.H, (2007), Oxidation of marcasite and pyrite by iron-oxidizing bacteria and archaea Original Research Article
Hydrometallurgy, Volume 88, Issues 1-4, August 2007, Pages 127-131

Wang X.H, (1996). Interfacial Electrochemistry of Pyrite Oxidation and Flotation. I: Effect of Borate on Pyrite Surface Oxidation
Journal of Colloid and Interface Science, Volume 178, Issue 2, 25 March 1996, Pages 628-637

Ward C.R., (2002). Analysis and significance of mineral matter in coal seams
International Journal of Coal Geology, Volume 50, Issues 1-4, May 2002, Pages 135-168

Waters K.E, Rowson N.A, Greenwood R.W, Williams A.J, (2007). Characterising the effect of microwave radiation on the magnetic properties of pyrite
Separation and Purification Technology, Volume 56, Issue 1, 1 August 2007, Pages 9-17

Waters K.E, Rowson N.A, Greenwood R.W, Williams A.J, (2008). The effect of heat treatment on the magnetic properties of pyrite
Minerals Engineering, Volume 21, Issue 9, August 2008, Pages 679-682

Wells J.J, Wigley F, Foster D.J, Gibb W.H, Williamson J, (2004). The relationship between excluded mineral matter and the abrasion index of a coal
Fuel, Volume 83, Issue 3, February 2004, Pages 359-364

Wells J.J, Wigley F, Foster D.J, Livingston W.R, Gibb W.H, Williamson J, (2005). The nature of mineral matter in a coal and the effects on erosive and abrasive behaviour
Fuel Processing Technology, Volume 86, Issue 5, 25 February 2005, Pages 535-550

Weng S, Wang J, (1992). Exploration on the mechanism of coal desulfurization using microwave irradiation / acid washing method
Fuel Processing Technology, Volume 31, Issue 3, September 1992, Pages 233-240

Whateley M. K. G, (2002). Measuring, understanding and visualising coal characteristics—innovations in coal geology for the 21st century
International Journal of Coal Geology, Volume 50, Issues 1-4, May 2002, Pages 303-315

Whittacker G.. (1997). A basic Introduction to Microwave Chemistry
Oxford, Oxford University Press

Whittles D. N, Kingman S.W, Reddish D.J, (2003). Application of numerical modelling for prediction of the influence of power density on microwave-assisted breakage
International Journal of Mineral Processing, Volume 68, Issues 1-4, January 2003, Pages 71-91

Wills B.A, (1988). Proceedings of the XVIth international mineral processing congress: E. Forssberg (Ed.) Elsevier Science Publishers, 1988. Price US$365.75. 1996 pps (in 2 volumes) ISBN 0-444-42975-1
Minerals Engineering, Volume 1, Issue 4, 1988, Pages 369-374

Winter F, Kimmich R, (1982). NMR field-cycling relaxation spectroscopy of bovine serum albumin, muscle tissue, micrococcus luteus and yeast: $^{14}N^{1}H$-quadrupole dips Original Research Article
Biochimica et Biophysica Acta (BBA) - General Subjects, Volume 719, Issue 2, 24 November 1982, Pages 292-298

Xia D.K, Pickles C.A, (1999). Caustic roasting and leaching of electric arc furnace dust
Canadian Metallurgical Quarterly, Volume 38, Issue 3, July 1999, Pages 175-186

Yan J, Xu L, Yang J, (2008). A study on the thermal decomposition of coal-derived pyrite
Journal of Analytical and Applied Pyrolysis, Volume 82, Issue 2, July 2008, Pages 229-234

Yu Ming-C, Wen-Bin Y, Pe-Ming H, (2007). Micro-injection molding with the infrared assisted mold heating system
Materials Science and Engineering: A, Volumes 460-461, 15 July 2007, Pages 288-295

Zandaryaa S, Gavasci R, Lombardi F, Fiore A, (2001). Nitrogen oxides from waste incineration: control by selective non-catalytic reduction
Chemosphere, Volume 42, Issues 5-7, February 2001, Pages 491-497

Zavitsanos P.D, Golden J.A, Bleiler, K.W, Kinkend K, (1978). Coal Desulfurization Using Microwave Energy. In: EPA-600/7-78-089, US Environmental Protection Agency (1978).

Zhang J, Jian-Wei Y, Chang-Dong S, Yi-Qian X, (2000). Characterization of coals utilized in power stations of China. Fuel, Volume 79, Issue 1, January 2000, Pages 95-102

APPENDIX

Appendix – A4

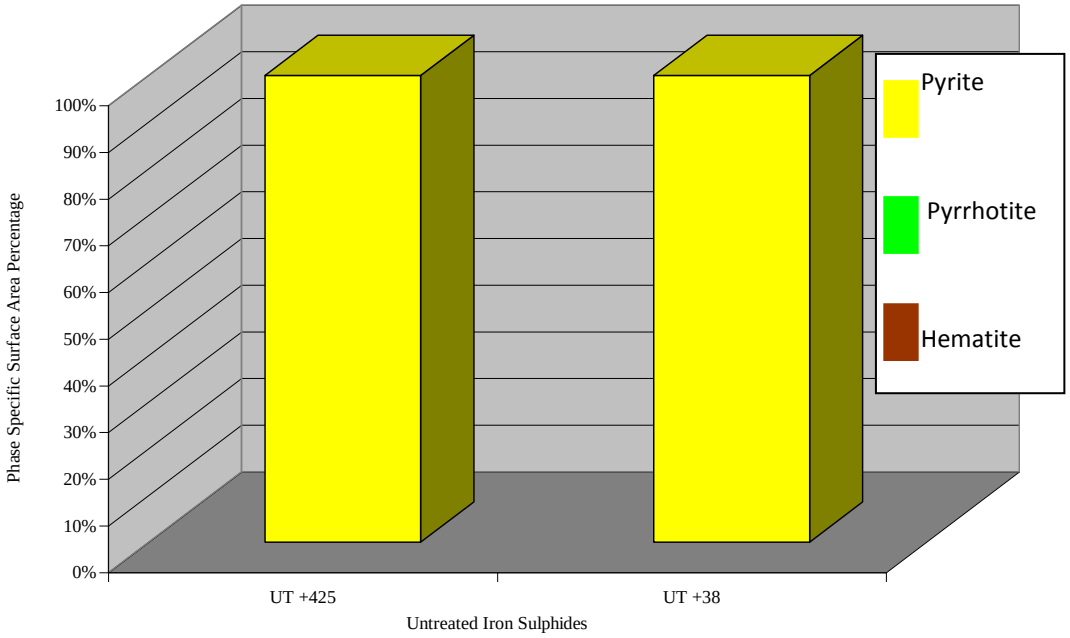

Figure 4.58 - Untreated samples of pyrite in-600+425µm and -53+38µm size fractions

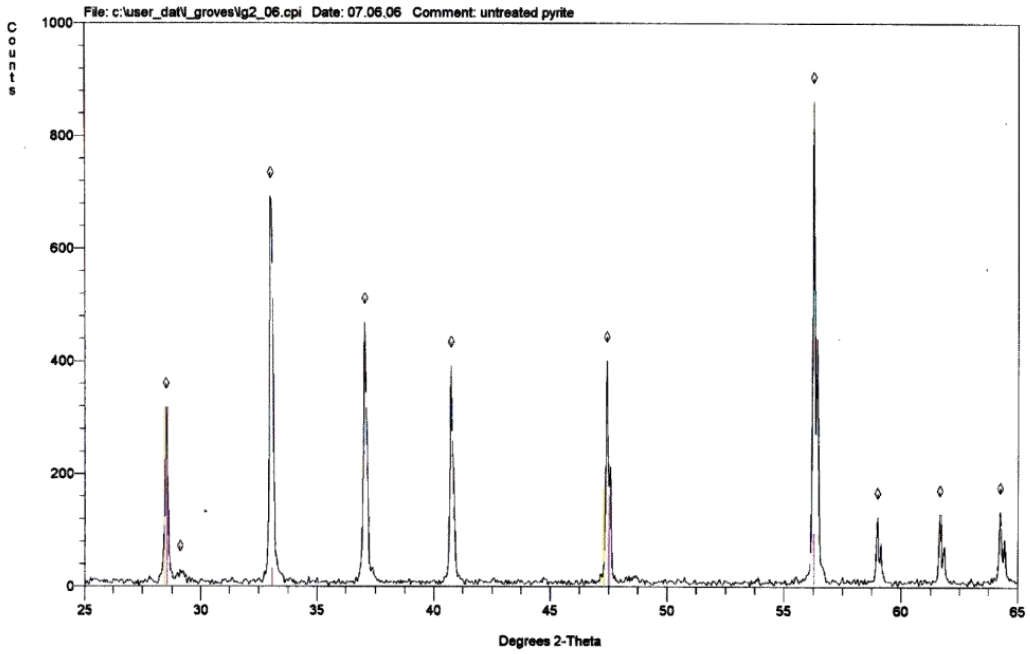

Figure 4.59 - XRD diffraction patterns of untreated -53+38µm pyrite

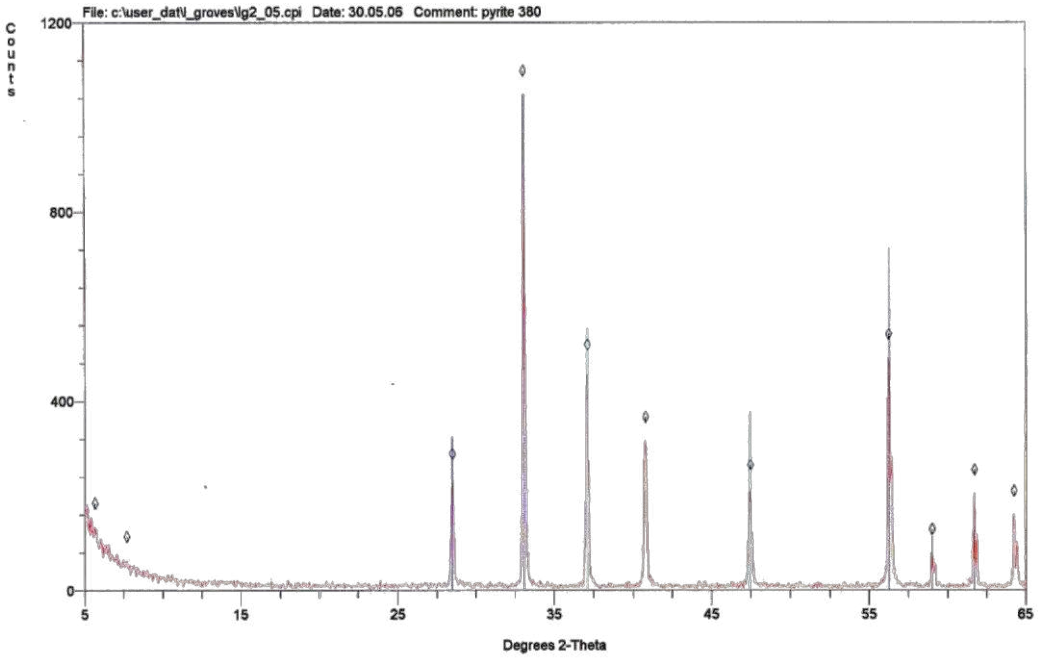

Figure 4.60 - XRD diffraction patterns of treated -53+38µm pyrite at 380°C

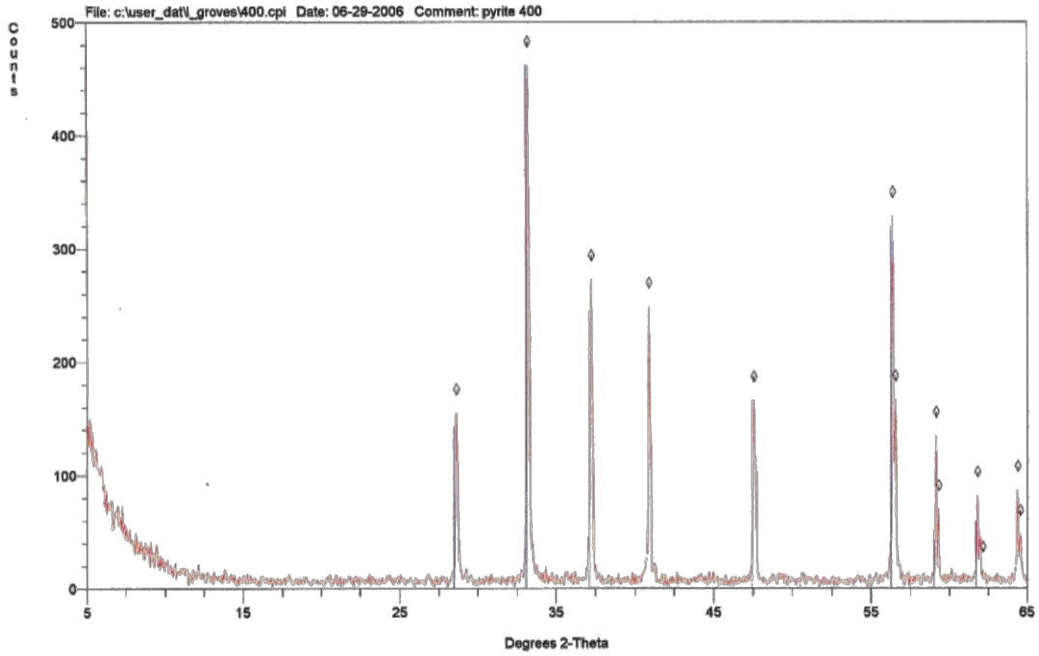

Figure 4.61 - XRD diffraction patterns of treated -53+38µm pyrite at 400°C

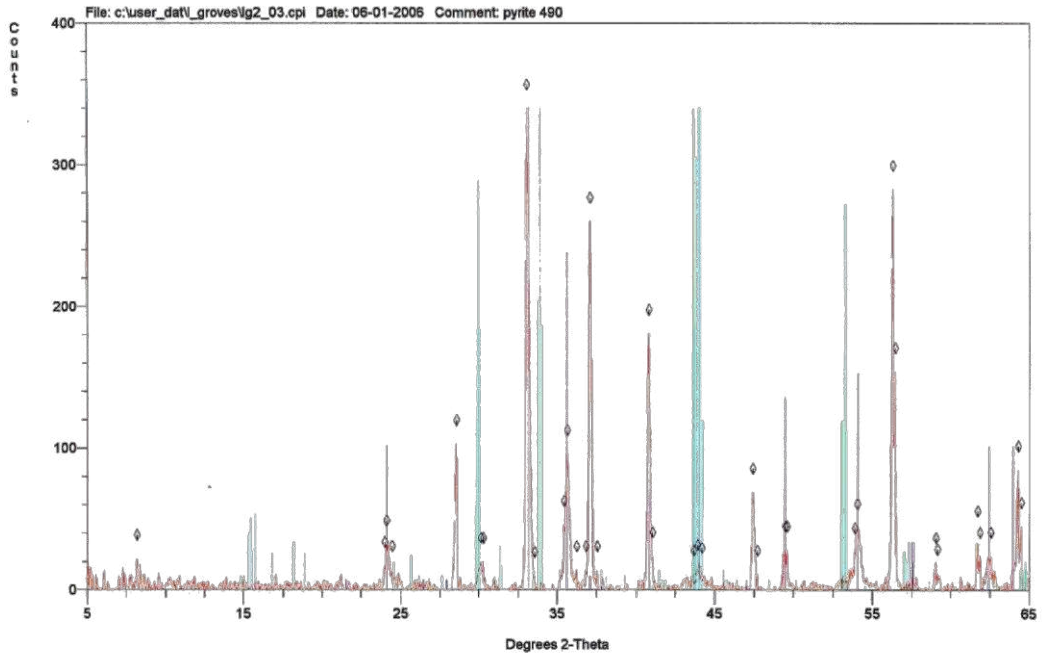

Figure 4.62 - XRD diffraction patterns of treated -53+38µm pyrite at 490°C

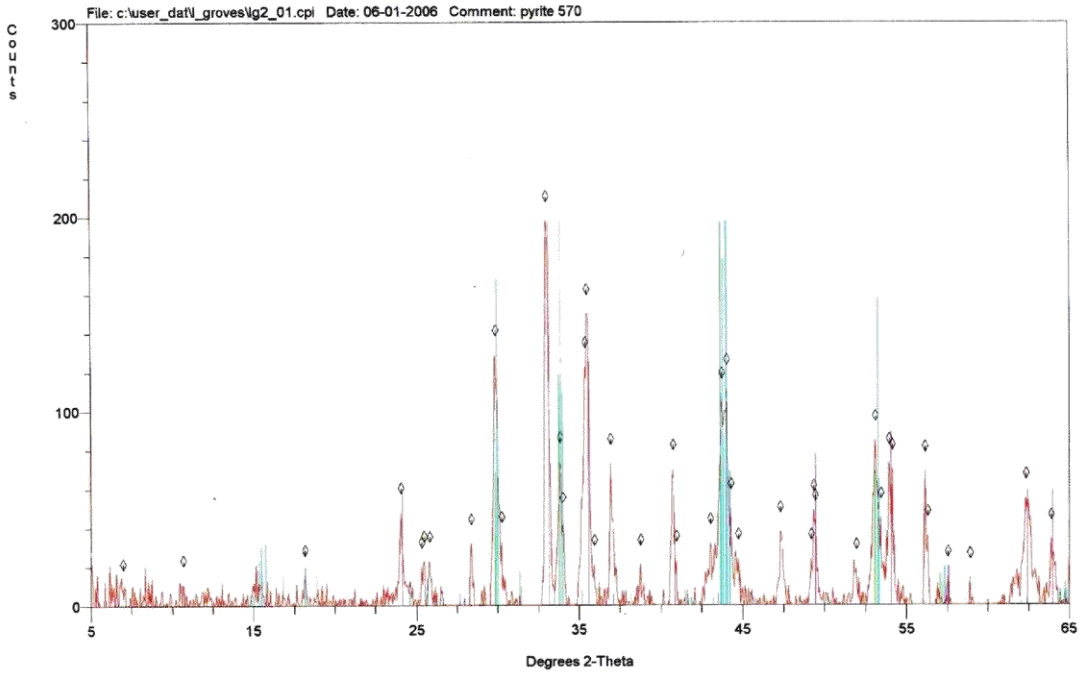

Figure 4.63 - XRD diffraction patterns of treated -53+38µm pyrite at 570°C

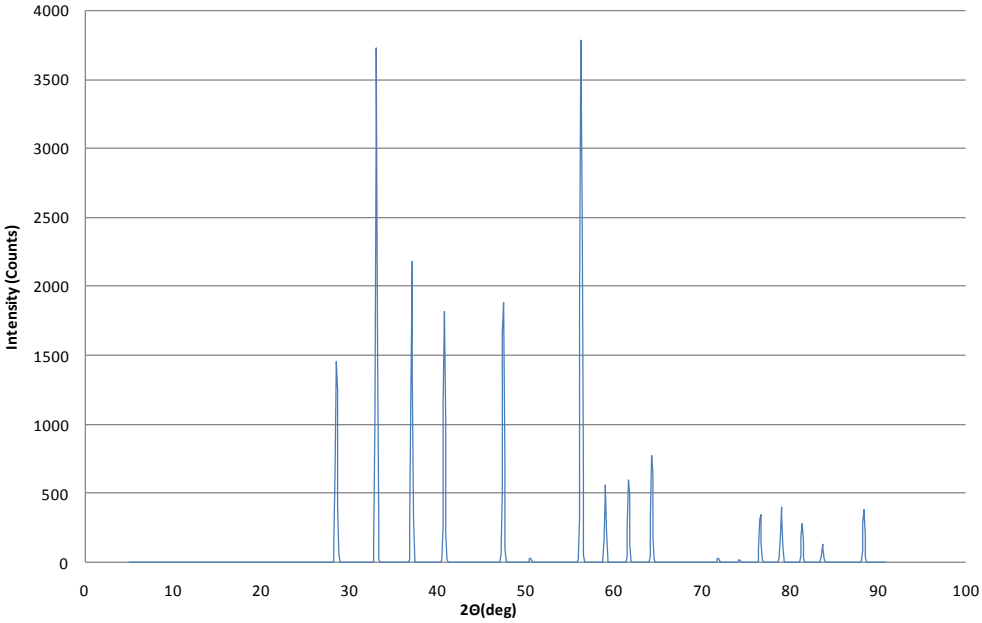

Figure 4.64 - Reference XRD diffraction pattern for Untreated Pyrite. (Source ICSD Database)

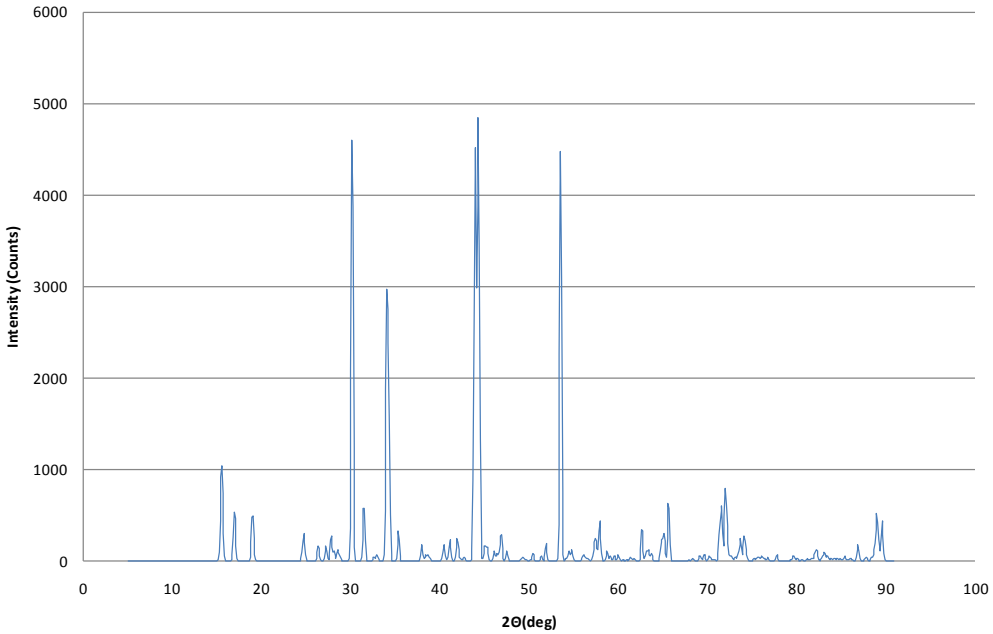

Figure 4.65 - Reference XRD diffraction pattern for Untreated Pyrrhotite. (Source ICSD Database)

Appendix – A5

Dielectric Loss Factor Predictions –Welbeck Coal

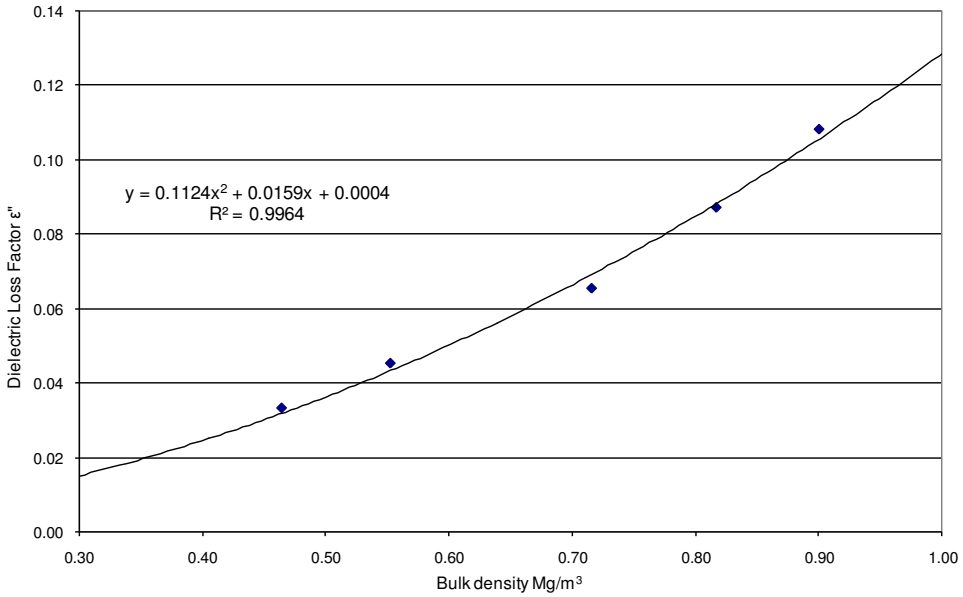

Figure 5.31 - Quadratic relationship between the dielectric Loss Factor of pulverised WelBeck coal samples and their bulk densities at 20°C and 912 MHz

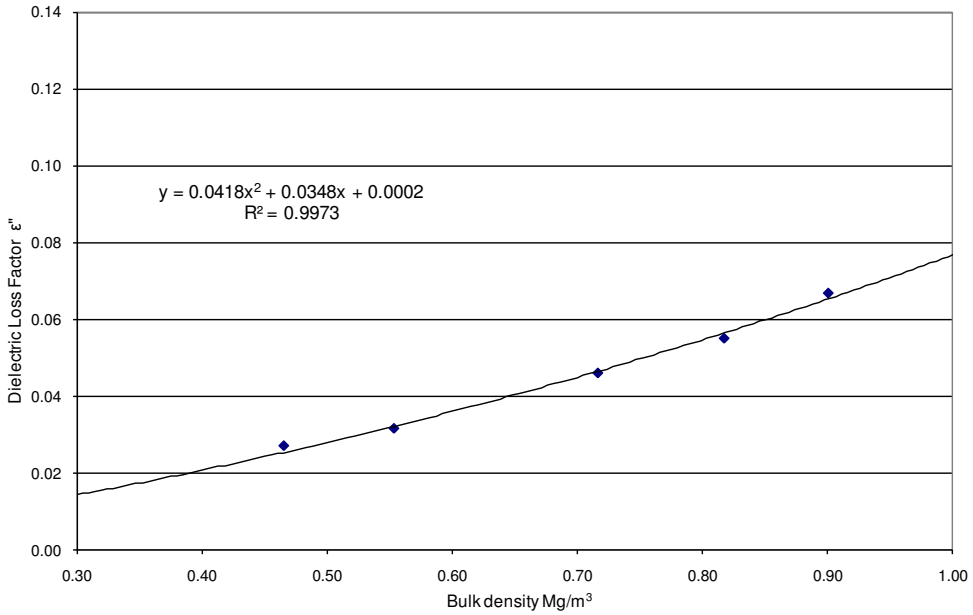

Figure 5.32 - Quadratic relationship between the dielectric Loss Factor

of pulverised WelBeck coal samples and their bulk densities at 20°C and 2.45GHz

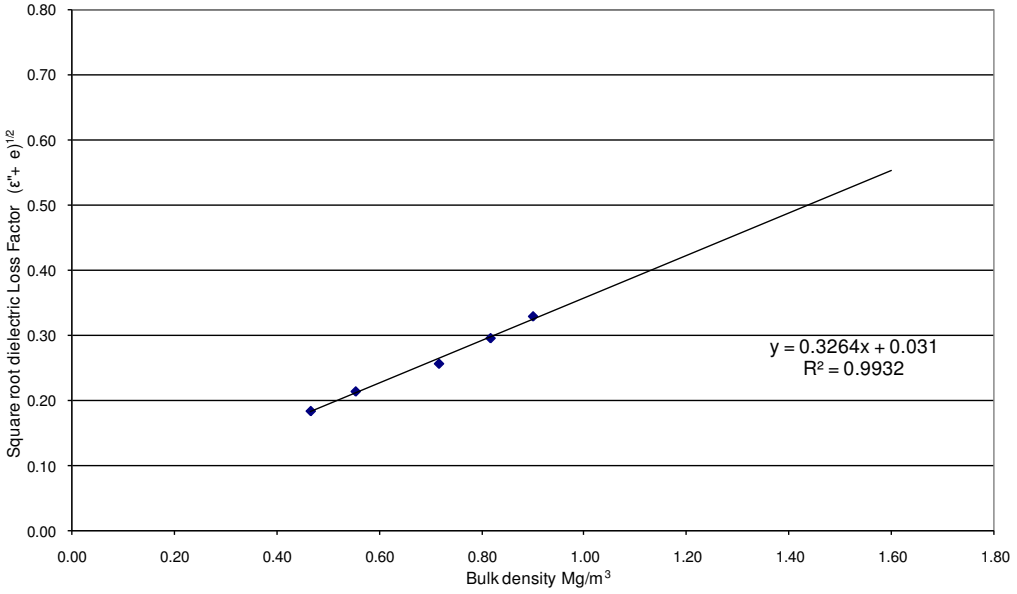

Figure 5.33 - Linear relationship of the Square roots of the dielectric Loss Factor of pulverised WelBeck coal samples and their bulk densities at 20°C and 912 MHz

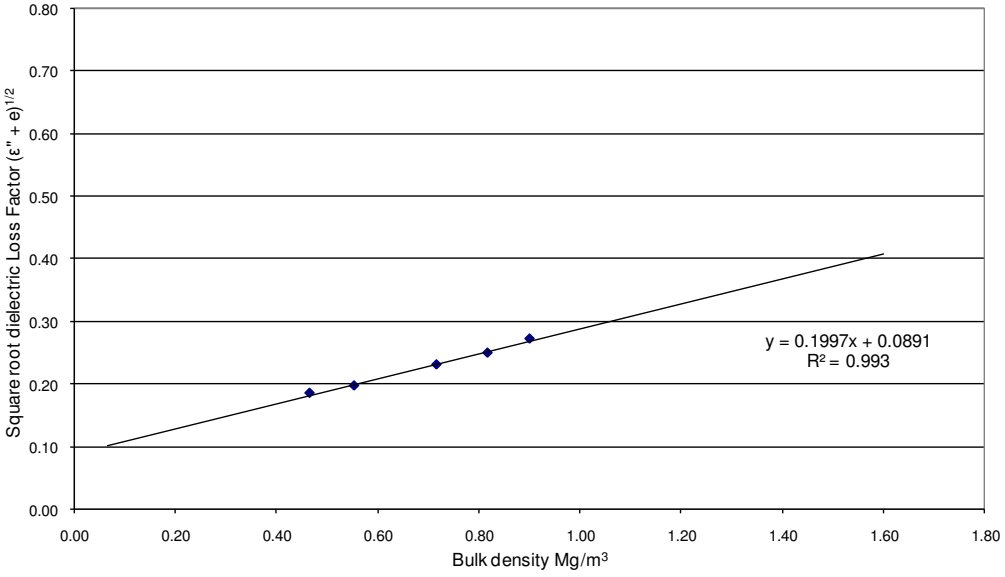

Figure 5.34 - Linear relationship of the Square roots of the dielectric Loss Factor of pulverised WelBeck coal samples and their bulk densities at 20°C and 2.45 GHz

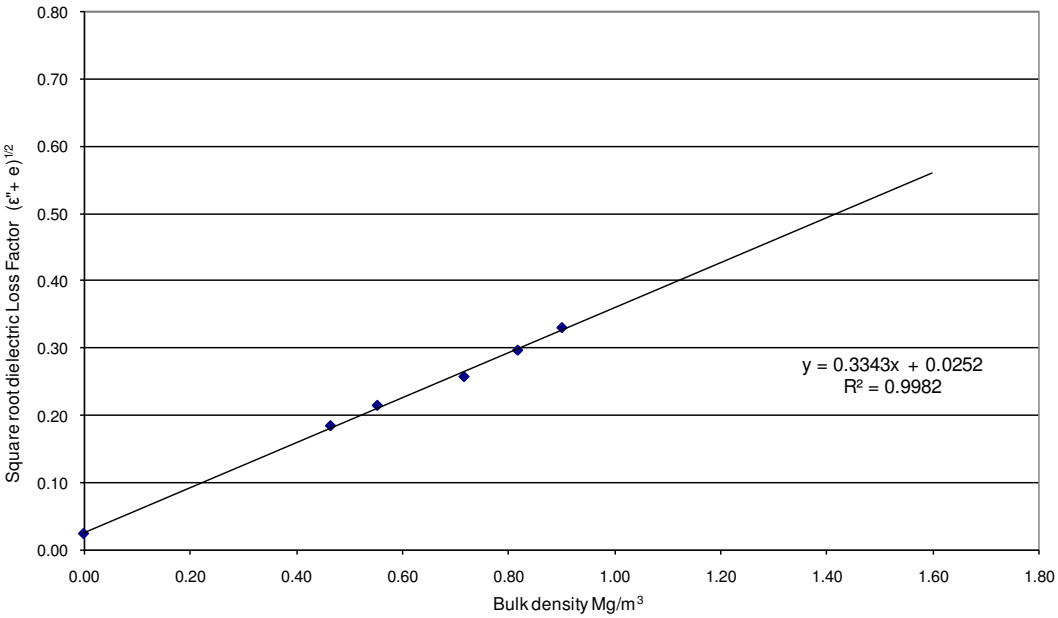

Figure 5.35 - Linear regression of the Square roots of the dielectric Loss Factor of pulverised WelBeck coal samples and their bulk densities at 20 ^{o}C and 911 MHz with point (0,$e^{1/2}$) included

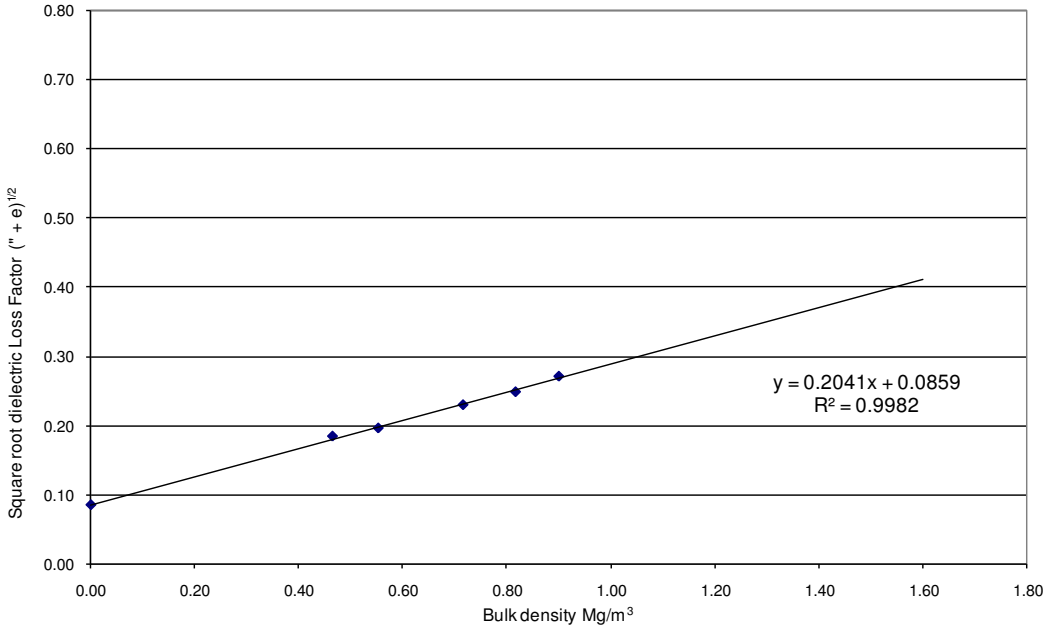

Figure 5.36 - Linear regression of the Square roots of the dielectric Loss Factor of pulverised WelBeck coal samples and their bulk densities at 20 ^{o}C and 2.45 GHz with point (0,$e^{1/2}$) included

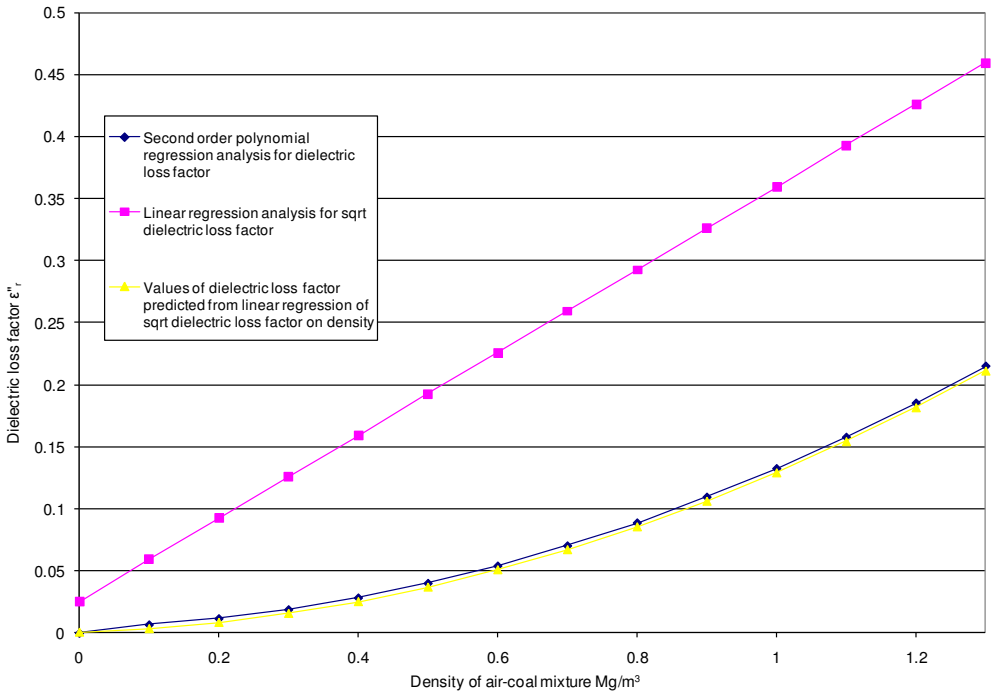

Figure 5.37 - Density dependence of the dielectric Loss Factor ε''_r and $(\varepsilon''_r)^{½}$ for Welbeck coal at 912 MHz and 20ºC

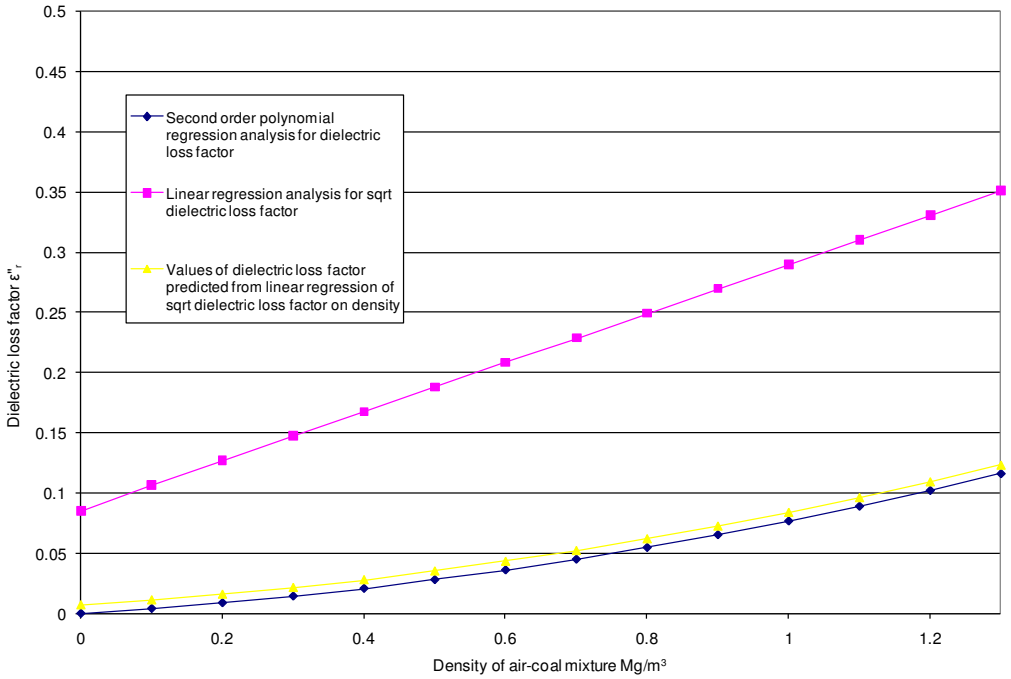

Figure 5.38 - Density dependence of the dielectric Loss Factor ε''_r and $(\varepsilon''_r)^{½}$ for Welbeck coal at 2.45 GHz and 20ºC

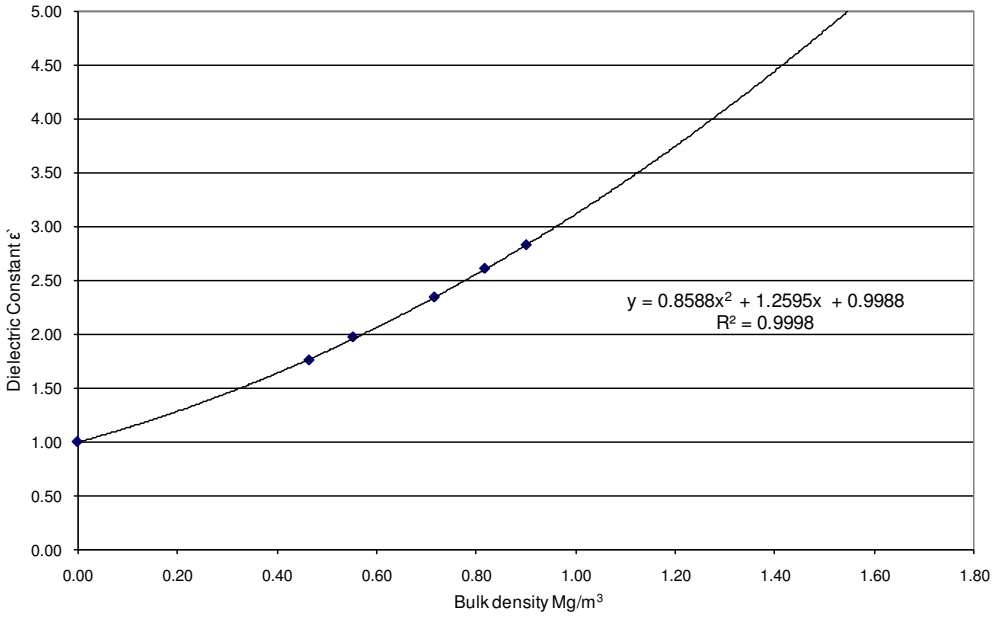

Figure 5.39 - Quadratic relationship between the dielectric Constant of pulverised WelBeck coal samples and their bulk densities at 20°C and 912 MHz

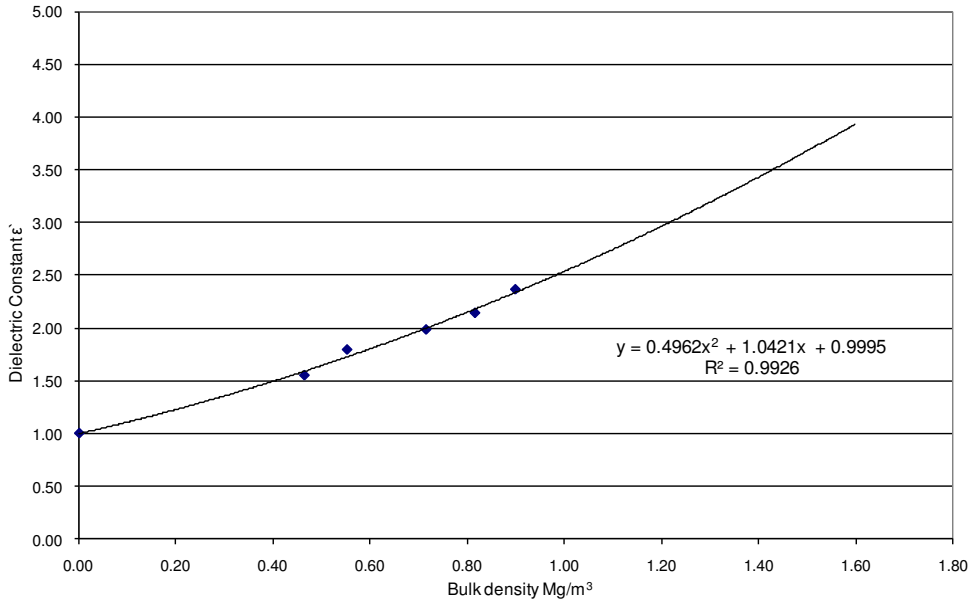

Figure 5.40 - Quadratic relationship between the dielectric Constant of pulverised WelBeck coal samples and their bulk densities at 20°C and 2.45 GHz

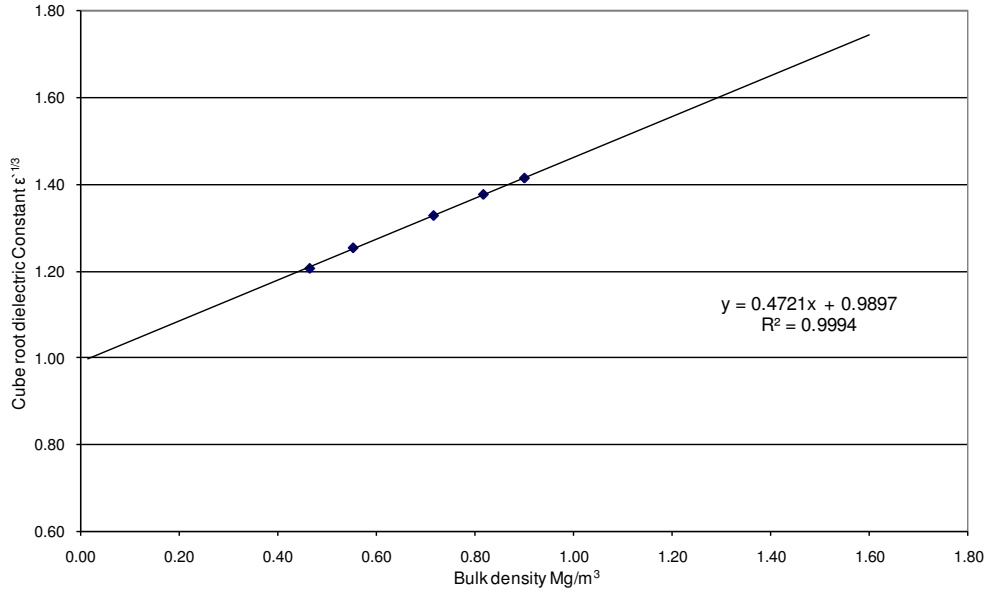

Figure 5.41 - Linear relationship between the cube roots of the dielectric constant of pulverised WelBeck coal samples and their bulk densities at 20°C and 911 MHz

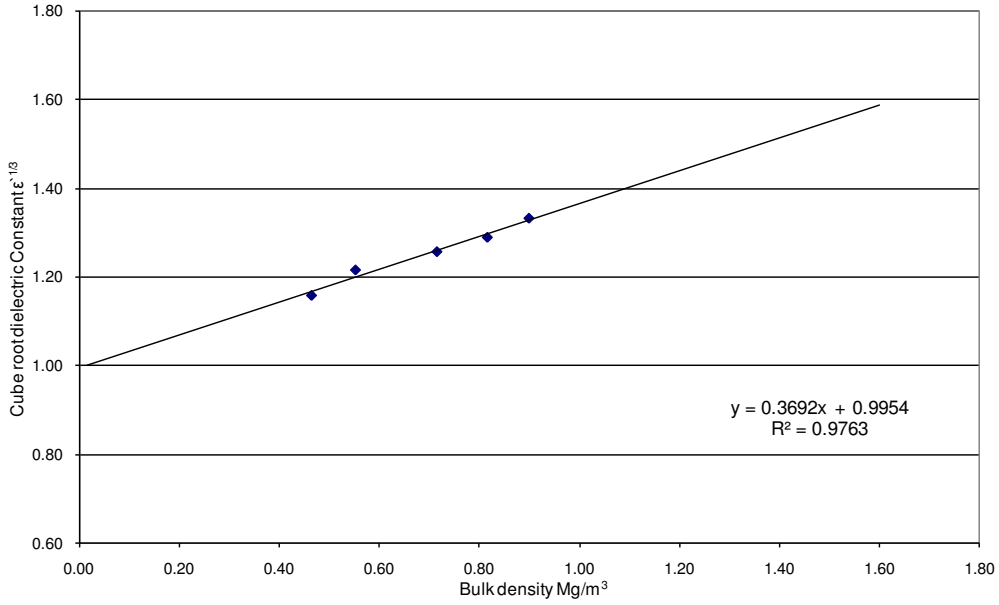

Figure 5.42 - Linear relationship between the cube roots of the dielectric constant of pulverised WelBeck coal samples and their bulk densities at 20°C and 2.45 GHz

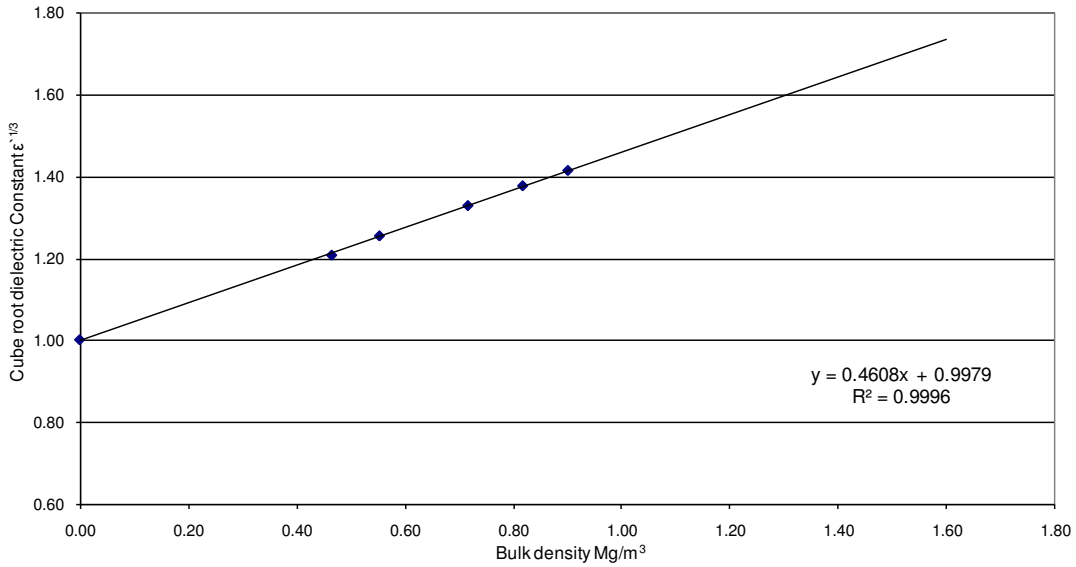

Figure 5.43 - Linear regression of the cube roots of the dielectric constant of pulverised WelBeck coal samples and their bulk densities at 20°C and 911 MHz with point (0,1) included

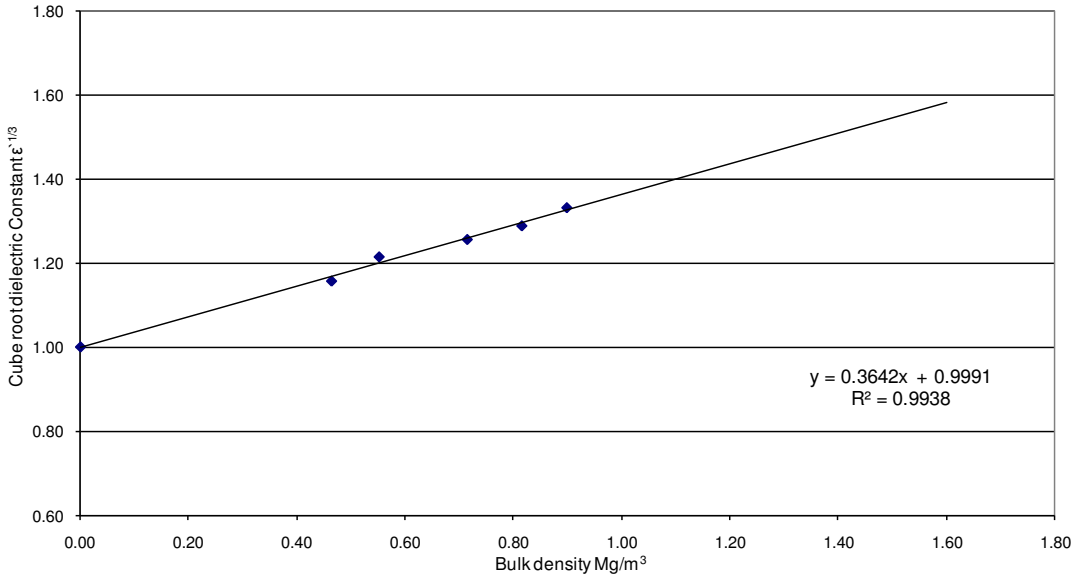

Figure 5.44 - Linear regression of the cube roots of the dielectric constant of pulverised WelBeck coal samples and their bulk densities at 20°C and 2.45 GHz with point (0,1) included

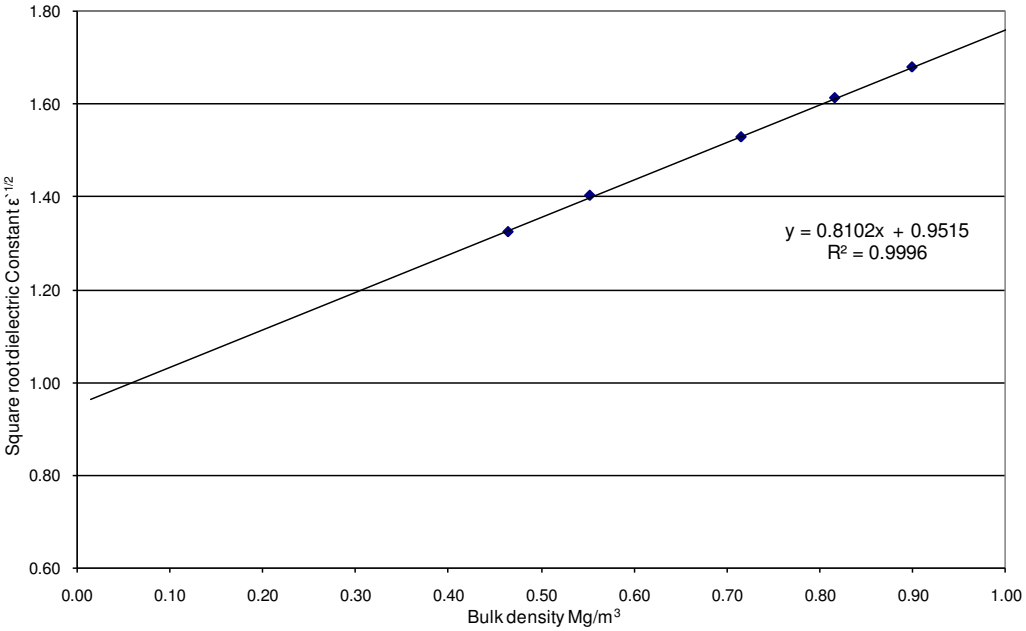

Figure 5.45 - Linear relationship between the Square roots of the dielectric constant of pulverised WelBeck coal samples and their bulk densities at 20°C and 911 MHz

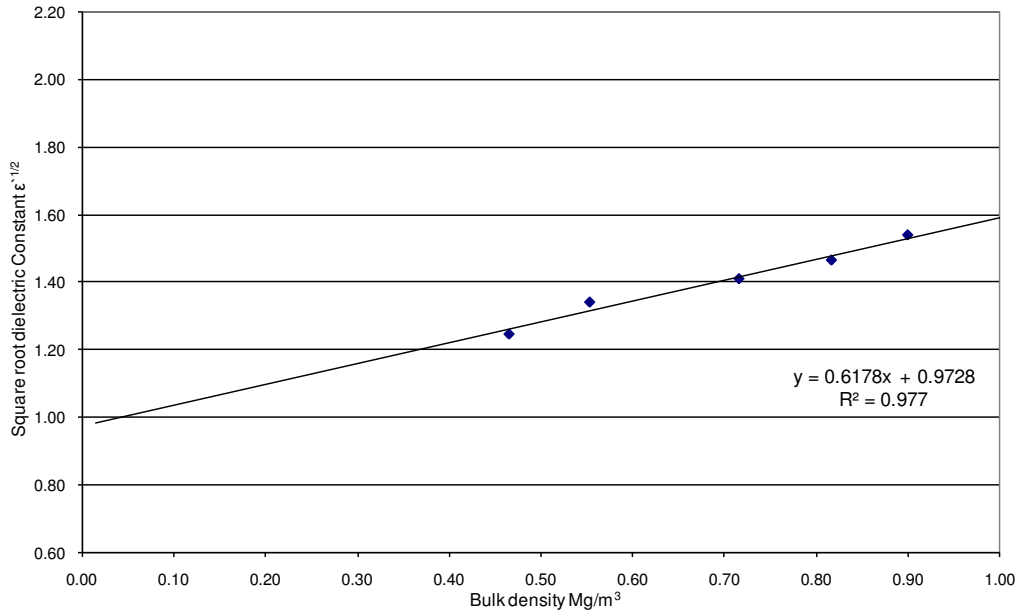

Figure 5.46 - Linear relationship between the Square roots of the dielectric constant of pulverised WelBeck coal samples and their bulk densities at 20°C and 2.45 GHz

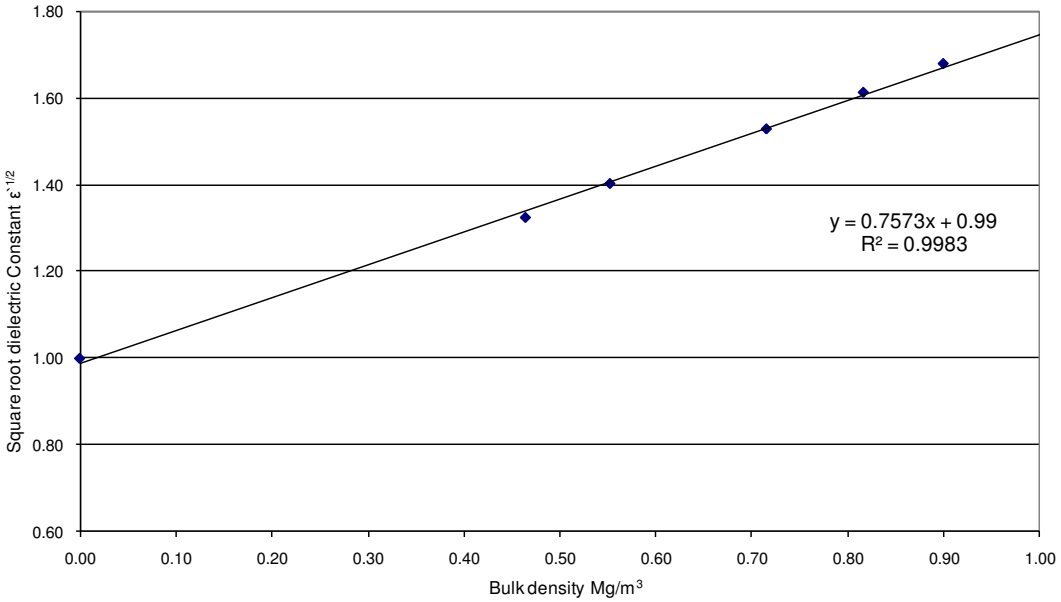

Figure 5.47 - Linear relationship between the Square roots of the dielectric constant of pulverised WelBeck coal samples and their bulk densities at 20°C and 911 MHz with point (0,1) included

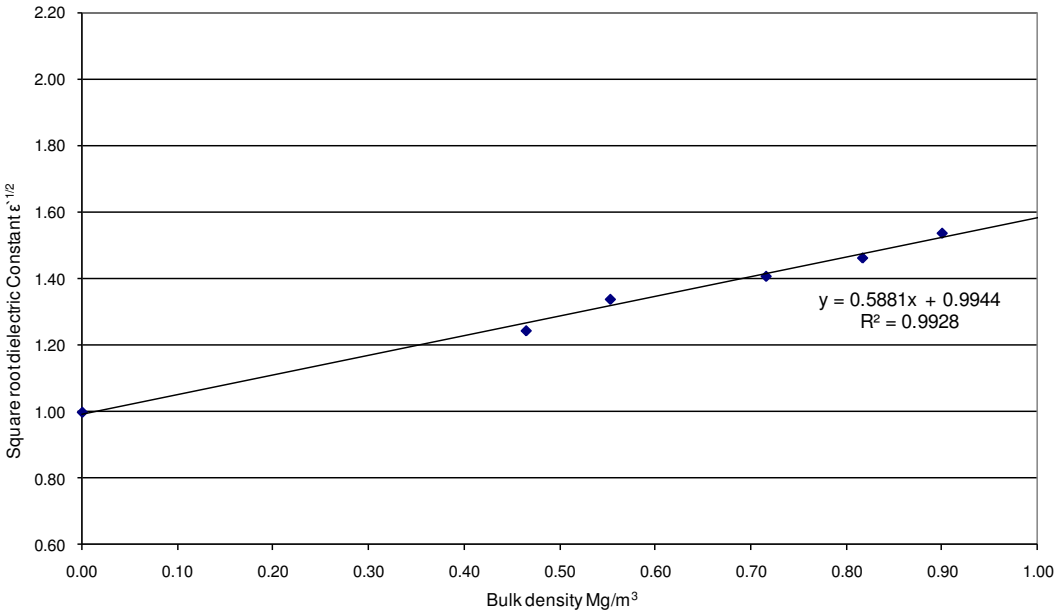

Figure 5.48 - Linear relationship between the Square roots of the dielectric constant of pulverised WelBeck coal samples and their bulk densities at 20°C and 2.45 GHz with point (0,1) included

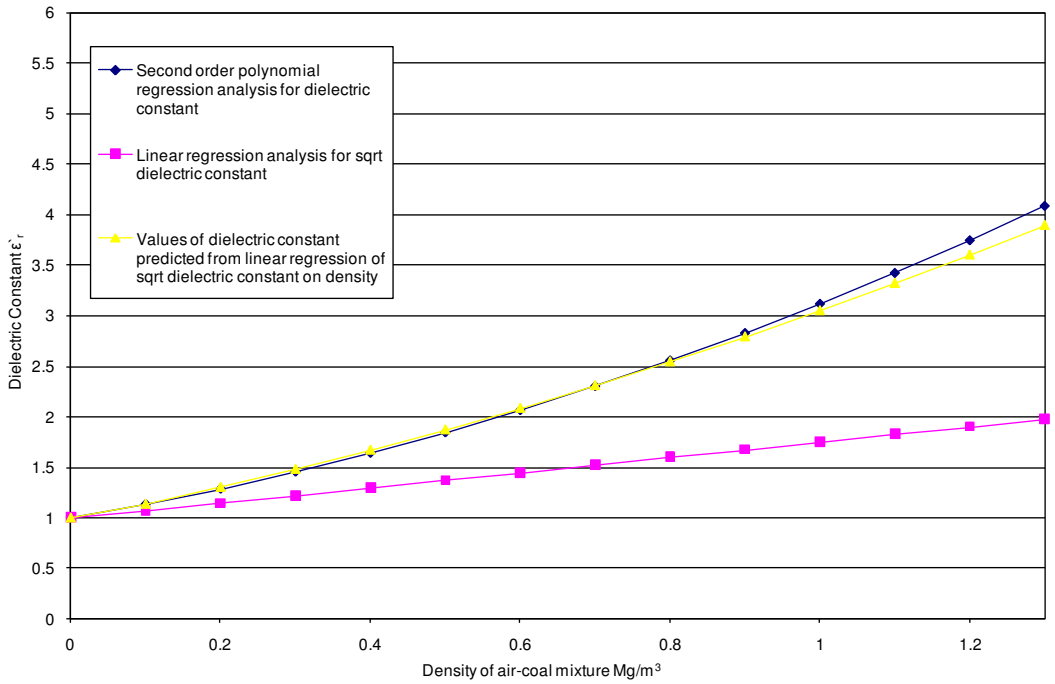

Figure 5.49 - Density dependence of the dielectric Constant $\varepsilon`_r$ and $(\varepsilon`_r)^{½}$ for Welbeck coal at 912 MHz and 20ºC

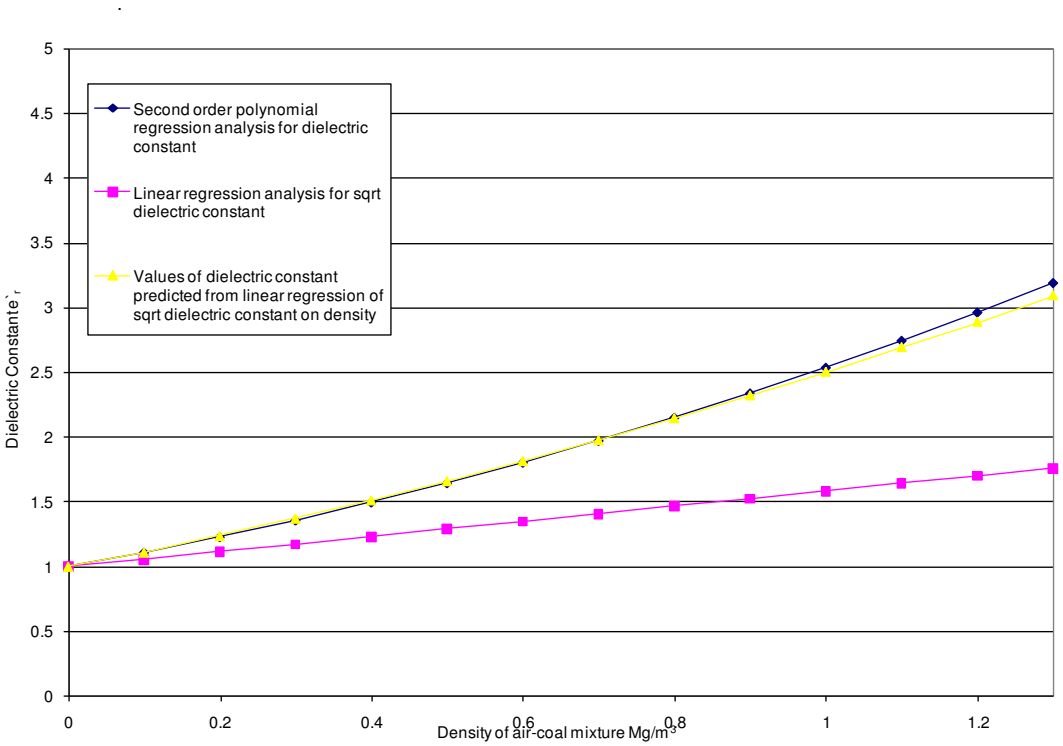

Figure 5.50 - Density dependence of the dielectric Constant $\varepsilon`_r$ and $(\varepsilon`_r)^{½}$ for Welbeck coal at 2.45 GHz and 20ºC

Dielectric Loss Factor Predictions –Dawmill Coal

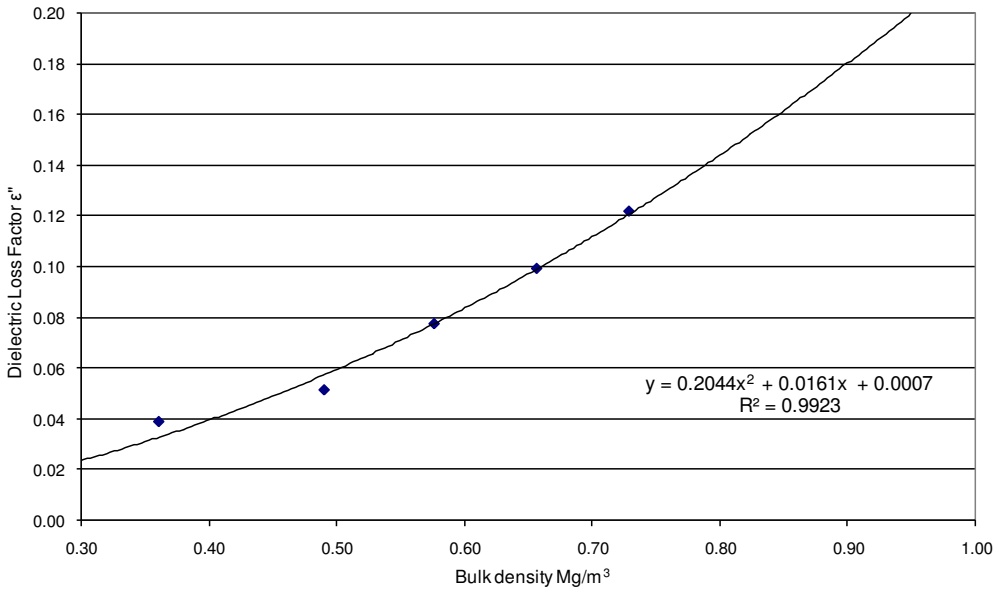

Figure 5.51 - Quadratic relationship between the dielectric Loss Factor of pulverised Dawmill coal samples and their bulk densities at 20°C and 912 MHz

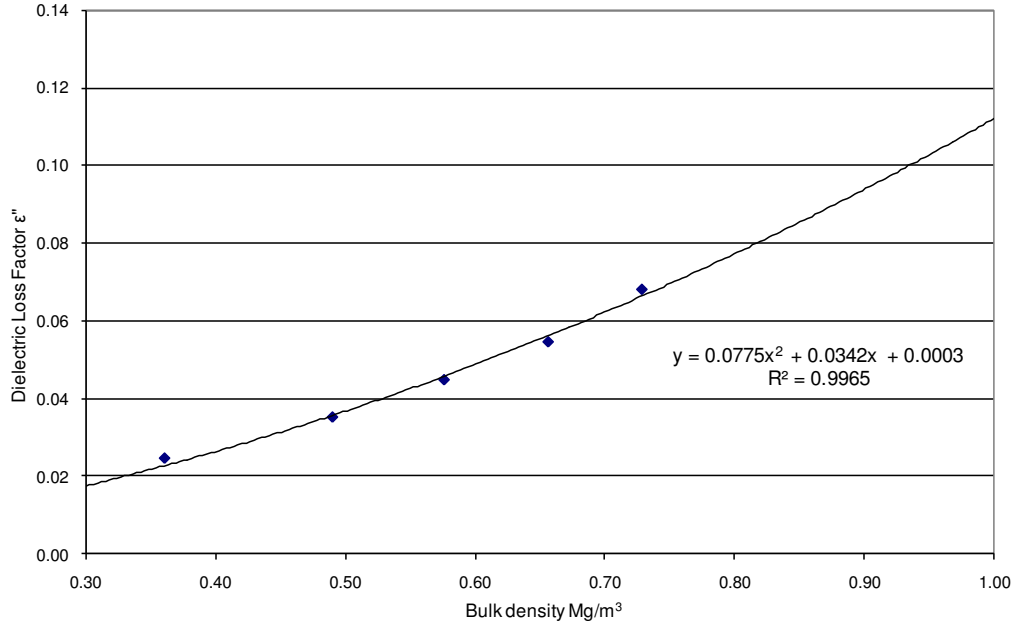

Figure 5.52 - Quadratic relationship between the dielectric Loss Factor of pulverised Dawmill coal samples and their bulk densities at 20°C and 2.45 GHz

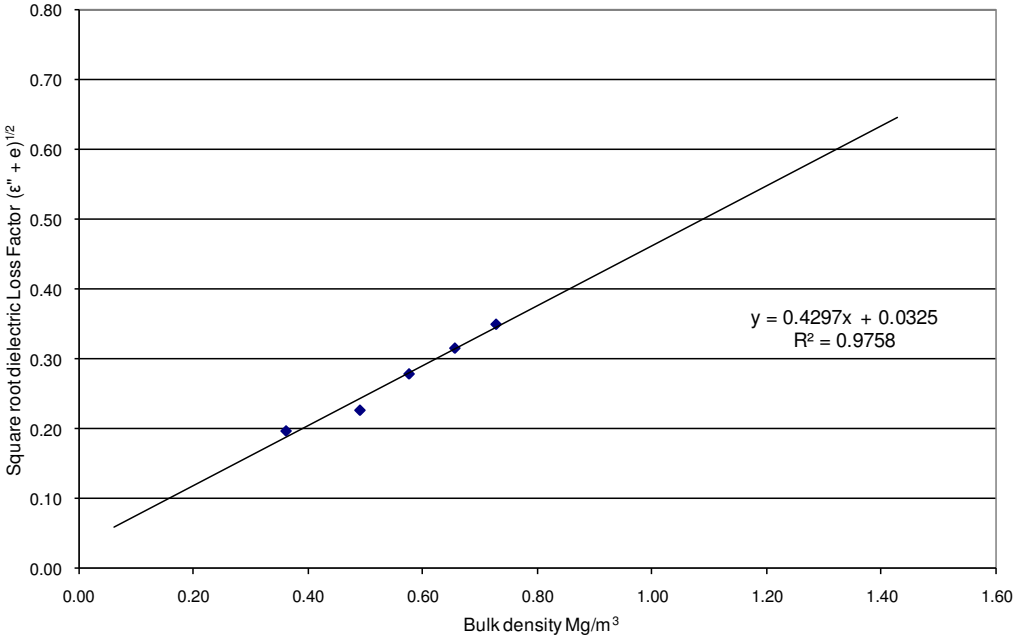

Figure 5.53 - Linear relationship of the Square roots of the dielectric Loss Factor of pulverised Dawmill coal samples and their bulk densities at 20°C and 912 MHz

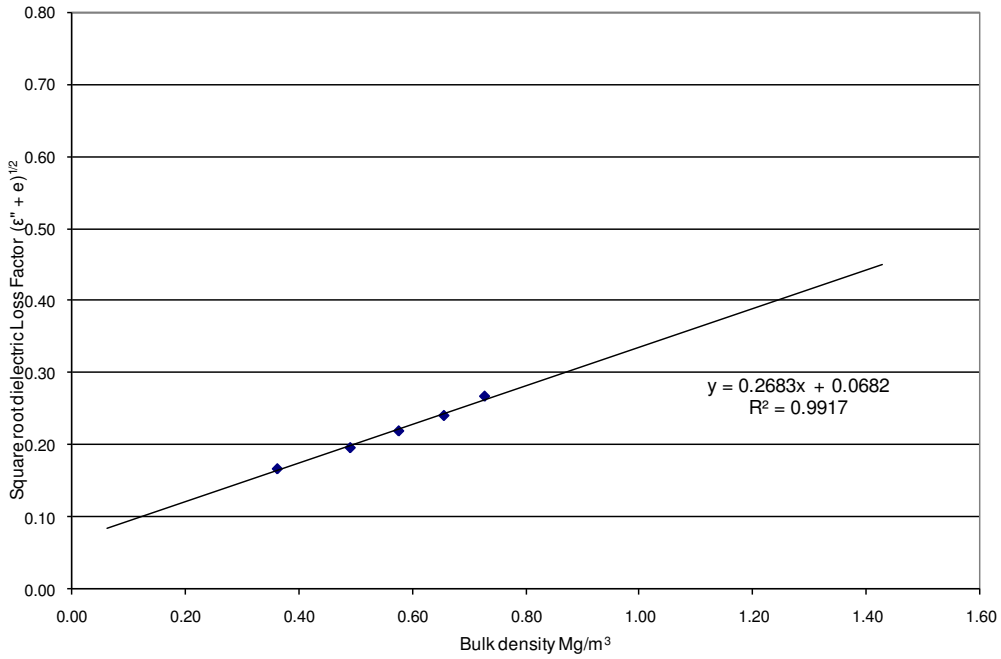

Figure 5.54 - Linear relationship of the Square roots of the dielectric Loss Factor of pulverised Dawmill coal samples and their bulk densities at 20°C and 2.45 GHz

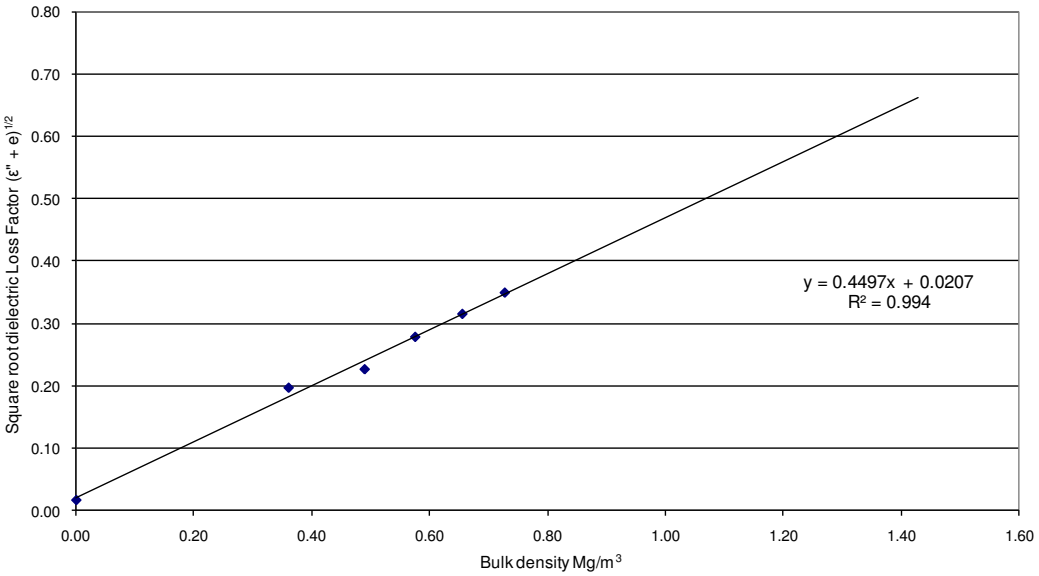

Figure 5.55 - Linear regression of the Square roots of the dielectric Loss Factorof pulverised Dawmill coal samples and their bulk densities at 20 ^{o}C and 911 MHz with point (0,e$^{1/2}$) included

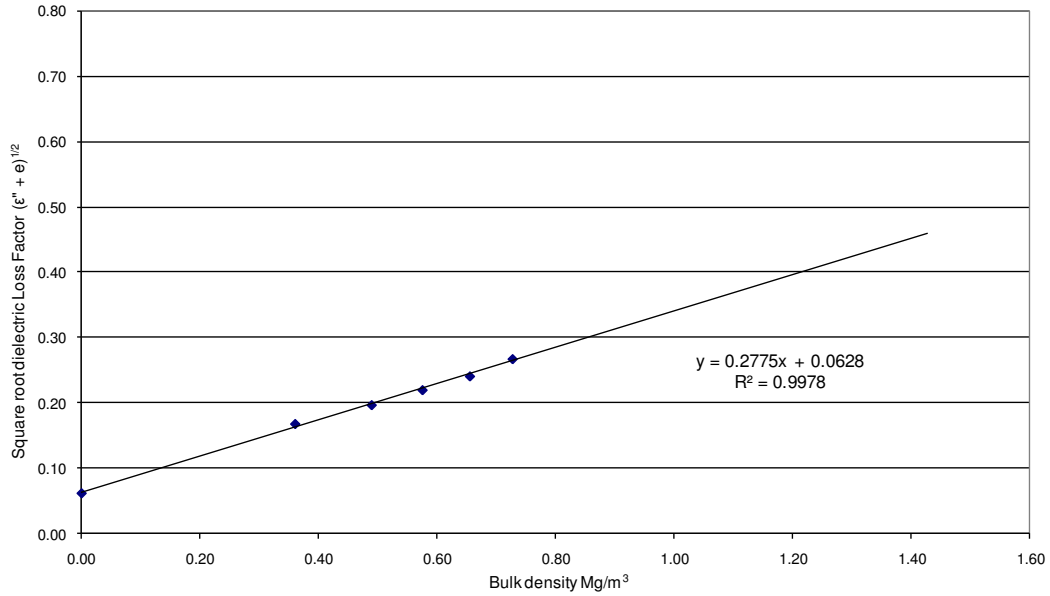

Figure 5.56 - Linear regression of the Square roots of the dielectric Loss Factor of pulverised Dawmill coal samples and their bulk densities at 20 ^{o}C and 2.45 GHz with point (0,e$^{1/2}$) included

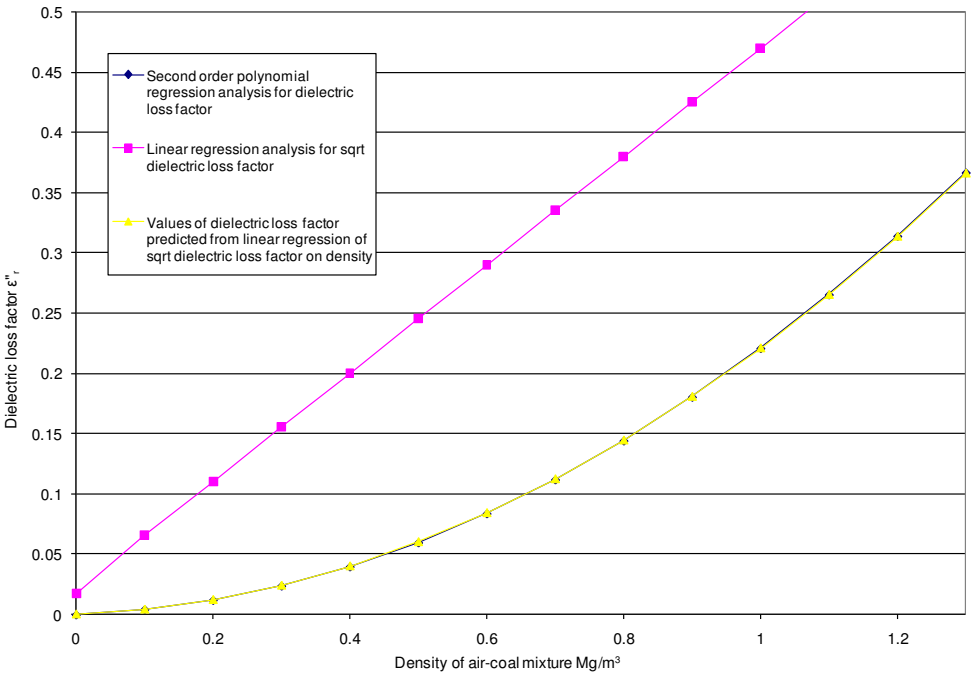

Figure 5.57 - Density dependence of the dielectric Loss Factor ε''_r and $(\varepsilon''_r)^{½}$ for Dawmill coal at 912 MHz and 20ºC

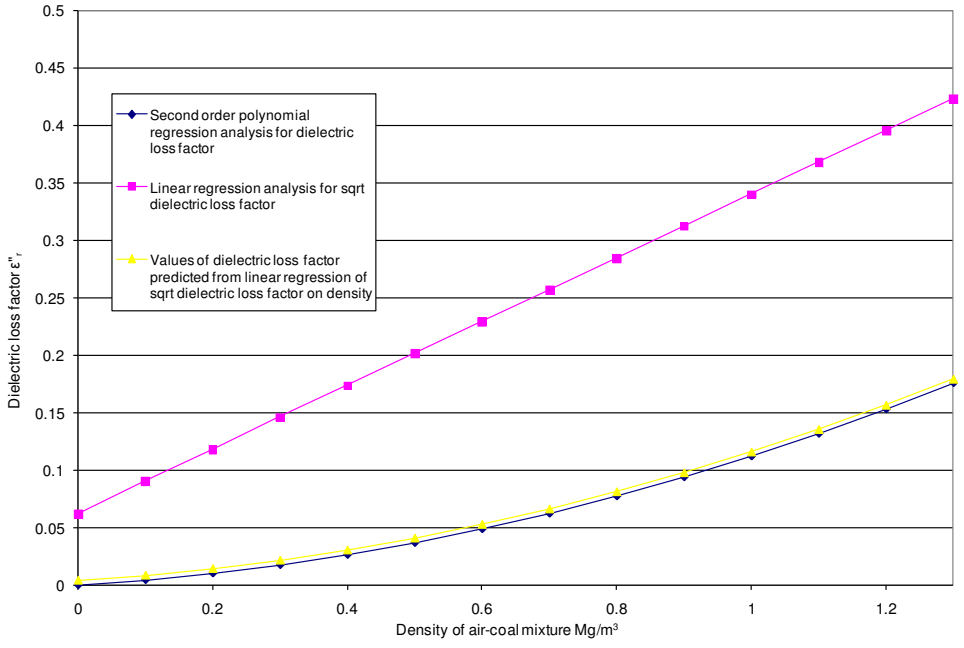

Figure 5.58 - Density dependence of the dielectric Loss Factor ε''_r and $(\varepsilon''_r)^{½}$ for Dawmill coal at 2.45 GHz and 20ºC

Dielectric Constant Predictions –Dawmill Coal

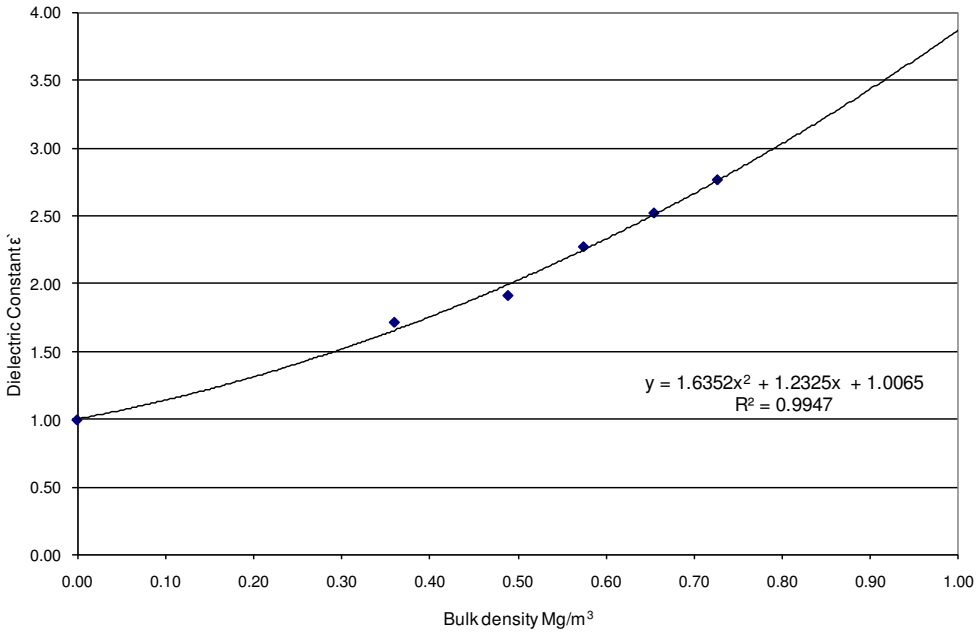

Figure 5.59 - Quadratic relationship between the dielectric Constant of pulverised Dawmill coal samples and their bulk densities at 20°C and 912 MHz

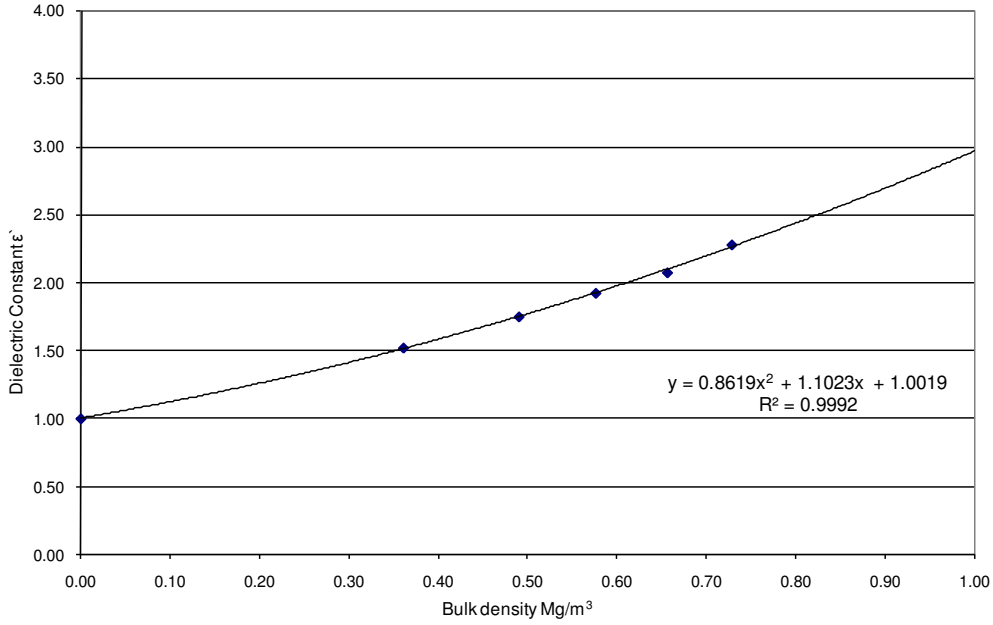

Figure 5.60 - Quadratic relationship between the dielectric Constant of pulverised Dawmill coal samples and their bulk densities at 20°C and 2.45 GHz

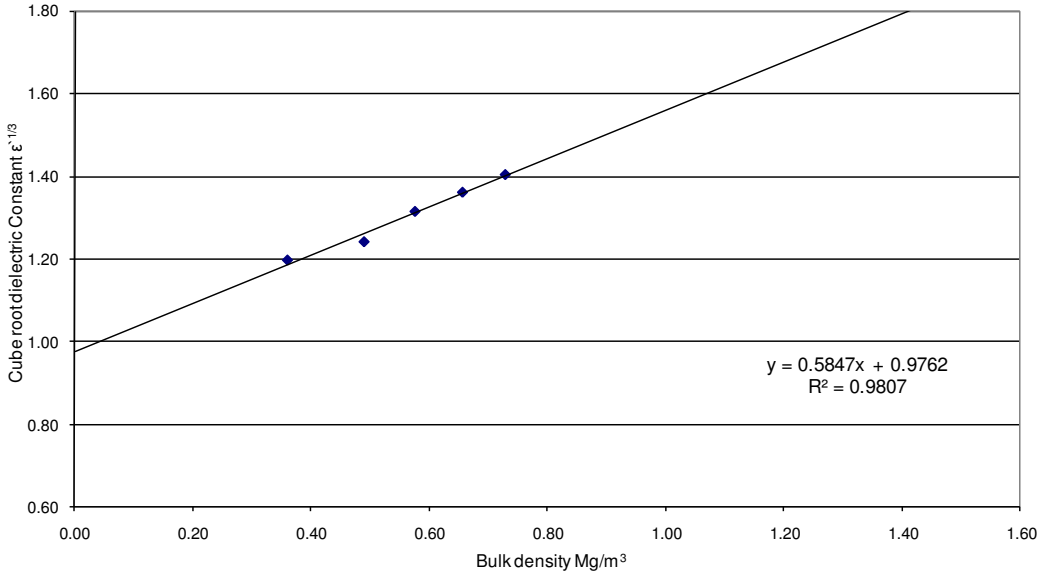

Figure 5.61 - Linear relationship between the cube roots of the dielectric constant of pulverised Dawmill coal samples and their bulk densities at 20°C and 911 MHz

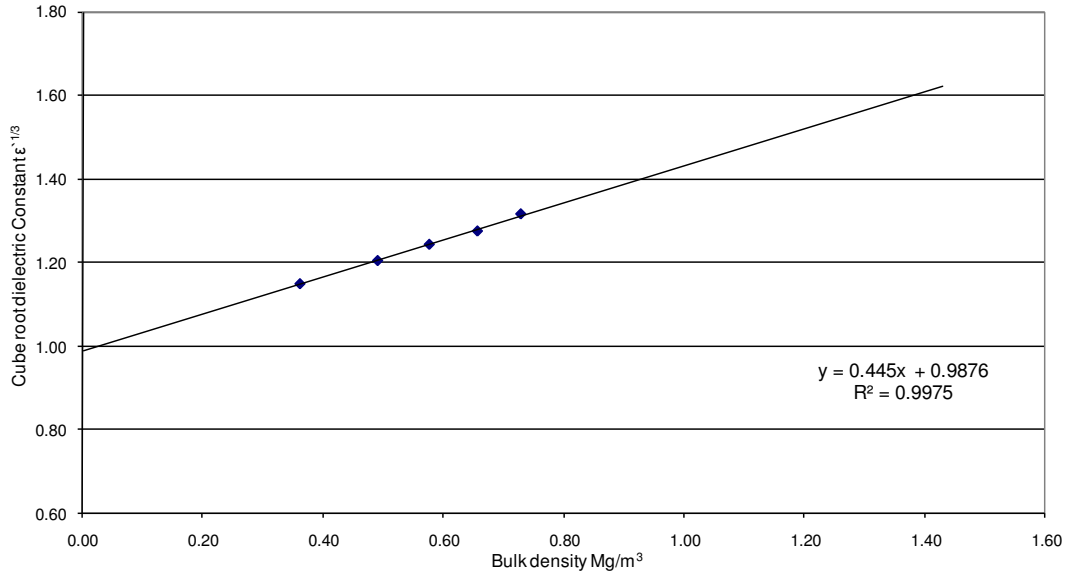

Figure 5.62 - Linear relationship between the cube roots of the dielectric constant of pulverised Dawmill coal samples and their bulk densities at 20°C and 2.45 GHz

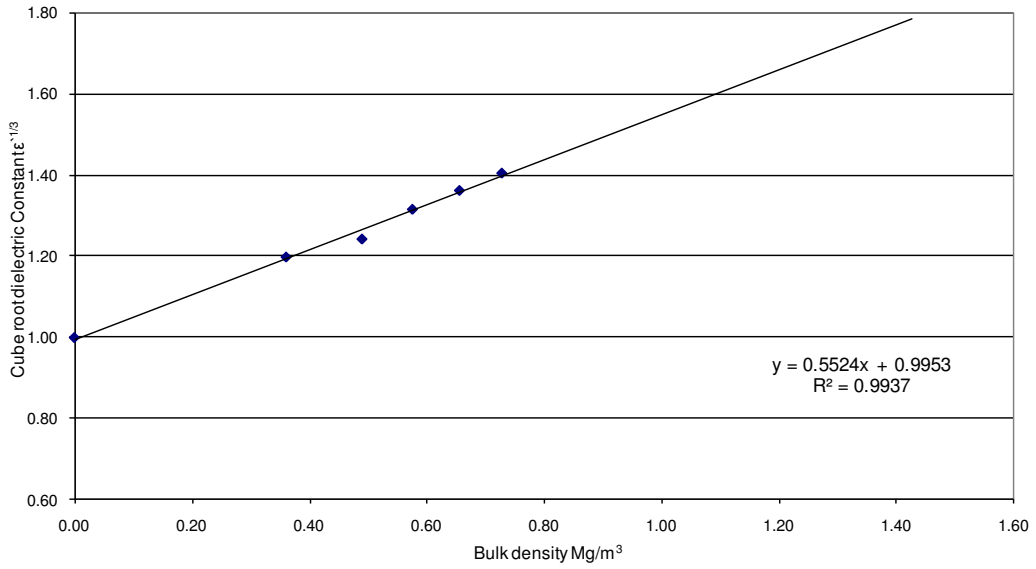

Figure 5.63 - Linear regression of the cube roots of the dielectric constant of pulverised Dawmill coal samples and their bulk densities at 20°C and 911 MHz with point (0,1) included

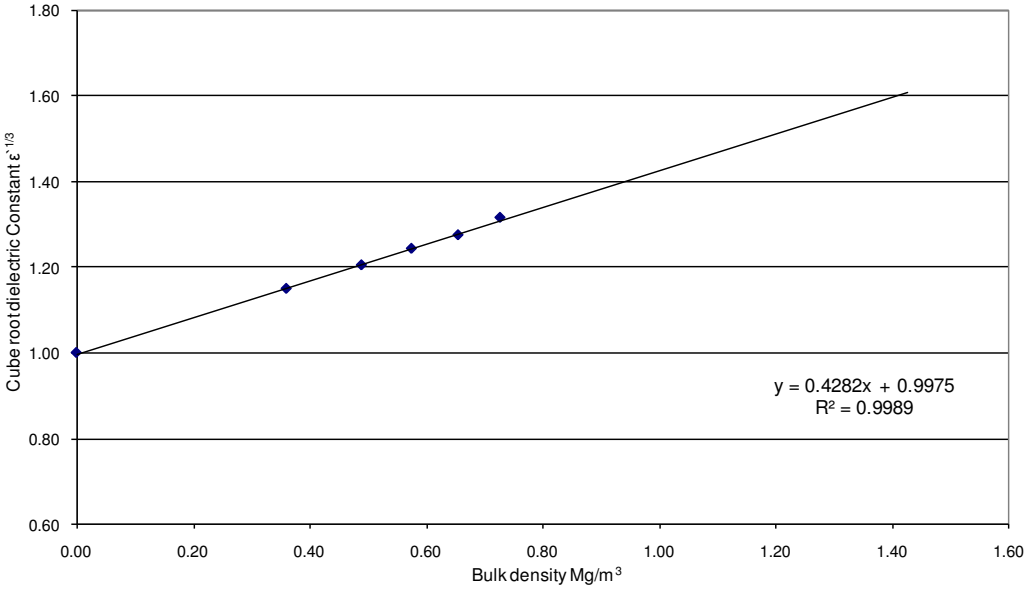

Figure 5.64 - Linear regression of the cube roots of the dielectric constant of pulverised Dawmill coal samples and their bulk densities at 20°C and 2.45 GHz with point (0,1) included

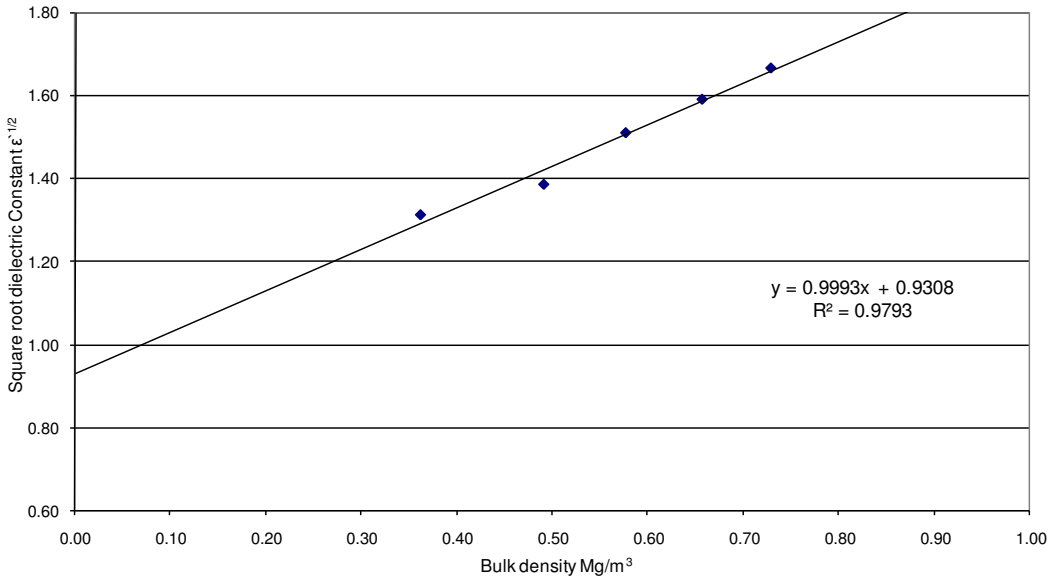

Figure 5.65 - Linear relationship between the Square roots of the dielectric constant of pulverised Dawmill coal samples and their bulk densities at 20°C and 911 MHz

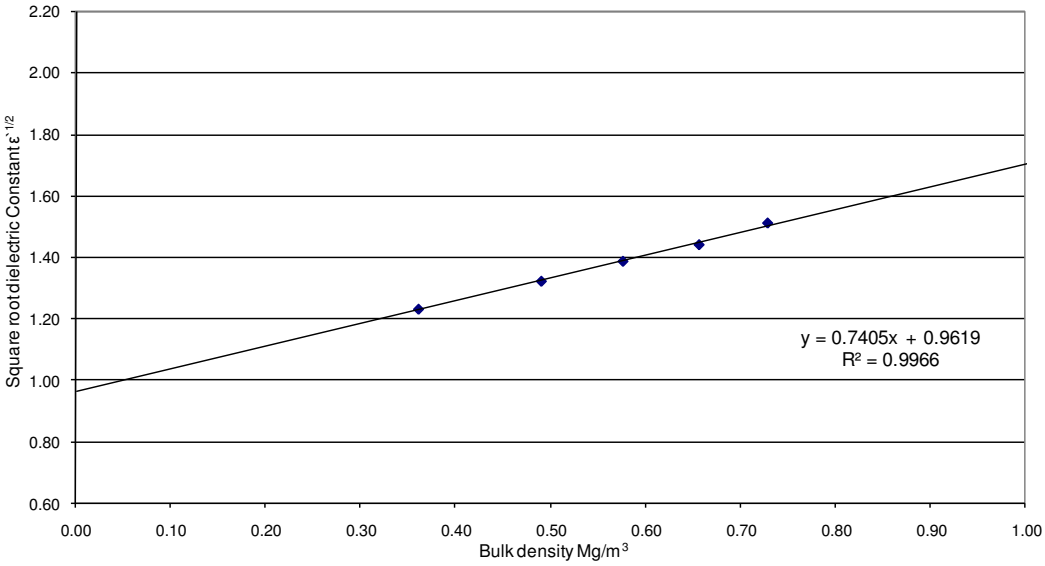

Figure 5.66 - Linear relationship between the Square roots of the dielectric constant of pulverised Dawmill coal samples and their bulk densities at 20°C and 2.45 GHz

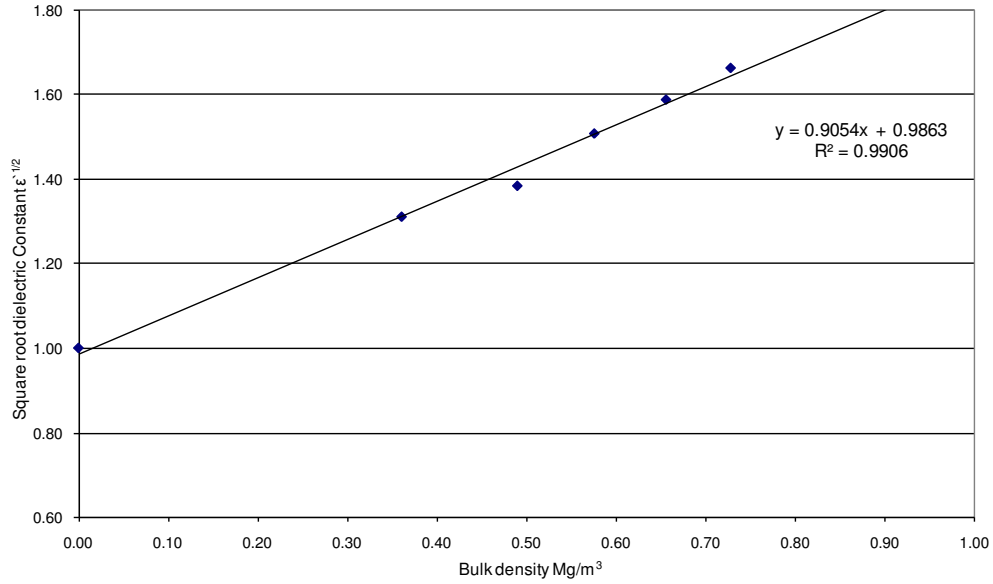

Figure 5.67 - Linear relationship between the Square roots of the dielectric constant of pulverised Dawmill coal samples and their bulk densities at 20^{o}C and 911 MHz with point (0,1) included

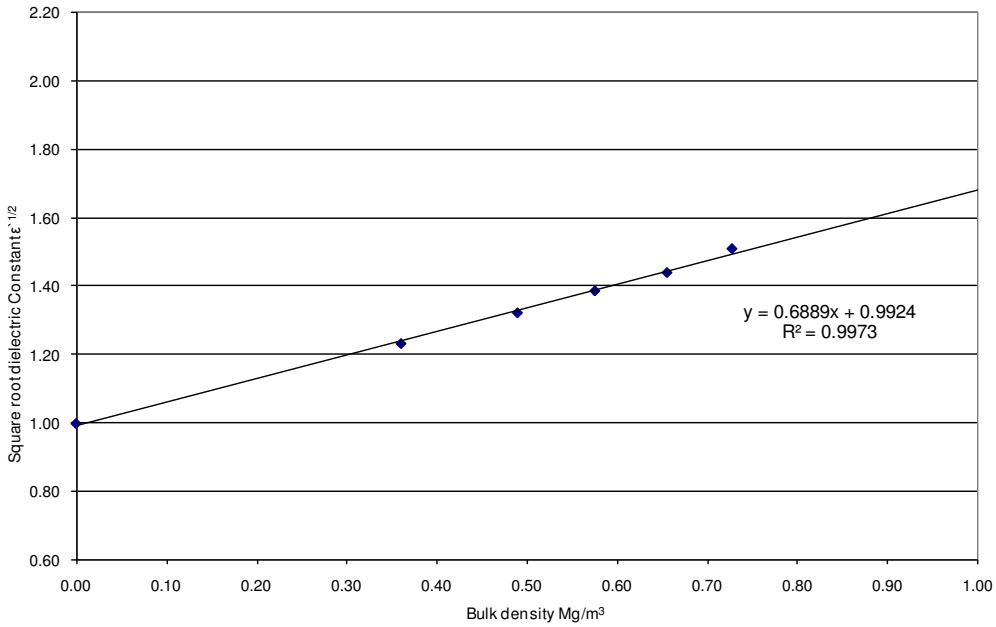

Figure 5.68 - Linear relationship between the Square roots of the dielectric constant of pulverised Dawmill coal samples and their bulk densities at 20^{o}C and 2.45 GHz with point (0,1) included

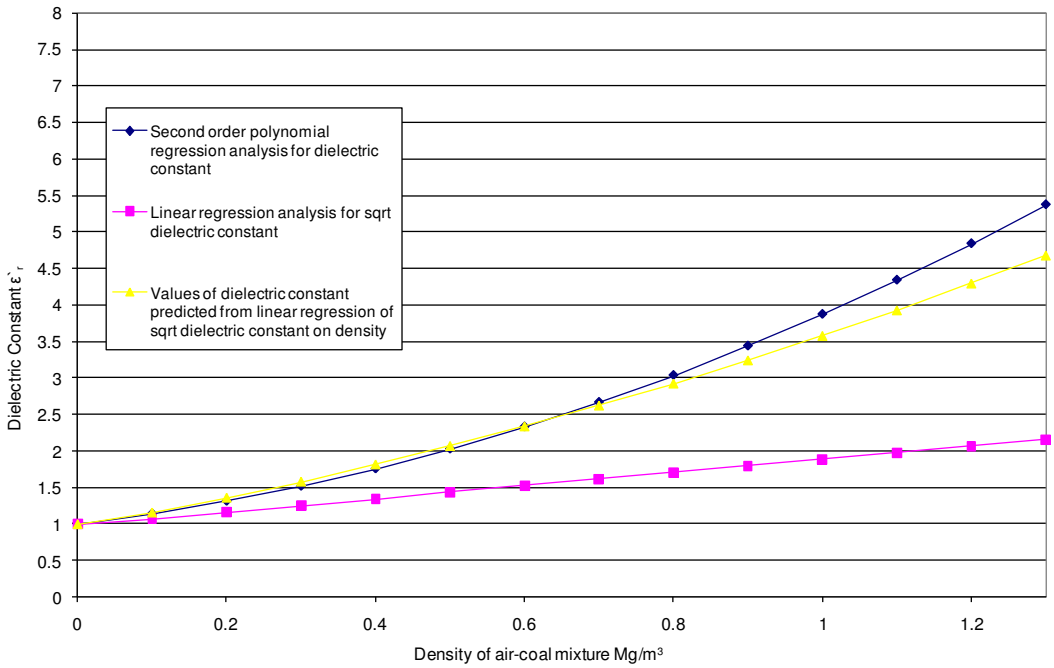

Figure 5.69 - Density dependence of the dielectric Constant $\varepsilon`_r$ and $(\varepsilon`_r)^{½}$ for Dawmill coal at 912 MHz and 20ºC

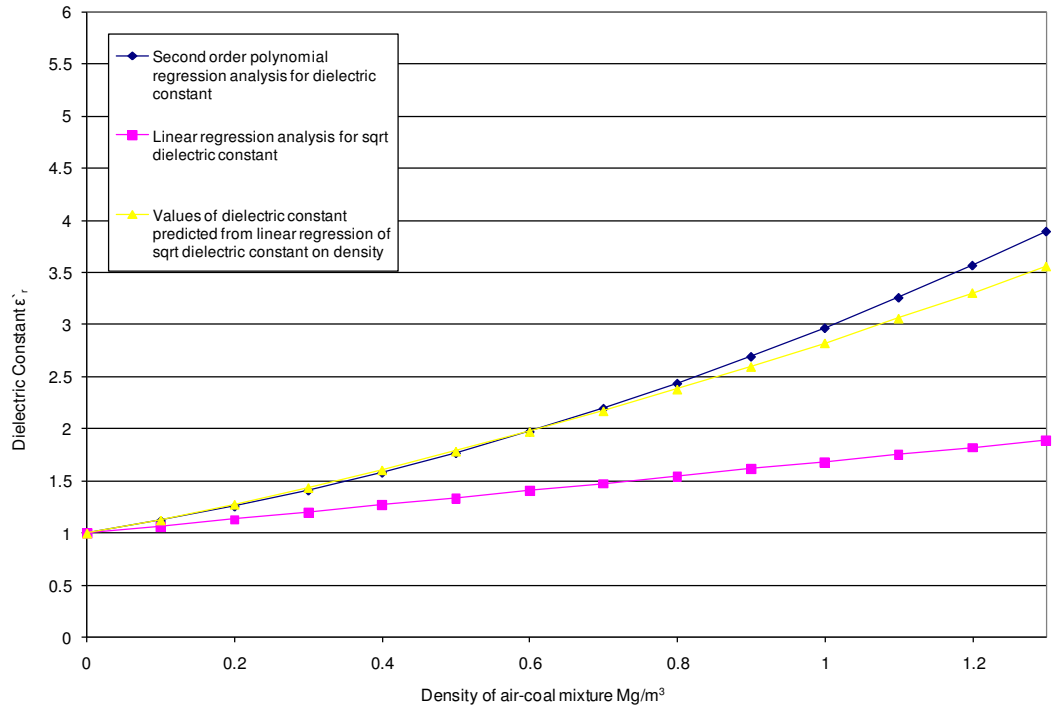

Figure 5.70 - Density dependence of the dielectric Constant $\varepsilon`_r$ and $(\varepsilon`_r)^{½}$ for Dawmill coal at 2.45 GHz and 20ºC

Appendix – A6

Modal Mineralogy Untreated –Kentucky Coal

Data Source: 1
Kentucky Coal -38µm (UT)

ID	Mineral	Mineral Weight (%)	Mineral Area (%)	Mineral Area (um2)	Particle Count	Grain Count
1	Pyrite	35.97	14.89	938944.34	3714	4076
2	Pyrrhotite	6.33	2.85	179677.42	1551	1609
3	Melanterite	5.15	5.64	355662.34	2698	2880
4	Maceral	43.70	69.58	4387383.14	20330	23058
5	Other_mineral	8.84	7.04	443875.13	3610	3935
0	Total	100.00	100.00	6305542.37	24138	35558

Table 6.7 – Modal Mineralogy –Untreated Kentucky Coal – (-38µm)

Data Source: 2
Kentucky Coal -53+38µm (UT)

ID	Mineral	Mineral Weight (%)	Mineral Area (%)	Mineral Area (um2)	Particle Count	Grain Count
1	Pyrite	33.95	13.50	1856878.90	4472	4813
2	Pyrrhotite	4.09	1.77	243094.17	1419	1454
3	Melanterite	7.39	7.77	1069596.50	3888	4165
4	Maceral	46.09	70.48	9696117.52	19751	22236
5	Other_mineral	8.48	6.48	892104.24	3528	3785
0	Total	100.00	100.00	13757791.33	24967	36453

Table 6.8 – Modal Mineralogy –Untreated Kentucky Coal – (-53+38µm)

Data Source: 5
Kentucky Coal -150+106µm (UT)

ID	Mineral	Mineral Weight (%)	Mineral Area (%)	Mineral Area (um2)	Particle Count	Grain Count
1	Pyrite	26.94	9.43	15636671.67	8391	8391
2	Pyrrhotite	2.86	1.09	1805754.87	4626	4626
3	Melanterite	5.31	4.91	8151014.36	8167	8167
4	Maceral	60.82	81.84	135775552.23	18970	18970
5	Other_mineral	4.06	2.73	4534447.05	9097	9097
0	Total	100.00	100.00	165903440.17	20635	49251

Table 6.9 – Modal Mineralogy –Untreated Kentucky Coal – (-150+106µm)

Data Source: 8
Kentucky Coal -425+300µm (UT)

ID	Mineral	Mineral Weight (%)	Mineral Area (%)	Mineral Area (um2)	Particle Count	Grain Count
1	Pyrite	26.56	9.20	15122481.14	9422	9422
2	Pyrrhotite	2.09	0.79	1294647.85	4788	4788
3	Melanterite	3.54	3.24	5332788.74	8210	8210
4	Maceral	62.44	83.19	136730207.89	16527	16527
5	Other_mineral	5.37	3.58	5876611.99	9951	9951
0	Total	100.00	100.00	164356737.60	19357	48898

Table 6.10 – Modal Mineralogy –Untreated Kentucky Coal – (-425+300µm)

Modal Mineralogy Microwave Treated [8kW 5s] –Kentucky Coal

Data Source: 10
Kentucky Coal -38µm (8kW 5s)

ID	Mineral	Mineral Weight (%)	Mineral Area (%)	Mineral Area (um2)	Particle Count	Grain Count
1	Pyrite	22.53	7.62	354546.78	2171	2258
2	Pyrrhotite	3.66	1.35	62628.57	806	819
3	Melanterite	3.70	3.31	153854.47	1650	1693
4	Maceral	64.73	84.23	3918154.71	30646	31741
5	Other_mineral	5.38	3.50	162820.22	1852	1900
0	Total	100.00	100.00	4652004.75	33413	38411

Table 6.11 – Modal Mineralogy –Microwave Treated Kentucky Coal – (-38µm)

Data Source: 11
Kentucky Coal -53+38µm (8kW 5s)

ID	Mineral	Mineral Weight (%)	Mineral Area (%)	Mineral Area (um2)	Particle Count	Grain Count
1	Pyrite	19.86	6.33	922782.06	2141	2274
2	Pyrrhotite	2.63	0.91	133020.53	670	686
3	Melanterite	0.32	0.27	39408.35	240	244
4	Maceral	73.85	90.45	13194309.47	18713	19601
5	Other_mineral	3.33	2.04	297545.92	945	984
0	Total	100.00	100.00	14587066.32	19785	23789

Table 6.12 – Modal Mineralogy –Microwave Treated Kentucky Coal – (-53+38µm)

Data Source: 14
Kentucky Coal -150+106µm (8kW 5s)

ID	Mineral	Mineral Weight (%)	Mineral Area (%)	Mineral Area (um2)	Particle Count	Grain Count
1	Pyrite	24.15	8.01	12728190.53	9822	9822
2	Pyrrhotite	1.39	0.50	796708.51	3506	3506
3	Melanterite	2.71	2.38	3780160.86	7309	7309
4	Maceral	67.95	86.69	137730883.82	20549	20549
5	Other_mineral	3.80	2.42	3847920.67	10039	10039
0	Total	100.00	100.00	158883864.39	21945	51225

Table 6.13 – Modal Mineralogy –Microwave Treated Kentucky Coal – (-150+106µm)

Data Source: 17
Kentucky Coal -425+300µm (8kW 5s)

ID	Mineral	Mineral Weight (%)	Mineral Area (%)	Mineral Area (um2)	Particle Count	Grain Count
1	Pyrite	20.81	6.91	7182258.21	4315	4315
2	Pyrrhotite	2.79	1.01	1045351.23	2226	2226
3	Melanterite	4.00	3.51	3651982.78	4996	4996
4	Maceral	66.40	84.75	88125748.18	11640	11640
5	Other_mineral	6.00	3.83	3981881.50	6508	6508
0	Total	100.00	100.00	103987221.91	12682	29685

Table 6.14 – Modal Mineralogy –Microwave Treated Kentucky Coal – (-425+300µm)

Modal Mineralogy Microwave Treated [8kW 10s] –Kentucky Coal

Data Source: 19
Kentucky Coal -38µm (8kW 10s)

ID	Mineral	Mineral Weight (%)	Mineral Area (%)	Mineral Area (um2)	Particle Count	Grain Count
1	Pyrite	64.10	36.64	2375557.16	9105	9997
2	Pyrrhotite	5.95	3.70	239604.10	2480	2564
3	Melanterite	0.92	1.40	90562.15	978	999
4	Maceral	23.98	52.72	3418392.34	20345	22556
5	Other_mineral	5.05	5.55	360175.89	2468	2547
0	**Total**	**100.00**	**100.00**	**6484291.64**	**27714**	**38663**

Table 6.15 – Modal Mineralogy –Microwave Treated Kentucky Coal – (-38µm)

Data Source: 20
Kentucky Coal -53+38µm (8kW 10s)

ID	Mineral	Mineral Weight (%)	Mineral Area (%)	Mineral Area (um2)	Particle Count	Grain Count
1	Pyrite	59.19	30.07	4134120.12	8750	10013
2	Pyrrhotite	3.93	2.17	298029.84	1913	1976
3	Melanterite	1.70	2.29	314168.03	944	965
4	Maceral	31.84	62.21	8551992.23	20701	23908
5	Other_mineral	3.34	3.27	448880.32	1695	1752
0	**Total**	**100.00**	**100.00**	**13747190.54**	**26125**	**38614**

Table 6.16 – Modal Mineralogy –Microwave Treated Kentucky Coal – (-53+38µm)

Data Source: 23
Kentucky Coal -150+106µm (8kW 10s)

ID	Mineral	Mineral Weight (%)	Mineral Area (%)	Mineral Area (um2)	Particle Count	Grain Count
1	Pyrite	33.58	12.71	18149000.40	15478	15478
2	Pyrrhotite	3.12	1.29	1835933.01	6042	6042
3	Melanterite	6.91	6.92	9880914.81	11189	11189
4	Maceral	52.28	76.10	108679910.51	23827	23827
5	Other_mineral	4.11	2.99	4274898.92	10788	10788
0	**Total**	**100.00**	**100.00**	**142820657.64**	**27266**	**67324**

Table 6.17 – Modal Mineralogy –Microwave Treated Kentucky Coal – (-150+106µm)

Data Source: 26
Kentucky Coal -425+300µm (8kW 10s)

ID	Mineral	Mineral Weight (%)	Mineral Area (%)	Mineral Area (um2)	Particle Count	Grain Count
1	Pyrite	21.60	7.24	11511550.92	5556	5556
2	Pyrrhotite	2.57	0.94	1490818.16	2393	2393
3	Melanterite	5.56	4.92	7834614.93	5395	5395
4	Maceral	64.63	83.27	132471495.09	13161	13161
5	Other_mineral	5.64	3.63	5775333.30	6765	6765
0	**Total**	**100.00**	**100.00**	**159083812.40**	**14237**	**33270**

Table 6.18 – Modal Mineralogy –Microwave Treated Kentucky Coal – (-425+300µm)

Modal Mineralogy Microwave Treated [8kW 15s] –Kentucky Coal

Data Source: 28
Kentucky Coal -38µm (8kW 15s)

ID	Mineral	Mineral Weight (%)	Mineral Area (%)	Mineral Area (um2)	Particle Count	Grain Count
1	Pyrite	52.05	24.33	1293318.22	6415	6892
2	Pyrrhotite	4.92	2.50	132880.86	1655	1689
3	Melanterite	0.47	0.59	31167.59	442	445
4	Maceral	38.18	68.65	3649008.39	26006	27883
5	Other_mineral	4.37	3.93	208913.98	1869	1931
0	**Total**	**100.00**	**100.00**	**5315289.03**	**30838**	**38840**

Table 6.19 – Modal Mineralogy –Microwave Treated Kentucky Coal – (-38µm)

Data Source: 29
Kentucky Coal -53+38µm (8kW 15s)

ID	Mineral	Mineral Weight (%)	Mineral Area (%)	Mineral Area (um2)	Particle Count	Grain Count
1	Pyrite	49.64	21.91	3121162.95	7091	7985
2	Pyrrhotite	3.80	1.82	259391.02	1541	1584
3	Melanterite	0.54	0.63	89064.45	597	610
4	Maceral	43.10	73.15	10422123.60	21621	24240
5	Other_mineral	2.94	2.49	354911.14	1486	1531
0	**Total**	**100.00**	**100.00**	**14246653.17**	**25766**	**35950**

Table 6.20 – Modal Mineralogy –Microwave Treated Kentucky Coal – (-53+38µm)

Data Source: 32
Kentucky Coal -150+106µm (8kW 15s)

ID	Mineral	Mineral Weight (%)	Mineral Area (%)	Mineral Area (um2)	Particle Count	Grain Count
1	Pyrite	30.87	11.08	16873811.22	10707	10707
2	Pyrrhotite	2.57	1.00	1528099.23	4355	4355
3	Melanterite	2.96	2.81	4280536.01	7609	7609
4	Maceral	59.65	82.37	125403391.95	20585	20585
5	Other_mineral	3.95	2.73	4154279.32	9695	9695
0	**Total**	**100.00**	**100.00**	**152240117.73**	**22183**	**52951**

Table 6.21 – Modal Mineralogy –Microwave Treated Kentucky Coal – (-150+106µm)

Data Source: 35
Kentucky Coal -425+300µm (8kW 15s)

ID	Mineral	Mineral Weight (%)	Mineral Area (%)	Mineral Area (um2)	Particle Count	Grain Count
1	Pyrite	18.04	5.73	8822563.23	7836	7836
2	Pyrrhotite	2.54	0.87	1347758.65	3250	3250
3	Melanterite	2.25	1.89	2913749.45	5260	5260
4	Maceral	72.70	88.77	136749942.37	12155	12155
5	Other_mineral	4.47	2.73	4208013.02	8115	8115
0	**Total**	**100.00**	**100.00**	**154042026.73**	**14885**	**36616**

Table 6.22 – Modal Mineralogy –Microwave Treated Kentucky Coal – (-425+300µm

Modal Mineralogy Microwave Treated [8kW 20s] –Kentucky Coal

Data Source: 37
Kentucky Coal -38µm (8kW 20s)

ID	Mineral	Mineral Weight (%)	Mineral Area (%)	Mineral Area (um2)	Particle Count	Grain Count
1	Pyrite	42.68	18.12	983953.78	5216	5670
2	Pyrrhotite	6.11	2.82	153192.95	1706	1752
3	Melanterite	0.84	0.95	51522.07	602	610
4	Maceral	45.28	73.95	4015201.60	24266	26569
5	Other_mineral	5.08	4.15	225380.73	1990	2069
0	Total	100.00	100.00	5429251.13	27880	36670

Table 6.23 – Modal Mineralogy –Microwave Treated Kentucky Coal – (-38µm)

Data Source: 38
Kentucky Coal -53+38µm (8kW 20s)

ID	Mineral	Mineral Weight (%)	Mineral Area (%)	Mineral Area (um2)	Particle Count	Grain Count
1	Pyrite	38.78	15.09	1850770.31	5559	6249
2	Pyrrhotite	4.33	1.83	224819.96	1502	1551
3	Melanterite	0.22	0.23	28188.77	258	260
4	Maceral	54.03	80.87	9916425.45	23362	25521
5	Other_mineral	2.63	1.97	241624.54	1245	1290
0	Total	100.00	100.00	12261829.03	26456	34871

Table 6.24 – Modal Mineralogy –Microwave Treated Kentucky Coal – (-53+38µm)

Data Source: 41
Kentucky Coal -150+106µm (8kW 20s)

ID	Mineral	Mineral Weight (%)	Mineral Area (%)	Mineral Area (um2)	Particle Count	Grain Count
1	Pyrite	27.84	9.69	16281851.08	11804	11804
2	Pyrrhotite	2.06	0.78	1307871.31	4631	4631
3	Melanterite	3.22	2.97	4984509.80	9053	9053
4	Maceral	62.46	83.61	140499875.50	26726	26726
5	Other_mineral	4.42	2.96	4970880.37	12395	12395
0	Total	100.00	100.00	168044988.07	28500	64609

Table 6.25 – Modal Mineralogy –Microwave Treated Kentucky Coal – (-150+106µm)

Data Source: 44
Kentucky Coal -425+300µm (8kW 20s)

ID	Mineral	Mineral Weight (%)	Mineral Area (%)	Mineral Area (um2)	Particle Count	Grain Count
1	Pyrite	22.82	7.70	12323295.82	8503	8503
2	Pyrrhotite	2.87	1.05	1682219.10	3651	3651
3	Melanterite	4.75	4.25	6792337.91	6819	6819
4	Maceral	64.44	83.68	133855434.66	12430	12430
5	Other_mineral	5.12	3.32	5315570.65	8533	8533
0	Total	100.00	100.00	159968858.14	15966	39936

Table 6.26 – Modal Mineralogy –Microwave Treated Kentucky Coal – (-425+300µm)

Modal Mineralogy Microwave Treated [8kW 25s] –Kentucky Coal

Data Source: 46
Kentucky Coal -38µm (8kW 25s)

ID	Mineral	Mineral Weight (%)	Mineral Area (%)	Mineral Area (um2)	Particle Count	Grain Count
1	Pyrite	33.62	12.63	735638.28	4474	4933
2	Pyrrhotite	5.01	2.05	119207.46	1441	1477
3	Melanterite	0.57	0.57	33269.30	482	490
4	Maceral	56.55	81.69	4759642.76	22781	24928
5	Other_mineral	4.24	3.06	178511.66	1760	1816
0	Total	100.00	100.00	5826269.46	25654	33644

Table 6.27 – Modal Mineralogy –Microwave Treated Kentucky Coal – (-38µm)

Data Source: 47
Kentucky Coal -53+38µm (8kW 25s)

ID	Mineral	Mineral Weight (%)	Mineral Area (%)	Mineral Area (um2)	Particle Count	Grain Count
1	Pyrite	31.03	11.10	1415537.14	4421	4813
2	Pyrrhotite	4.09	1.59	202686.24	1230	1258
3	Melanterite	0.25	0.24	30525.11	232	233
4	Maceral	61.89	85.18	10858060.85	24349	25732
5	Other_mineral	2.74	1.88	240111.27	1153	1184
0	Total	100.00	100.00	12746920.60	26978	33220

Table 6.28 – Modal Mineralogy –Microwave Treated Kentucky Coal – (-53+38µm)

Data Source: 50
Kentucky Coal -150+106µm (8kW 25s)

ID	Mineral	Mineral Weight (%)	Mineral Area (%)	Mineral Area (um2)	Particle Count	Grain Count
1	Pyrite	59.49	33.52	16801911.14	9844	9844
2	Pyrrhotite	6.24	3.82	1916906.99	4347	4347
3	Melanterite	4.24	6.31	3164598.67	6016	6016
4	Maceral	21.97	47.61	23864984.59	17666	17666
5	Other_mineral	8.06	8.73	4378551.44	9980	9980
0	Total	100.00	100.00	50126952.83	20704	47853

Table 6.29 – Modal Mineralogy –Microwave Treated Kentucky Coal – (-150+106µm)

Data Source: 53
Kentucky Coal -425+300µm (8kW 25s)

ID	Mineral	Mineral Weight (%)	Mineral Area (%)	Mineral Area (um2)	Particle Count	Grain Count
1	Pyrite	26.04	9.15	13158469.22	8777	8777
2	Pyrrhotite	2.53	0.97	1389452.70	3609	3609
3	Melanterite	6.45	6.00	8620879.78	7710	7710
4	Maceral	59.11	79.92	114884521.52	14187	14187
5	Other_mineral	5.87	3.96	5699609.04	9270	9270
0	Total	100.00	100.00	143752932.26	18450	43553

Table 6.30 – Modal Mineralogy –Microwave Treated Kentucky Coal – (-425+300µm)

Modal Mineralogy Microwave Treated [8kW 30s] –Kentucky Coal

Data Source: 55
Kentucky Coal -38µm (8kW 30s)

ID	Mineral	Mineral Weight (%)	Mineral Area (%)	Mineral Area (um2)	Particle Count	Grain Count
1	Pyrite	30.29	12.30	726988.24	4472	4853
2	Pyrrhotite	14.73	6.50	384242.95	2934	3085
3	Melanterite	1.23	1.33	78402.56	899	921
4	Maceral	48.59	75.85	4484623.02	26292	28900
5	Other_mineral	5.15	4.02	237885.03	2065	2167
0	**Total**	**100.00**	**100.00**	**5912141.80**	**29799**	**39926**

Table 6.31 – Modal Mineralogy –Microwave Treated Kentucky Coal – (-38µm)

Data Source: 56
Kentucky Coal -53+38µm (8kW 30s)

ID	Mineral	Mineral Weight (%)	Mineral Area (%)	Mineral Area (um2)	Particle Count	Grain Count
1	Pyrite	16.90	5.41	631017.49	2332	2495
2	Pyrrhotite	7.15	2.49	290281.06	1419	1452
3	Melanterite	0.51	0.43	50028.97	398	402
4	Maceral	73.45	90.44	10545235.52	25747	26805
5	Other_mineral	1.99	1.22	142750.64	902	924
0	**Total**	**100.00**	**100.00**	**11659313.67**	**27397**	**32078**

Table 6.32 – Modal Mineralogy –Microwave Treated Kentucky Coal – (-53+38µm)

Data Source: 59
Kentucky Coal -150+106µm (8kW 30s)

ID	Mineral	Mineral Weight (%)	Mineral Area (%)	Mineral Area (um2)	Particle Count	Grain Count
1	Pyrite	26.99	9.71	13912758.51	11115	11115
2	Pyrrhotite	5.56	2.18	3116638.42	4482	4482
3	Melanterite	2.55	2.43	3475723.59	7462	7462
4	Maceral	58.91	81.54	116806647.24	18874	18874
5	Other_mineral	6.00	4.15	5945611.40	7721	7721
0	**Total**	**100.00**	**100.00**	**143257379.16**	**20857**	**49654**

Table 6.33 – Modal Mineralogy –Microwave Treated Kentucky Coal – (-150+106µm)

Data Source: 62
Kentucky Coal -425+300µm (8kW 30s)

ID	Mineral	Mineral Weight (%)	Mineral Area (%)	Mineral Area (um2)	Particle Count	Grain Count
1	Pyrite	25.63	9.27	12027916.96	12241	12241
2	Pyrrhotite	7.59	2.98	3873348.03	6311	6311
3	Melanterite	5.20	4.98	6461199.59	8155	8155
4	Maceral	57.46	79.91	103723266.99	18977	18977
5	Other_mineral	4.11	2.86	3713789.40	6172	6172
0	**Total**	**100.00**	**100.00**	**129799520.96**	**23727**	**51856**

Table 6.34 – Modal Mineralogy –Microwave Treated Kentucky Coal – (-425+300µm)

Modal Mineralogy Microwave Treated [15kW 5s] –Kentucky Coal

Data Source: 64
Kentucky Coal -38µm (15kW 5s)

ID	Mineral	Mineral Weight (%)	Mineral Area (%)	Mineral Area (um2)	Particle Count	Grain Count
1	Pyrite	28.66	13.04	797227.15	3655	3899
2	Pyrrhotite	19.99	9.89	604434.11	3726	3984
3	Melanterite	3.61	4.35	265951.36	2175	2277
4	Maceral	35.35	61.87	3782288.62	20512	23104
5	Other_mineral	12.40	10.85	663222.92	4537	4947
0	Total	100.00	100.00	6113124.15	25993	38211

Table 6.35 – Modal Mineralogy –Microwave Treated Kentucky Coal – (-38µm)

Data Source: 65
Kentucky Coal -53+38µm (15kW 5s)

ID	Mineral	Mineral Weight (%)	Mineral Area (%)	Mineral Area (um2)	Particle Count	Grain Count
1	Pyrite	28.62	11.59	1829376.35	2603	2720
2	Pyrrhotite	14.81	6.52	1028617.37	2004	2093
3	Melanterite	2.61	2.79	440951.05	1302	1355
4	Maceral	47.58	74.13	11697367.42	19997	21573
5	Other_mineral	6.38	4.97	784148.77	2194	2331
0	Total	100.00	100.00	15780460.96	22662	30072

Table 6.36 – Modal Mineralogy –Microwave Treated Kentucky Coal – (-53+38µm)

Data Source: 68
Kentucky Coal -150+106µm (15kW 5s)

ID	Mineral	Mineral Weight (%)	Mineral Area (%)	Mineral Area (um2)	Particle Count	Grain Count
1	Pyrite	38.69	18.76	8196024.36	4696	4696
2	Pyrrhotite	19.09	10.06	4395589.79	2953	2953
3	Melanterite	2.74	3.52	1535769.28	3753	3753
4	Maceral	33.06	61.67	26938862.90	10473	10473
5	Other_mineral	6.43	6.00	2619033.78	4520	4520
0	Total	100.00	100.00	43685280.09	11566	26395

Table 6.37 – Modal Mineralogy –Microwave Treated Kentucky Coal – (-150+106µm)

Data Source: 71
Kentucky Coal -425+300µm (15kW 5s)

ID	Mineral	Mineral Weight (%)	Mineral Area (%)	Mineral Area (um2)	Particle Count	Grain Count
1	Pyrite	29.03	11.43	12668460.25	7430	7430
2	Pyrrhotite	10.89	4.66	5166570.34	6938	6938
3	Melanterite	4.32	4.50	4988402.16	7720	7720
4	Maceral	49.10	74.37	82417427.84	30245	30245
5	Other_mineral	6.65	5.04	5583544.98	12223	12223
0	Total	100.00	100.00	110824405.56	33572	64556

Table 6.38 – Modal Mineralogy –Microwave Treated Kentucky Coal – (-425+300µm)